ISTITUTO NAZIONALE DI FISICA NUCLEARE
Laboratori Nazionali di Frascati

FRASCATI PHYSICS SERIES

ECT*

EUROPEAN CENTRE FOR THEORETICAL STUDIES
IN NUCLEAR PHYSICS AND RELATED AREAS
TRENTO, ITALY
Institutional Member of the ESF Expert Committee NuPECC

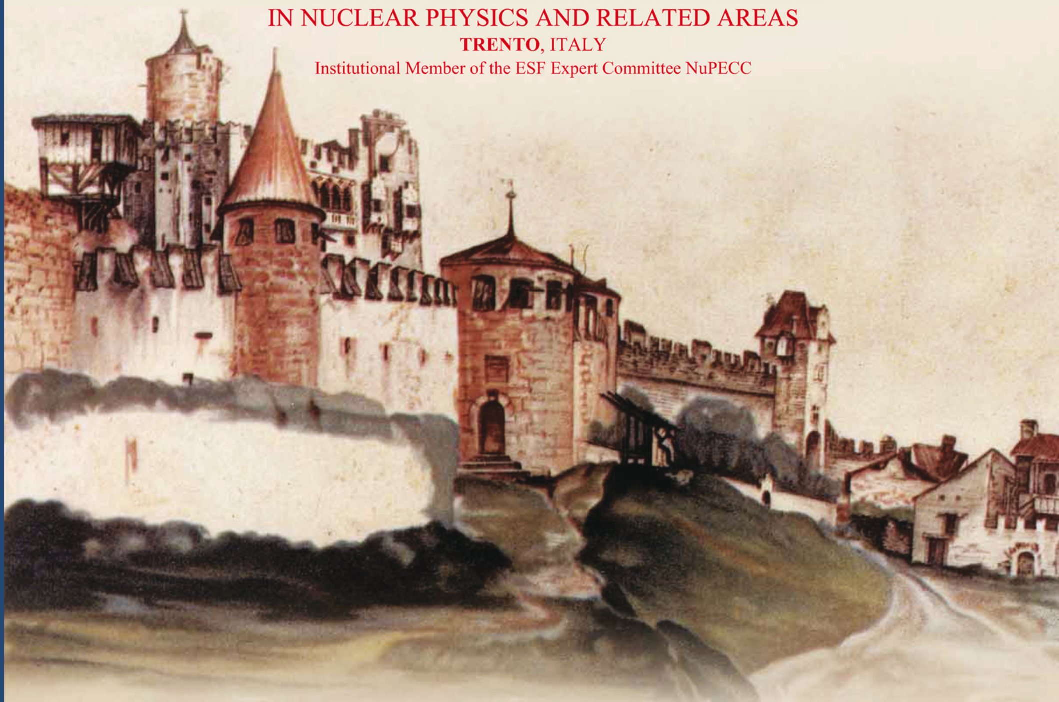

Castello di Trento ("Trint"). watercolour, 19.8 x 27.7, painted by A. Dürer on his way back from Venice (1495) British Museum, London.

LFC15: Physics prospects for Linear and other Future Colliders after the discovery of the Higgs

Trento, September 7-11, 2015

Editors:

Gennaro Corcella, Stefania De Curtis, Stefano Moretti,
Giulia Pancheri

FRASCATI PHYSICS SERIES

Series Editor
Rossana Centioni

Technical Editor
Debora Bifaretti

Cover by Claudio Federici

Volume LXI

Istituto Nazionale di Fisica Nucleare – Laboratori Nazionali di Frascati
Divisione Ricerca
SIDS – Servizio Informazione e Documentazione Scientifica
Ufficio Biblioteca e Pubblicazioni
P.O. Box 13, I-00044 Frascati Roma Italy
email: sis.publications@lnf.infn.it

ISBN 978-88-86409-88-9

LFC15:
Physics prospects for Linear and other Future Colliders
after the discovery of the Higgs
2015

CONTENTS

PREFACE

The workshop 'LFC15: physics prospects for Linear and other Future Colliders after the discovery of the Higgs' was held at the European Center for Theoretical Physics (ECT*), Villazzano (TN), Italy, on September 7-11 2015. It is part of a series which started as forums to discuss the physics of high-energy electron-positron Linear Colliders, and have lately become meetings wherein all projects of future accelerators, both linear and circular, as well as lepton and hadron colliders, are debated.

All workshops took place in Italy and gathered the Italian community working on the phenomenology of future colliders and scientists from everywhere in the world. Previous editions were held in Florence (2007), Perugia (2009), Frascati National Laboratories (2008 and 2010) and again at ECT* (2011 and 2013).

Our meetings consist of plenary sessions, organized with a few general presentation and working groups with more specific talks on Quantum Chromodynamics, top-quark phenomenology, electroweak interactions, Higgs physics, Monte Carlo event generators, supersymmetry, physics beyond the Standard Model (BSM) and astroparticle physics. Furthermore, along the lines of the ECT* workshops, a colloquium on topics of wide interest was organized: in the 2015 edition, the speaker was Francois Richard and the title ‘The future of accelerator physics’.

In detail, we scheduled general talks on the most challenging objectives of the LHC Run II at 13 TeV, the perspectives for muon colliders, neutrino factories, as well as e^+e^- colliders, in both linear (ILC) and circular (FCC-ee) options. The BSM session had presentations on the searches for new physics carried out by the ATLAS and CMS collaborations at the LHC and, on the theory side, on the status of the naturalness paradigm after the LHC Run I, heavy leptons at present and future colliders, Dark Matter candidates, the status of supersymmetry after the Higgs discovery, the minimal flavour-violating CMSSM.

The Higgs working group dealt with Higgs physics both within and beyond the Standard Model: in fact, the latest LHC experimental results, presented at the workshop, confirmed the hint that the discovered particle with mass about 125 GeV should be the Standard Model Higgs boson. Besides, composite models, as well as the prospects for singlet-like, off-shell and double Higgs production, were thoroughly debated.

In the top-quark session, the recent measurements and the theory status on the determination of the top mass and couplings were topics which led to wide discussions among speakers and participants. Moreover, the prospects for top phenomenology at future colliders, in particular electroweak corrections, $t\bar{t}H$ production and BSM effects in $t\bar{t}$ events in e^+e^- collisions, were reported within the working group. It was also shown how flavour and electroweak data can be used to obtain an indirect determination of the top mass which, within the errors, is in agreement with the direct extraction; as far as the flavour sector is concerned, the most interesting LHCb results were reviewed.

As happened also in previous meetings, a special session was devoted to the lepton magnetic moment, the so-called g-2. This issue was tackled from both experimental and theoretical viewpoints, taking particular care about the new ‘g-2 experiment’ at Fermilab.

In the Standard Model and QCD session, the main issues investigated were four-fermion production, total pp cross section, status and prospects for QCD measurements and computations, namely fixed-order and resummed calculation, as well as parton shower implementation and updates on parton distribution functions. Finally, we had a working group on cosmology and astrophysics, which scheduled talks on the cosmological history of the Higgs vacuum, results from the AMS-02 experiment and open problems in the galacting cosmic ray origin and propagation.

These proceedings can therefore be, from several viewpoints, a useful collections of contributions, discussing the state of the art of particle physics after the LHC Run I and a number of astrophysics observations, and underlining the prospects for future hadron and lepton colliders. More details, as well as the slides of the talks, can be found at: `http://www.ectstar.eu/node/1233` and `http://www.lnf.infn.it/conference/LFC15/`

Before concluding, we wish to warmly thank all the conveners, whose names are listed below, for their remarkable effort to invite the speakers and manage the sessions, in such a way to achieve a fruitful workshop and release the present volume. We also acknowledge the ECT* for financial support and, in particular, Gianmaria Ziglio for his invaluable help with the organization of the logistics.

Organizing Committee:

Gennaro Corcella, INFN, Laboratori Nazionali di Frascati
Stefania De Curtis, INFN, Florence
Stefano Moretti, NExT Institute, Southampton University
Giulia Pancheri, INFN, Laboratori Nazionali di Frascati
Francois Richard, Laboratoire de l'Accélérateur Linéaire, Orsay

Conveners:

Carlo Carloni Calame, Pavia University (Electroweak Physics and g-2)
Denis Comelli, INFN, Ferrara (Dark Matter and Astroparticle Physics)
Aldo Deandrea, IPN, Lyon (BSM and Supersymmetry)
Giancarlo Ferrera, Milan University (QCD)
Roberto Franceschini, CERN (BSM and Higgs Phenomenology)
Orlando Panella, INFN, Perugia (BSM and Exotic Physics)
Fulvio Piccinini, INFN, Pavia (Tools for High Energy Physics)
Francesco Tramontano, Naples University (Top-quark Phenomenology)

APPROACHING A NEW ENERGY FRONTIER AT THE LHC

Barbara Mele
INFN, Sezione di Roma, Rome, Italy

Abstract

After reviewing the latest great achievements in the field of Collider Physics, we sketch the main criticalities of the present theory of particle interactions. The latter substantiate the expectations for possible new discoveries at the forthcoming Run II at the Large Hadron Collider (LHC). We discuss the LHC potential in mass reach for the production of new heavy states, and we argue that any kind of clear discrepancy from the Standard Model predictions which will be observed will imply a revolution in the field.

1 Collider Physics: where we stand today

The Large Hadron Collider (LHC), the CERN proton-proton collider with c.m. collision energies of up to 14 TeV, has yet to enter its full running regime, and still has already produced a wealth of most remarkable results. In the

LHC Run 1, spanning the years 2009-2013, the ATLAS and CMS experiments collected each a data set of about 5 fb^{-1} of integrated luminosity at $\sqrt{s} = 7$ TeV plus about 20 fb^{-1} at $\sqrt{s} = 8$ TeV[1]. This was just the initial phase of the machine, which is now expected to collect about 100 fb^{-1} at $\sqrt{s} = 13-14$ TeV in the Run 2 during the years 2015-2018. In the subsequent Run 3, by the year 2023 the LHC should reach a data set of 300 fb^{-1} at the same $\sqrt{s}$, possibly followed by a High-Luminosity phase aiming at collecting about 3000 fb^{-1} at $\sqrt{s} = 14$ TeV in the following 10 years [1).

Although Run 1 was just the initial LHC phase, both the machine and the experiments had an amazing performance, obtaining results very much above expectations. The standard model (SM) theory has been tested at high accuracy in a new $\sqrt{s}$ range. QCD has been probed in many different regimes, and knowledge of the proton parton distribution functions (PDF's) has been widely extended. Many new results on top quark physics, flavor physics, and electroweak (EW) processes have been collected [2).

Most importantly, the direct exploration of the SM EW symmetry breaking (EWSB) sector has started up with the observation of a (quite light) Higgs-boson resonance at 125 GeV. The Higgs observation (which was the last missing object among the states predicted by the SM to be experimentally observed) was a triumph for both the SM theory [3) and the LHC enterprise [4). Although the particle observed looks quite similar to the boson predicted in the SM, there is presently still a lot of room for a non-SM EWSB/Higgs sector.

Apart from SM studies, at the Run1, a lot of searches for new heavy states predicted by many beyond-SM (BSM) models have been performed, and the corresponding mass bounds have been widely extended with respect to the pre-LHC era. There are just a few very mild hints at the moment possibly pointing to non-SM phenomena in proton collisions (see e.g. the ATLAS analysis [5)). Altogether, one can say that the SM theory provides an excellent description of all phenomena studied up to now in high-energy collisions.

The LHC Run-2 just started with stable beams in June 2015, with ATLAS and CMS having already collected about 200 pb^{-1} today [1), and great expectations for fore-coming results.

---

[1]Here we are not covering physics studies at the LHCb and ALICE experiments.

2 The Higgs boson sector: criticalities and opportunities

The actual identity of the newly observed particle with mass 125 GeV can be established by measuring with high precision the magnitude and structure of its couplings to known particles. The SM predicts the intensity of the Hpp Higgs coupling is set by the mass of the coupled p particle. Once, the Higgs mass is known, the SM also predicts the scalar boson self-coupling magnitude. From the ATLAS and CMS analysis of the Run 1 data set, one can infer that the observed particle is not a *generic* scalar state, because it really matches the nontrivial coupling pattern predicted in the SM well within errors. The brand new combined ATLAS and CMS results for the measurement of the couplings [6] agrees within 1σ with the SM Higgs-coupling predictions. The measurement of the scalar resonance mass in the $\gamma\gamma$ and 4ℓ channels by the two experiments agrees very well, and provides the result $m_H = 125.09 \pm 0.24$ GeV [7], with the amazing precision of 0.2%.

The test of the SM Lagrangian looks then about to be completed by the direct measurements of all the parameters involved in its Higgs-sector part. Actually, it should be stressed that the main *theoretical shortcomings* of the SM Lagrangian are connected to just its Higgs sector, notably the Yukawa-coupling mysterious hierarchy (which spans many many orders of magnitudes), the fact that the Higgs mass term is not protected by any symmetry, and finally the Higgs self-coupling magnitude which affects the vacuum stability, and the possibility of explaining the Baryogenesis via cosmological EW phase transition.

The unprotected Higgs mass term in the SM Lagrangian motivates the expectation for a New Physics energy threshold as low as o(1) TeV in order to avoid fine-tuning in the fundamental parameters of the theory. Such a low threshold could well give rise to detectable effects at the LHC. After LHC Run 1 searches, the simplest versions of many proposed models able to cure the SM fine-tuning (or *naturalness*) problem look quite fine-tuned. Run 2 will widely expand the coverage of BSM searches, as discussed in the following. It is anyhow important to stress that a general prediction of *natural* models (like the MSSM or the minimal Composite Higgs models), apart from the existence of new heavy states with o(1) TeV masses, is a deviation in the Higgs-boson couplings at the few percents level. The deviation pattern depends on the particular extension of the SM Lagrangian. A very accurate measurement of the

Higgs boson couplings could then detect the inadequacy of the SM even before the direct observation of the predicted heavy states, and point to a particular kind of SM extension. One Higgs coupling which is in general most sensitive to *natural* modifications of the SM Lagrangian is the Higgs self-coupling. Its corresponding measurement, which is unfortunately quite challenging at the LHC, as well as the measurement of all Higgs couplings, will be extremely helpful in characterizing possible SM extensions at the TeV scale, even if they do not manifest in direct production of new states.

3 LHC Run 2 versus LHC Run 1

LHC Run 2 is at the moment characterized by a 13 TeV c.m. collision energy, that could soon be updated to the nominal value of 14 TeV foreseen by the LHC design. This corresponds to a 62% (75% at 14 TeV) increase in the c.m. energy available for the production of new heavy states, with a total integrated luminosity expected to be about 100 fb^{-1} at the end of Run 2 by 2018.

The exploration of a yet unexplored energy domain has just started with a huge discovery potential! Indeed, the mass reach M_{reach} (defined as the heaviest mass of a BSM state that can be directly produced and observed either singly or in pairs) will be drastically extended in Run 2 with respect to the 8-TeV Run. Although the exact mass-reach increase from Run 1 to Run 2 is in general model dependent, it is interesting to approximatly estimate the M_{reach} variation just from the scaling of parton luminosities and PDF's, with the assumption that cross sections scale with the inverse squared system mass [8]. In general, given the higher c.m. energy and related integrated luminosity, starting from the Run-1 8-TeV mass reach M^{R1}_{reach} and event number N_{ev} (corresponding to the 20 fb^{-1} collected data set) for a given signal process, in order to estimate the LHC increase in mass reach at larger $\sqrt{s}$, one can just require the number of events corresponding to Run-2 to be the same N_{ev}, neglecting scaling differences in backgrounds, reconstruction, and detector behavior [8]. For quite large masses (not too close to the edges of available kinematical range), one then finds simple approximate rules governing M_{reach} versus $\sqrt{s}$ and integrated luminosity $\int L$. For instance, one finds that, by increasing $\sqrt{s}$ by a factor x, in order to also extend M_{reach} by a factor x, one needs to increase the integrated luminosity by x^2, which compensates the $1/M^2$ cross section dependence. On the other hand, at fixed $\sqrt{s}$, M_{reach} depends almost logarithmically on $\int L$. For

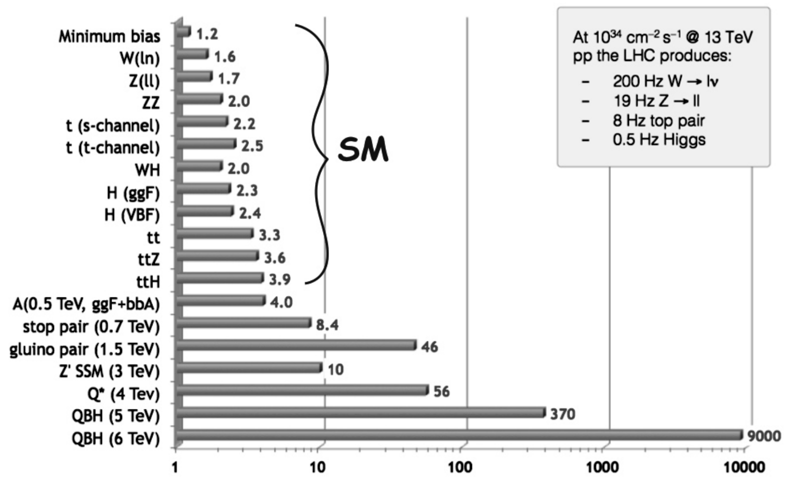

Figure 1: *Cross-section enhancement x factors for different production processes when going from LHC collisions at $\sqrt{s} = 8$ GeV to LHC collisions at $\sqrt{s} = 13$ GeV. The 13-TeV potential approximately equals the Run-1 8-TeV one, after collecting (20/x) fb^{-1} at 13 TeV.*

instance, for $0.15 < M_{reach}/\sqrt{s} < 0.6$, increasing $\int L$ by a factor 10, M_{reach} grows up to about $M_{reach} + 0.07\sqrt{s}$, which for $\sqrt{s} = 14$ TeV corresponds to a 1-TeV rise. This is relevant for example when going from the LHC projected luminosity of $\int L$ 300 fb^{-1} to the High-Luminosity expected data set of about $\int L$ 3000 fb^{-1}.

In Figure 1, we report the enhancement factor x for cross sections at $\sqrt{s} = 13$ TeV with respect to the 8 TeV cross sections for different production processes. These factors fold the *partonic* cross-section and *partonic* luminosity scaling. At 13 TeV, the Run 1 potential in searches will be approximately matched after collecting just about $(20/x)$ fb^{-1}, which, for particularly heavy states such as gluino pairs in Supersymmetry, requires less than 1 pb^{-1}.

4 Summary and Outlook

The SM has proven to be beautifully successful in any possible test involving c.m. energies covered up to today in collider experiments. Nevertheless, the SM theory many limitations lead us to believe that this framework is not a complete one. In particular, the Higgs boson is the first *possibly* elementary scalar observed in nature, and its theoretical features present a number of criticalities. As a consequence, the precise measurement of the Higgs properties will be, in the forthcoming LHC program, one of the most promising way to "indirectly" discover New Physics and to discriminate among BSM extensions. The search of exotic signatures in Higgs decays and of further heavier Higgs degrees of freedom will also provide a valuable handle for extending our knowledge of the actual (possibly non-standard) Higgs sector.

Indeed, the Higgs-boson observation opened up an entire new chapter of BSM exploration. Even in case of no observation of new heavy states in the next LHC runs, precision Higgs physics will have a key role in paving the way for extending the SM theory.

In any case, LHC Run 2 just started with a great potential for discoveries. There are many different possibilities ahead of us. We might observe new resonances and/or *robust* modifications of distributions or physical observables. This would surely imply a revolution in our understanding of particle interactions. It would also require a huge amount of work in the following years to set the actual SM extension that could accomodate the observed new phenomena. Another option ahead is that we will not observe at the LHC any significant deviation from the SM predictions, and will just keep measuring observables with more and more precision. This latter option would anyway imply a deepening of our knowledge of fundamental interactions at shorter distances, that will have to be taken into account by any possible SM extension.

After the Run-1 completion and the observation of all SM degrees of freedom, however "revolutionary" the forthcoming LHC outcome at 14 TeV will be, it will lay just the first stage of a new path of exploration, which will in no way be a conclusive one for Particle Physics.

5 Acknowledgements

I wish to thank the organizers of the LFC15 workshop at the ETC* in Trento for inviting me to such an inspiring and fruitful workshop.

References

1. M. Lamont, talk at the 27th International Symposium on Lepton Photon Interactions at High Energies (LP2015), 17-22 Aug 2015, Ljubljana, Slovenia.

2. J. Ellis, talk at the 27th International Symposium on Lepton Photon Interactions at High Energies (LP2015), 17-22 Aug 2015, Ljubljana, Slovenia.

3. F. Englert and R. Brout, Phys. Rev. Lett. **13**, 321 (1964); P. W. Higgs, Phys. Lett. **12**, 132 (1964); P. W. Higgs, Phys. Rev. Lett. **13**, 508 (1964); G. S. Guralnik, C. R. Hagen and T. W. B. Kibble, Phys. Rev. Lett. **13**, 585 (1964).

4. G. Aad *et al.* [ATLAS Collaboration], Phys. Lett. B **716**, 1 (2012) [arXiv:1207.7214 [hep-ex]]; S. Chatrchyan *et al.* [CMS Collaboration], Phys. Lett. B **716**, 30 (2012) [arXiv:1207.7235 [hep-ex]].

5. V. Khachatryan *et al.* [CMS Collaboration], JHEP **1408**, 174 (2014) doi:10.1007/JHEP08(2014)174 [arXiv:1405.3447 [hep-ex]]; G. Aad *et al.* [ATLAS Collaboration], JHEP **1512**, 055 (2015) doi:10.1007/JHEP12(2015)055 [arXiv:1506.00962 [hep-ex]].

6. The ATLAS and CMS Collaborations, "Measurements of the Higgs boson production and decay rates and constraints on its couplings from a combined ATLAS and CMS analysis of the LHC pp collision data at $\sqrt{s} = 7$ and 8 TeV," ATLAS-CONF-2015-044, CMS-PAS-HIG-15-002.

7. G. Aad *et al.* [ATLAS and CMS Collaborations], Phys. Rev. Lett. **114**, 191803 (2015) doi:10.1103/PhysRevLett.114.191803 [arXiv:1503.07589 [hep-ex]].

8. G. Salam and A. Weiler, http://collider-reach.web.cern.ch/

PERSPECTIVES FOR MUON COLLIDERS AND NEUTRINO FACTORIES

M. Bonesini
Sezione INFN Milano Bicocca, Dipartimento di Fisica G. Occhialini, Università di Milano Bicocca, Milano, Italy.

Abstract

High brilliance muon beams are needed for future facilities such as a Neutrino Factory, an Higgs-factory or a multi-TeV Muon Collider. The *R&D* path involves many aspects, of which cooling of the incoming muon beams is essential.

1 Introduction

Since the 1960's, Muon Colliders (MC) [1] and Neutrino Factories (NF) [2], based on high brilliance muon beams, have been proposed. Their design has been optimized in references [3], [4], [5], [6] and [7]. While a MC addresses the high-energy frontier: looking at precise Higgs physics [8] and beyond, a NF will provide the ultimate tool for neutrino oscillation studies, looking at CP-violation. The current design of a NF or a MC front-end is similar, up to

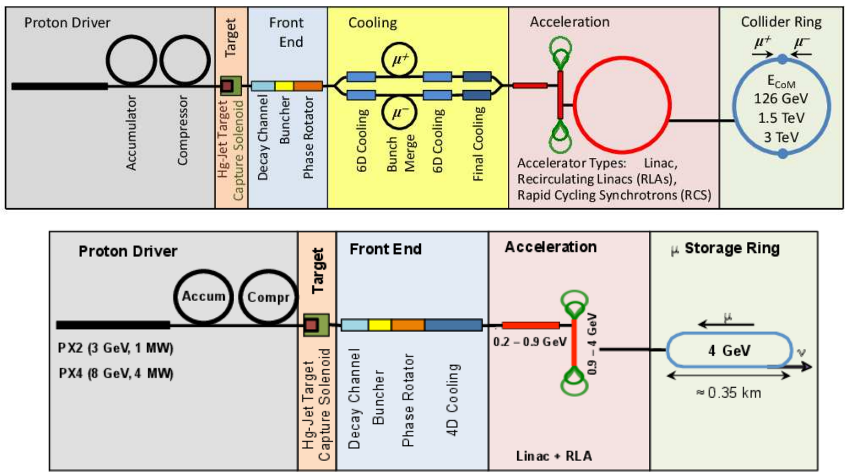

Figure 1: Schematic layout of a MC (top) and a NF (bottom).

the beginning of the cooling section , as can be seen from the layouts reported in figure 1.

MC's may be developed with c.m.s energy up to many TeV and, due to the large μ mass as compared to the electron one, may easily fit in the footprint of existing HEP laboratories [1]

s-channel scalar Higgs production is greatly enhanced in a $\mu^+\mu^-$ collider (as respect to e^+e^-) as the coupling is proportional to the lepton mass. Precision measurements in the Higgs sector are thus feasible: at $m_{H^0} \sim 126$ GeV$/c^2$ only a $\mu^+\mu^-$ collider may directly measure the H^0 lineshape. With an integrated luminosity of 0.5 fb^{-1}, the H^0 mass may be determined, in the Standard Model case, with a precision of 0.1 MeV$/c^2$ and its width $\Gamma_{H^0}(\sim 4$ MeV$/c^2)$ with a precision of 0.5 MeV$/c^2$.

Through the processes $\mu^- \mapsto e^-\nu_\mu\overline{\nu_e}$ and $\mu^+ \mapsto e^+\overline{\nu_\mu}\nu_e$, neutrino beams with a flux known at better than 1% and well-known composition (50%ν_μ or

[1] A $\sqrt{s} = 3$ TeV Muon Collider ($\mu^+\mu^-$ Higgs Factory) has a ring circumference of $\sim 6.3(\sim 0.3)$ km, to be compared to the ~ 26 km of the LHC tunnel.

$\overline{\nu_\mu}$, 50%$\overline{\nu_e}$ or ν_e) may be produced in a NF [9]. The "golden channel" linked to $\nu_e \mapsto \nu_\mu$ (or $\overline{\nu_e} \mapsto \overline{\nu_\mu}$) oscillations, manifests itself by wrong sign muons, as respect to initial beam charge, suggesting the use of large magnetized far detectors. After the experimental discovery of a large θ_{13} value, $\sim 5\%$, the design of the NF has been revised to improve precision in the study of sub-leading effects in neutrino oscillations and provide better capabilities for the measurement of the phase δ, if leptonic CP-violation occurs [7].

2 R&D towards a muon collider and a neutrino factory

Many R&D issues are relevant for the development of a NF or a MC, such as the availability of a suitable proton driver or a high-power target, but the most critical one is still the muon cooling. Muons are produced as tertiary particles in the process chain $pA \mapsto \pi X, \pi \mapsto \mu\nu$ and thus occupy a large longitudinal and transverse phase space. Conventional accelerator technologies require input beams with small phase space. To alleviate this problem one may use either new large aperture accelerators, such as "fixed field alternating-gradient" (FFAG) machines [10] or try to reduce ("cool") the incoming muon beam phase space. While for a NF the required cooling factor is small: around 2.4 for the 75 m cooling section in the IDS-NF design [5], [7], for a MC a longitudinal emittance reduction ~ 14 and a transverse emittance reduction ~ 400 in both transverse coordinates are needed, requiring a total cooling factor $\sim 2 \times 10^6$.

2.1 Ionization cooling and the MICE experiment at RAL

Conventional beam cooling methods do not work on the short timescale of the muon lifetime ($\tau \sim 2.2\mu$s). The only effective way is the so-called "ionization cooling" that is accomplished by passing muons through a low-Z absorber, where they loose energy by ionization and the longitudinal component of momentum is then replenished by RF cavities [11].

The initial goal of the MICE experiment [12] to study a fully engineered cooling cell of the proposed US Study 2 [4], has been downsized in 2014 to a demonstration of ionization cooling with a simplified lattice based on the available RF cavities and absorber-focus coils (see the top panel of figure 2). A dedicated muon beam from ISIS (140-240 MeV/c momentum, tunable between $3 - 10\pi\cdot$ mm rad input emittance) enters the MICE cooling section after a Pb

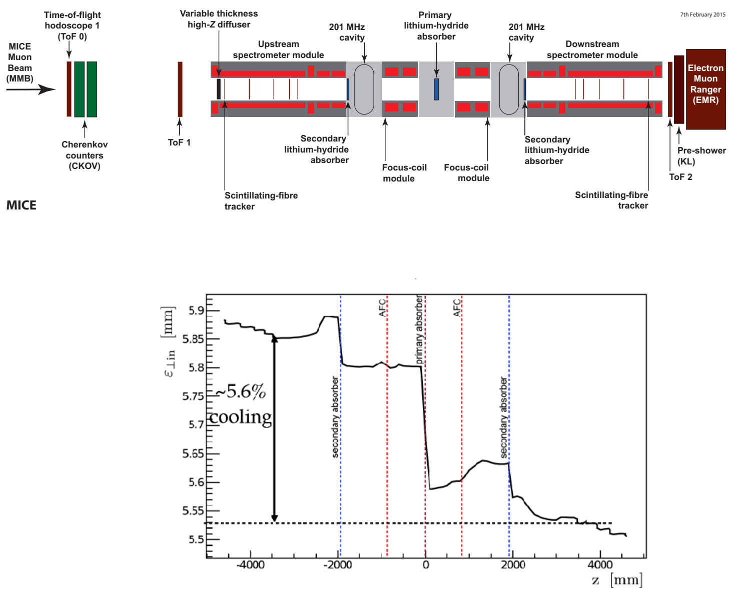

Figure 2: Top panel: view of the MICE experiment at RAL (for more details see [16]). The cooling channel is put between two magnetic spectrometers [13] and two TOF stations [14] to measure particle parameters. Bottom panel: evolution of the 4D emittance in the MICE ionization-colling demo lattice, for a $6\pi\cdot$ mm, 200 MeV/c muon beam.

diffuser of adjustable thickness. The MICE beamline has been characterized by the use of the TOF detectors (with ~ 50 ps resolution), with data taken mainly in summer 2010 [17]. As conventional emittance measurement techniques reach barely a 10% precision, the final measure of emittance will be done in MICE on a particle-by-particle basis by measuring $x, y, x' = p_x/p_z, y' = p_y/p_z, E, t$ with the trackers and the TOF system. Foreseen performances of the MICE cooling cell are shown in the bottom panel of figure 2.

2.1.1 6D cooling

Both a reduction in transverse emittance and longitudinal emittance are needed for a $\mu^+\mu^-$ Higgs factory or a multi-TeV collider, as shown in the left panel of figure 3 from reference [15]. As a direct longitudinal cooling is not feasible, due to the energy-loss straggling that increases the energy spread, the only practical solution is to transfer a fraction of the cooling effect from transverse to longitudinal phase space (via "emittance exchange"), as shown schematically in figure 3. Dispersion is used to create an appropriate correlation between momentum and transverse position/path length. Clearly this is at the expense of a reduced transverse cooling. Some aspects of the "emittance exchange " will be addressed also in the MICE experiment, by inserting LiH wedge absorbers.

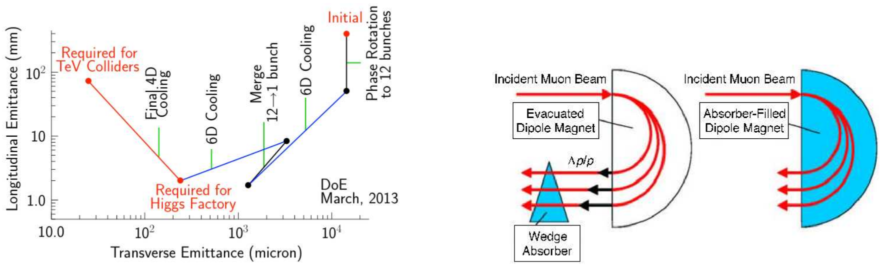

Figure 3: Left panel: emittance evolution path for a $\mu^+\mu^-$ Higgs factory and a multi-TeV collider. Right panel: approaches to emittance exchange, to get 6D cooling [courtesy of Muons Inc.].

One may envisage multi-pass cooling rings [18] and then extract the cooled beams, with a substantial cost reduction, instead of single-pass linear cooling channels, as in MICE. These designs are based on solenoidal focussing strictly interleaved with RF accelerating cavities [19], [20], [21]. Difficult beam dynamics must be handled and performance limits or cost-effectiveness are not completely defined. In a multi-turn cooling ring, the main problems will be connected to beam injection and extraction.

3 Conclusions

The recent discovery of the Standard Model Higgs at about 126 GeV has revived the interest for a compact muon collider: the Higgs-factory. As cooling factors up to 10^6 are needed for a MC, the optimization of the cooling channel is essential. A vigorous *R&D* program is thus needed.

References

1. F.F. Tikhonin, JINR P2-4120 (1968) Dubna; G.I. Budker, AIP Conf. Proc. **352** (1996) 4; D.V. Neuffer, R.B. Palmer, Proc. EPAC94(1994) 52.
2. D.G. Koshkarev,CERN/ISR-DI/74-62; S. Geer,Phys.Rev. **D57**(1998)6989.
3. S. Geer S, LINAC10 Conference, Tsukuba, Japan, 2010.
4. S.Ozaki *et al.*, BNL-52623, June 2001 ; M.M. Alsharo'a *et al.*,Phys. Rev. ST. Accel. Beams **6**, 081001 (2003).
5. S. Choubey *et al*, IDS-NF-20,2011.
6. M. Apollonio *et al.*, CERN-TH-2002-208, 2002.
7. M. Bogomilov *et al.*, Phys. Rev. ST. Accel.Beams. **17**(2014)18,121002.
8. D. Cline, Nucl. Instr. Meth. **A350** (1994) 24; C. Rubbia, arXiv:1308.6612.
9. M. Bonesini and A. Guglielmi, Phys.Rep. **433** (2006) 65.
10. G.H. Rees and D.J. Kelliher, Proceedings Workshop HB2010, 2010, 54.
11. A.N. Skrinsky and V.V. Parkhomchuk, Sov. J. Part. Nucl **12** (1981) 3; M. Bonesini, JINST **9** (2014)01,C01064.
12. G. Gregoire *et al.*, proposal to RAL, 2003.
13. M. Ellis *et al.*, Nucl. Instr. and Meth. **A655** (2011) 136.
14. R. Bertoni *et al.*, Nucl. Instr. and Meth. A615 (2010) 14, arXiv:001.4426.
15. M.A. Palmer, proceedings COOL13, FERMILAB-CONF-13-253-APC.
16. M. Bogomilov *et al.* [MICE Collaboration] JINST **7** (2012) P05009; M. Bonesini, PoS EPS-HEP2015 (2015) 521.
17. D. Adams *et al.* [MICE Collaboration] Eur. Phys. J. **C73** (2013) 2582.
18. R.C. Fernow, R.B. Palmer, Phys. Rev. ST. Accel Beams **10** (2007) 064001.
19. A. Garren *et al.* Nucl. Instr. Meth. **A654** (2011) 40.
20. V.Babelkov *et al.*, proceedings PAC 2001, (2001) 3867.
21. R.Palmer *et al.*, Phys. Rev. ST Accel. Beams **8** (2005) 061003.

PHYSICS CASE OF FCC-ee

David d'Enterria
CERN, PH-EP Department, 1211 Geneva, Switzerland

Abstract

The physics case for electron-positron beams at the Future Circular Collider (FCC-ee) is succinctly summarized. The FCC-ee core program involves e^+e^- collisions at $\sqrt{s}$ = 90, 160, 240, and 350 GeV with multi-ab^{-1} integrated luminosities, yielding about 10^{12} Z bosons, 10^8 W$^+$W$^-$ pairs, 10^6 Higgs bosons and $4{\cdot}10^5$ $t\bar{t}$ pairs per year. The huge luminosities combined with $\mathcal{O}\,(100$ keV) knowledge of the c.m. energy will allow for Standard Model studies at unrivaled precision. Indirect constraints on new physics can thereby be placed up to scales $\Lambda_{\rm NP} \approx 7$ and 100 TeV for particles coupling respectively to the Higgs and electroweak bosons.

1 Introduction

The Standard Model (SM) of particle physics is a renormalizable quantum field theory encoding our knowledge of the fundamental particles and their (electroweak and strong) interactions. Despite its tremendous success to describe many phenomena with high accuracy for over 40 years –including the recent experimental confirmation of the existence of its last missing piece, the Higgs boson– fundamental questions remain open (such as the small Higgs boson mass compared to the Planck scale, dark matter, matter-antimatter asymmetry, neutrino masses,...) which may likely *not* be fully answered through the study of proton-proton collisions at the Large Hadron Collider (LHC). Notwithstanding their lower center-of-mass energies, high-energy e^+e^- colliders feature several advantages in new physics studies compared to hadronic machines, such as direct model-independent searches of new particles coupling to Z^*/γ^* with masses up to $m \approx \sqrt{s}/2$, and clean experimental environment with initial and final states very precisely known theoretically, (i.e. well understood backgrounds without "blind spots" of p-p searches). Combined with high-luminosities, an e^+e^- collider can thus provide access to studies with δX precision at the permille level, allowing indirect constraints to be set on new physics up to very-high energy scales $\Lambda_{\rm NP} \propto (1\ \mathrm{TeV})/\sqrt{\delta X}$. Plans exist to build future circular (FCC-ee [1]), CEPC [2])) and/or linear (ILC [3]), CLIC [4])) e^+e^- colliders (Fig. 1).

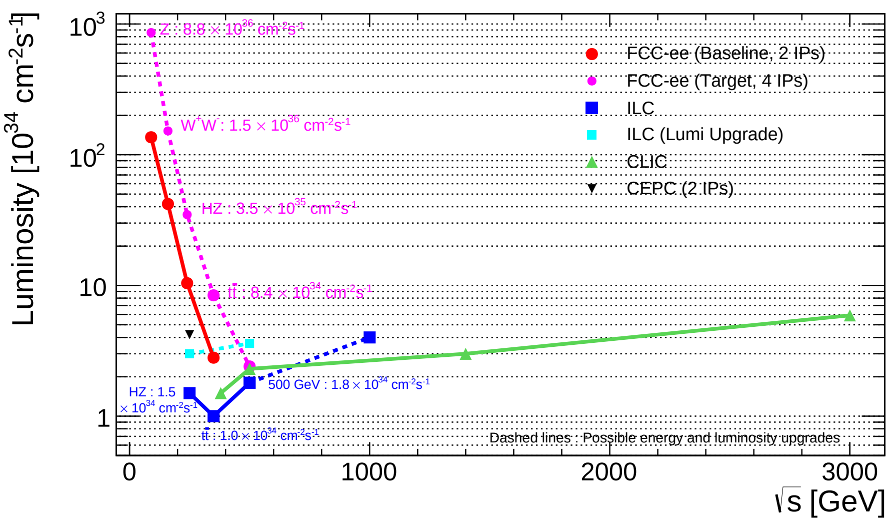

Figure 1: *Target luminosities as a function of center-of-mass energy for future circular (FCC-ee, CEPC) and linear (ILC, CLIC) e^+e^- colliders under consideration.*

The advantages of circular machines are (i) their much higher luminosity below $\sqrt{\mathrm{s}} \approx 400$ GeV (thanks to much larger collision rates, adding continuous top-up injection to compensate for luminosity burnoff), (ii) the possibility to have several interaction points (IPs), and (iii) a precise measurement of the beam energy $\mathrm{E}_{\mathrm{beam}}$ through resonant transverse depolarization [5]. Linear colliders, on the other hand, feature (i) much larger $\sqrt{\mathrm{s}}$ reach (circular colliders are not competitive above $\sqrt{\mathrm{s}} \approx 400$ GeV due to synchroton radiation scaling as $\mathrm{E}_{\mathrm{beam}}^4/\mathrm{R}$), and (ii) easier longitudinal beam polarization. At the FCC (with a radius R = 80–100 km), e^+e^- collisions present clear advantages with respect to LEP (e.g. $\times 10^4$ more bunches, and $\delta E_{\mathrm{beam}} \approx \pm 0.1$ MeV compared to ± 2 MeV) and to ILC (crab-waist optics scheme, up to 4 IPs) yielding luminosities $\times(10^4$–$10)$ larger in the $\sqrt{\mathrm{s}} = 90$–350 GeV range [6]. Table 1 lists the target FCC-ee luminosities, and the total number of events collected at each $\sqrt{\mathrm{s}}$ obtained for the following cross sections (including initial state radiation, and smearings due to beam-energy spreads): $\sigma_{\mathrm{e^+e^-\to Z}} = 43$ nb, $\sigma_{\mathrm{e^+e^-\to H}} = 0.29$ fb, $\sigma_{\mathrm{e^+e^-\to WW}} = 4$ pb, $\sigma_{\mathrm{e^+e^-\to HZ}} = 200$ fb, $\sigma_{\mathrm{e^+e^-\to t\bar{t}}} = 0.5$ pb, and $\sigma_{\mathrm{e^+e^-\to VV\to H}} = 30$ fb. With these target luminosities, the completion of the FCC-ee core physics program (described in the next sections) requires 10 years of running.

$\sqrt{\mathrm{s}}$ (GeV):	90 (Z)	125 (eeH)	160 (WW)	240 (HZ)	350 ($t\bar{t}$)	350 (VV $\to$ H)
$\mathcal{L}$/IP (cm^{-2} s^{-1})	$2.2{\cdot}10^{36}$	$1.1{\cdot}10^{36}$	$3.8{\cdot}10^{35}$	$8.7{\cdot}10^{34}$	$2.1{\cdot}10^{34}$	$2.1{\cdot}10^{34}$
$\mathcal{L}_{\mathrm{int}}$ (ab^{-1}/yr/IP)	22	11	3.8	0.87	0.21	0.21
Events/year (4 IPs)	$3.7{\cdot}10^{12}$	$1.3{\cdot}10^{4}$	$6.1{\cdot}10^{7}$	$7.0{\cdot}10^{5}$	$4.2{\cdot}10^{5}$	$2.5{\cdot}10^{4}$
Years needed (4 IPs)	2.5	1.5	1	3	0.5	3

Table 1: *Target luminosities, events/year, and years needed to complete the W, Z, H and top programs at FCC-ee.* [$\mathcal{L} = 10^{35}$ cm^{-2} s^{-1} *corresponds to* $\mathcal{L}_{\mathrm{int}} = 1$ ab^{-1}/yr *for 1 yr =* 10^7 s].

2 Indirect constraints on BSM via high-precision Z, W, top physics

Among the main goals of the FCC-ee is to collect multi-ab^{-1} at $\sqrt{\mathrm{s}} \approx 91$ GeV (Z pole), 160 GeV (WW threshold), and 350 GeV ($t\bar{t}$ threshold) in order to measure with unprecedented precision key properties of the W and Z bosons and top-quark, as well as other fundamental parameters of the SM. The combination of huge data samples available at each $\sqrt{\mathrm{s}}$, and the precise knowledge of the c.m. energy leading to very accurate threshold scans, allows for improvements in their experimental precision by factors around $\times 25$ (dominated by systematics uncertainties) compared to the current state-of-the-art (Table 2) [7]. In many cases, the dominant uncertainty will be of theoretical origin, and developments in the calculations are needed in order to match the expected experimental uncertainty. The FCC-ee experimental precision targets are e.g. ± 100 keV for $m_{\rm Z}$, ± 500 keV for $m_{\rm W}$, ± 10 MeV for $m_{\rm t}$, a relative statistical uncertainty of the order of $3{\cdot}10^{-5}$ for the QED α coupling (through muon forward-backward asymmetries above and below the Z peak) [8], 1-permille for the QCD coupling $\alpha_{\rm s}$ (through hadronic Z and W decays) [9], and 10^{-3} on the electroweak top couplings $F^{\gamma t, Z t}_{\rm 1V,2V,1A}$ (through differential distributions in $e^+e^- \to t\bar{t} \to \ell\nu q\bar{q}b\bar{b}$) [10].

Observable	Measurement	Current precision	FCC-ee stat.	Possible syst.	Challenge
$m_{\rm Z}$ (MeV)	Z lineshape	91187.5 ± 2.1	0.005	< 0.1	QED corrs.
$\Gamma_{\rm Z}$ (MeV)	Z lineshape	2495.2 ± 2.3	0.008	< 0.1	QED corrs.
R_ℓ	Z peak	20.767 ± 0.025	0.0001	< 0.001	QED corrs.
$R_{\rm b}$	Z peak	0.21629 ± 0.00066	0.000003	< 0.00006	$g \to {\rm b\bar{b}}$
$A^{\mu\mu}_{\rm FB}$	Z peak	0.0171 ± 0.0010	0.000004	< 0.00001	$E_{\rm beam}$ meas.
N_ν	Z peak	2.984 ± 0.008	0.00004	0.004	Lumi meas.
N_ν	$\rm e^+e^- \to \gamma\, Z(inv.)$	2.92 ± 0.05	0.0008	< 0.001	–
$\alpha_{\rm s}(m_{\rm Z})$	$R_\ell, \sigma_{\rm had}, \Gamma_{\rm Z}$	0.1196 ± 0.0030	0.00001	0.00015	New physics
$1/\alpha_{\rm QED}(m_{\rm Z})$	$A^{\mu\mu}_{\rm FB}$ around Z peak	128.952 ± 0.014	0.004	0.002	EW corr.
$m_{\rm W}$ (MeV)	WW threshold scan	80385 ± 15	0.3	< 1	QED corr.
$\alpha_{\rm s}(m_{\rm W})$	$B^{\rm W}_{\rm had}$	$B^{\rm W}_{\rm had} = 67.41 \pm 0.27$	0.00018	0.00015	CKM matrix
$m_{\rm t}$ (MeV)	threshold scan	173200 ± 900	10	10	QCD
$F^{\gamma t, Z t}_{\rm 1V,2V,1A}$	${\rm d}\sigma^{t\bar{t}}/{\rm d}x\,{\rm d}\cos(\theta)$	4%–20% (LHC-14 TeV)	(0.1–2.2)%	(0.01–100)%	–

Table 2: *Examples of achievable precisions in representative Z, W and top measurements.*

Figure 2 shows limits in the W-mass vs. top-mass plane (left), and the energy reaches of a subset of dimension-6 operators of an Effective Field Theory of the SM parametrizing possible new physics (right) [11]. Such measurements impose unrivaled constraints on new weakly-coupled physics. Whereas electroweak precision tests (EPWT) at LEP bound any BSM physics to be above $\Lambda_{\rm NP} \gtrsim 7$ TeV, FCC-ee would reach up to $\Lambda_{\rm NP} \approx 100$ TeV.

3 Indirect constraints on BSM via high-precision Higgs physics

In the range of c.m. energies covered by the FCC-ee, Higgs production peaks at $\sqrt{\rm s} \approx 240$ GeV dominated by Higgsstrahlung ($e^+e^- \to$ HZ), with some

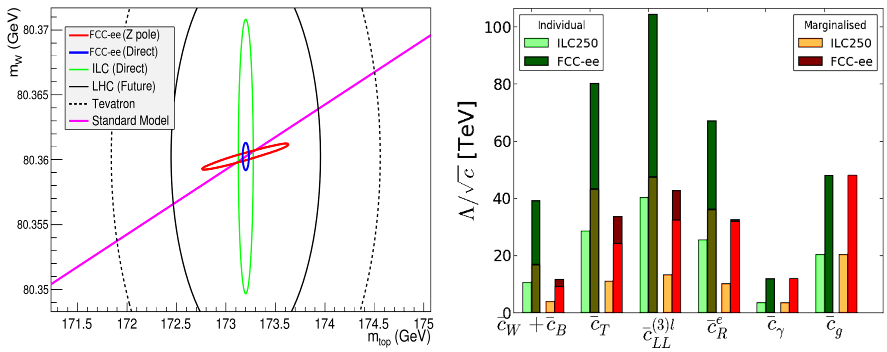

Figure 2: *Left: 68% C.L. limits in the* m_t*–*m_W *plane at FCC-ee and other colliders* [1]*. Right: Energy reaches for dim-6 operators sensitive to EWPT, obtained from precision measurements at FCC-ee and ILC* [11]*.*

sensitivity also to vector-boson-fusion ($VV \to$ H $e^+e^-, \nu\nu$) and the top Yukawa coupling ($e^+e^- \to t\bar{t}$ with a virtual Higgs exchanged among the top quarks) at $\sqrt{\mathrm{s}} = 350$ GeV. The target total number of Higgs produced at the FCC-ee (4 IPs combined, all years) amounts to 2.1 million at 240 GeV, 75 000 in $VV \to$ H at 350 GeV, and 19 000 in s-channel $e^+e^- \to$ H at $\sqrt{\mathrm{s}} = 125$ GeV (Table 1). With such large data samples, unique Higgs physics topics are accessible to study:

- High-precision model-independent determination of the Higgs couplings, total width, and exotic and invisible decays (Table 3) [1].
- Higgs self-coupling through loop corrections in HZ production [12].
- First-generation fermion couplings: (u,d,s) through exclusive decays H$\to$ $V\gamma$ ($V = \rho, \omega, \phi$) [13], and electron Yukawa through resonant $e^+e^- \to$ H at $\sqrt{\mathrm{s}} = m_{\mathrm{H}}$ [14].

The recoil mass method in $e^+e^- \to$ HZ is unique to lepton colliders and allows for a high-precision tagging of Higgs events irrespective of their decay mode (Fig. 3). It provides, in particular, a high-precision ($\pm 0.05\%$) measurement of $\sigma_{\mathrm{e^+e^-\to HZ}}$ and, therefore, of g^2_{HZ}. From the measured value of $\sigma_{\mathrm{e^+e^-\to H(XX)Z}} \propto \Gamma_{\mathrm{H\to XX}}$ and different known decays fractions $\Gamma_{\mathrm{H\to XX}}$, one can then obtain the total Higgs boson width with $\mathcal{O}\,(1\%)$ uncertainty combining different final states. The $\ell^+\ell^-$H final state and the distribution of the mass recoiling against the lepton pair can also be used to directly measure the invisible decay width of the Higgs boson in events where its decay products escape undetected. The Higgs boson invisible branching fraction can be measured with an absolute precision of 0.2%. If not observed, a 95% C.L. upper limit of 0.5% can be set on this branching ratio [1]. In addition, loop corrections to the Higgsstrahlung cross sections at different center-of-mass energies are sensitive to the Higgs self-coupling [12]. The effect is tiny but visible at FCC-ee thanks to the extreme precision achievable on the $g_{\rm HZ}$ coupling. Indirect and model-dependent limits on the trilinear $g_{\rm HHH}$ can be set with a $\mathcal{O}\,(70\%)$ uncertainty, comparable to that expected at HL-LHC.

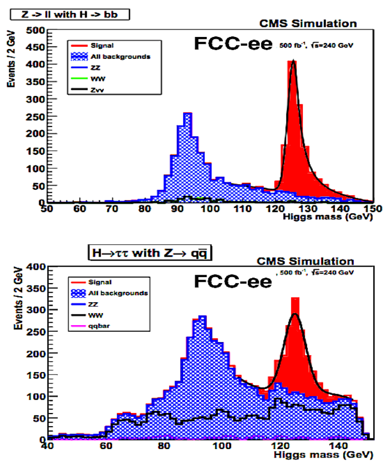

Figure 3: Distribution of recoil mass against $\rm Z \to \ell\ell$ (top) and $\rm Z \to q\overline{q}$ (bottom) in the $e^+e^- \to$ HZ process with H$\to b\bar{b}$ (top) and H$\to \tau\tau$ (bottom).

Observable	240 GeV	240+350 GeV
$g_{\rm HZZ}$	0.16%	0.15%
$g_{\rm HWW}$	0.85%	0.19%
$g_{\rm Hbb}$	0.88%	0.42%
$g_{\rm Hcc}$	1.0%	0.71%
$g_{\rm Hgg}$	1.1%	0.80%
$g_{\rm H\tau\tau}$	0.94%	0.54%
$g_{\rm H\mu\mu}$	6.4%	6.2%
$g_{\rm H\gamma\gamma}$	1.7%	1.5%
$\Gamma_{\rm tot}$	2.4%	1.2%
$\rm BR_{inv}$	0.25%	0.2%
$\rm BR_{exo}$	0.48%	0.45%

Table 3: Expected model-independent uncertainties on Higgs couplings, total width, and branching ratios into invisible and exotic particles (invisible or not) [1].

The large Higgs data samples available also open up to study exotic (e.g. flavour-violating Higgs) and very rare SM decays. First- and second-generation couplings to fermions are accessible via exclusive decays $\rm H \to V\gamma$, for $V = \rho, \omega, \phi$, with sensitivity to the u,d,s quark Yukawas [13]. The $\rm H \to \rho\gamma$ channel appears the most promising with $\mathcal{O}\,(50)$ events expected. The low mass of the electron translates into a tiny $\rm H \to e^+e^-$ branching ratio $\rm BR_{e^+e^-} = 5\cdot 10^{-9}$ which precludes any experimental observation of this decay mode and, thereby a determination of the electron Yukawa coupling. The resonant s-channel production, despite its small cross section [15], is not completely hopeless and preliminary studies indicate that one could observe it at the 5σ-level accumulating 75 ab^{-1} at FCC-ee running at $\sqrt{\mathrm{s}} = 125$ GeV with a c.m. energy spread commensurate with the Higgs boson width itself (≈4 MeV) which requires beam monochromatization [14].

Summarizing in terms of new physics constraints, deviations δg_{HXX} of the Higgs boson couplings to gauge bosons and fermions with respect to the SM predictions can be translated into BSM scale limits through: $\Lambda_{\mathrm{NP}} \gtrsim (1\,\mathrm{TeV})/\sqrt{(\delta \mathrm{g}_{\mathrm{HXX}}/\mathrm{g}^{\mathrm{SM}}_{\mathrm{HXX}})/5\%}$. The expected 0.15% precision for the most precise coupling, g_{HZZ}, would thus set competitive bounds, $\Lambda_{\mathrm{NP}} \gtrsim 7$ TeV, on any new physics coupled to the scalar sector of the SM.

4 Direct constraints on BSM physics: dark matter and right-handed neutrinos

The precision electroweak and Higgs boson studies, summarized previously, not only impose competitive constraints on new physics at multi-TeV scales but can also be interpreted in terms of limits in benchmark SUSY models (CMSSM and NUHM1) [1]. Other studies exist that have analyzed the impact of FCC-ee on other key BSM extensions such as e.g. direct searches of dark matter (DM) [16] and right-handed neutrinos [17] through Z and H bosons rare decays. Figure 4 (left) shows the limits in the plane (branching ratio, DM mass) for the decays $\mathrm{Z, H} \to \mathrm{DM\,DM}$. Measurements of the invisible Z and H widths are the best collider options to test DM lighter than $m_{\mathrm{Z,H}}/2$ that couples via SM mediators. Figure 4 (right) shows the unrivaled limits that can be set in sterile neutrinos searches via decays $\mathrm{Z} \to \mathrm{N}\nu_{\mathrm{i}}$ with $\mathrm{N} \to \mathrm{W}^*\ell, \mathrm{Z}^*\nu_{\mathrm{j}}$ as a function of their mass and mixing to light neutrinos [17].

5 Summary

Electron-positron collisions at $\sqrt{\mathrm{s}} \approx 90$–$350$ GeV at the FCC-ee provide unique means to address many of the fundamental open problems in particle physics via high-precision studies of the W, Z, Higgs, and top-quark with permil-level uncertainties, thanks to the huge luminosities $\mathcal{O}(1-100)$ ab^{-1} and the exquisite beam energy calibration. Such measurements set indirect constraints

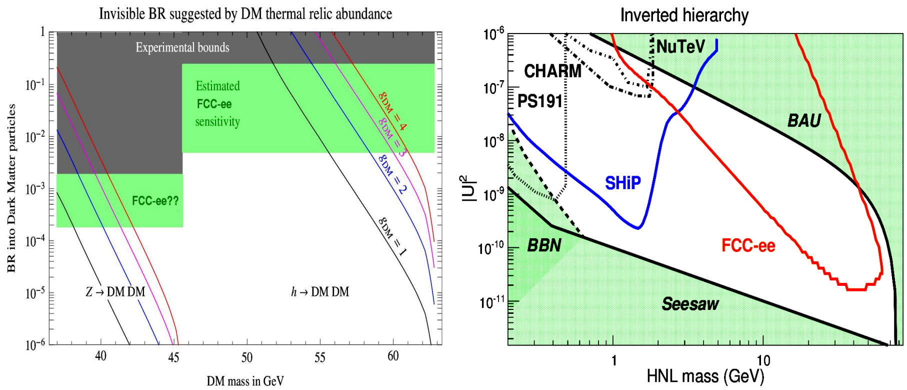

Figure 4: *Regions of sensitivity of FCC-ee for: (i) Z and H decays into DM in the* $\mathrm{BR}_{\mathrm{Z,H\to DM\,DM}}$ *vs.* m_{DM} *plane (left)* [16]*, and (ii) sterile neutrinos as a function of their mass and mixing to light neutrinos (inverted hierarchy) for* 10^{12} *Z decays (right)* [17]*.*

on BSM physics up to scales $\Lambda_{\mathrm{NP}} \approx 7, 100$ TeV for new particles coupling to the scalar and electroweak SM sectors, respectively. Rare Higgs and Z bosons decays are sensitive to dark matter and sterile neutrinos with masses up to $m_{\mathrm{DM,HNL}} \approx 60$ GeV.

References

1. M. Bicer *et al.* [TLEP Design Study Working Group], JHEP **1401**, 164 (2014).

2. M. Ahmad *et al.* [CEPC-SPPC Study Group], IHEP-CEPC-DR-2015-01, IHEP-TH-2015-01, HEP-EP-2015-01 (2015).

3. T. Behnke *et al.* [ILC Collaboration], arXiv:1306.6327 [physics.acc-ph]

4. L. Linssen, A. Miyamoto, M. Stanitzki and H. Weerts [CLIC Collaboration], arXiv:1202.5940 [physics.ins-det].

5. M. Koratzinos, A. Blondel, E. Gianfelice-Wendt and F. Zimmermann, arXiv:1506.00933 [physics.acc-ph].

6. F. Zimmermann, Talk given at 1st FCC annual workshop, Washington (USA), March 2015.

7. R. Tenchini, arXiv:1412.2928 [hep-ex].

8. P. Janot, arXiv:1512.05544 [hep-ph].

9. D. d'Enterria *et al.*, arXiv:1512.05194 [hep-ph].

10. P. Janot, JHEP **1504**, 182 (2015).

11. J. Ellis and T. You, arXiv:1510.04561 [hep-ph].

12. M. McCullough, Phys. Rev. D **90**, 015001 (2014).

13. A. L. Kagan, G. Perez, F. Petriello, Y. Soreq, S. Stoynev and J. Zupan, Phys. Rev. Lett. **114**, 101802 (2015).

14. D. d'Enterria, G.Wojcik, R.Aleksan, Talk given at 8th FCC-ee Physics Workshop, LPNHE, Paris, 2014.

15. S. Jadach and R. A. Kycia, arXiv:1509.02406 [hep-ph].

16. A. Strumia, Talk given at 9th FCC-ee Physics Workshop, SNS, Pisa, Feb. 2015.

17. A. Blondel *et al.* [FCC-ee Study Team Collaboration], arXiv:1411.5230 [hep-ex].

NATURALNESS AFTER LHC RUN I

Andrea Romanino
SISSA/ISAS and INFN, I–34136 Trieste, Italy
ICTP, Strada Costiera 11, I–34151 Trieste, Italy

Abstract

Thanks to the discovery of the Higgs boson, the 8 TeV run of the LHC was a tremendous success. At the same time, the lack of signals of physics beyond the Standard Model was unexpected. Waiting for the first results of the 13 TeV run, as assessment of the implications of such a puzzling situation is appropriate. After a critical appraisal of the naturalness argument, we will discuss i) the status of models addressing the naturalness problem (supersymmetry and composite Higgs as prototypical examples) and ii) possible alternative models evading the naturalness argument.

1 The naturalness argument: a critical appraisal

The naturalness problem arises from the longing for a complete understanding of the electroweak (EW) scale. A first aspect of the problem is whether the description of the EW scale provided by the SM is correct. Data definitely support the SM parameterisation: the Higgs particle i) is a scalar with positive parity, ii) is neutral under color and charge, iii) it respects the custodial symmetry, and iii) it couples to the SM fermions and gauge bosons proportionally to their masses, within the present experimental accuracy. While there is still room for the Higgs couplings to deviate from the SM prediction, it is fair to say that possible departures are bound to be corrections to a leading order picture in agreement with the SM one.

The second aspect, more relevant for our purposes, is whether the SM description of the EW scale is complete. The SM parameterises the EW scale in terms of its only dimensionful parameter, the Higgs mass parameter μ^2, provided that the latter has a negative sign. On the other hand, a deeper understanding of the origin of that parameter, in the context of the standard reductionist paradigm of particle physics, should allow to compute that parameter in terms of more fundamental physics lying at a higher scale. A simple quantum field theory calculation then shows that the physical Higgs mass develops a quadratic dependence on the physical scale M associated to the high scale degrees of freedom (dofs), weighted by their coupling to the Higgs and a loop factor: $m_H^2 \sim -2\mu^2 + \lambda^2/(4\pi)^2 M^2$. If $M = 10^{15}\,\text{GeV}$ and $\lambda \sim 1$, for example, the second term in the RHS would be 24 orders of magnitude larger than m_H^2, requiring an extremely fine-tuned cancellation. Hence the expectation that some new physics should exist at a much lower scale taming the sensitivity of the Higgs mass to M. This is the celebrated naturalness argument.

The above formulation of the naturalness argument does not involve an arbitrary cutoff, nor quadratic divergences, and needless to say still holds in dimensional regularisation, where quadratic divergences are not seen. Also, it clarifies the assumptions on which it is based, and the corresponding way outs. The argument assumes the existence of high scale physical dofs coupled to the SM, and can be evaded if no such states exist. Or, the cancellation in the Higgs mass could take place, but not be accidental. On the other hand, if high scale coupled dofs do exist, and a cancellation can only be explained by an accident, the need to make the Higgs mass natural by getting rid of the M^2 dependence becomes compelling. This is the standard case, in which the "natural" scale m_{NP} of the new physics in charge of cancelling the M^2

dependence can be estimated by computing the top loop corrections to the Higgs mass in the presence of the new physics. Which typically gives $m_H^2 \sim -2\mu^2 + 12\lambda_t^2/(4\pi)^2 m_{\rm NP}^2$. In the absence of large cancellations, we expect $m_{\rm NP} \sim 0.5\,{\rm TeV}$.

2 "Quasi-natural" new physics

Let us consider in greater detail the standard case in which the Higgs mass is protected by new dofs at a scale in turn subject to the naturalness constraint, and briefly discuss the two prototypical examples: supersymmetric models and composite Higgs models.

A few preliminary comments are in order. First of all, the scale $m_{\rm NP}$, although undoubtedly tied to the weak scale, is not precisely determined. According to the previous qualitative estimate, any value of $m_{\rm NP}$ is viable, as long as a cancellation of one part out of $\Delta \sim (m_{\rm NP}/(0.5\,{\rm TeV}))^2$ is accepted, where Δ is called the fine-tuning parameter. The amount of fine-tuning one is willing to accept is of course subjective. For example, $\Delta \sim 10$ corresponds to $m_{\rm NP} \sim 1.5\,{\rm TeV}$, while $\Delta \sim 100$ corresponds to $m_{\rm NP} \sim 5\,{\rm TeV}$. Note that the reach in terms of fine-tuning grows quadratically with the reach in terms of $m_{\rm NP}$. A second comment is that the previous estimate of Δ is actually model dependent. A broad distinction arises, depending on the possible residual dependence on the superheavy scale M. "Natural" models are supposed to get rid of the quadratic dependence on M, but they may still have a residual logarithmic dependence on M ("soft" models), or they can completely decouple the Higgs mass from M ("supersoft" models). The above fine-tuning estimate is appropriate for supersoft models, such as composite Higgs. In soft models, on the other hand, Δ is enhanced by the (possibly large) logarithm $\log(M/m_{\rm NP})$. This is the case of supersymmetry, where the role of M is played by the scale at which supersymmetry breaking is mediated.

2.1 Supersymmetry

The $\log(M/m_{\rm NP})$ enhancement of Δ lowers the scale at which new physics, the stop mass in this case, is expected, as now $\Delta \sim (m_{\rm NP}/(0.5\,{\rm TeV}/\log))^2$, where $\log = \log(M/m_{\rm NP})^2$. This in turn is the reason why the first expectations on the scale of supersymmetric particles, based on supergravity, were not far from the Z-boson mass scale. Indeed, in the case of supergravity, $M = M_{\rm Pl}$, giving $m_{\rm NP} \sim 0.5\,{\rm TeV}/\log \sim M_Z$ for $\Delta \sim 1$. As a consequence, minimal realisations of supergravity have been known to have a fine-tuning problem since LEP2 failed to discover supersymmetry [1]. A first message that the present lack of signal may be sending is then that supersymmetry is communicated at a relatively low scale M.

Another well known source of pressure on minimal supersymmetric models comes from the value of the Higgs mass. When nothing but the SM dofs and their supersymmetric partners are assumed to be part of the TeV-scale spectrum, multi-TeV stop masses or A-terms are needed in order to account for the fact that m_H^2 exceeds M_Z^2 by almost a factor of 2. On the other hand, the independently motivated, harmless introduction of a gauge singlet in the TeV spectrum (NMSSM) significantly helps from this point of view [2].

The naturalness status of supersymmetric models, and its model dependence, can be summarised in Fig. 1 [3], where two different set-up are considered. On the left panel, a minimal supergravity model with $M = M_{\rm Pl}$ is considered, while the right panel refers to a model with $M = 100\,{\rm TeV}$ and a gauge singlet relaxing the bounds on the Higgs mass. The fine-tuning isolines are shown in the stop-gluino mass plane, where representative values of run I and expected future bounds are also shown. The minimal supergravity case is not very promising from the point of view of future searches: a large part of the experimentally accessible parameter space is excluded by the indirect Higgs mass bound on stop masses (a conservative one, corresponding to large stop mixing) and the remaining one is significantly fine-tuned. On the other hand, the low M set up, while as simple and motivated as the minimal supergravity one, is in better shape, with the parameter space opened up by the possibility to account for the Higgs mass through the tree level contribution of the singlet, and significantly lower values of the fine-tuning.

2.2 Composite Higgs

From the point of view of naturalness, composite Higgs models do not suffer from large $\log(M/m_{\rm NP})$ enhancements of the sensitivity to $m_{\rm NP}$, as they are supersoft. In the expression $\Delta \sim (m_{\rm NP}/(0.5\,{\rm TeV}))^2$, $m_{\rm NP}$ can be interpreted as the mass of the first stop resonances. The composite Higgs arises as the pseudo-Goldstone boson of new strong interactions characterised by a compositeness

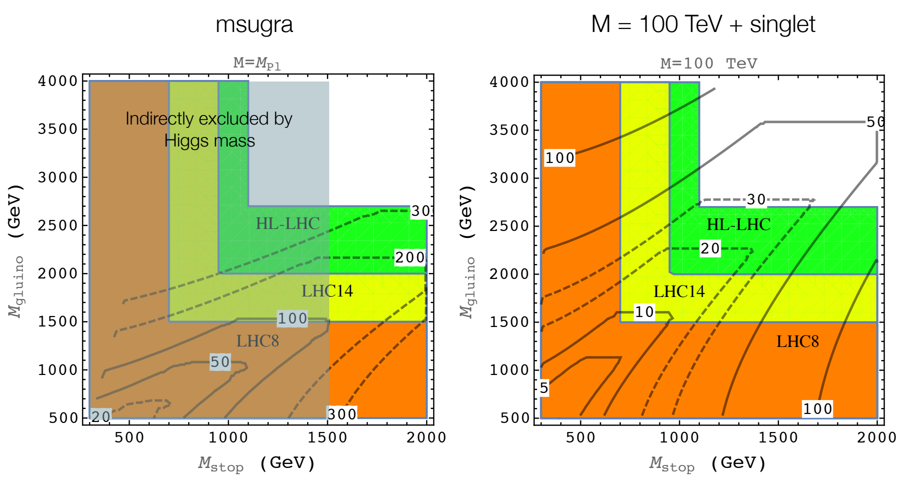

Figure 1: *Representative present and future bounds on stop and gluino masses and naturalness status of two types of supersymmetric models: minimal supergravity (left) and a NMSSM model with low-scale mediation of supersymmetry breaking (right)* [3].

scale $\Lambda \gtrsim 3\,\mathrm{TeV}$, with the bound due to electroweak precision tests. If the scale of the stop resonances is near Λ, as expected, the fine-tuning still turns out to be of the order of a few percent. On the other hand, the value Higgs mass (largish and forcing large stop masses in minimal supersymmetric models) turns out to be smallish and forcing small top resonance masses in minimal composite Higgs models. Lighter top resonances then naively correspond to a smaller fine-tuning, but their lightness may actually itself represent a source of fine-tuning.

Fig. 2 [4, 3] corresponds to a simple model where the Higgs arises as the pseudo-Goldstone boson of the spontaneous breaking to SO(4) of an approximate global SO(5) symmetry. Present bounds and future prospects for the detection of the lightest top resonance, here assumed to be a hypercharge 7/6 doublet X, are shown. Both single and double production are considered, with the latter relatively model independent and the former depending on the model-dependent dimensionless parameter c_R on the vertical axis in the Figure. The naive estimate of the fine-tuning parameter is also shown and correspond

Composite Higgs: Limits on $X_{5/3}$ top partner

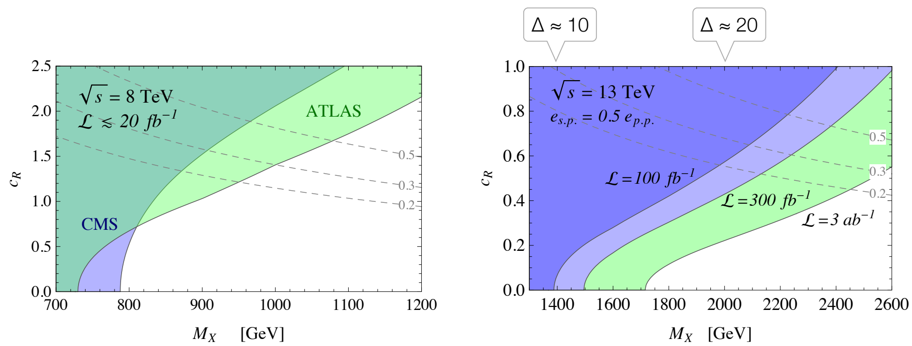

[Matsedonskyi, Panico, Wulzer]

Figure 2: *Present and future bounds on the lightest stop resonances in a representative composite Higgs model. A naive, possibly underestimated, estimate of the fine-tuning parameter is shown* [4, 3].

3 Alternatives

Evading the naturalness argument is possible but not painless.

As discussed, the argument is based on the assumption that superheavy dofs exist with a non-negligible coupling to the SM dofs. An easy way out is then offered by the possibility that this is not the case. Of course, there are many reasons to believe that new dofs exist, at the Planck, GUT, lepton number breaking scales, for example. But it turns out that it is actually possible to account for the experimental shortcomings of the SM (neutrino masses, dark matter, baryon asymmetry) with new dofs, light or weakly coupled enough not to represent a problem for naturalness [5]. At the price of course of giving up two of the most compelling ideas about physics beyond the electroweak scale: i) the understanding of the smallness of neutrino masses in terms of a breaking of lepton number at very high scales and ii) the understanding of the peculiar pattern of SM fermion gauge quantum numbers in terms of a unified description of gauge interactions. Above all, a viable understanding of gravity not involving Planck scale dofs is not known so far (for an interesting attempt see [6]).

If high scale dofs exist, and an unnatural contribution to the Higgs mass does arise at those scales, the fine-tuned cancellation needed to reproduce the much smaller Higgs mass can in principle be accounted for by a dynamical mechanism or by anthropic selection [7].

The first example of an alternative solution of the Higgs mass puzzle was obtained using anthropic considerations [8]. Such a solution is compatible with an unified description of gauge interactions at superheavy scales and with a high scale origin of neutrino masses; it can be realised in a calculable supersymmetric context that can be extrapolated up to the Planck scale and is non-trivially consistent with gauge coupling unification and WIMP dark matter; it predicts a Higgs mass significantly above the M_Z bound even in minimal models. On the other hand, it is based on highly non-trivial assumptions, such as the existence of the huge landscape of vacua of string theory, and of a cosmology populating that landscape. And of course, it requires giving up a reductionist understanding of the EW scale.

A perhaps more satisfying way to account for a fine-tuned cancellation, would be through a dynamical mechanism forcing that cancellation. An example, though in another domain, is the almost complete cancellation of the θ_{QCD} parameter of the QCD lagrangian in the minimum of the axion potential. Recently, a possible mechanism based on a cosmological relaxation of the EW scale has been proposed [9]. Interestingly enough, such a proposal makes again use, in its simplest realisation, of an axion. The role of the axion ϕ is twofold. First, it slowly scans a broad range of scales during its cosmological evolution, and is initially larger than the scale of the radiative corrections to the Higgs mass $\lambda^2/(4\pi)^2 M^2$. Through a coupling to the Higgs, this allows the Higgs mass to scan a correspondingly broad range of values, starting from large, positive values in the first part of the evolution, down to negative values (much) later on. The second role is to be itself, an axion, thus developing an oscillating potential $\sim \lambda\Lambda^3|H|\cos(\phi/f)$ when the Higgs mass turns negative, the EW symmetry is broken, and the SM fermions get a mass through the Higgs vev $|H|$. The new contribution to the axion potential then adds to the terms responsible for the slow roll and generates local minima separated by the oscillation period. If certain conditions are satisfied, the axion might relax in one of those minima, where the Higgs mass, which had just turned negative, is still much smaller than the $\mathcal{O}\left(\lambda^2/(4\pi)M^2\right)$ corrections to it. An apparently accidental large cancellation in the Higgs mass has been forced. The value $m_H^2 \approx 0$ is special in this case not because of a symmetry, but because it corresponds to a phase transition. It is early to judge anything but the cuteness of the mechanism. It is fair to say, though, that realising the simplest axion scenario requires a low cut-off; extreme values of the parameters, such as a (technically natural) axion-Higgs coupling of order of 10^{-30}, or an extremely long cosmological evolution, corresponding to $\mathcal{O}\left(10^{30}\right)$ e-foldings; and it spoils the axion solution of the CP problem. Variations on the theme have just begun to be studied, addressing some of those issues [10]. Conceptual issues, related to the tunnelling to larger, negative values of the Higgs mass, might also need to be addressed.

4 Final remark

The new LHC run at higher energy will hopefully very soon wipe out the above considerations with the discovery of new physics around the TeV scale, as widely expected since decades. Even in that case, though, once the excitement for the discovery and its interpretation in terms of dofs and interactions will settle, the understanding in a grander context will still require, I believe, an understanding of the question: why not earlier?

References

1. L. Giusti, A. Romanino, and A. Strumia, Nucl. Phys. **B550**, 3 (1999), hep-ph/9811386.

2. U. Ellwanger, C. Hugonie, and A. M. Teixeira, Phys. Rept. **496**, 1 (2010), 0910.1785. P. Fayet, Nucl. Phys. **B90**, 104 (1975).

3. A. Andreazza *et al.*, Frascati Phys. Ser. **60**, 1 (2015).

4. O. Matsedonskyi, G. Panico, and A. Wulzer, JHEP **12**, 097 (2014), 1409.0100.

5. M. Farina, D. Pappadopulo, and A. Strumia, JHEP **08**, 022 (2013), 1303.7244.

6. A. Salvio and A. Strumia, JHEP **06**, 080 (2014), 1403.4226.

7. V. Agrawal, S. M. Barr, J. F. Donoghue, and D. Seckel, Phys.Rev. **D57**, 5480 (1998), hep-ph/9707380.

8. N. Arkani-Hamed and S. Dimopoulos, JHEP **0506**, 073 (2005), hep-th/0405159. G. Giudice and A. Romanino, Nucl.Phys. **B699**, 65 (2004), hep-ph/0406088. N. Arkani-Hamed, S. Dimopoulos, G. Giudice, and A. Romanino, Nucl.Phys. **B709**, 3 (2005), hep-ph/0409232.

9. P. W. Graham, D. E. Kaplan, and S. Rajendran, Phys. Rev. Lett. **115**, 221801 (2015), 1504.07551.

10. E. Hardy, JHEP **11**, 077 (2015), 1507.07525. J. R. Espinosa *et al.*, Phys. Rev. Lett. **115**, 251803 (2015), 1506.09217. O. Antipin and M. Redi, JHEP **12**, 031 (2015), 1508.01112. R. S. Gupta, Z. Komargodski, G. Perez, and L. Ubaldi, (2015), 1509.00047.

EFT ANALYSIS OF OFF-SHELL HIGGS PRODUCTION IN GLUON FUSION AT FCC

Aleksandr Azatov
Abdus Salam International Centre for Theoretical Physics, 34151, Trieste, Italy
Theory Division, CERN, Geneva, Switzerland

Abstract

I will present the prospects to resolve the gluon-fusion loop, by studying off-shell Higgs producition at FCC.

1 Introduction

The discovery of the Higgs boson at LHC [1] moved us into the new era of the high energy physics: the precision Higgs boson measurements. This program has already started since the first measurements of the Higgs couplings at LHC [1] and will continue in the future. The next hadron collider FCC (Future Circular Collider), whose main aim will be to discover new resonances, will provide us with new opportunities to measure the Higgs boson couplings. One of the couplings, which are hard to measure directly at LHC, is the top quark Yukawa

Table 1: 95% *credibility intervals.*

full analysis	$c_t \in [0.96, 1.07]$
linear analysis	$c_t \in [0.93, 1.07]$
analysis with $\sqrt{s} < 1.5$ TeV	$c_t \in [0.92, 1.13]$

coupling. Even though the dominant production of the Higgs boson occurs in gluon fusion, which in the Standard Model (SM) is dominated by the top quark loop, we cannot differentiate between the SM and new physics contributions to gluon fusion. To make this discussion more clear, let us consider an effective Higgs interaction in the following form:

$$\mathcal{L}^h = -c_t \frac{h}{v} m_t \bar{t}t + \frac{c_g g_s^2}{48\pi^2} \frac{h}{v} G_{\mu\nu} G^{\mu\nu}. \tag{1}$$

We can see that the rate of inclusive Higgs production is proportional to $|c_t + c_g|$. This well-known fact can be explained by the Higgs low-energy theorems [2], which fix the strength of the Higgs-gluon interactions for particles in the loop much heavier than the Higgs field. This degeneracy of the Higgs couplings can be broken by studying Higgs production in association with a $t\bar{t}$ pair. Recently, it was shown [3] that off-shell Higgs production [4] can be an alternative way to break this degeneracy. Even though the prospects of the constraints coming from off-shell Higgs production are weaker than the ones from tth, both analyses probe the same ball-park of deviations of the Higgs couplings.

2 Breaking the (c_t, c_g) degeneracy

We will start by reviewing the results on the constraints on the c_t and c_g couplings at 100 TeV collider at 3 ab^{-1} luminosity. The details of the collider simulation are presented in [3].

The results are presented in Fig.1 and Table 1. We can see that the off-shell Higgs analysis will be sensitive to few percent deviations of the top Yukawa couplings. So far, we have not said anything about the origin of the couplings c_t and c_g; however, assuming that the Higgs boson appears as a doublet of $SU(2)_L$, these modifications can appear as effects of dimension-six operators :

$$\mathcal{L}^{dim=6} = c_u \frac{y_t |H|^2}{v^2} \bar{Q}_L \tilde{H} t_R + h.c. + \frac{c_g g_s^2}{48\pi^2 v^2} |H^2| G_{\mu\nu} G^{\mu\nu}. \tag{2}$$

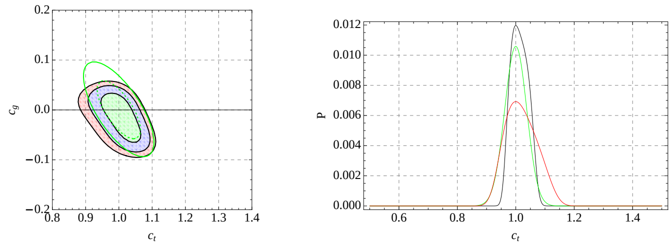

Figure 1: *Left - $68, 95, 99\%$ credibility contours in the (c_t, cg) plane; the green contours correspond to the linear analysis. Right - posterior probability as a function of c_t once the condition $c_t + c_g = 1$ is imposed; the green curve corresponds to the linear analysis, the red one to the analysis with only the low-energy bins.*

The EFT (effective field theory) expansion is valid only if the effects of the operators with higher dimension are much smaller. Note that EFT provides us with the following self-consistency test: the contribution proportional to the squares of the dimension-six operators scales as a dimension-eight operator. So, the expansion is valid only if the effects proportional to $c_{u,g}^2$ are subleading with respect to the linear ones. We show in Fig.1 and Table 1 that indeed the FCC analysis will probe the deviation of the Higgs couplings, which are small enough to be described within the EFT expansion.

3 Constraining the ttZ interactions

Another application of off-shell Higgs production could be the constraints on the ttZ interactions. We remind the reader that the current collider constraints on this interaction are still weak. Generically, we can parameterise the ttZ interactions in the following form:

$$\mathcal{L} = e\bar{t}\left[c_v + \gamma_5 c_A\right] tZ^{\mu};$$
$$c_V^{SM} = \frac{3-8\sin^2\theta_W}{12\sin\theta_W\cos\theta_W}\ ,\ c_A^{SM} = -\frac{1}{4\sin\theta_W\cos\theta_W}, \tag{3}$$

where we have indicated the SM values of the couplings. By performing a similar analysis, we can show that at 3 ab^{-1} we can constrain the deviations of c_A to be of the order of 5% and, at the same time, the constraints on c_V are very weak (see Fig. 2). This deviation of the Z boson couplings can appear as

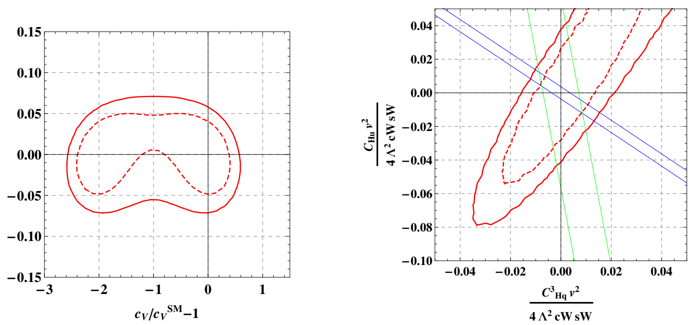

Figure 2: *Left -68, 95% credibility contours for the deviations of the* (c_V, c_A) *couplings. Right - credibility contours for the Wilson coefficients* (C_{Hu}, C^3_{Hq})*; on the top, the current constraints the electroweak precision tests (blue:* ΔT*, green:* $\Delta\epsilon_B$*) are presented.*

a result of the dimension six operators:

$$O^3_{Hq} = i(H^\dagger \tau^I \overset{\leftrightarrow}{D}_\mu H)(\bar{q}_L \gamma_\mu \tau^I q_L),\ O^1_{Hq} = i(H^\dagger \overset{\leftrightarrow}{D}_\mu H)(\bar{q}_L \gamma_\mu q_L),$$
$$O_{Hu} = i(H^\dagger \tau^I \overset{\leftrightarrow}{D}_\mu H)(\bar{u}_R \gamma_\mu u_R). \tag{4}$$

The Zbb constraints from LEP [5] rule out any possibility of large modifications of the Zbb coupling, thus fixing $C^1_{Hq} = -C^3_{Hq}$. Then, we can easily relate the Wilson coefficients to the c_V, c_A couplings:

$$c_{V,A} = c^{SM}_{V,A} + \frac{v^2}{4\Lambda^2 \sin\theta_W \cos\theta_W} \left(\pm 2C^3_{Hq} - C_{Hu}\right). \tag{5}$$

The results of the fit are shown in Fig.2. Note that the same operators at one-loop order will contribute to the electroweak precision observables, namely ΔT and $\Delta\epsilon_B$ [6], which right now lead to constraints as strong as our predictions for the off-shell production sensitivity. However, since the precision constraints result as an effect of one-loop insertions of the dimension-six operators, they are more model-dependent than our analysis.

4 Conclusion

We have studied the FCC prospects on constraining the effective field theories in the off-shell Higgs boson production via gluon fusion. We have shown that this channel can be used to put new constraints on the tth, ttZ and ggH interactions. The results, even though weaker than the other channels, still lead to interesting constraints on these interactions.

5 Acknowledgements

I would like to thank my collaborators on this project C. Grojean, A. Paul and E. Salvioni. I also wish to thank the ECT* center for partial support during the LFC15 meeting.

References

1. G. Aad *et al.* [ATLAS Collaboration], Phys. Lett. B **716**, 1 (2012);
   S. Chatrchyan *et al.* [CMS Collaboration], Phys. Lett. B **716**, 30 (2012).

2. M. A. Shifman, A. I. Vainshtein, M. B. Voloshin and V. I. Zakharov, Sov. J. Nucl. Phys. **30**, 711 (1979) [Yad. Fiz. **30**, 1368 (1979)];
   J. R. Ellis, M. K. Gaillard and D. V. Nanopoulos, Nucl. Phys. B **106**, 292 (1976).

3. A. Azatov, C. Grojean, A. Paul and E. Salvioni, Zh. Eksp. Teor. Fiz. **147**, 410 (2015) [J. Exp. Theor. Phys. **120**, 354 (2015)];
   A. Azatov, C. Grojean, A. Paul and E. Salvioni, to appear soon.

4. CMS Collaboration, CMS-PAS-HIG-14-002;
   V. Khachatryan *et al.* [CMS Collaboration], Phys. Lett. B **736**, 64 (2014);
   ATLAS collaboration, ATLAS-CONF-2014-042.

5. R. Barbieri, A. Pomarol, R. Rattazzi and A. Strumia, Nucl. Phys. B **703**, 127 (2004)

6. A. Pomarol and J. Serra, Phys. Rev. D **78**, 074026 (2008)

HEAVY NEUTRINOS AT FUTURE COLLIDERS

P. S. Bhupal Dev[1,2] and Alejandro Ibarra[1]

[1] *Physik-Department T30d, Technische Univertität München, James-Franck-Straße 1, D-85748 Garching, Germany*

[2] *Max-Planck-Institut für Kernphysik, Saupfercheckweg 1, D-69117 Heidelberg, Germany*

Abstract

We discuss the current status and future prospects of heavy neutrino searches at the energy frontier, which might play an important role in vindicating the simplest seesaw paradigm as the new physics responsible for neutrino mass generation. After summarizing the current search limits and potential improvements at hadron colliders, we highlight the unparalleled sensitivities achievable in the clean environment of future lepton colliders.

1 Introduction

Despite the spectacular experimental progress in the past two decades in determining the neutrino oscillation parameters, the nature of new physics responsible for non-zero neutrino masses and mixing is still unknown. Given this lack of information, it is essential to explore *all* possible ways the neutrino mass mechanism can be probed at various frontiers. In the era of the Large Hadron Collider (LHC), it is therefore natural to ask whether any of the existing theories of neutrino mass can be tested at the energy frontier.

A simple paradigm for neutrino masses is the so-called type-I seesaw mechanism [1], which postulates the existence of sterile neutrinos (N) with Majorana mass M_N. Together with the Dirac mass M_D, they induce a tree-level active neutrino mass matrix after electroweak symmetry breaking:

$$M_\nu \simeq -M_D M_N^{-1} M_D^T \,. \tag{1}$$

In a bottom-up phenomenological approach [2], the mass scale of the sterile neutrinos, synonymous with the seesaw scale, is *a priori* unknown, and could be anywhere ranging from sub-eV all the way up to the grand unification theory scale $\sim 10^{15}$ GeV. However, there are arguments based on naturalness of the Standard Model (SM) Higgs mass which suggest the seesaw scale to be below $\sim 10^7$ GeV [3]. Of particular interest to us are TeV-scale seesaw models which are kinematically accessible at the current and foreseeable future collider energies [4]. Under favorable circumstances, the hadron collider experiments can *simultaneously* probe both the key aspects of seesaw, namely, the Majorana nature of the neutrinos and the active-sterile neutrino mixing parameters $V_{\ell N} \equiv M_D M_N^{-1}$ through the "smoking gun" lepton number violating (LNV) signature of same-sign dilepton plus two jets: $pp \to N\ell^\pm \to \ell^\pm \ell^\pm jj$ [5, 6, 7] and other related processes [8]. On the other hand, the complementary low-energy probes at the intensity frontier [9, 10] are mostly sensitive to only one aspect, e.g. neutrinoless double beta decay ($0\nu\beta\beta$) for the Majorana nature and lepton flavor violation (LFV) searches for the active-sterile neutrino mixing.

2 Low-scale Seesaw with Large Mixing

In the traditional "vanilla" seesaw mechanism [1], the active-sterile neutrino mixing parameter is suppressed by the light neutrino mass $M_\nu \lesssim 0.1$ eV:

$$V_{\ell N} \simeq \sqrt{\frac{M_\nu}{M_N}} \lesssim 10^{-6}\sqrt{\frac{100 \text{ GeV}}{M_N}} \,. \tag{2}$$

Thus for a TeV-scale seesaw, the experimental effects of the light-heavy neutrino mixing are naively expected to be too small, unless the heavy neutrinos have additional interactions, e.g. when they are charged under an additional $U(1)$ or $SU(2)$ gauge group. However, there exists a class of low-scale Type-I seesaw scenarios [11, 12, 13], where $V_{\ell N}$ can be sizable due to specific textures of the Dirac and Majorana mass matrices in Eq. (1).

Another natural realization of a low-scale seesaw scenario with potentially large light-heavy neutrino mixing is the inverse seesaw mechanism [14]. In this case, the magnitude of the neutrino mass becomes decoupled from the heavy neutrino mass, thus allowing for a large mixing

$$V_{\ell N} \simeq \sqrt{\frac{M_\nu}{\mu_S}} \approx 10^{-2}\sqrt{\frac{1 \text{ keV}}{\mu_S}} , \tag{3}$$

where μ_S is the only LNV parameter in the theory, whose smallness is 'technically natural, i.e. in the limit of $\mu_S \to \mathbf{0}$, lepton number symmetry is restored and the light neutrinos are exactly massless to all orders in perturbation theory.

In the absence of any additional gauge interactions beyond the SM, the amplitudes of the LNV processes in most of the low-scale seesaw models are suppressed by the small mass splitting between the relevant heavy neutrinos, if not by their small mixing with the active neutrino sector, as required to satisfy the light neutrino mass and $0\nu\beta\beta$ constraints [12, 15]. For collider studies in such situations, one can either use the opposite-sign dilepton signal, relying on the specific kinematic features to separate the signal from the huge SM background, or use the trilepton channel $pp \to N\ell^\pm \to \ell^\pm\ell^\mp\ell^\pm + \not{E}_T$ [16], which has a relatively smaller cross section, but a smaller SM background as well. Introducing new gauge groups beyond the SM and making the sterile neutrinos charged under them enriches the collider phenomenology [4], but here we will limit ourselves only to the SM seesaw due to lack of space/time.

3 Searches at Hadron Colliders

The current direct search limits using the same-sign dilepton channel at $\sqrt{s} = 8$ TeV LHC [17] range from $|V_{\ell N}|^2 \lesssim 10^{-2} - 1$ (with $\ell = e, \mu$) for $M_N = 100 - 500$ GeV. This is shown by the 'LHC8' curve in Fig. 1 for the electron sector at 95% confidence level (CL). These limits could be improved by roughly an order of magnitude and extended for heavy neutrino masses up to a TeV or so with the run-II phase of the LHC, as shown by 'LHC14' in Fig. 1 for 300 fb^{-1}

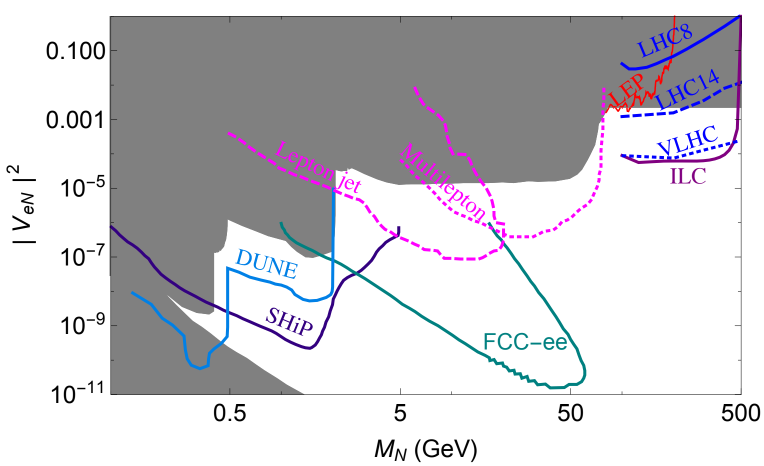

Figure 1: Current (shaded) and future limits in the heavy neutrino mass-mixing plane for the electron flavor. For details and for limits in other flavors, see [4, 7].

luminosity. Further improvements by another order of magnitude are possible at the proposed 100 TeV pp collider, as shown by the 'VLHC' curve for 1 ab^{-1} luminosity. The corresponding limits for opposite-sign dilepton signal are expected to be weaker due to the larger SM background. It is worth emphasizing here that the $W\gamma$ vector boson fusion processes [8] become increasingly important at higher center-of-mass energies and/or higher masses, and must be taken into account, along with the usual Drell-Yan production mechanism with an s-channel W boson so far considered in the experimental analyses of the LHC data.

Note that the LFV processes (such as $\mu \to e\gamma$) put stringent constraints on the product $|V_{\ell N} V^*_{\ell' N}|$ (with $\ell \neq \ell'$), but do not restrict the individual mixing parameters $|V_{\ell N}|^2$ in a model-independent way. Similarly in the electron sector, the $0\nu\beta\beta$ constraints are the most stringent for a large range of the heavy neutrino masses, but are subject to a large uncertainty due to the unknown CP phases in the seesaw matrix, and hence, do not necessarily render the direct searches redundant. The current exclusion limits from various other experiments are shown by the shaded region in Fig. 1 [4, 7].

4 Searches at Lepton Colliders

The dominant production channel for heavy neutrinos at e^+e^- colliders is $e^+e^- \to N\nu$ mediated by an s-channel Z (for all flavors) and a t-channel W (for electron flavor) [18]. Using the decay channel $N \to eW$ with $W \to jj$, which would lead to a single isolated electron plus hadronic jets, 95% CL upper limits on $|V_{eN}|^2$ for heavy neutrino mass range between 80 and 205 GeV was derived by LEP [19], as shown by the 'LEP' contour in Fig. 1. Similar limits were derived [20] using the LEP data on $e^+e^- \to W^-W^+ \to \bar{\nu}\ell^-\ell^+\nu$. Future lepton colliders can significantly improve the sensitivity in this mass region, as illustrated by the 'ILC' curve for $\sqrt{s} = 500$ GeV with 500 fb^{-1} luminosity [21]. Due to its relatively cleaner environment, as compared to hadron colliders, a linear collider thus provides better sensitivity up to heavy neutrino mass values very close to its kinematic threshold. Also note that these limits are valid, irrespective of the Majorana or (pseudo-)Dirac nature of the heavy neutrinos.

In addition, for heavy Majorana neutrinos, one can explicitly look for LNV processes, such as $e^+e^- \to Ne^\pm W^\mp \to \ell^\pm e^\pm + 4j$ [21]. Also, switching the beam configuration from e^+e^- to e^-e^- mode, one can also search for the LNV signal $e^-e^- \to W^-W^- \to 4j$ mediated by a t-channel Majorana neutrino [22].

Before concluding, we should mention that the direct searches discussed above are mostly effective for heavy neutrino masses above 100 GeV or so. For smaller masses, there exist a number of interesting proposals both at energy and intensity frontiers, some of which are shown in Fig. 1 labeled as 'DUNE' [23], 'SHiP' [10], 'FCC-ee' [24], 'lepton jet and mulitlepton' at the LHC [25] .

5 Conclusion

Heavy neutrinos are essential constituents of the simplest seesaw scenario, and hence, their direct searches are important to test the neutrino mass mechanism at the energy frontier. We have briefly reviewed the current status and future prospects of these direct searches for heavy neutrinos at both hadron and lepton colliders. We find that while up to an order of magnitude improvement over the current limit is possible at the LHC, the lepton colliders provide a much better sensitivity due to their clean, almost background-free environment.

6 Acknowledgements

P.S.B.D. thanks the LFC15 workshop organizers for the invitation and the local hospitality provided by ECT*, Trento. This work was partially supported by the DFG cluster of excellence "Origin and Structure of the Universe". P.S.B.D. was also supported in part by a TUM University Foundation Fellowship, and during the completion of this proceedings, by the DFG with grant RO 2516/5-1.

References

1. P. Minkowski, Phys. Lett. B **67**, 421 (1977); R. N. Mohapatra and G. Senjanović, Phys. Rev. Lett. **44**, 912 (1980); T. Yanagida, Conf. Proc. C **7902131**, 95 (1979); M. Gell-Mann, P. Ramond and R. Slansky, Conf. Proc. C **790927**, 315 (1979).

2. M. Drewes, Int. J. Mod. Phys. E **22**, 1330019 (2013); M. Drewes and B. Garbrecht, arXiv:1502.00477 [hep-ph].

3. F. Vissani, Phys. Rev. D **57**, 7027 (1998); J. A. Casas, J. R. Espinosa and I. Hidalgo, JHEP **0411**, 057 (2004); J. D. Clarke, R. Foot and R. R. Volkas, Phys. Rev. D **91**, 073009 (2015).

4. F. Deppisch, P. S. B. Dev and A. Pilaftsis, New J. Phys. **17**, 075019 (2015).

5. W. Y. Keung and G. Senjanović, Phys. Rev. Lett. **50**, 1427 (1983).

6. A. Datta, M. Guchait and A. Pilaftsis, Phys. Rev. D **50**, 3195 (1994); O. Panella, M. Cannoni, C. Carimalo and Y. N. Srivastava, Phys. Rev. D **65**, 035005 (2002); T. Han and B. Zhang, Phys. Rev. Lett. **97**, 171804 (2006); S. Bray, J. S. Lee and A. Pilaftsis, Nucl. Phys. B **786**, 95 (2007); F. del Aguila, J. A. Aguilar-Saavedra and R. Pittau, JHEP **0710**, 047 (2007); R. Leonardi, L. Alunni, F. Romeo, L. Fanó and O. Panella, arXiv:1510.07988 [hep-ph].

7. A. Atre, T. Han, S. Pascoli and B. Zhang, JHEP **0905**, 030 (2009).

8. P. S. B. Dev, A. Pilaftsis and U. K. Yang, Phys. Rev. Lett. **112**, 081801 (2014); D. Alva, T. Han and R. Ruiz, JHEP **1502**, 072 (2015); A. Das and N. Okada, arXiv:1510.04790 [hep-ph].

9. A. de Gouvea and P. Vogel, Prog. Part. Nucl. Phys. **71**, 75 (2013).

10. S. Alekhin *et al.*, arXiv:1504.04855 [hep-ph].

11. J. Kersten and A. Y. Smirnov, Phys. Rev. D **76**, 073005 (2007);

12. A. Ibarra, E. Molinaro and S. T. Petcov, JHEP **1009**, 108 (2010); Phys. Rev. D **84**, 013005 (2011).

13. A. Pilaftsis, Z. Phys. C **55**, 275 (1992); D. Tommasini, G. Barenboim, J. Bernabeu and C. Jarlskog, Nucl. Phys. B **444**, 451 (1995); J. Gluza, Acta Phys. Polon. B **33**, 1735 (2002); Z. z. Xing, Prog. Theor. Phys. Suppl. **180**, 112 (2009); M. B. Gavela, T. Hambye, D. Hernandez and P. Hernandez, JHEP **0909**, 038 (2009); X. G. He, S. Oh, J. Tandean and C. C. Wen, Phys. Rev. D **80**, 073012 (2009); R. Adhikari and A. Raychaudhuri, Phys. Rev. D **84**, 033002 (2011); F. F. Deppisch and A. Pilaftsis, Phys. Rev. D **83**, 076007 (2011); M. Mitra, G. Senjanovic and F. Vissani, Nucl. Phys. B **856**, 26 (2012); C. H. Lee, P. S. B. Dev and R. N. Mohapatra, Phys. Rev. D **88**, 093010 (2013).

14. R. N. Mohapatra, Phys. Rev. Lett. **56**, 561 (1986); R. N. Mohapatra and J. W. F. Valle, Phys. Rev. D **34**, 1642 (1986).

15. J. Lopez-Pavon, E. Molinaro and S. T. Petcov, JHEP **1511**, 030 (2015); E. Fernandez-Martinez, J. Hernandez-Garcia, J. Lopez-Pavon and M. Lucente, JHEP **1510**, 130 (2015).

16. F. del Aguila and J. A. Aguilar-Saavedra, Phys. Lett. B **672**, 158 (2009); C. Y. Chen and P. S. B. Dev, Phys. Rev. D **85**, 093018 (2012); A. Das and N. Okada, Phys. Rev. D **88**, 113001 (2013); A. Das, P. S. B. Dev and N. Okada, Phys. Lett. B **735**, 364 (2014); G. Bambhaniya, S. Goswami, S. Khan, P. Konar and T. Mondal, Phys. Rev. D **91**, 075007 (2015).

17. V. Khachatryan *et al.* [CMS Collaboration], Phys. Lett. B **748**, 144 (2015); G. Aad *et al.* [ATLAS Collaboration], JHEP **1507**, 162 (2015).

18. W. Buchmuller and C. Greub, Nucl. Phys. B **363**, 345 (1991); A. Djouadi, Z. Phys. C **63**, 317 (1994); G. Azuelos and A. Djouadi, Z. Phys. C **63**, 327 (1994); J. Gluza and M. Zralek, Phys. Lett. B **372**, 259 (1996); J. Gluza, J. Maalampi, M. Raidal and M. Zralek, Phys. Lett. B **407**, 45 (1997).

19. P. Achard *et al.* [L3 Collaboration], Phys. Lett. B **517**, 67 (2001).

20. S. Antusch and O. Fischer, JHEP **1505**, 053 (2015).

21. S. Banerjee, P. S. B. Dev, A. Ibarra, T. Mandal and M. Mitra, Phys. Rev. D **92**, 075002 (2015).

22. T. G. Rizzo, Phys. Lett. B **116**, 23 (1982); G. Belanger, F. Boudjema, D. London and H. Nadeau, Phys. Rev. D **53**, 6292 (1996); B. Ananthanarayan and P. Minkowski, Phys. Lett. B **373**, 130 (1996); W. Rodejohann, Phys. Rev. D **81**, 114001 (2010); T. Asaka and T. Tsuyuki, Phys. Rev. D **92**, 094012 (2015).

23. C. Adams *et al.* [LBNE Collaboration], arXiv:1307.7335 [hep-ex].

24. A. Blondel, E. Graverini, N. Serra and M. Shaposhnikov, arXiv:1411.5230 [hep-ex].

25. E. Izaguirre and B. Shuve, Phys. Rev. D **91**, 093010 (2015).

TOP MASS AND COUPLINGS IN ATLAS AND CMS

Marina Cobal
Università di Udine and INFN Gruppo Collegato di Udine

Abstract

Top-quark physics became a sector of high precision measurements since top-quark discovery at Tevatron in 1995. Nowadays, in the LHC era, it is a system of prior importance where to hunt for New Physics. In this presentation, the most recent results on top-quark mass measurements and searches for anomalous top-quark couplings from the LHC experiments are presented.

1 Introduction

The top-quark with its mass of $\simeq$ 175 GeV is the heaviest known elementary particle and may have a special role in electro-weak symmetry breaking due to its large coupling to the Higgs boson. Top-quark pairs produced via strong interaction in proton-proton (pp) collision at the Large Hadron Collider (LHC), decay before they can form bound states and before their spins de-correlate.

As a consequence one can study the top-quark properties, which are nowadays determined with increasing level of precision, to test the SM and have the possibility to probe New Physics effects. Data presented in this review have been collected in pp collisions at $\sqrt{s} = 7$ and 8 TeV in 2011 and 2012, at the LHC experiments ATLAS [1] and CMS [2]. At these energies the top-quark pairs production cross section is significantly larger than the Tevatron collider one, and dominantly driven by gluon-gluon fusion. Single top-quark production can occur via electro-weak interactions too. According to the Standard Model (SM), top-quarks decay almost exclusively to a W-boson and a b-quark. The decay channel of the W-boson into leptons or quarks is then generally used to distinguish different top-quark decay channels.

Between 2010 and 2012 more than five million top-quark events have been collected by each of the ATLAS and CMS experiments. Based on this amount of data, top-quark physics has entered a new realm of precision, and experimental results are used to further constrain the SM parameters, to probe improved QCD calculations and to search for New Physics signals. In all those scenarios in which new physics would couple to mass, the top-quark may show a particular sensitivity.

2 Top-Quark Mass

The top-quark mass (m_t) is a free parameter of the SM. For a given m_t and the CKM matrix elements corresponding to the top-quark, predictions for all top-quark properties are possible. Conversely, precise property measurements can be used to get stringent consistency tests of the SM. Theoretically, the m_t definition requires a renormalisation scheme. In the so-called pole mass scheme (which is related to the intuitive understanding of the mass of a free particle) the mass is defined as the pole in the re-normalised quark propagator. In the experiments, m_t is usually determined through the comparison of certain reconstructed distributions of the top-quark decay products in data with those obtained from a given Monte Carlo simulation (standard measurement). The mass parameter in the simulation is then varied in order to better describe the data. With this technique, m_t has been measured with a precision of better than 1 GeV. Albeit there is no well-defined relation of the mass parameters in simulations with a theoretically well defined top-quark mass, the pole mass and the mass measured from final state reconstruction are expected to agree within O(1 GeV) [3]. It is clear then that the mass measurement is dominated by the uncertainty on the definition of the mass itself.

2.1 Standard Top-Quark Mass Measurement

In the following a few of the most recent results using the above mentioned technique are described in more detail. Using the full dataset at $\sqrt{s} = 8$ TeV, the CMS experiment performed a m_t measurement using $t\bar{t}$ events in which both top-quarks decay hadronically [4]. The presence of six jets is required, two of them originated from b-quark fragmentation. A kinematic fit is used to assign the final-state jets to W-bosons and top-quark candidates. In the fit m_t is determined simultaneously with an overall jet energy scale factor (JSF), constrained by the known mass of the W-boson. In fig. 1 a) the mass distribution is shown. A clear narrow peak is seen on a relatively small background. The mass is determined in a joint maximum-likelihood fit to the selected events. Dominant uncertainties arise from the jet energy scale, the modelling of flavour-dependent jet energy corrections and the modelling of pile-up events. The top-quark mass is measured to be $172.08 \pm 0.36(\text{stat} + \text{JSF}) \pm 0.83(\text{syst})$ GeV.

The ATLAS experiment has measured m_t in the di-lepton and lepton+jets channels [5]. A kinematic likelihood fit allowed to reconstruct the event kinematics and to find the most likely assignment of reconstructed jets to partons. In the lepton+jets channel a 3D-template technique was used to determine m_t simultaneously with a correction for the global jet energy scale, using a constraint to the mass of the W-boson, and an additional correction for the b-jet energy scale using the observable R_{bq}. The latter observable, derived as the ratio of the scalar sum of transverse momenta of b-tagged jets over the scalar sum of transverse momenta of the two jets associated with the hadronic W-boson decay, is sensitive to the b-jet energy response, and independent of m_t. In fig. 1 b) the reconstructed distributions of data and simulation are displayed for m_t. The combination of the 3D-template analysis in the lepton+jets channel with the di-lepton analysis resulted in a $m_t = 172.99 \pm 0.48(\text{stat}) \pm 0.78(\text{syst})$ GeV. Both statistical and systematic uncertainties are expected to diminish with increasing statistics.

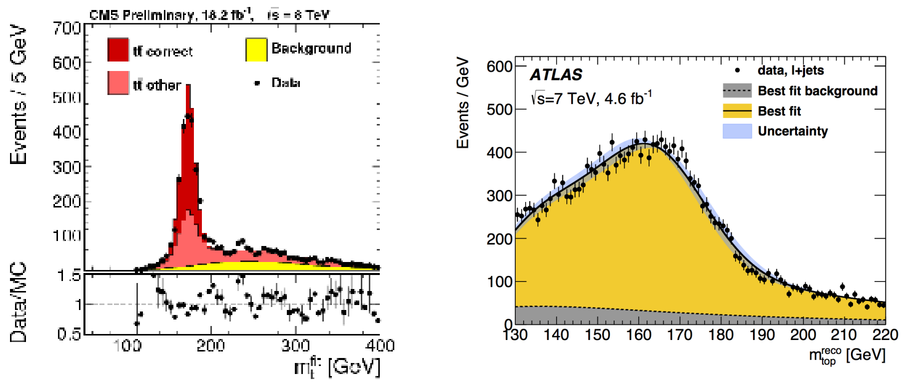

Figure 1: *a) Reconstructed m_t from the CMS kinematic fit. The simulated signal and the background from event mixing are normalized to the data b) Fitted ATLAS m_t distribution The fitted probability density functions for the background alone and for signal-plus-background are also shown. The uncertainty bands indicate the total uncertainty on the signal-plus-background fit obtained from pseudo-experiments.*

2.2 *Top-Quark Pole Mass Measurement*

Several alternative approaches to measure m_t have been developed, like extracting its value from the measured inclusive $\sigma_{t\bar{t}}$ cross section. This approach has the advantage that the cross section and the pole mass are directly related, such that the extraction yields a theoretically well-defined quantity. The D0, CMS and ATLAS experiments have used their measured $t\bar{t}$ cross section to extract the top-quark pole mass as defined at NNLO accuracy [6]. The ATLAS experiment has presented a measurement of the top-quark pole mass using the $t\bar{t}$ differential cross section as a function of the invariant mass of the $t\bar{t}+$ 1-jet system [7]. This distribution provides information on m_t via the mass-dependent threshold and cone effects for the radiation of hard gluons. The ATLAS analysis is based on the dataset taken at the energy of 7 TeV. The measured distribution is compared to the NLO prediction in QCD. The measured value of the top-quark pole mass is $173.7 \pm 1.5(\text{stat}) \pm 1.4(\text{syst}) \pm 1.0 \pm 0.5(\text{theory})$ GeV.

3 Flavour Changing Neutral currents

In the SM, FCNCs are forbidden at tree level due to the GIM mechanism and are characterised by branching ratios (BRs) smaller than 10^{-12}. There are numerous SM extensions (like quark singlet, 2HDM, MSSM) which predict higher BRs, up to 10^{-4}, 10^{-5} and the LHC data are expected to be able to discover or exclude some of these models [8]. ATLAS recently published a search for the decay $t \to qZ$, where $q{=}u, c$, based on the full 8 TeV dataset [9] and giving an observed (expected) limit on BR of 0.07% (0.08%) is set at 95% C.L.. FCNCs can occur also in top-quark production: the CMS experiment recently presented a search for single top-quark production in association with a photon [10]. Observed (expected) limits BR($t \to u\gamma$) $<$ 0.0161%(0.0279%) and BR($t \to c\gamma$) $<$ 0.182%(0.261%), respectively have been obtained. Both ATLAS and CMS performed the search in single top-quark production where the top-quark would be produced in pp collisions from the coupling of an initial state gluon with an u, c quark [11]. The ATLAS experiment used the full 8 TeV dataset looking at both the electron and muon channel, and got the most stringent limits: BR($t \to ug$) $< 4.0{\times}10^{-5}$ and BR($t \to cg$) $< 17{\times}10^{-5}$. Searches were also performed for scenarios where the top-quark decays to a quark (u or c) and a H. Both ATLAS and CMS reported searches for top pair events in which one top-quark decays to qH and the other decays to bW [12]. None of these many searches for FCNCs has been successful up to now, however the reached upper limits are getting close to expectations for some of the New Physics scenarios. Some of these scenarios could be soon discovered or excluded, already based on the LHC Run 2 datasets.

4 Top-Quark Couplings

The top-quark couples to other SM fields through its gauge and Yukawa interactions. The $t \to Wb$ coupling has been measured already at Tevatron: with the high statistics top physics at LHC also $t\bar{t}\gamma$, $t\bar{t}Z$ and $t\bar{t}H$ became accessible. These measurements test the SM and offer a direct measurement of the top couplings which can be used in searches for New Physics.

With the full 7 TeV dataset, the ATLAS collaboration measured the production cross section of top-quark pairs with additional photons (which is sensitive to the $t\bar{t}\gamma$ coupling) and reported observation of this process with a significance of 5.3 σ [13]. The measurement is performed in the single-lepton channel in a fiducial region: with 362 selected events the fiducial cross section is measured with an uncertainty of $\simeq$30%, dominated by uncertainties on the jet energy scale and b-tagging efficiency. The associated production cross section of $t\bar{t}$ with either a W or a Z boson has been measured by both CMS and ATLAS at $\sqrt{s} = 8$ TeV. The interest in the measurement of the $t\bar{t}Z$ process lies in the determination of the top-quark coupling to the Z-boson. The $t\bar{t}W$ process probes the proton structure and is a source of same-sign di-lepton events, which is an important background in many searches. Several signal categories are considered such as same-sign and opposite-sign di-lepton, tri-lepton and four-lepton channels. In a simultaneous extraction of $\sigma_{t\bar{t}Z}$ and $\sigma_{t\bar{t}W}$, ATLAS measured both cross sections with a significance of 5.0 and 4.2 σ respectively, over the background-only hypothesis [14]. The measured cross sections are $\sigma_{t\bar{t}W} = 369{+}^{100}_{-91}$ fb and $\sigma_{t\bar{t}Z} = 176{+}^{58}_{-52}$ fb, with uncertainties dominated by the statistical component (see fig. 2 a)). CMS determined the cross sections of these processes, as well, with significances of 4.8 and 6.4 σ respectively [15], using the same final states. Their analysis reduces the statistical uncertainty by lowering the requirements on the reconstructed objects quality: of course this gives rise to larger systematic uncertainties. The measured cross sections are $\sigma_{t\bar{t}W} = 382{+}^{117}_{-102}$ fb and $\sigma_{t\bar{t}Z} = 242{+}^{65}_{-55}$ fb (see fig. 2 b)). The result allows to constraint the axial and vector components of the $t\bar{t}Z$ coupling and on dimension-six operators in an effective field theory framework.

Studies related to the $t\bar{t}H$ associated productions are discussed elsewehere [16]. Top-quark pairs can be produced with additional energetic jets, and the measurement of such jet multiplicities provides an important test of QCD predictions at NLO. Recently, the production of additional b-quarks has been studied. The $t\bar{t}b\bar{b}$ final state is an irreducible non-resonant background to the $t\bar{t}H$ process. CMS measured $\sigma_{t\bar{t}b\bar{b}}$ and the quantity $\mathrm{R}_{HF} = \sigma_{t\bar{t}b\bar{b}} / \sigma_{t\bar{t}jj}$ in the di-lepton and single-lepton channels [17]. Results are in the range $\mathrm{R}_{HF} = 0.012 - 0.022$, depending on the phase space and whether particle or parton level is considered, with uncertainties of $0.004 - 0.006$, and are in general in good agreement with predictions. ATLAS performs four measurements of heavy flavour production in top-quark pair events in a fiducial volume [18]. The ratio R_{HF} is determined to be 0.013 ± 0.004 with comparable systematic and statistical uncertainties.

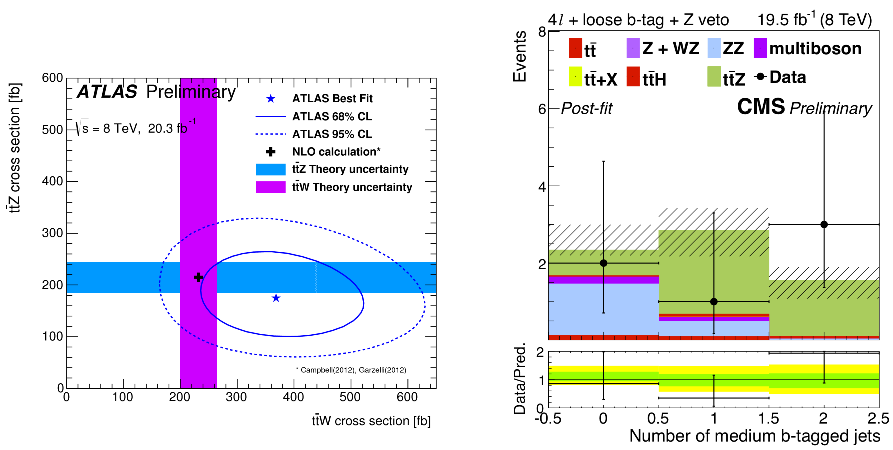

Figure 2: *a) Result of the combined two-dimensional simultaneous fit to the $t\bar{t}W$ and $t\bar{t}Z$ cross sections along with the 68% and 95% CL uncertainty contours. The shaded areas correspond to 14% uncertainty, which includes renormalisation and factorisation scale uncertainties as well as and PDF uncertainties including alpha$_s$ variations. b) Post-fit plots of the final discriminant for the four leptons $t\bar{t}Z$ channel with exactly one lepton pair consistent with a $Z \to l^+l^-$ decay,*

5 Conclusions

Top-quark physics is a key element to understand QCD and electro-weak model and maybe to enter in a New Physics era. With the statistics collected with Run 1 LHC data, top-quark properties have been precisely scrutinized and it has been possible to observe for the first time several processes involving the heaviest top ($t\bar{t} + W/Z$). Also the electroweak production of single top events starts to be useful for property measurements. So far, no deviations from what expected by the SM have been detected, but with Run 2 we should be able to collect around 100 fb^{-1} per experiment by 2018 at 13 TeV, which means 80 million of $t\bar{t}$ events and 20 million single top events. This, together with more refined experimental techniques and theory advances, may open up new scenarios.

References

1. ATLAS Collaboration, JINST 3 (2008) S08003.
2. CMS Collaboration, JINST 3 (2008) S08004.
3. S. Moch et al., arXiv:1405.4781 [hep-ph].
4. CMS Collaboration, CMS-PAS-TOP-14-002.
5. ATLAS Collaboration, Eur. Phys. J. C 75 (2015) 7, 330.
6. CMS Collaboration, Phys. Lett. B 728 (2014) 496;
   ATLAS Collaboration, Eur. Phys. J. C 74 (2014) 10, 3109;
   D0 Collaboration, D0 Note 6453-CONF.
7. ATLAS Collaboration, JHEP 1510 (2015) 121.
8. J. A. Aguilar-Saavedra, Acta Phys. Pol. B 35, 2695 (2004).
9. ATLAS Collaboration, Eur. Phys. J. C76 (2016) 12.
10. CMS Collaboration, CMS-PAS-TOP-14-003.
11. ATLAS Collaboration, arXiv:1509.00294 [hep-ex];
    CMS Collaboration, CMS-PAS-TOP-14-007.
12. ATLAS Collaboration, JHEP 1406 (2014) 008, JHEP 12 (2015) 061;
    CMS Collaboration, CMS-PAS-TOP-13-017, CMS-PAS-TOP-14-019, CMS-PAS-TOP-14-020
13. ATLAS Collaboration, Phys. Rev. D 91 (2015) 072007.
14. ATLAS Collaboration, arXiv:1509.05276 [hep-ex].
15. CMS Collaboration, arXiv:1510.01131 [hep-ex].
16. C. Bini, these proceedings.
17. CMS Collaboration, Phys. Lett. B 746 (2015) 132.
18. ATLAS Collaboration, arXiv:1508.06868 [hep-ex].

INDIRECT DETERMINATIONS OF THE TOP QUARK MASS

Paride Paradisi
Dipartimento di Fisica dell'Università di Padova and INFN, Italy

Abstract

We give a complete analysis of indirect determinations of the top quark mass in the Standard Model using flavour and electroweak data. Although present data give only a poor determination, we show how future theoretical and experimental progress in flavour physics can lead to an accuracy in M_t well below 2 GeV. We revisit determinations of M_t from electroweak data, showing how an improved measurement of the W mass leads to an accuracy at the level of 1 GeV.

1 Introduction

The top quark mass (M_t) is a key input parameter of the Standard Model (SM). Since the top quark is the heaviest particle in the SM, its Yukawa coupling y_t is sizeable and plays a crucial role in determining the predictions of the theory at the quantum level. A precise determination of M_t is crucial for stability of the electroweak vacuum [1] or to establish the viability of scenarios of Higgs inflation [2]. Therefore, a more precise determination of M_t will add important information to our knowledge of particle physics and cosmology.

The most precise quoted value of the top-quark pole mass comes from the combination of LHC and Tevatron measurements $(M_t)_{\text{pole}} = 173.34 \pm 0.76$ GeV [3]. A theoretical concern about the extraction of M_t from data is that the pole top mass is not a physical observable. This means that its experimental determination is done through the measurement of other physical observables (final-state invariant masses, kinematic distributions, total rates) that are especially sensitive to M_t. These measurements are compared to the results of theoretical calculations, which are expressed in terms of M_t in a well-defined renormalisation scheme. In the context of hadron colliders, the extraction of M_t suffers from a variety of effects linked to hadronization that are not fully accountable by perturbative QCD calculations, like bound-state effects of the $t\bar{t}$ pairs, parton showering, and other non-perturbative corrections (see [4] for a thorough discussion). In practice, the extraction of M_t relies on modelling based on Monte-Carlo generators, and this is why [5] refers to M_t as "Monte-Carlo mass".

These considerations justify the search for alternative strategies to determine M_t. Given that the top is the only quark associated to a sizeable Yukawa coupling, loop effects in the SM are potentially very sensitive to M_t. Our goal is to identify all processes that receive quantum corrections enhanced by powers of M_t (in the limit $M_t \gg M_W$) and infer M_t from their measurements.

In ref. [6] we have proposed to use the comparison between experimental data and theoretical predictions of flavour processes as a way to extract the top quark mass, under the assumption that the SM is valid up to very short distance scales. The use of flavour data for an indirect determination of M_t is fairly robust from the theoretical point of view, since it relies on controllable SM calculations, in which non-perturbative effects are restricted to a few well-known hadronic parameters, now under careful scrutiny by lattice calculations. The current status of the extraction of the top mass from the fit of flavour data is $(M_t)_{\text{flavour}} = (173.4 \pm 7.8)$ GeV [6]. The uncertainty of this extraction is too large to be competitive with the direct measurements. However, taking into account foreseeable progress in perturbative and lattice calculations, on one side, and experimental measurements, on the other side, our projection for the future is that the error can be brought to about 1.7 GeV [6].

With the aim of an indirect determination of the top mass, in ref. [6] we have also reconsidered global fits of electroweak observables, finding $(M_t)_{\rm EW} = (177.0 \pm 2.6)\,$GeV. We find that the determination of M_t is dominated by the measurement of M_W. A reduction of the error in the measurement of M_W to about 8 MeV, as foreseeable at the LHC [7], can bring down the uncertainty on M_t to 1.2 GeV.

2 M_t dependence of observables in the heavy-top limit

The large top Yukawa coupling offers the possibility of reconstructing M_t from SM quantum effects. In order to identify the physical observables that are most sensitive to the top mass at the one-loop level, we have developed here a systematic procedure to extract the leading M_t dependence predicted by the SM [6]. We work in the heavy-top limit [8], in which the masses of the W and Z bosons are neglected with respect to M_t. This is achieved by considering a gauge-less theory with massive quarks, the Higgs boson h, and 3 Goldstone bosons $\vec{\chi}$ (related by the equivalence theorem to the longitudinal components of the W and Z), where the only quark interaction is

$$\mathcal{L} = y_t\, \bar{t}_R\, H^T \begin{pmatrix} V_{ti}\, d_{iL} \\ -t_L \end{pmatrix} + \text{h.c.}\,, \qquad H = \frac{1}{\sqrt{2}} e^{\frac{i\vec{\sigma}\cdot\vec{\chi}}{v}} \begin{pmatrix} 0 \\ v+h \end{pmatrix}\,. \tag{1}$$

Here y_t is the top Yukawa coupling, V is the CKM matrix, H is the Higgs doublet, $v = 246\,$GeV is the symmetry breaking scale and $\vec{\sigma}$ are the Goldstone bosons. The next step is to integrate out the top quark. The top-less effective theory will contain a set of effective operators whose coefficients describe the leading top-mass dependence in the large M_t limit, as illustrate in Fig. 1.

3 Extracting M_t from flavour data

When searching for new physics, it is customary to determine the four independent CKM parameters from tree-level observables, which are presumed to be well described by the SM, and then use this determination to predict loop processes, which are expected to hide new effects beyond the SM.

In ref. [6], we took a different perspective: we have assumed the SM to be exactly valid and we have extracted M_t from flavour processes. We have then

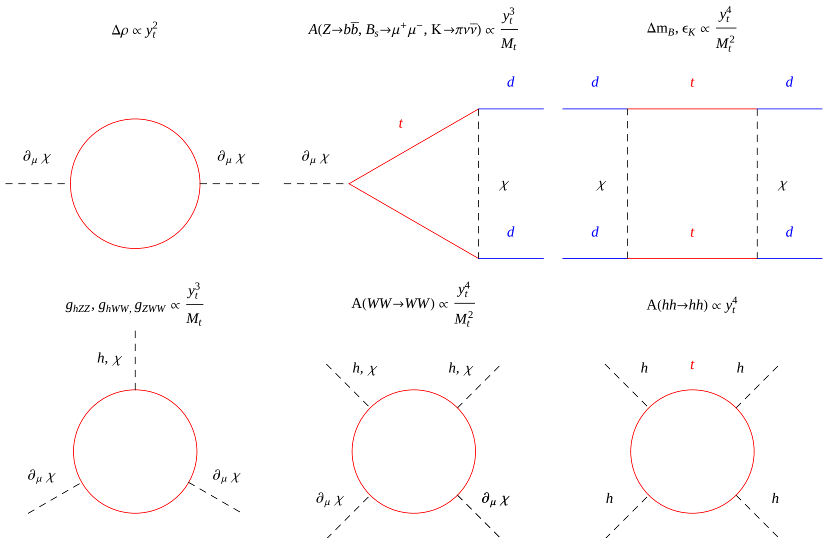

Figure 1: *Feynman diagrams illustrating the effective operators generated by integrating out the top quark. Also shown is the power counting estimate of their sensitivity to the top mass. Dashed lines denote the Higgs boson (h) or the Goldstones (χ); solid lines denote the quarks.*

fixed the four CKM parameters from the most precise measurements that do not depend on M_t, even if they arise at loop level:

$$|V_{us}|, \qquad |V_{cb}|, \qquad \gamma, \qquad \beta\,. \tag{2}$$

In principle, the extraction of $(M_t)_{\rm flavour}$ would require a global fit of all flavour observables in which the CKM parameters and the top mass are allowed to float independently. However, in practice, our procedure of fixing the CKM parameters in eq. (2) from processes that are insensitive to M_t and then determine M_t from the remaining observables is perfectly adequate and leads to results identical to those from a global fit. Actually, as shown in fig. 2, the determination of M_t is dominated by Δm_{B_s}, which depends on the CKM parameters only through the combination $|V_{ts}V_{tb}^*|$ which is equal to $|V_{cb}|$, up to a dependence on the angles γ and β suppressed by two powers of λ. This means that essentially $|V_{cb}|$ alone drives the error on the determination of M_t attributable to CKM

Observable	Now (2015)		Error 2020		Error 2025	
M_W(GeV)	80.385(15)	[9]	8	[7]	5	[10]
$\sin^2\theta_{\rm W}$	0.23116(13)	[9]	13	[7]	1.3	[7]
$\alpha_{\rm em}^{-1}(M_Z)$	128.952(13)	[9]	–		–	
$\alpha_s(M_Z)$	0.1184(7)	[9]	7	[7]	7	[7]
m_{B_s}(MeV)	5366.8(2)	[9]	–		–	
Δm_{B_s}(ps^{-1})	17.757(21)	[11]	–		–	
τ_H^s(ps)	1.607(10)	[11]	–		–	
$\lvert V_{cb}\rvert \times 10^3$	40.9(11)	[12]	4	[13, 14]	3	[13, 14]
$\mathcal{B}(B_s \to \mu^+\mu^-) \times 10^9$	2.8(7)	[11]	3	[13, 14]	1.3	[13, 14]
η_B	0.55(1)	[15]	0.5	[16]	0.2	[16]
f_{B_s}(MeV)	226(5)	[12]	2	[13]	1	[13]
$\hat{B}_{B_s}$	1.33(6)	[12]	2	[13]	0.7	[13]

Table 1: *Present values and future uncertainties for the most relevant quantities of our analysis. In the predictions for future errors we use the symbol "–" when no significant improvement is expected.*

elements, while the less precisely known parameters γ and β play only a minor role. Moreover, $B_s \to \mu^+\mu^-$ will soon become an equally important process for the determination of M_t and its CKM dependence, as in the case of Δm_{B_s}, is given by $|V_{ts}V_{tb}^*|$. So our conclusion that $|V_{cb}|$ is the most important CKM parameter for M_t extraction is likely to hold true even after future theoretical and experimental improvements. Let us turn now to discuss our forecast for the future of M_t determinations from flavour processes focusing on Δm_{B_s} and $B_s \to \mu^+\mu^-$.

Δm_{B_s}

The mass differences of the $B^0_{s,d}$–$\bar{B}^0_{s,d}$ systems in the SM can be written as [17]

$$\Delta m_{B_q} = \frac{G_F^2}{6\pi^2} m_{B_q} M_W^2 \hat{B}_{B_q} f_{B_q}^2 \eta_B S_0(x_t) |V_{tq}V_{tb}^*|^2 , \qquad q = d, s , \tag{3}$$

where η_B accounts for NLO QCD corrections. The LO loop function $S_0(x_t)$ depends on $x_t = 2y_t^2/g_2^2$, where g_2 is the coupling of the SM gauge group $SU(2)_L$ and y_t is the top-Yukawa coupling.

From eq. (3) we obtain the following value for Δm_{B_s}

$$\Delta m_{B_s} = \frac{16.9 \pm 1.4}{\text{ps}} \left(\frac{\sqrt{\hat{B}_{B_s}} f_{B_s}}{261\,\text{MeV}} \right)^2 \left(\frac{M_t}{173.34\,\text{GeV}} \right)^{1.52} \left(\frac{|V_{ts} V_{tb}^*|}{0.0401} \right)^2 \left(\frac{\eta_B}{0.55} \right) . \tag{4}$$

Matching this expression with the measurement of Δm_{B_s} reported in table 1, we find

$$(M_t)_{\Delta m_{B_s}} = (179.3 \pm 9.7)\ \text{GeV} . \tag{5}$$

Assuming the expected improvements by about 2020 and 2025, see table 1, we have [6]

$$\delta(M_t)_{\Delta m_{B_s}} \approx \left\{ \begin{array}{ll} \pm 3.6\ \text{GeV} & (2020) \\ \pm 2.1\ \text{GeV} & (2025) \end{array} \right. . \tag{6}$$

in good agreement with our numerical results.

$B_s \to \mu^+ \mu^-$

The SM prediction for $\text{BR}(B_s \to \mu^+\mu^-)$, which accounts for NNLO QCD and NLO electroweak corrections [18] reads

$$\text{BR}(B_s \to \mu^+\mu^-) = (3.33 \pm 0.05) \times 10^{-9}\, R_{t\alpha}\, R_s\,, \tag{7}$$

where $R_{t\alpha}$ and R_s are given by

$$R_{t\alpha} = \left(\frac{\alpha_s(M_Z)}{0.1184} \right)^{-0.18} \left(\frac{M_t}{173.34\,\text{GeV}} \right)^{3.06} , \tag{8}$$

$$R_s = \left(\frac{f_{B_s}}{226\,\text{MeV}} \right)^2 \left(\frac{|V_{cb}|}{0.0409} \right)^2 \left(\frac{|V_{ts} V_{tb}^*/V_{cb}|}{0.980} \right)^2 \frac{\tau_H^s}{1.607\,\text{ps}} , \tag{9}$$

where the uncertainty comes mostly from V_{cb} and f_{B_s}. Comparing the experimental result for $\text{BR}(B_s \to \mu^+\mu^-)$ quoted in table 1 with eq. (7), we end up with the following prediction for M_t [6]

$$(M_t)_{B_s \to \mu\mu} = (163.8 \pm 14.7)\ \text{GeV}. \tag{10}$$

On the other hand, assuming the expected improvements of table 1, we have [6]

$$\delta(M_t)_{B_s \to \mu\mu} \approx \left\{ \begin{array}{ll} \pm 5.3\ \text{GeV} & (2020) \\ \pm 2.4\ \text{GeV} & (2025) \end{array} \right. . \tag{11}$$

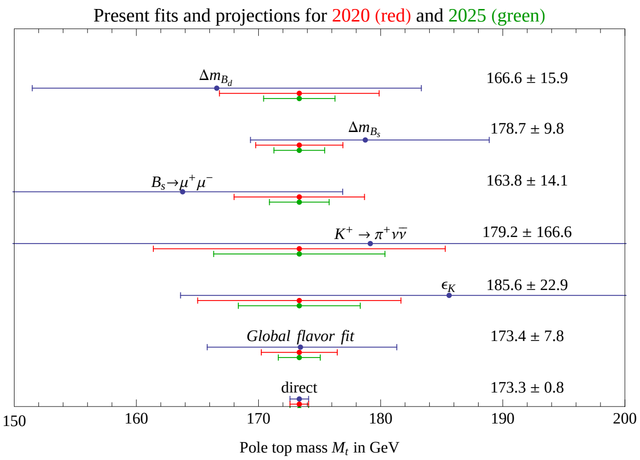

Figure 2: *Summary of present and future determinations of M_t from flavour data. For future projections, we have fixed the central value of M_t to the present direct measurement.*

4 Extracting M_t from electroweak precision data

Electroweak observables depend on the top mass (and on the Higgs mass) only through the $\varepsilon_1, \varepsilon_2, \varepsilon_3$ parameters that describe corrections to the tree-level propagators of the weak gauge bosons, and through the ε_b parameter that describes corrections to the $Zb\bar{b}$ vertex [19].

The measurement of M_W plays the key role, since we find $\delta M_t/M_t = 69\,\delta M_W/M_W$ [6]. This means that measuring M_W with a precision of 8 MeV (as foreseeable after combination of the full LHC dataset [7]) can lead to a determination of M_t within about 1.2 GeV [6].

5 Conclusions

In ref. [6], we have analysed indirect determinations of the top quark mass M_t by means of flavour and electroweak observables.

Among flavour processes, Δm_{B_s} and $B_s \to \mu^+\mu^-$ provide the best probe of M_t. Δm_{B_s} and $B_s \to \mu^+\mu^-$ require only V_{cb} as CKM input and, combined with a determination of V_{cb} and the lattice parameters $\hat{B}^{1/2} f_{B_s}$ and f_{B_s}, are sufficient to extract a fairly accurate estimate of the M_t determination from flavour physics. Our results are summarised in fig. 2: at present flavour data determine $M_t = (173.4 \pm 7.8)$ GeV and we have estimated that the uncertainty on M_t can be brought down to 3 GeV by 2020 and to 1.7 GeV by 2025 [6].

On the other hand, electroweak data, at present, determine $M_t = (177.0 \pm 2.6)$ GeV [6]. A more precise measurement of M_W is the key player for an improved determination of M_t from electroweak observables. As experiments at the LHC are expected to reduce the uncertainty on M_W to about 8 MeV [7], it is foreseeable that electroweak physics will determine M_t with a precision of about 1.2 GeV [6].

In the future, a global fit of all indirect determinations of M_t, from both electroweak and flavour data, will provide significant information. Even if indirect measurements do not surpass direct determinations in precision, the comparison between indirect and direct analyses will carry essential information, especially in view of the theoretical ambiguities in the extraction of M_t from collider experiments.

References

1. G. Degrassi *et al.*, JHEP 1208 (2012) 098.
2. J. R. Espinosa *et al.*, JHEP 1509 (2015) 174.
3. [ATLAS and CDF and CMS and D0 Collaborations], arXiv:1403.4427 [hep-ex].
4. A. Juste *et al.*, Eur. Phys. J. C 74 (2014) 10, 3119.
5. K. Agashe *et al.* [Top Quark Working Group Collaboration], arXiv:1311.2028 [hep-ph].
6. G. F. Giudice, P. Paradisi and A. Strumia, JHEP 1511 (2015) 192.
7. Gfitter Group Collaboration, Eur. Phys. J. C 74 (2014) 3046.
8. R. Barbieri, M. Beccaria, P. Ciafaloni, G. Curci and A. Vicere, Phys. Lett. B 288 (1992) 95.
9. Particle Data Group Collaboration, Chin. Phys. C 38 (2014) 090001.

10. H. Baer *et al.*, arXiv:1306.6352 [hep-ph].

11. Y. Amhis *et al.* [Heavy Flavor Averaging Group (HFAG) Collaboration], arXiv:1412.7515 [hep-ex].

12. G. Martinelli, talk at the EPS 2015 conference and UTfit website.

13. A. Andreazza *et al.*, Frascati Phys. Ser. 60 (2015) 1.

14. T. Aushev *et al.*, arXiv:1002.5012 [hep-ex].

15. A. J. Buras, M. Jamin and P. H. Weisz, Nucl. Phys. B 347 (1990) 491;

16. M. Gorbahn et al., work in progress.

17. G. Buchalla, A. J. Buras and M. E. Lautenbacher, Rev. Mod. Phys. 68 (1996) 1125.

18. C. Bobeth *et al.*, Phys. Rev. Lett. 112 (2014) 101801.

19. G. Altarelli *et al.*, Nucl. Phys. B 369 (1992) 3; Nucl. Phys. B 405 (1993) 3.

TOP QUARK PHYSICS AT LINEAR COLLIDERS

Roman Pöschl
CNRS/IN2P3/LAL

Abstract

Top quark production in the process $e^+e^- \to t\bar{t}$ at a future linear electron positron collider is an essential pillar of the physics programme that will be carried out with such a machine. For the first time it will be possible to study top quark pair production through electro-weak processes. This offers exciting possibilities to make high precision measurements at the top-pair threshold and, at higher energies, to determine the electroweak couplings of the top quark in an unambiguous way.

1 Introduction

With the discovery of the Higgs Boson with a mass of $m_h \approx 125$ GeV by the LHC, the Standard Model of particle physics is complete. The Standard Model is a quantum field theory featuring $SU(2)_L \times U(1)_Y$ symmetry. This symmetry is spontaneously broken at the electroweak scale leading to non-zero masses of the gauge bosons and the fermions. The breaking of the symmetry is associated to a scalar field that develops a non-zero vacuum expectation value. Today it is however unknown what is at the origin of the symmetry breaking and what generates the detailed shape of the Higgs potential. A special role in the search for physics beyond the Standard Model will be played by the top quark, or t quark. With a mass of about $m_t \approx 173$ GeV [1)], it is the heaviest known elementary particle today and tantalisingly close to the electroweak symmetry breaking scale. Text passages in the following summary are largely inspired by Refs. [2)] and [3)].

2 The top quark

A linear electron positron collider such as ILC [4)] or CLIC [5)], briefly named LC hereafter, would be the first machine at which the t quark is studied using a precisely defined leptonic initial state. Therefore, individual events can be analysed in more detail. It also changes the production mechanism for t quark pairs from the strong to the electro-weak interactions, which are a step closer to the phenomena of electro-weak symmetry breaking. Finally, this change brings into play new experimental observables – weak interaction polarisation and parity asymmetries – that are very sensitive to the coupling of the t quark to possible new interactions. It is very possible that, while the t quark might respect Standard Model expectations at the LHC, it will break those expectations when studied at the LC. Unless stated otherwise, all results presented in the following are based on full simulation studies of the LC detectors ILD and CLIC-detector.

2.1 $e^+e^- \to t\bar{t}$ at threshold

One of the unique capabilities of an e^+e^- linear collider is the ability to carry out cross section measurements at particle production thresholds. The accurately known and readily variable beam energy of a LC makes it possible to measure the shape of the cross section at any pair-production threshold within its range. Because of the leptonic initial state, it is also possible to tune the initial spin state, giving additional options for precision threshold measurements. The $t\bar{t}$ pair production threshold at a centre-of- mass energy $\sqrt{s} \approx 2m_t$ allows for precise measurements of the t quark mass m_t as well as the t quark total

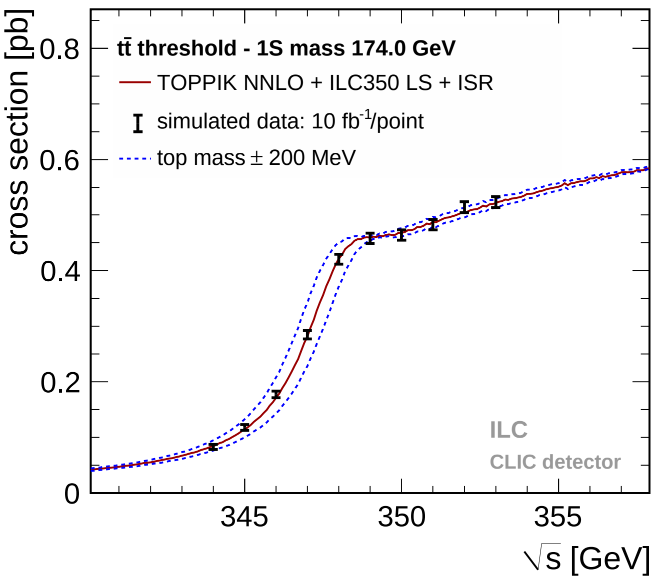

Figure 1: *Result of a simulation study of a top threshold scan that includes the luminosity spectrum of the ILC beams. The figure is taken from* [6]

width Γ_t and the QCD coupling α_s. Because the top is a spin-$\frac{1}{2}$ fermion, the $t\bar{t}$ pair is produced in an angular S-wave state. This leads to a clearly visible rise of the cross section even when folded with e.g. the ILC luminosity spectrum as shown in Fig. 1. From this rise the t quark mass can be extracted to a statistical precision of about 25 MeV, which increases to 50 MeV once theoretical uncertainties are taken into account [6].

A simultaneous fit may allow to extract simultaneously the t-quark mass, its width Γ_t and the top-Yukawa coupling y_t. In this case the expected statistical accuracies for 200 fb^{-1} of integrated luminosity are: $\delta m_t \approx 17$ MeV, $\delta\Gamma_t \approx 26$ MeV and $\delta y_t = 4.2\%$ [7]. The measurement of the latter becomes possible since the virtual exchange of the Standard Model Higgs boson enhances the cross section at threshold by about 9% The dependence of the t-quark cross section shape on the t-quark mass and interactions is computable to high precision with full control over the renormalisation scheme dependence of the top mass parameter. A recent publication [8] shows that the 1S mass as resulting from the described analysis can be translated to, e.g., the $\overline{\mathrm{MS}}$ mass, typically used in theoretical calculations, to a precision of about 10 MeV.

2.2 Open top production

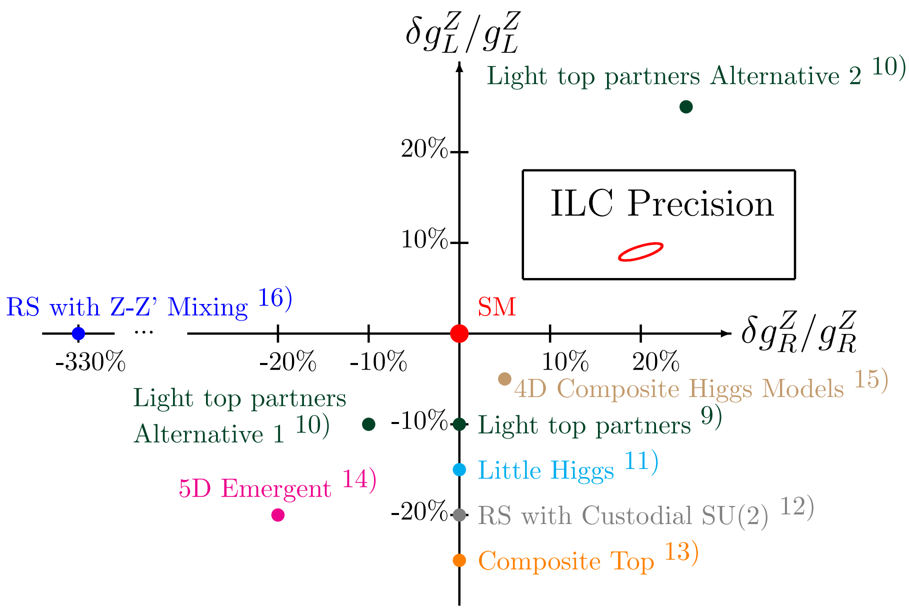

Figure 2: *Predictions of several models that incorporate Randall-Sundrum (RS) models and/or compositeness or Little Higgs models on the deviations of the left- and right-handed couplings of the t quark to the Z^0 boson. The ellipse in the frame in the upper right corner indicates the precision that can be expected for the ILC running at a centre-of-mass energy of $\sqrt{s} = 500$ GeV after having accumulated $\mathcal{L} = 500\,\mathrm{fb}^{-1}$ of integrated luminosity shared equally between the beam polarisations $\mathcal{P}_{e^-}, \mathcal{P}_{e^+} = \pm 0.8, \mp 0.3$. The original version of this figure can be found in [17].*

Refs. [18, 3] report on the determination of CP conserving form factors and couplings based on a full simulation study of the reaction $e^+e^- \to t\bar{t}$ at a centre-of-mass energy of $\sqrt{s} = 500$ GeV with 80% polarised electron beams and 30% polarised positron beams. The unique feature of linear colliders to provide polarised beams allow for a largely unbiased disentangling of the individual *L*eft and *R*ight handed couplings of the t quark to the Z^0 boson and the photon, $g^{\gamma,Z}_{L,R}$, or equivalently of the form factors $F^{\gamma,Z}_{(1,2),(V,A)}$. These quantities can be measured at the sub-percent level at a LC. This is, when referring to the results in [19, 20], considerably better than it will be possible at the LHC even with an integrated luminosity of $\mathcal{L} = 3000\,\mathrm{fb}^{-1}$. The improving analyses of the LHC experiments, as e.g. [21], will however be observed with great interest.

Beam polarisation is a critical asset for the high precision measurements of the electroweak t quark couplings. Experimental and theoretical effects manifest themselves differently for different beam polarisations. It seems to be that the configuration positive electron-beam polarisation is more benign in both experimental aspects, due to the suppression of migrations in the polar angle spectrum of the final state t quark, see e.g. [18, 3], and theoretical aspects due to the somewhat simpler structure of higher order electroweak corrections [22]. It is intuitively clear that the described facts would greatly support the discovery of effects due to new physics. The precision, as expected for a LC, would allow for the verification of a great number of models for physics beyond the Standard Model. Examples for these models are extra dimensions and compositeness, see Fig. 2. The current results constitute therefore a perfect basis for discussions with theoretical groups. Note at this point that the community has adopted a running scenario for the ILC that would yield up to eight times more luminosity [23] than has been assumed so far. Moreover, it can be expected that the event reconstruction will be improved by e.g. the measurement of the b quark charge. Already from the achieved precision it is mandatory that experiment and theoretical systematic uncertainties are controlled well below the 1% level. A study of systematic errors will therefore become very important and is addressed in ongoing studies.

Finally, the study presented in [22], based on generated events, suggests that, by exploiting the polarisation of the final state t quarks, a simultaneous extraction of all anomalous top form factors, including the CP violating $F^{\gamma,Z}_{2,A}$, to a precision below the percent level is feasible. A detailed comparison between the advantages and drawbacks of the method applied there and the method presented in [3] is left for a future study.

3 Summary and outlook

Parameter	Initial Phase	Lumi-Upgrade	units	ref.
m_t	50	50	MeV (m_t(1S))	6)
Γ_t	60	60	MeV	7)
g_L^γ	0.8	0.6	%	3)
g_R^γ	0.8	0.6	%	3)
g_L^Z	1.0	0.6	%	3)
g_R^Z	2.5	1.0	%	3)
F_2^γ	0.001	0.001	absolute	3)
F_2^Z	0.002	0.002	absolute	3)

Table 1: Projected accuracies for top physics parameters at the two stages of the ILC program proposed in the report of the Joint Working Group on ILC Beam Parameters [23]. The relevant running phases for these projections are an initial phase with 500 fb^{-1} at 500 GeV, 200 fb^{-1} at 350 GeV, and a luminosity-upgraded phase with an additional 3500 fb^{-1} at 500 GeV . Initial-state polarisations are taken according to the prescriptions of [23]. Uncertainties are listed as 1σ errors computed cumulatively at each stage of the program. These estimated errors include both statistical uncertainties and theoretical and experimental systematic uncertainties. The table has been extracted from [2].

At the example of the ILC the results discussed in the previous sections are summarised in Table 1. These are all based on full simulation studies of linear collider detectors and prove the outstanding potential for top physics at a LC. The studies at threshold and in the continuum have reached a level of maturity and precision that now the experimental sensitivity to higher-order effects (QCD and electroweak) has to be studied as well as the impact of issues arising from the full six-fermion final state. The results presented at the conference have triggered already considerable efforts on theoretical and experimental side that will be interesting to follow in the near future.

References

1. **Particle Data Group**, K. Olive *et al.*, "Review of Particle Physics" *Chin.Phys.* **C38** (2014) 090001.

2. K. Fujii *et al.*, "Physics Case for the International Linear Collider" `arXiv:1506.05992 [hep-ex]`.

3. M. S. Amjad *et al.*, "A precise characterisation of the top quark electro-weak vertices at the ILC" *accepted by European Journal of Physics C* (2015) , `arXiv:1505.06020 [hep-ex]`.

4. T. Behnke *et al.*, "ILC TDR and DBD" *ILC-Report-2013-040* . `http://www.linearcollider.org/ILC/Publications/Technical-Design-Report`.

5. P. Lebrun, L. Linssen, A. Lucaci-Timoce, D. Schulte, F. Simon, *et al.*, "The CLIC Programme: Towards a Staged e+e- Linear Collider Exploring the Terascale : CLIC Conceptual Design Report" `arXiv:1209.2543 [physics.ins-det]`.

6. K. Seidel, F. Simon, M. Tesar, and S. Poss, "Top quark mass measurements at and above threshold at CLIC" *arXiv:1303.3758 [hep-ex]* (2013) , `arXiv:1303.3758 [hep-ex]`.

7. T. Horiguchi, A. Ishikawa, T. Suehara, K. Fujii, Y. Sumino, *et al.*, "Study of top quark pair production near threshold at the ILC" `arXiv:1310.0563 [hep-ex]`.

8. P. Marquard, A. V. Smirnov, V. A. Smirnov, and M. Steinhauser, "Quark Mass Relations to Four-Loop Order in Perturbative QCD" *Phys.Rev.Lett.* **114** (2015) no. 14, 142002, `arXiv:1502.01030 [hep-ph]`.

9. C. Grojean, O. Matsedonskyi, and G. Panico, "Light top partners and precision physics" `arXiv:1306.4655 [hep-ph]`.

10. G. Panico, A. Wulzer, private communication, Possible deviations of couplings in framework described in [9].

11. C. Berger, M. Perelstein, and F. Petriello, "Top quark properties in little Higgs models" `arXiv:hep-ph/0512053 [hep-ph]`.

12. M. S. Carena, E. Ponton, J. Santiago, and C. E. Wagner, "Light Kaluza Klein States in Randall-Sundrum Models with Custodial SU(2)" *Nucl.Phys.* **B759** (2006) 202–227, `arXiv:hep-ph/0607106 [hep-ph]`.

13. A. Pomarol and J. Serra, "Top Quark Compositeness: Feasibility and Implications" *Phys.Rev.* **D78** (2008) 074026, `arXiv:0806.3247 [hep-ph]`.

14. Y. Cui, T. Gherghetta, and J. Stokes, "Fermion Masses in Emergent Electroweak Symmetry Breaking" *JHEP* **1012** (2010) 075, `arXiv:1006.3322 [hep-ph]`.

15. D. Barducci, S. De Curtis, S. Moretti, and G. M. Pruna, "Top pair production at a future e^+e^- machine in a composite Higgs scenario" `arXiv:1504.05407 [hep-ph]`.

16. A. Djouadi, G. Moreau, and F. Richard, "Resolving the A(FB)**b puzzle in an extra dimensional model with an extended gauge structure" *Nucl.Phys.* **B773** (2007) 43–64, `arXiv:hep-ph/0610173 [hep-ph]`.

17. F. Richard, "Present and future constraints on top EW couplings" `arXiv:1403.2893 [hep-ph]`.

18. M. Amjad, M. Boronat, T. Frisson, I. Garcia, R. Poschl, *et al.*, "A precise determination of top quark electro-weak couplings at the ILC operating at $\sqrt{s} = 500$ GeV" `arXiv:1307.8102 [hep-ex]`.

19. U. Baur, A. Juste, L. Orr, and D. Rainwater, "Probing electroweak top quark couplings at hadron colliders" *Phys.Rev.* **D71** (2005) 054013, `arXiv:hep-ph/0412021 [hep-ph]`.

20. U. Baur, A. Juste, D. Rainwater, and L. Orr, "Improved measurement of ttZ couplings at the CERN LHC" *Phys.Rev.* **D73** (2006) 034016, `arXiv:hep-ph/0512262 [hep-ph]`.

21. **CMS**, V. Khachatryan *et al.*, "Observation of top quark pairs produced in association with a vector boson in pp collisions at sqrt(s) = 8 TeV" `arXiv:1510.01131 [hep-ex]`.

22. P. Khiem, E. Kou, Y. Kurihara, and F. L. Diberder, "Probing New Physics using top quark polarization in the $e^+e^- \to t\bar{t}$ process at future Linear Colliders" `arXiv:1503.04247 [hep-ph]`.

23. T. Barklow, J. Brau, K. Fujii, J. Gao, J. List, N. Walker, and K. Yokoya, "ILC Operating Scenarios" `arXiv:1506.07830 [hep-ex]`.

ELECTROWEAK CORRECTIONS TO TOP-PAIR PRODUCTION AT LEPTON COLLIDERS

P.H. Khiem
Deutsches Elektronen-Synchrotron (DESY),
Platanenallee 6, D-15738 Zeuthen, Germany
E. Kou & F. Le Diberder
Laboratoire de l'Accélérateur Linéaire,
IN2P3/CNRS et Université Paris-Sud 11,
B. P. 34, F-91898 Orsay Cedex, France
Y. Kurihara & N.M.U. Quach
High Energy Accelerator Research Organization (KEK),
1-1 Oho, Tsukuba, Ibaraki 305-0801, Japan

Abstract

We investigate the sensitivity to new physics of the process $e^+e^- \to t\bar{t}$ when the top polarization is analyzed using the leptonic final states $e^+e^- \to t\ \bar{t} \to l^+l^-b\ \bar{b}\ \nu_l\bar{\nu}_l$. The matrix element method is applied for the statistical analysis. In this talk, we presented various tests of LO analysis, of the 6 fermion background and of the GRACE $t\bar{t}$ events including NLO contribution.

1 Introduction

We discuss in this talk the use of the polarization of the top and anti-top pairs produced from e^+e^- collisions. The top quark, which does not hadronize due to its short life time, is the only quark whose spin polarization can be exploited. The study of polarization allows us to probe the interactions between the top quark and the gauge bosons γ and Z or any new particles beyond the SM.

The top quark polarization pattern can be reached by using the angular distributions of the top quark decay products. In the previous studies using the semi-leptonic final states [1)], it has been found that the so-called form factor of $t\bar{t}V$ ($V = \gamma, Z$) can be measured at a per-mill level at ILC ($\sqrt{s} = 500$ GeV). While this study has been done at the Leading Order (LO) level, it has been pointed out that then, the large electroweak corrections (∼5 % in cross-section), which are only known at the Next-to-Leading order (NLO), may hamper the analysis.

In this study, we use the fully leptonic final state, $e^+e^- \to t\,\bar{t} \to l^+l^- b\,\bar{b}\,\nu_l\bar{\nu}_l$ ($l^+l^- = e^+e^-, e^+\mu^-, \mu^+e^-, \mu^+\mu^-$). This talk includes the continuation of our previous work [2)] where we applied the matrix element method to determine the deviation from the LO SM values (we refer to this as the bias method in the following). The main findings of [2)] are:

1. The kinematics of fully leptonic final state can be accurately reconstructed (so far, the detector effects have not been studied including in the new analysis presented in this talk).
2. The expected statistical uncertainties at the LO level are comparable to the semi-leptonic final state analysis.
3. Multi-parameter fits can be achieved which are beyond the reach of the (current) semi-leptonic analysis.
4. Beam polarization is not essential at the LO level.
5. On the other hand, the electroweak NLO contributions show a very strong correlation to the beam polarization and it can be instrumental to analyze the NLO effects.

In this work, we

1. Quantify the impact on the analysis of the errors in the kinematical reconstruction coming form the top's and W widths effects, and wrong b-jet assignment.
2. Estimate the irreducible background coming from the 6-fermion finals state $e^+e^- \to l^+l^- b\;\bar{b}\;\nu_l\bar{\nu}_l$.
3. The first analysis of the GRACE NLO events by using the bias method.

2 Estimating the errors coming from the imperfect kinematical reconstruction

We first estimate the effect of the top and W width effects which can potentially worsen the kinematical reconstruction. As an example, we choose the form factor $r = \mathcal{R}\text{e}\ \delta F_{2V}^{Z}$ (see [2] for the definition). This choice is interesting since the azimuthal angles of the leptons play an important role in the measurement. Being two Lorentz boosts away from the ILC frame, the kinematical reconstruction of these angles is the most fragile: it depends critically on both the top's and both the W's to be close to onshell. It is thus expected that the width effects observed for this variable will be among the most prominent ones.

The measurement of r is performed through the minimization of the $\chi^2(r)$ function described in [2]:

$$\chi^2(r) = -2\left(\sum_{\text{event}=1}^{N_{\text{exp}}} \ln|\mathcal{M}_{\text{event}}(r)|^2 - N_{\text{th}}(r)\right) \tag{1}$$

where $\mathcal{M}_{\text{event}}(r)$ is the matrix element and the $N_{\text{th}}(r)$ is the SM prediction at LO, where the real part of the F_{2V}^{Z} form factor can depart from its SM value by r. By using 10^4 GRACE LO events [3], we obtained the bias and its statistical uncertainty due to badly reconstructed kinematics caused by the widths of the top and W as

$$\delta r = -0.004 \pm 0.001 \tag{2}$$

Although, optimization should be done after all the other effects are included, we found that this bias can be strongly reduced by imposing a cut on the quality of the kinematical reconstruction, keeping 90% of the events.

Next we assess the errors induced by the wrong b-assignment. In the absence of b-jet charge tagging, the kinematical reconstruction must consider both assignments, the correct one and the inverted one. For most of the events the inverted assignment leads to a very bad kinematical reconstruction and is thus harmless. However, for 5% of the events the inverted assignment leads to a better kinematical reconstruction than the correct one. For these events the angular information is meaningless, and induces a bias. Without any cut, the bias is found to be $\delta r = -0.009$, even larger than the statistical accuracy. In this case, it turned out that the previous quality cut does not improve the result while by performing the fit with masses free to vary, the inverted assignment is preferred for only 2% of the events. In that case, by keeping 90% of the events as before, the bias is reduced down to $\delta r = -0.002$, while the sample now contains only 0.3% of events with a wrong b-jet assignment.

3 Irreducible background

The final state $e^+e^- \rightarrow l^+l^-b\ \bar{b}\ \nu_l\bar{\nu}_l$ can be reached without involving the $e^+e^- \rightarrow t\ \bar{t}$ pair production. Although the total cross section is only slightly affected by the numerous additional diagram contributions (the $t\bar{t}$ pair cross section accounts for $\sim 95\%$ of the total cross section) interference effects should be scrutinize since they could be much larger and they may distort the distribution of events in phase space, and thus induce a potentially significant bias in the measurement.

The study is performed using 10^5 GRACE 6-fermions (referred to as 6fLO-Data) events to which is applied the kinematical reconstruction with top's and W's masses free to vary, and taking into account wrongly assigned b-jets. To enhance the $t\bar{t}$ dominance, the previously defined 90% cut is applied and the reconstructed masses are requested to be within 10 GeV of the nominal masses of top and W, which reject and additional 6% of the events: finally 85% of the events of the initial sample are kept, among which 0.2% have a wrong b-jet assignment.

The fit performed on the truth kinematics yields $r = 0.0134 \pm 0.0022$ (a 6 sigma effect) thereby confirming the existence of a percent level bias, at truth level, within the 85% selection efficiency.

In conclusion, requesting an acceptable $t\bar{t}$ kinematical reconstruction ensures that the bias induced by the numerous non $t\bar{t}$ diagrams involved in the 6fLO-Data is at the level of the percent.

At this stage, owing to the percent level bias observed with a single parameter fit, it is relevant to perform a multi parameter fit . Using the set of 10 parameters used in [2], and keeping 85% of 10^4 events, the truth fit gives the values indicated in the first line of the table below; the second line gives the statistical uncertainties from the fit; the third line gives the shift observed with the reconstructed events.

$$\begin{bmatrix} \mathcal{R}\mathrm{e}\delta\tilde{F}^{\gamma}_{1V} & \mathcal{R}\mathrm{e}\delta\tilde{F}^{Z}_{1V} & \mathcal{R}\mathrm{e}\delta\tilde{F}^{\gamma}_{1A} & \mathcal{R}\mathrm{e}\delta\tilde{F}^{Z}_{1A} & \mathcal{R}\mathrm{e}\delta\tilde{F}^{\gamma}_{2V} & \mathcal{R}\mathrm{e}\delta\tilde{F}^{Z}_{2V} & \mathcal{R}\mathrm{e}\delta\tilde{F}^{\gamma}_{2A} & \mathcal{R}\mathrm{e}\delta\tilde{F}^{Z}_{2A} & \mathcal{I}\mathrm{m}\delta\tilde{F}^{\gamma}_{2A} & \mathcal{I}\mathrm{m}\delta\tilde{F}^{Z}_{2A} \\ -0.0039 & +0.0047 & -0.0097 & -0.0154 & +0.0030 & -0.0305 & -0.0068 & -0.0094 & +0.0183 & +0.0135 \\ 0.0062 & 0.0134 & 0.0097 & 0.0135 & 0.0204 & 0.0340 & 0.0114 & 0.0255 & 0.0185 & 0.0163 \\ -0.0008 & +0.0012 & -0.0019 & +0.0002 & -0.0041 & +0.0058 & -0.0005 & +0.0021 & -0.0039 & -0.0006 \end{bmatrix}$$

4 First analysis of the NLO effect

Next we investigate further beyond the tree level, namely including the one-loop electroweak corrections. It has been a long time since a large electroweak NLO correction for $e^+e^- \to t\bar{t}$ was recognized [4] and confirmed independently in [5]. However, this effect has not yet been taken into account for the top polarization study. The NLO corrections to the $e^+e^- \to t\bar{t}$ process are large: they amount to $\sim 5\%$ for the total cross section and $\sim 10\%$ for the forward-backward asymmetry, which is much larger than the foreseen experimental errors. Therefore, it is important to have good control of the NLO contribution by investigating the precise source of this large contributions and more importantly, by assessing the systematical uncertainties associated to it. Interestingly, we find in [2] that in the case of $e_L^- e_R^+$, the NLO contributions are negative (positive) for positive (negative) $\cos\theta$ while for $e_R^- e_L^+$, the NLO contributions are always positive. This kind of strong dependence on the kinematical variables can be most useful to investigate the NLO corrections in detail. Indeed, the top quark polarization analysis developed here may provide the best handle to control the NLO contributions.

The GRACE program [3] can provide the SM prediction for $e^+e^- \to t\bar{t}$ including the full one-loop electroweak corrections which contain 150 diagrams [6]. Recently the initial and the final state polarization as well as the decay of top quarks have been implemented into the GRACE program, which are used in our study.

NLO events are analyzed using the method applied in the previous sections: we use the true level LO amplitude and estimate the NLO contribution as a bias. The discussion is limited to the truth level, since it was shown previously that reconstruction effects have little impact.
By using 2.5×10^4 NLO GRACE events, one obtains:

$$r = -0.1070 \pm 0.0050 \tag{3}$$

that is to say a huge 21 sigma effect which utterly rules out SM-LO.

Performing the 10-parameter fit[1], one obtain the table below. The χ^2 with respect to SM is very large: $\chi^2 = 977$, and some large biases are observed,

[1]We removed some outliers events amounting to about 1 % of the NLO sample.

the most important one being for $\mathcal{R}\mathrm{e}\ \delta\tilde{F}_{2V}^{Z}$.

$$\begin{bmatrix} \mathcal{R}\mathrm{e}\delta\tilde{F}_{1V}^{\gamma} & \mathcal{R}\mathrm{e}\delta\tilde{F}_{1V}^{Z} & \mathcal{R}\mathrm{e}\delta\tilde{F}_{1A}^{\gamma} & \mathcal{R}\mathrm{e}\delta\tilde{F}_{1A}^{Z} & \mathcal{R}\mathrm{e}\delta\tilde{F}_{2V}^{\gamma} & \mathcal{R}\mathrm{e}\delta\tilde{F}_{2V}^{Z} & \mathcal{R}\mathrm{e}\delta\tilde{F}_{2A}^{\gamma} & \mathcal{R}\mathrm{e}\delta\tilde{F}_{2A}^{Z} & \mathcal{I}\mathrm{m}\delta\tilde{F}_{2A}^{\gamma} & \mathcal{I}\mathrm{m}\delta\tilde{F}_{2A}^{Z} \\ +0.0131 & -0.0094 & +0.0592 & +0.0924 & -0.0176 & +0.4416 & -0.0071 & +0.0916 & -0.0326 & +0.0243 \\ 0.0049 & 0.0105 & 0.0077 & 0.0108 & 0.0136 & 0.0262 & 0.0083 & 0.0211 & 0.0210 & 0.0133 \end{bmatrix}$$

A test of goodness of fit (not described here for brevity) shows that this 10 parameter fit is enable to reproduce the feature of the angular distributions that bear the imprint of the NLO corrections.

5 Conclusion

We have confirmed that the matrix element method developed in [2] can be reliably applied for the LO analysis. We have also shown that at the LO level, the wrong reconstruction effects are small, as far as top's and W's widths effects and improper b-jet assignment are concerned. The analysis of LO signal and background (i.e. 6 fermion final states) events validate the method since they do not exhibit large biases (and successfully pass the test of goodness of fit) by using the LO amplitudes as the truth level.

On the other hand, the NLO analysis reveals very large effects, much larger than the expected statistical uncertainties. Stated differently if we use the LO amplitude as reference, the NLO effects can not be absorbed into deviations of the form factors. Not only the observed deviations are large, but the test of goodness of fit fails utterly. If confirmed, this implies that the LO framework is not appropriate to search for new physics, since the latter would be hidden behind large biases: the overall credibility of the discovery of new physics would be severely hindered. One must move from the LO framework to the NLO framework, where the amplitude used in the analysis is the full NLO amplitude.

Our next step is to study the detector and hadronization+QCD effects which could be significant.

References

1. M. S. Amjad *et al.*, Eur. Phys. J. C **75** (2015) 10, 512.
2. P. H. Khiem, E. Kou, Y. Kurihara and F. Le Diberder, arXiv:1503.04247 [hep-ph].

3. F. Yuasa, J. Fujimoto, T. Ishikawa, M. Jimbo, T. Kaneko, K. Kato, S. Kawabata and T. Kon *et al.*, Prog. Theor. Phys. Suppl. **138** (2000) 18.

4. J. Fujimoto and Y. Shimizu, Mod. Phys. Lett. **3A** (1988) 581.

5. J. Fleischer, A. Leike, T. Riemann and A. Werthenbach, Eur. Phys. J. C **31** (2003) 37.

6. P. H. Khiem, J. Fujimoto, T. Ishikawa, T. Kaneko, K. Kato, Y. Kurihara, Y. Shimizu and T. Ueda, J.A.M. Vermaseren and Y. Yasui, Eur. Phys. J. C **73** (2013) 4, 2400.

NON-QCD CONTRIBUTIONS TO TOP-PAIR PRODUCTION NEAR THRESHOLD

Martin Beneke
Physik Department T31, James-Franck-Straße 1,
Technische Universität München, 85748 Garching, Germany

Andreas Maier
IPPP, Department of Physics,
University of Durham, DH1 3LE, United Kingdom

Jan Piclum
Albert Einstein Center for Fundamental Physics,
Institute for Theoretical Physics, Sidlerstrasse 5, 3012 Bern, Switzerland

Thomas Rauh
Physik Department T31, James-Franck-Straße 1,
Technische Universität München, 85748 Garching, Germany

Abstract

The threshold scan of top pair production at a future lepton collider allows to determine several Standard Model parameters with very high precision. The recent completion of the third-order QCD corrections to the inclusive top-pair production cross section demonstrated that strong dynamics are under control. We investigate effects from P-wave production and Higgs contributions at third order and from QED and the nonresonant production of the physical $W^+W^-b\bar{b}$ final state at first order. We discuss the sensitivity of the cross section to the top mass, width and Yukawa coupling as well as to the strong coupling.

1 Introduction

The top-quark mass is an important parameter for many observables in the Standard Model and beyond, including the stability of the vacuum, due to the often large radiative corrections involving virtual top quarks. Currently, the highest precision is achieved in the direct reconstruction of (anti-) top quarks from their decay products at the Tevatron and LHC with a total uncertainty of ±0.76 GeV [1]. However, this value is plagued by the lack of understanding of the precise relationship between the measured Monte Carlo mass and a "proper" mass definition from the theory point of view, which could add an additional uncertainty of the order of 1 GeV. This can be circumvented by determinations of the top-quark mass from the measurement of the total top pair production cross section in hadron collisions [2, 3] or indirectly, from flavour and electroweak precision observables [4]. The drawback is an increased uncertainty at the level of several GeV. A measurement of the top quark mass with an uncertainty substantially below ±1 GeV can be achieved by performing a threshold scan at a future lepton collider, which consists of the measurement of the total inclusive top pair production cross section for about ten center-of-mass energies near the production threshold $\sqrt{s} \sim 2m_t$ [5, 6, 7]. By comparison of the shape of the cross section with the theory prediction the top mass can be measured directly in a well-defined short-distance mass scheme and with very high accuracy. Furthermore the top width can be determined precisely and modifications of the top Yukawa coupling through new physics effects could possibly be detected. For this program it is crucial that the level of accuracy provided by a lepton collider is matched on the theory side. The recent completion of the QCD contributions up to NNNLO precision [8] showed that the theory uncertainty is now greatly reduced with respect to the NNLO predictions [9] and at the level of just $\pm3\%$. Thus non-QCD effects, which can affect the cross section by up to 10% [10], have now become the focus of further theoretical efforts. In the following we give a very brief outline of the special dynamics near the production threshold, then discuss various non-QCD effects and present numerical results for the cross section and its sensitivity to different input parameters.

Threshold dynamics. In the vicinity of the top-pair production threshold $\sqrt{s} \sim 2m_t$ the tops are nonrelativistic with a small velocity of the order of the strong coupling constant $v \sim \alpha_s$. Thus the top mass m_t, momentum $m_t v$ and energy $m_t v^2$ are vastly different and set the relevant scales, denoted as the hard, soft and ultrasoft scale. In addition terms scaling like $(\alpha_s/v)^n$ appear which are not suppressed in the nonrelativistic counting and indicate the breakdown of conventional perturbation theory. Hence these so-called Coulomb singularities have to be resummed to all orders. This can be achieved in the effective field theory of potential non-relativistic QCD (PNRQCD), which is obtained by subsequently integrating out the hard and soft scale. A distinguishing aspect of PNRQCD is that the LO Lagrangian does not describe free fields, but nonrelativistic top fields which are interacting through an instantaneous colour Coulomb potential. Consequently the leading order Coulomb interaction is treated nonperturbatively while higher order corrections can be obtained systematically by expanding in α_s and v around the resummed solution. For more details on the EFT framework we refer to the literature [11], where everything required for the NNNLO cross section is described. The cross section, normalized as usual to the muon pair production cross section, can be expressed using the optical theorem as

$$R(s) \equiv \frac{\sigma(e^+e^- \to \gamma^*, Z^* \to t\bar{t}X)}{\sigma_0(e^+e^- \to \mu^+\mu^-)} = 12\pi\, f(s)\; \mathrm{Im}\left[\Pi^{(v)}(s)\right], \tag{1}$$

where $f(s) = e_t^2 + \ldots$ is a prefactor depending on the top couplings to photons and Z bosons and kinematic variables. The vector polarization function $\Pi^{(v)}(s)$ has the form

$$\Pi^{(v)}(s) = \frac{3}{2m_t^2} c_v \left[c_v - \frac{E}{m_t}\left(c_v + \frac{d_v}{3}\right)\right] G(E) + \ldots, \tag{2}$$

where $E = \sqrt{s} - 2m_t$ is the energy of the top pair, c_v, d_v are hard matching coefficients for the external vector current, and the Green function $G(E)$ describes the propagation of the top pair within PNRQCD, subject to interactions from various potentials and the exchange of ultrasoft gluons. The imaginary part of the vector polarization function is known to third order in the reorganized and resummed expansion in α_s and v, see Figure 1 of [8].

2 Non-QCD and P-wave contribution

In the following we discuss further effects not contained in the QCD vector polarization function, which are parametrically or numerically of similar size as the remaining $\pm 3\%$ theoretical uncertainty on the contribution from $\Pi^{(v)}(s)$.

P-wave contribution. In addition to the dominant contribution from the vector current as described above, the top pair can also be produced through

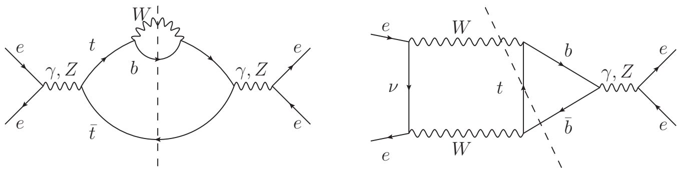

Figure 1: Sample diagrams for the nonresonant production of the $W^+W^-b\bar{b}$ final state.

an axial-vector current from the exchange of a s-channel Z boson. This yields top pairs in a P-wave state which are suppressed by a factor v^2 with respect to the leading S-wave production and thus constitutes a NNLO effect. The full contribution up to NNNLO has been computed and discussed in [12]. This correction is only of the order of 1% relative to the third-order S-wave QCD result [8], and is included in what is referred to as the QCD prediction below.

Higgs effects. In the following we consider only Higgs effects that come from the top Yukawa coupling. Contributions involving the coupling to gauge bosons will be regarded as general electroweak effects and treated separately. The former manifest themselves as corrections to the hard matching coefficient c_v of the external vector current and in a local contribution to the $t\bar{t}$ potential.[1] The pure Higgs contribution to c_v has been computed in [13, 14, 15] and mixed Higgs and QCD corrections in [15]. The insertion of the Higgs potential into the Green function was calculated recently in [10], such that the full NNNLO Higgs correction to the cross section is now known.

Nonresonant effects. Since the cross section near threshold is also sensitive to the small ultrasoft scale and the top width is of the same order, the narrow-width approximation cannot be used here to factorize the production and decay of the top pair. This implies that, assuming $V_{tb} = 1$, the physical final state is $W^+W^-b\bar{b}$. It is dominantly produced through a resonant top pair, where the replacement $E \to E + i\Gamma_t$ accounts for the effects of top instability [18]. At higher orders in the nonrelativistic counting the $W^+W^-b\bar{b}$ final state can

[1]Earlier work included the potential induced by Higgs exchange in the form of a Yukawa potential [16, 17]. Consistency with the implementation of the matching coefficients requires that the Yukawa potential is approximated by a local potential when the Higgs mass is much larger than the typical potential momentum exchange, and treated as a perturbation.

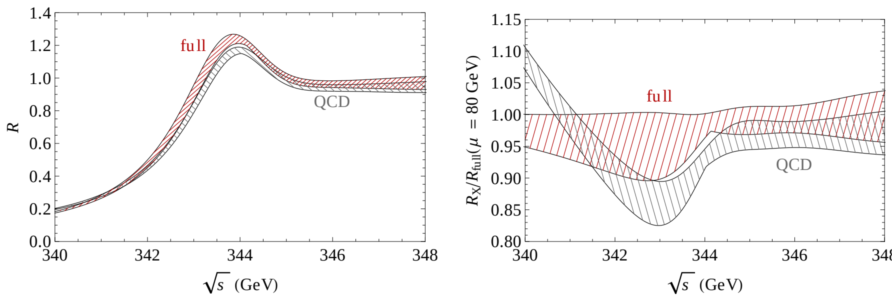

Figure 2: Overall effect of non-QCD corrections on the cross section. The uncertainty band is spanned by variation of the renormalization scale $\mu \in [50\text{ GeV}, 350\text{ GeV}]$. In the right plot the cross section is normalized to the full one at the central scale $\mu = 80$ GeV. Figures from [10].

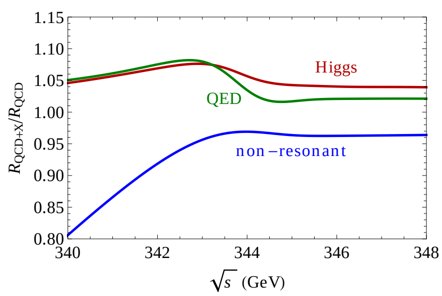

Figure 3: Relative size of the different non-QCD corrections to the top-pair production cross section with respect to the pure QCD result at $\mu = 80$ GeV. Figure from [10].

however also be produced with just one or no resonant tops. Two sample diagrams at NLO without an on-shell top (left) or anti-top (right) are shown in Figure 1. Only the sum of both processes constitutes a physical quantity as is also apparent from singularities that appear in both parts at NNLO and only cancel in the sum. In a systematic way the two contributions can be organized within Unstable Particle Effective Theory [19, 20]. The nonresonant NLO effects have been calculated in [21] and have been included in [10]. At NNLO only partial results are available [22, 23, 24], which we have not considered yet.

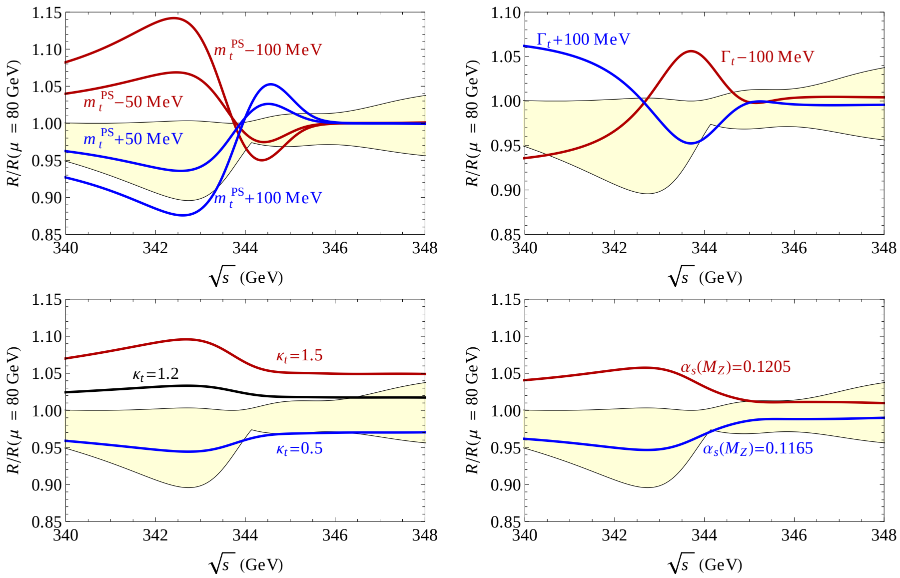

Figure 4: The relative change of the cross section under variations of the top mass, width and Yukawa coupling as well as the strong coupling constant is shown in comparison to the uncertainty band obtained by scale variation. Figures in the second row from [10]; those in the first row are similar to the ones shown in [8], except that now the cross section includes the P-wave and non-QCD contributions discussed in [10] and this proceeding.

QED effects. The leading electroweak correction is the QED Coulomb potential at NLO. Its contribution can be inferred from the results available from the QCD calculation and has been included in [10]. Further electroweak effects at NNLO [13, 14, 25, 26] and even at NNNLO [15, 27] are known, but have not been included yet, since the full NNLO nonresonant correction is not available yet and thus no complete description of EW effects at this order is possible at the moment.

3 Phenomenology

We compare the non-QCD effects described above to the pure QCD cross section. The latter is given by the results of [8] to which we add the small P-wave contribution [12]. The net effect is shown in Figure 2, where the uncertainty bands for the pure QCD and the full result are displayed (see [10]) for the adopted parameter values). We observe that the non-QCD contributions change the cross section by up to about 10% and particularly affect the shape of the cross section at and below threshold. The shift is larger than the QCD uncertainty estimate, thus it is very important to include these contributions. Based on the shift in the peak position we estimate that the effect on the measurement of the top mass is approximately 50 MeV, which is the expected total uncertainty. The separate corrections relative to the QCD prediction are shown in Figure 3. The Higgs and QED contributions both increase the cross section by $4-8\%$ and $2-8\%$, respectively, since they provide an additional attraction between the top pair. Furthermore they shift the peak slightly towards smaller center-of-mass energies.[2] On the other hand the nonresonant contribution is negative, insensitive to the special dynamics near threshold, and roughly energy-independent at NLO. This implies that the relative correction can reach up to 20% below threshold, where the cross section becomes small.

To get an idea of the physics potential of a top threshold scan at a future lepton collider we discuss the dependence of the cross section on the input parameters and compare it to the theory uncertainty. Relative to the full result at $\mu = 80$ GeV this is shown in Figure 4. A change in the top mass mainly manifests itself in a horizontal shift of the cross section by twice that amount. An increase/decrease of the top width changes the degree to which the toponium resonances are smeared out and thus makes the peak in the cross section less/more pronounced. The parameter κ_t parametrizes possible new physics effects in the relation between the top Yukawa coupling and mass $y_t = \sqrt{2}\kappa_t m_t/v$, where $\kappa_t = 1$ corresponds to the Standard Model. Variation of κ_t as well as the strong coupling mainly changes the normalization of the cross section. Due to the similar effect on the cross section the sensitivity to the individual parameters κ_t, α_s in a threshold scan is reduced if both are extracted in a simultaneous fit. For the peak position and height these dependences are illustrated in Figure 5. Given the small error of the strong coupling constant it can also be used as an external input, in which case the added uncertainty relative to the scale variation is small.

A rough estimate of the theory uncertainty in measurements of these

[2]The peak arises from the smeared out toponium resonances, whose binding energy is increased by the additional attractive potentials.

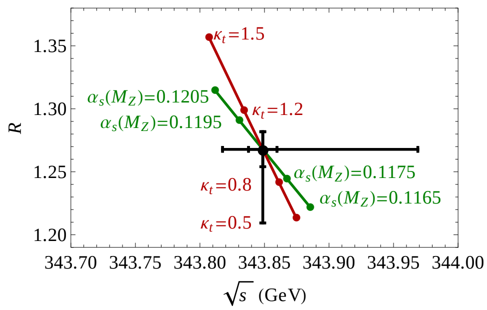

Figure 5: Changes in peak height and position due to variation of the Yukawa coupling (red line) and the strong coupling (green line). The black error bars denote the α_s and combined scale and α_s uncertainty for $y_t = y_t^{\mathrm{SM}}$ ($\kappa_t = 1$) and $\alpha_s(M_Z) = 0.1185$. Figure from [10].

parameters can be obtained by determining the parameter shifts for which the change of cross section lies outside of the uncertainty band in Figure 4. This however underestimates the sensitivity, since in the threshold scan the cross section is measured for multiple points and the theory uncertainty is (at least to some degree) correlated. A reliable estimate on the sensitivity can thus only be obtained by an experimental study using the full theory result. Unfortunately this is not available yet, but existing studies [5, 6, 7] with less complete theory input suggest that the experimental uncertainties are about one half of the present theoretical ones for the top width and mass, specifically of the order of 20 MeV for the mass and 20−30 MeV for the width, respectively, and 0.001 for the strong coupling and $5 - 15\%$ for the top Yukawa coupling.

Acknowledgements

This work was supported by the Gottfried Wilhelm Leibniz programme of the Deutsche Forschungsgemeinschaft (DFG) and the DFG cluster of excellence "Origin and Structure of the Universe".

References

1. ATLAS and CDF and CMS and D0 Collaborations, arXiv:1403.4427 [hep-ex].

2. ATLAS Collaboration, Eur. Phys. J. C **74** (2014) 10, 3109 [arXiv:1406.5375 [hep-ex]].

3. CMS Collaboration, Phys. Lett. B **728** (2014) 496, Corrigendum-ibid. B **728** (2014) 526 [arXiv:1307.1907 [hep-ex]].

4. G. F. Giudice, P. Paradisi and A. Strumia, arXiv:1508.05332 [hep-ph].

5. M. Martinez and R. Miquel, Eur. Phys. J. C **27** (2003) 49 [hep-ph/0207315].

6. K. Seidel, F. Simon, M. Tesař and S. Poss, Eur. Phys. J. C **73** (2013) 8, 2530 [arXiv:1303.3758 [hep-ex]].

7. T. Horiguchi, A. Ishikawa, T. Suehara, K. Fujii, Y. Sumino, Y. Kiyo and H. Yamamoto, arXiv:1310.0563 [hep-ex].

8. M. Beneke, Y. Kiyo, P. Marquard, A. Penin, J. Piclum and M. Steinhauser, Phys. Rev. Lett. **115** (2015) 192001, [arXiv:1506.06864 [hep-ph]].

9. A. H. Hoang *et al.*, Eur. Phys. J. direct C **3** (2000) 1 [hep-ph/0001286].

10. M. Beneke, A. Maier, J. Piclum and T. Rauh, Nucl. Phys. B **899** (2015) 180 [arXiv:1506.06865 [hep-ph]].

11. M. Beneke, Y. Kiyo and K. Schuller, arXiv:1312.4791 [hep-ph].

12. M. Beneke, J. Piclum and T. Rauh, Nucl. Phys. B **880** (2014) 414 [arXiv:1312.4792 [hep-ph]].

13. B. Grzadkowski, J. H. Kühn, P. Krawczyk and R. G. Stuart, Nucl. Phys. B **281** (1987) 18.

14. R. J. Guth and J. H. Kühn, Nucl. Phys. B **368** (1992) 38.

15. D. Eiras and M. Steinhauser, Nucl. Phys. B **757** (2006) 197 [hep-ph/0605227].

16. M. J. Strassler and M. E. Peskin, Phys. Rev. **D43** (1991) 1500.

17. R. Harlander, M. Ježabek and J. H. Kühn, Acta Phys. Polon. **B27** (1996) 1781 [hep-ph/9506292].

18. V. S. Fadin and V. A. Khoze, JETP Lett. **46** (1987) 525 [Pisma Zh. Eksp. Teor. Fiz. **46** (1987) 417].

19. M. Beneke, A. P. Chapovsky, A. Signer and G. Zanderighi, Phys. Rev. Lett. **93** (2004) 011602 [hep-ph/0312331].

20. M. Beneke, A. P. Chapovsky, A. Signer and G. Zanderighi, Nucl. Phys. B **686** (2004) 205 [hep-ph/0401002].

21. M. Beneke, B. Jantzen and P. Ruiz-Femenía, Nucl. Phys. B **840** (2010) 186 [arXiv:1004.2188 [hep-ph]].

22. A. A. Penin and J. H. Piclum, JHEP **1201** (2012) 034 [arXiv:1110.1970 [hep-ph]].

23. B. Jantzen and P. Ruiz-Femenía, Phys. Rev. D **88** (2013) 5, 054011 [arXiv:1307.4337].

24. P. Ruiz-Femenía, Phys. Rev. D **89** (2014) 9, 097501 [arXiv:1402.1123 [hep-ph]].

25. A. H. Hoang and C. J. Reißer, Phys. Rev. D **71** (2005) 074022 [hep-ph/0412258].

26. A. H. Hoang and C. J. Reißer, Phys. Rev. D **74** (2006) 034002 [hep-ph/0604104].

27. Y. Kiyo, D. Seidel and M. Steinhauser, JHEP **0901** (2009) 038 [arXiv:0810.1597 [hep-ph]].

COMPOSITE HIGGS MODELS AND $t\bar{t}$ PRODUCTION AT FUTURE e^+e^- COLLIDERS

D. Barducci
LAPTh, Université Savoie Mont Blanc CNRS
B.P. 100, F-74941 Annecy-le-Vieux, France
S. De Curtis
INFN, Sezione di Firenze and
Dept. of Physics and Astronomy
University of Florence, Italy
S. Moretti
School of Physics and Astronomy
University of Southampton
Highfield, Southampton SO17 1BJ, U.K.
Particle Physics Department, Rutherford Appleton Laboratory
Chilton, Didcot, Oxon OX11 0QX, UK
G.M. Pruna
Paul Scherrer Institut, CH-5232 Villigen PSI, Switzerland

Abstract

The study of the top quark properties will be an integral part of any particle physics activity at future leptonic colliders. In this proceeding we discuss the possibility of testing composite Higgs scenarios at e^+e^- prototypes through deviations from the Standard Model predictions in $t\bar{t}$ production observables for various centre of mass energies, ranging from 370 GeV up to 1 TeV. These proceedings draw from Ref. [1)]

1 Introduction

The large hierarchy between the masses of the first two and the third generation of Standard Model (SM) quarks seems to point to an intrinsic difference between the nature of these particles and suggest that the top quark plays a special role in the underlying mechanisms of electroweak symmetry breaking (EWSB). While this problem is not addressed in the SM, various new physics (NP) scenarios attempt to find a solution to this puzzle, with composite Higgs models (CHMs) being nowadays one of the most compelling SM extension.

Within this framework the Higgs is assumed to be a bound state of a new strongly interacting sector with a cut-off at a scale $\Lambda \sim 4\pi f \gg v_{\rm SM}$, thus resolving the so-called *big hierarchy problem* of the SM, while the little hierarchy between the Higgs mass and the cut-off scale is further ensured by the pseudo Nambu Goldstone boson (pNGB) nature of the Higgs. While this idea goes back to the '80s [2], one modern ingredient of CHMs is the mechanism of *partial compositeness* [3], which addresses the mass hierarchy between the SM fermions by postulating a sizable mixing of the third generation of quarks with the strong sector to which the Higgs belongs.

The simplest realisation of this idea is the minimal composite Higgs model (MCHM) [4], where the Higgs arises from the symmetry breaking pattern $SO(5) \to SO(4)$, thus providing only four GBs and a custodial symmetry to prevent the ρ parameter from large corrections. This idea was originally considered in the context of 5-dimensional (5D) scenarios while deconstructed 4D effective descriptions were more recently proposed [5, 6]. These explicit CHM realisations present features of phenomenological relevance at colliders (see *e.g.* [7] for a recent review), as they include in their spectrum a full sector of composite resonances of the strong sector, both of spin 1 and spin 1/2, below the cut-off Λ and allow for a dynamical calculation of the Higgs potential through the Coleman-Weinberg technique [8]. In particular, the 4D Composite Higgs model (4DCHM) predicts a finite one loop Higgs potential that, for a natural choice of the model parameters, results in a Higgs mass consistent with the ATLAS and CMS measurements [9].

In order to shed light on the possibility of NP intimately correlated with the top sector, the measurement of the top quark properties, and in particular of its couplings to the Higgs and SM gauge bosons, are of primary importance. In this respect a leptonic collider will greatly increase the precision achievable the the Large Hadron Collider (LHC), due to the cleaner experimental environment with respect to a hadronic machine and the possibility of having a well defined initial state and controllable centre of mass (COM) energy. Moreover, the possibility of having polarised initial state or of measuring top quark polarisation in the final state will be important to measure independently the $t\bar{t}\gamma$ and $t\bar{t}Z$ couplings, both contributing to $e^+e^- \to t\bar{t}$ production. Future leptonic facilities will also be an excellent environment to measure the top quark mass, because of the colourless initial state.

In these proceedings we will show how the new particle content present in the 4DCHM can affect $t\bar{t}$ production at future e^+e^- facilities in two ways. Firstly, potentially large deviations of the $Zt\bar{t}$ coupling with respect to the SM prediction can arise due to mixing between the top quark and composite spin 1/2 resonances, the so-called top partners, and between the Z and additional composite spin 1 resonances, hereafter referred to as ρ. Secondly, the ρ's can enter as propagating particles in the diagrams describing $t\bar{t}$ production, thus contributing either on their own or via interference effect with the SM background. In order to cover different machines prototypes, as the International Linear Collider (ILC), the Compact Linear Collider (CLIC) and the Future Circular Collider (FCC), we will work in an COM energy ranging from $\sim 2m_{\text{top}}$ up to 1 TeV.

2 Top quark coupling measurements

Many extensions of the SM predict large deviations of the Z couplings to a top quark pair. In CHMs these deviations are a consequence of the mixing between the right and left handed top quark components and the top partners present in the composite sector.

The top quark couplings to the Z and the photon can be conveniently parametrised in terms of form factors defined by

$$\Gamma_\mu^{ttX}(k^2,q,\bar{q}) = -ie\big[\gamma_\mu(F_{1V}^X(k^2)+\gamma_5 F_{1A}^X(k^2))+\frac{\sigma_{\mu\nu}}{2m_t}(q+\bar{q})_\mu(iF_{2V}^X(k^2)+\gamma_5 F_{2A}^X(k^2))\big] \tag{1}$$

where e is the proton charge, m_t is the top-quark mass, q ($\bar{q}$) is the outgoing top (antitop) quark four-momentum and $k^2 = (q+\bar{q})^2$. The terms $F_{1V,A}^X(0)$ in the low energy limit are the ttX vector and axial-vector form-factors, which can be easily translated into left- and right-handed top quark couplings to the Z boson. While the LHC sensitivity to these quantities is quite limited, future e^+e^- facilities will improve the accuracy of these measurements of at least one order of magnitude, depending on the machine prototype details, the COM energy, the luminosity, the selected final state and the possibility of using polarised beams. This is shown in Fig. 1, where the expected sensitivity in determining the form factors is illustrated for various collider prototypes. Also reported in the right panel of the same figure are the typical deviations for the $Zt_L\bar{t}_L$ and $Zt_R\bar{t}_R$ couplings for various new physics scenarios and the 4DCHM, the latter represented as black dots. These figures make therefore clear the importance of e^+e^- machines also in comparison to the high luminosity LHC options, at the end of which the 4DCHM might not be disentangled from the SM.

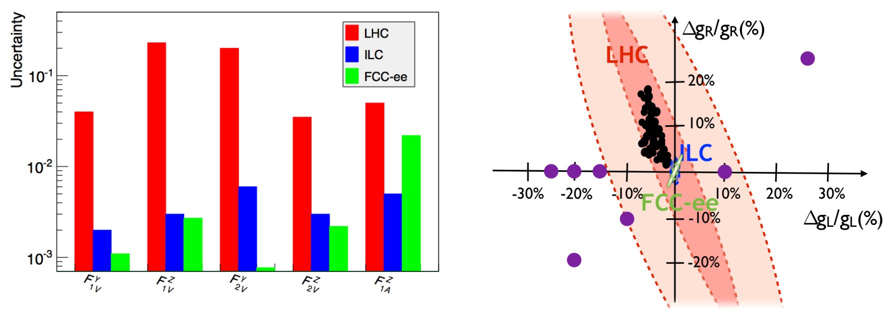

Figure 1: *Statistical uncertainties on the axial and vector form factors expected at the LHC-13 with 300 fb^{-1}, at ILC-500 with 500 fb^{-1} and at FCC-ee-360 with 2.6 ab^{-1} (left panel). Typical deviations of the Zt_Lt_L and Zt_Rt_R couplings for various NP models (purple points) and for the 4DCHM (black points) together with the sensitivity expected at LHC-13 with 300 and 3000 fb^{-1}, outer and inner red lines, from ILC-500, blue dashed lines, and FCC-ee green lines (see* [1] *and refs. therein.)*

3 $e^+e^- \to t\bar{t}$ production in the 4DCHM

Electroweak (EW) precision data and current LHC measurements bound top partners and ρ resonances to have a mass above ~ 800 GeV and 2 TeV respectively. While top partners only affect $t\bar{t}$ production via modifications of the $Zt\bar{t}$ coupling, ρ resonances can directly enter into the diagrams describing the e^+e^- process both for the inclusive cross section as well as for asymmetry observables [1]. This is well illustrated in Fig. 2, where we present deviations from the SM predictions for the total cross section and for the Forward Backward asymmetry (AFB) [1] without (left panel) or with (right panel) the inclusions of the ρ's present in the 4DCHM, as propagating particles in the production diagrams for $\sqrt{s} = 500$ GeV. The blue points are compliant with current EW precision data and LHC measurements, and clearly illustrate the importance of ρ exchange even at a COM energy well below the ρs mass scale of ~ 2 TeV, due to their interference effect with the SM background.

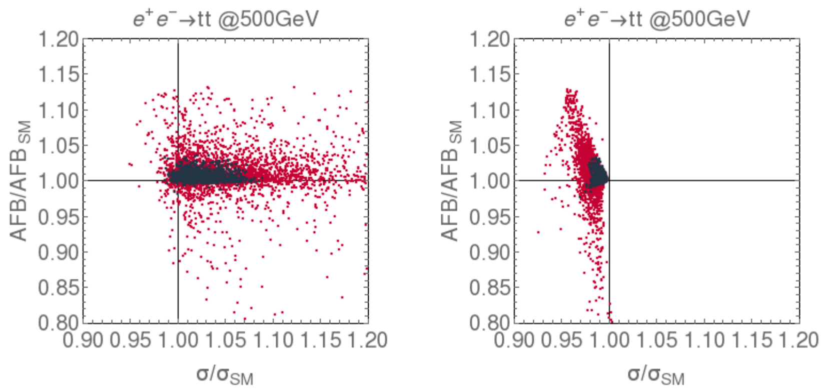

Figure 2: *Predicted deviations for the cross section versus AFB for the process* $e^+e^- \to t\bar{t}$ *with* $\sqrt{s} = 500$ *GeV without (left) and with (right) the inclusion of the* ρ*s present in the 4DCHM as propagating particles in the production diagrams. The points correspond to* f *=0.75-1.5 TeV,* g_ρ *=1.5-3 and a scanning over the fermion parameter. Blue points are compliant with current EW precision data and LHC measurements.*

We can then extract the sensitivity of an e^+e^- prototype to the relevant parameters of a typical CHM. In Fig. 3 we plot, by using different colours, the predicted deviations for the cross section at $\sqrt{s}$= 500 and 1000 GeV in the 4DCHM compared with the SM as functions of $m_\rho = fg_\rho$, with g_ρ the typical coupling strength of the ρ resonances, and $\xi = v^2/f^2$, the compositeness parameter. For each point we have selected the configuration yielding the maximal deviation defined as $\Delta = (\sigma^{\text{4DCHM}} - \sigma^{\text{SM}})/\sigma^{\text{SM}}$. The points correspond to f = 0.75–1.5 TeV, g_ρ = 1.5–3 and are obtained scanning over the other

[1]Defined as $A_{FB} = (N(\cos\theta^* > 0) - N(\cos\theta^* < 0))/(N_{\text{tot}})$ with θ^* the polar angle in the $t\bar{t}$ rest frame and N denoting the number of observed events in a given hemisphere.

model parameters. We see that, by requiring a deviation larger than 2% to be detected, a 500 GeV machine is sensitive to ρ resonances with mass up to 3.5 TeV.

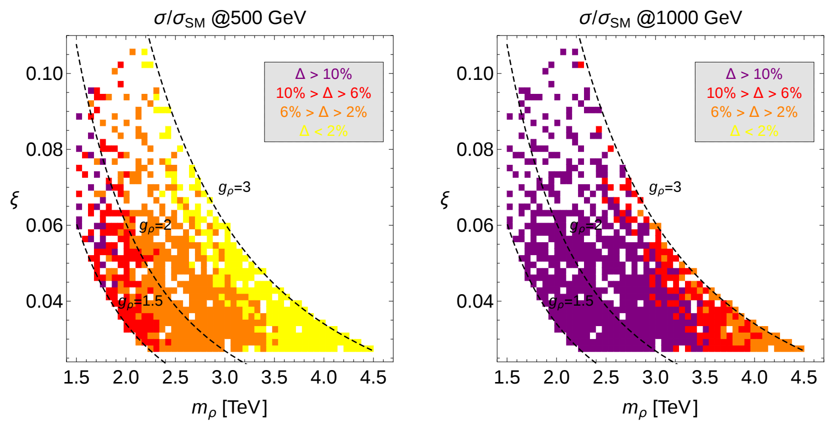

Figure 3: *Predicted deviations for the cross section of the process* $e^+e^- \to t\bar{t}$ *at 500 and 1000 GeV in the 4DCHM compared with the SM as functions of* $m_\rho = fg_\rho$ *and* $\xi = v^2/f^2$. *For each point we have selected the configuration yielding the maximal deviation defined as* $\Delta = (\sigma^{4DCHM} - \sigma^{SM})/\sigma^{SM}$. *The points correspond to* f *=0.75-1.5 TeV,* g_ρ*=1.5-3. All points are compliant with EW precision data and current LHC measurements.*

4 Conclusions

In this proceeding, based on Ref. [1], we have exploited a calculable version of a CHM in order to test the sensitivity of future e^+e^- colliders to deviations in the cross section and FB asymmetry of $t\bar{t}$ production from the SM values. We have illustrated how these observables can be affected by both deviations in the $Zt\bar{t}$ couplings and by the presence of spin-1 resonances. The latter in particular can lead to sizable deviations also at COM energies well below their mass scale, due to interference effects with the SM background. We have then finally mapped such predicted deviations into typical parameter of CHMs, namely the mass scale of the spin-1 resonances, m_ρ, and the compositeness parameter, $\xi = v^2/f^2$.

References

1. D. Barducci, S. De Curtis, S. Moretti and G. M. Pruna, JHEP **1508** (2015) 127.
2. D. B. Kaplan and H. Georgi, Phys. Lett. B **136** (1984) 183.
3. D. B. Kaplan, Nucl. Phys. B **365** (1991) 259.
4. K. Agashe, R. Contino and A. Pomarol, Nucl. Phys. B **719** (2005) 165.
5. G. Panico and A. Wulzer, JHEP **1109** (2011) 135.
6. S. De Curtis, M. Redi and A. Tesi, JHEP **1204** (2012) 042.
7. G. Panico and A. Wulzer, Lect. Notes Phys. **913** (2016) pp, [arXiv:1506.01961 [hep-ph]].
8. S. R. Coleman and E. J. Weinberg, Phys. Rev. D **7** (1973) 1888.
9. G. Aad *et al.* [ATLAS and CMS Collaborations], Phys. Rev. Lett. **114** (2015) 191803.

HIGGS PHYSICS AT THE LHC

Cesare Bini
Sapienza Universitá and INFN Roma

Abstract

In Summer 2012 the ATLAS and CMS collaborations announced the first observation of a particle compatible with the Higgs boson at a mass of 125 GeV. After that discovery, the two collaborations have started a complete analysis program aiming to establish the main properties of the Higgs boson, using the full data sample collected in 2011 and 2012 at 7 and 8 TeV center of mass energies. A precision measurement of the Higgs boson mass is obtained by combining the results of the two experiments and limits on the Higgs boson width are obtained by both experiments with different methods. The Higgs boson standard model spin/CP assignment together with the pattern of its couplings with the standard model particles are also tested. All results turn out to be compatible with the standard model predictions.

1 Introduction

The Standard Model of the elementary particle physics (SM) predicts the existence of the Higgs boson field in the context of the spontaneous symmetry breaking mechanism accounting for the mass generation of the elementary particles [1]. The Higgs boson has been observed in 2012 by the ATLAS and CMS collaborations at a mass of about 125 GeV [2]. The SM predicts that it is a scalar particle with spin CP assignments 0^{++} and that, given the observed value of the mass, it is characterized by well defined values of the decay width and of the couplings with all the SM particles. In the following the results of the studies of the properties done by the two experiments, together with the first combinations, are described.

All the analyses are based on the full Run1 dataset, consisting in ~ 5 fb^{-1} proton-proton collisions at a center of mass energy of 7 TeV taken in 2011 and ~ 20 fb^{-1} at 8 TeV taken in 2012.

2 Higgs properties from LHC Run1

2.1 Higgs mass and width

The mass of the Higgs boson is measured by fitting the mass peaks in the two clean and high resolution final states $\mathrm{H} \to \gamma\gamma$ and $\mathrm{H} \to \mathrm{ZZ} \to 4$ leptons. The results of each experiment together with the combination [3] are shown in fig.1. The overall p-value compatibility of the different mass measurements is 10%. The uncertainty on the combined value is still statistically dominated. The best value of the Higgs boson mass from LHC Run1 is:

$$M_{\mathrm{H}} = 125.09 \pm 0.24 \text{ GeV} = 125.09 \pm 0.21(stat) \pm 0.11(syst) \text{ GeV} \qquad (1)$$

For a Higgs mass of 125 GeV the decay width Γ_{H} is expected to be around 4 MeV, well below the direct experimental sensitivity. Indirect upper limits of 23 and 22 MeV are reported by ATLAS and CMS respectively [4] obtained by analyzing the ZZ and WW high mass distributions that are sensitive to the Higgs width through the interference of the high mass Higgs boson off-shell tail with the gg$\to$ZZ,WW background.

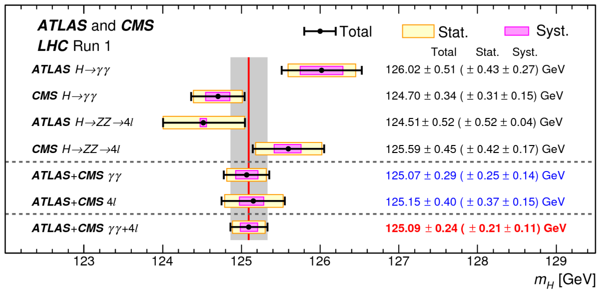

Figure 1: *Summary of the results of the Higgs mass measurement for the two high resolution channels, namely $\gamma\gamma$ and ZZ→ 4leptons. The combinations of ATLAS and CMS for each channel together with the global combination are also shown.*

2.2 Higgs spin/CP

The spin/CP nature of the Higgs boson determines the kinematics of the diboson decays. Hypothesys tests comparing the SM assignment 0^{++} with several alternative assignments are done using multivariate techniques based on angular and kinematical variables. All alternative spin/CP scenarios are excluded with confidence levels larger than 99.9% [5]. Moreover BSM additional parameters in the lagrangian are checked and found to be compatible with 0.

2.3 Higgs couplings

A complete combined ATLAS+CMS analysis of the Higgs couplings has been recently published [6]. The aim of the analysis is to combine all the production and decay channels to extract informations on the way the Higgs couples with particles to be compared with SM expectations. The following definitions are used here: $\mu = \sigma_{meas}/\sigma_{SM}$ is the "signal strength" while κ namely the ratio of a measured Higgs couplings to the SM value is the "coupling modifier".

The initial state μ_i and final state μ_f signal strengths can be related to the observed number of events in the category c, n_s^c according to the expression:

$$n_s^c = \Sigma_i \Sigma_f \mu_i (\sigma_i)_{SM} \times \mu_f (BR_f)_{SM} \times A_{if}^c \times \epsilon_{if}^c \times L^c \qquad (2)$$

where A_{if}^c, ϵ_{if}^c and L^c are the acceptance, the efficiency and the integrated

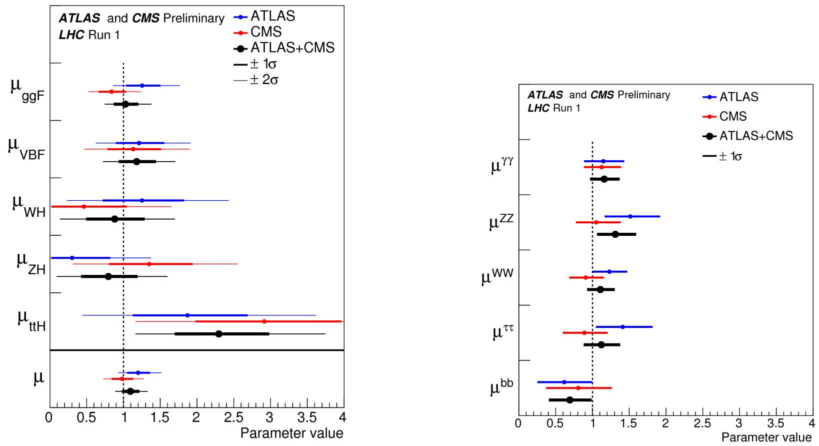

Figure 2: *Results of the signal strength fit to the data of ATLAS, of CMS and on the combination of the two experiments. (left) production signal strengths and (right) decay signal strengths.*

luminosities respectively. By fitting the rate of events in the different categories the signal strengths for all initial and final states are obtained. The results are shown in fig.2. All values are in good agreement with the SM expectation μ=1. By fitting an overall value of μ the following value is obtained:

$$\mu = 1.09^{+0.11}_{-0.10} = 1.09^{+0.07}_{-0.07}(stat)^{+0.04}_{-0.04}(exp)^{+0.03}_{-0.03}(thbgd)^{+0.07}_{-0.06}(thsig) \qquad (3)$$

where the systematic uncertainties are split into an experimental contribution (expt) and two theoretical contributions either related to the background (thbgd) or the signal (thsig) modellization. In this case the statistical uncertainty is at the same level of the systematic uncertainty dominated by the theoretical systematic error.

In order to extract the coupling modifiers the cross-section for a given initial and final state is parametrized according to the:

$$\sigma(i \to \mathrm{H} \to f) = \frac{\sigma_i(\kappa_j) \cdot \Gamma_f(\kappa_j)}{\Gamma_\mathrm{H}(\kappa_j)} \qquad (4)$$

where production cross-sections and decay widths are expressed in terms of the coupling modifiers k_j. The results of the combined fit of the coupling modifiers

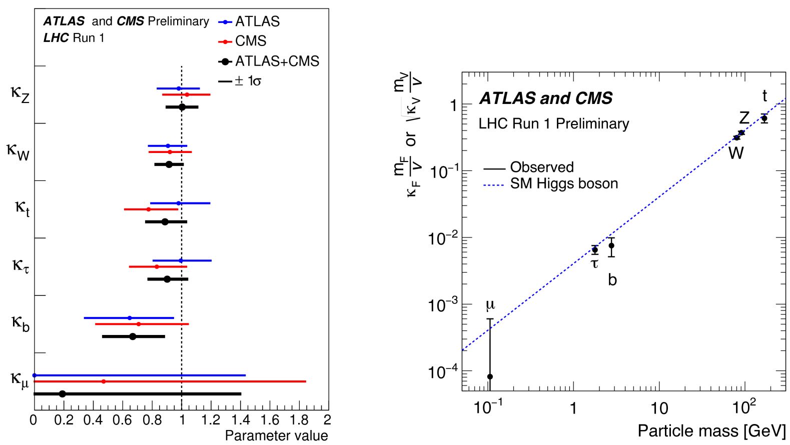

Figure 3: *Results of the coupling modifier fit to the data of ATLAS, of CMS and on the combination of the two experiments. The left plot reports directly the best values of the coupling modifiers, the right plot reports the adimensional couplings entering the lagrangian. The linear dependence shows the property of the Higgs boson couplings to scale with the mass of the particle.*

is shown in fig.3. Again the observed couplings are well consistent with the SM expected pattern. The result of a fit with the overall couplings to fermions and to vectors κ_F and κ_V, as free parameters is shown in fig.4.

3 LHC Run2 and prospects in future LHC runs

The timeline of the LHC project includes three main steps: the Run2 that has started now with pp collisions at 13 TeV center of mass energy aiming to collect an integrated luminosity of 100 fb^{-1}; the Run3 that is expected to start in 2019 aiming to collect 300 fb^{-1} at 14 TeV; the HL-LHC project that aims to reach 3000 fb^{-1} also at 14 TeV on a longer timescale.

The prospects for the Higgs physics include (evidence is a 3σ effect and observation a 5σ effect): the observation of the VBF, VH and ttH production modes, of the di-fermion decays H→ $\tau\tau$ and H→ $b\bar{b}$ and of rare decays like H→ $\mu\mu$ and H→Zγ; a precision measurement of the couplings at the 10% level. Under scrutiny is also the possibility to obtain evidence of HH production and

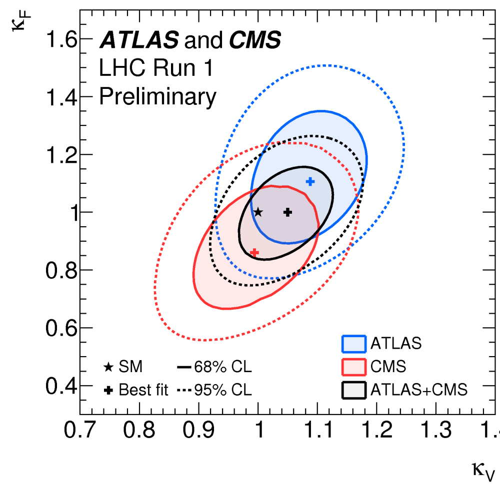

Figure 4: *Result of the two parameter fit with two overall coupling modifiers to fermions and to vectors, κ_F and κ_V as free parameters. Results are shown for ATLAS, for CMS and for the combination of the two experiments.*

to reach the sensitivity to measure the Higgs decay width $\Gamma_{\rm H}$.

References

1. P.W.Higgs, Phys.Lett.**12** 132 (1964), Phys.Rev.Lett.**13** 508 (1964); F.Englert, R.Brout, Phys.Rev.Lett.**13** 321 (1964).

2. ATLAS collaboration, Phys.Lett.**B716** 1 (2012); CMS collaboration Phys.Lett.**B716** 30 (2012).

3. ATLAS and CMS collaborations, Phys.Rev.Lett. **114** 191803.

4. ATLAS collaboration, Eur.Phys.J. **C75** 335 (2015); CMS collaboration, Phys.Lett. **B736** 64 (2014).

5. ATLAS collaboration, Eur.Phys.J. **C75** 476 (2015); CMS collaboration, Phys.Rev. **D92** 012004 (2015).

6. ATLAS and CMS collaborations, ATLAS-CONF-2015-044, .

PROSPECTS FOR DOUBLE HIGGS PRODUCTION

Giuliano Panico
IFAE, Universitat Autònoma de Barcelona, Bellaterra, Barcelona, Spain

Abstract

A concise review of the double Higgs production channel at the LHC and at future hadron and lepton machines is presented.

1 Introduction

Double Higgs production is one example of scattering process that can disclose key information on the electroweak symmetry breaking dynamics, in particular its underlying symmetries and strength. It is one of the few channels that can give direct access to the quartic couplings among two Higgs bosons and a pair of gauge bosons or of top quarks, as well as to the Higgs trilinear self-coupling.

Due to the small cross section, the precision achievable at the LHC on these couplings is quite limited. The large increase in cross section at high-energy hadron machines and the improved precision possible at future lepton colliders could overcome the LHC limitations providing an ideal environment to test this process.

In the absence of light new states, the new-physics effects can be parametrized via low-energy effective Lagrangians. Two formulations are useful for the study of Higgs physics [1]. The first one, the "linear" Lagrangian, is based on the assumption that the Higgs is part of an $\mathrm{SU}(2)_L$ doublet, as in the SM. In the second, more general formulation, $\mathrm{SU}(2)_L \times \mathrm{U}(1)_Y$ is non-linearly realized, hence the name of "non-linear" Lagrangian, and the physical Higgs is a singlet of the custodial symmetry, not necessarily part of a weak doublet. The run 1 LHC indicates that the couplings of the newly discovered boson are close to the values predicted for the SM Higgs. This clearly motivates the use of the linear Lagrangian for future studies. Indeed, small deviations from the SM are naturally expected if the Higgs boson belongs to a doublet, provided the new states are much heavier than the weak scale. The non-linear formulation is still useful, however, when large deviations in the Higgs couplings are allowed. This is especially true for double Higgs production, from which additional couplings not accessible via single Higgs processes can be extracted [2, 3].

In the linear Lagrangian, the operators can be organized as

$$\mathcal{L}_{\mathrm{lin}} = \mathcal{L}_{\mathrm{SM}} + \Delta\mathcal{L}_6 + \Delta\mathcal{L}_8 + \ldots \tag{1}$$

The lowest-order terms coincide with the usual SM Lagrangian $\mathcal{L}_{\mathrm{SM}}$, whereas $\mathcal{L}_n$ contains the deformations due to operators of dimension n, with $n > 4$. For our purposes it is sufficient to focus on the operators involving the Higgs boson. The ones in $\Delta\mathcal{L}_6$ relevant for double Higgs production are (for simplicity we only include the CP-conserving operators)

$$\begin{aligned}\Delta\mathcal{L}_6 \supset\ & \frac{\overline{c}_H}{2v^2}\left[\partial_\mu(H^\dagger H)\right]^2 + \frac{\overline{c}_u}{v^2} y_u H^\dagger H \overline{q}_L H^c u_R - \frac{\overline{c}_6}{v^2}\frac{m_h^2}{2v^2}(H^\dagger H)^3 \\ & + \frac{c_g}{m_W^2} g_s^2 H^\dagger H G^a_{\mu\nu} G^{a\,\mu\nu}\,,\end{aligned} \tag{2}$$

where H denotes the Higgs doublet, $v = 246$ GeV and $m_h = 125$ GeV is the Higgs mass. The linear Lagrangian relies on a double expansion. The first one is an expansion in derivatives, in which higher-order terms are suppressed by additional powers of E^2/m_*^2. To derive this estimate we assumed that the new dynamics can be broadly characterized by a single mass scale m_*, at which new states appear, and by one coupling strength g_* (this is the so called SILH power counting [4]). The second expansion is in powers of the Higgs doublet: each extra insertion is weighted by a factor $1/f \equiv g_*/m_*$. In order to be under control, the linear Lagrangian requires $E^2/m_*^2 < 1$ and $v/f < 1$.

In the case of the non-linear Lagrangian, the relevant operators are

$$\mathcal{L} \supset \left(m_W^2 W_\mu W^\mu + \frac{m_Z^2}{2} Z_\mu Z^\mu\right)\left(1 + 2c_V \frac{h}{v} + c_{2V}\frac{h^2}{v^2}\right) - c_3 \frac{m_h^2}{2v} h^3$$
$$- m_t \bar{t}t \left(1 + c_t \frac{h}{v} + c_{2t}\frac{h^2}{2v^2}\right) + \frac{g_s^2}{4\pi^2}\left(c_g \frac{h}{v} + c_{2g}\frac{h^2}{2v^2}\right) G^a_{\mu\nu} G^{a\,\mu\nu}\,, \quad (3)$$

where h denotes the physical Higgs field (with vanishing expectation value). With respect to the linear parametrization, the operators in Eq. (3) effectively resum all the corrections of order v^2/f^2. The non-linear Lagrangian only relies on the derivative expansion, but not on the expansion in powers of the Higgs field. When the linear and non-linear parametrizations are both valid, the coefficients of the two effective Lagrangians are related by

$$c_t = 1 - \bar{c}_H/2 - \bar{c}_u\,, \qquad c_{2t} = -(\bar{c}_H + 3\,\bar{c}_u)/2\,, \qquad c_3 = 1 - 3\,\bar{c}_H/2 + \bar{c}_6\,,$$
$$c_g = c_{2g} = \bar{c}_g\left(16\pi^2/g^2\right)\,, \qquad c_V = 1 - \bar{c}_H/2\,, \qquad c_{2V} = 1 - 2\,\bar{c}_H\,. \quad (4)$$

Notice that single operators in the linear Lagrangian induce correlated modifications in different Higgs vertices. For instance the $\mathcal{O}_u$ operator, which gives a modification of the top Yukawa, also generates a new quartic interaction $\bar{t}thh$.

2 Double Higgs at hadron colliders

Double Higgs production at hadron colliders is mainly due to three processes: Gluon Fusion (GF), Vector Boson Fusion (VBF) and $tthh$ associated production. In the following we will focus on the GF and VBF channels, for which dedicated analyses at high-energy colliders exist. The $tthh$ channel, for which only LHC studies are currently available [5], can provide some information on the Higgs trilinear coupling, but it seems not competitive with the GF channel.

2.1 Gluon fusion

The GF channel is the dominant production mode at hadron colliders. The NNLO SM cross section at the 14 TeV LHC is $\sigma_{\rm SM} \simeq 37\,\text{fb}$, while it becomes $\sigma_{\rm SM} \simeq 1.5\,\text{pb}$ at a 100 TeV collider. The relatively small cross sections imply

	LHC_{14}	HL-LHC	FCC_{100}	Reference
$\overline{c}_6$	$[-1.2, 6.1]$	$[-1.0, 1.8] \cup [3.5, 5.1]$	$[-0.33, 0.29]$	Azatov *et al.* [3]
Δc_{2V}	$[-0.18, 0.22]$	$[-0.08, 0.12]$	$[-0.01, 0.03]$	Contino *et al.* [8]

Table 1: *Estimated precision on the Higgs trilinear coupling $\overline{c}_6$ and $\Delta c_{2V} = c_{2V} - 1$ at hadron machines. The table reports the 68% probability intervals.*

that only a few final states are relevant. In spite of the small branching fraction ($BR \simeq 0.264\%$) the $hh \to \gamma\gamma b\bar{b}$ channel has been recognized as the most promising one due to the clean signal and small backgrounds [6, 3]. Other channels, whose exploitation is more difficult due to the large backgrounds, have been also considered, among which $hh \to b\bar{b}\tau^+\tau^-$, $hh \to b\bar{b}WW^*$ and $hh \to b\bar{b}b\bar{b}$ [7]. Due to the larger cross section these channels could be relevant for an analysis of the high-energy tail of the kinematic distributions, where boosted jet techniques could enhance the signal reconstruction efficiency.

The GF channel is sensitive to several new-physics effects. In the non-linear formalism, it depends on the Higgs self-coupling (c_3), on the top couplings (c_t, c_{2t}) and on the contact interactions with the gluons (c_g, c_{2g}). It is thus a privileged channel to test the non-linear Higgs couplings (c_3, c_{2t}, c_{2g}) that can not be directly accessed in single-Higgs processes. Interestingly, the various new physics effects affect in different ways the kinematic distributions (in particular, the Higgs-pair invariant mass m_{hh}). An exclusive analysis taking into account the m_{hh} distribution can thus be used to disentangle the various coefficients in the effective Lagrangian [3]. This is relevant at high-energy colliders, where the sizable cross section allows to reconstruct the m_{hh} distribution, it is instead of limited applicability at the LHC due to the small number of signal events.

To conclude the discussion we report in table 1 the precision on the determination of the Higgs trilinear coupling $\overline{c}_6$ for three benchmark scenarios: 14 TeV LHC with $L = 300\,\mathrm{fb}^{-1}$ integrated luminosity (LHC_{14}), high-luminosity LHC with $L = 3\,\mathrm{ab}^{-1}$ (HL-LHC) and a future 100 TeV pp collider with $L = 3\,\mathrm{ab}^{-1}$ (FCC_{100}). It is important to stress that the precision on the $\overline{c}_6$ coefficient is affected by the uncertainty on the other parameters in the effective Lagrangian and in particular on the top Yukawa, $\overline{c}_u$ (the result in table 1 was derived by assuming $\Delta\overline{c}_u \simeq 0.05$). With no uncertainty on $\overline{c}_u$, the Higgs trilinear coupling could be extracted at FCC_{100} with precision $\Delta\overline{c}_6 \simeq 0.18$.

	COM Energy	Precision	Process	Reference
ILC	500 GeV [$L = 500$ fb^{-1}]	$\Delta c_3 \sim 104\%$	DHS	ILC TDR, Volume 2 [10]
	1 TeV [$L = 1$ ab^{-1}]	$\Delta c_3 \sim 28\%$	VBF	ILC TDR, Volume 2 [10]
		$\Delta c_{2V} \sim 20\%$	DHS	Contino *et al.* [11]
CLIC	1.4 TeV [$L = 1.5$ ab^{-1}]	$\Delta c_3 \sim 24\%$	VBF	P. Roloff (CLICdp Coll.) [12]
		$\Delta c_{2V} \sim 7\%$		
	3 TeV [$L = 2$ ab^{-1}]	$\Delta c_3 \sim 12\%$		
		$\Delta c_{2V} \sim 3\%$		

Table 2: *Expected* 68% *CL precision on the Higgs trilinear coupling* c_3 *and on the* c_{2V} *coupling at future lepton colliders.*

2.2 Vector boson fusion

The VBF channel is sensitive to the Higgs self-coupling c_3 and, more importantly, to the single and double Higgs coupling to the vector bosons (c_V, c_{2V}). Analogously to WW scattering, a modification of the Higgs coupling to the gauge fields spoils the cancellation present in the SM, so that the VBF amplitude grows at high energy as $\mathcal{A} \sim \hat{s}/v^2(c_V^2 - c_{2V})$. The tail of the distribution is thus particularly sensitive on c_V and c_{2V}. The Higgs trilinear, on the contrary, affects the m_{hh} distribution mostly at threshold and has a limited impact.

The small cross section forces to consider Higgs decay channels with large branching fractions. The most relevant final state is $hh \to 4b$. Estimates of the precision achievable on c_{2V} are given in table 1 for three benchmark scenarios.

3 Double Higgs at lepton colliders

The main channels for double Higgs production at lepton colliders are Double Higgs-Strahlung (DHS) and Vector Boson Fusion (VBF). The DHS channel is dominant for center of mass energies below $s \lesssim 1$ TeV, while above this threshold the VBF cross section becomes the largest one [9].

Both production channels are sensitive to deviations in the Higgs trilinear coupling and in the double Higgs coupling to vector bosons. The expected precision on the determination of Δc_3 and Δc_{2V} for different benchmark scenarios are listed in table 2. In order to obtain a fair determination of these parameters a center of mass energy $s \gtrsim 1$ TeV and an integrated luminosity $L \gtrsim 1$ ab^{-1} are necessary. With these minimal requirements a precision of the order $20 - 30\%$ can be achieved. Further improvements in the collider energy could significantly boost the precision on c_{2V}, up to a $\sim 3\%$ accuracy, since the effects mediated by this coupling are enhanced at high m_{hh}. The deviations in the Higgs trilinear coupling, on the contrary, affect mostly the distribution at threshold, hence an improvement in the precision at higher energies is mainly related to the luminosity increase. The precision on c_3 and c_{2V} that can be obtained at lepton machines with $s \gtrsim 1$ TeV is roughly comparable to the one estimated for a 100 TeV hadron collider (see the FCC_{100} column in table 1).

References

1. R. Contino *et al.*, JHEP **1307** (2013) 035 [arXiv:1303.3876 [hep-ph]].
2. R. Grober, M. Muhlleitner, JHEP **1106** (2011) 020 [arXiv:1012.1562 [hep-ph]]; R. Contino *et al.*, JHEP **1208** (2012) 154 [arXiv:1205.5444 [hep-ph]].
3. A. Azatov *et al.*, Phys. Rev. D **92** (2015) 3, 035001.
4. G. F. Giudice *et al.*, JHEP **0706** (2007) 045 [hep-ph/0703164]. For a pedagogical review see: G. Panico and A. Wulzer, Lect. Notes Phys. **913** (2016) [arXiv:1506.01961 [hep-ph]].
5. C. Englert *et al.*, Phys. Lett. B **743** (2015) 93 [arXiv:1409.8074 [hep-ph]].
6. J. Baglio *et al.*, JHEP **1304** (2013) 151; W. Yao, arXiv:1308.6302 [hep-ph]; A. J. Barr *et al.*, JHEP **1502** (2015) 016.
7. See for instance: M. J. Dolan *et al.*, JHEP **1210** (2012) 112; D. E. Ferreira de Lima *et al.*, JHEP **1408** (2014) 030; A. J. Barr *et al.*, Phys. Lett. B **728** (2014) 308; F. Goertz *et al.*, JHEP **1504** (2015) 167.
8. F. Bishara, R. Contino, J. Rojo, in progress. R. Contino talk at HPPC2015.
9. J. Tian *et al.* [ILD Collaboration], PoS EPS **HEP2013** (2013) 316.
10. H. Baer *et al.*, arXiv:1306.6352 [hep-ph].
11. R. Contino *et al.*, JHEP **1402** (2014) 006 [arXiv:1309.7038 [hep-ph]].
12. P. Roloff (CLICdp Collaboration), talk at LCWS14.

SCALAR SINGLETS AT PRESENT AND FUTURE COLLIDERS

Dario Buttazzo
Physik-Institut, Universität Zürich, CH-8057 Zürich, Switzerland

Abstract

A scalar singlet, coupled to the other particles only through its mixing with the Higgs boson, appears in several motivated extensions of the Standard Model. The prospects for the discovery of a generic singlet at the various stages of the LHC, as well as at future high-energy colliders, are studied, and the reach of direct searches is compared with the precision attainable with Higgs couplings measurements. The results are then applied to the NMSSM and Twin Higgs.

1 Introduction

Is the Higgs boson recently found by the ATLAS and CMS experiments the only scalar particle, or are there other Higgs-like states around the Fermi scale? This question is of fundamental importance for particle physics, and motivates a detailed study of the phenomenology of additional scalars, as well as the prospects for their discovery at the LHC and future colliders [1].

The simplest example of an extended Higgs sector is realised adding just a real scalar field, singlet under all the known gauge groups, to the Standard Model (SM). Despite its great simplicity, this scenario is of considerable physical relevance, since it can easily arise in many of the most natural extensions of the SM – e.g. the Next-to-Minimal Supersymmetric SM (NMSSM), Twin Higgs, some Composite Higgs models.

In general, such a singlet will mix with the Higgs boson. As a consequence, both physical scalar states are coupled to SM particles, hence they can both be produced at colliders and be observed by means of their visible decays. In the following, after briefly reviewing the main properties of a generic singlet-like scalar, I shall present the constraints on the existence of such a particle that arise from both direct searches and Higgs couplings precision measurements.

2 General properties

Let us call h and ϕ the two neutral, CP-even propagating degrees of freedom, with masses $m_h = 125.1$ GeV and m_ϕ. They are related to the Higgs and singlet gauge eigenstates via a mixing angle γ.

In a weakly interacting theory, the couplings of h and ϕ are just the ones of a standard Higgs boson with the same mass, rescaled by a universal factor of c_γ or s_γ, respectively. As a consequence, their signal strengths $\mu_{h,\phi}$ are

$$\begin{aligned}
\mu_h &= \mu_{\rm SM}(m_h) \times c_\gamma^2, &(1)\\
\mu_{\phi\to VV,ff} &= \mu_{\rm SM}(m_\phi) \times s_\gamma^2 \times (1 - {\rm BR}_{\phi\to hh}), &(2)\\
\mu_{\phi\to hh} &= \sigma_{\rm SM}(m_\phi) \times s_\gamma^2 \times {\rm BR}_{\phi\to hh}, &(3)
\end{aligned}$$

where $\mu_{\rm SM}(m)$ is the corresponding signal strength of a SM Higgs with mass m, and ${\rm BR}_{\phi\to hh}$ is the branching ratio of ϕ into two 125 GeV Higgs bosons. The phenomenology of the Higgs system is therefore completely described by three parameters: m_ϕ, s_γ, and ${\rm BR}_{\phi\to hh}$. The second state ϕ behaves like a heavy SM Higgs boson, with reduced couplings and an additional decay width into hh.

Notice that the mixing angle γ and m_ϕ are not independent quantities, since the former has to vanish when the mass tends to infinity. Indeed,

$$\sin^2\gamma = \frac{M_{hh}^2 - m_h^2}{m_\phi^2 - m_h^2}, \tag{4}$$

where M_{hh} is the first diagonal entry of the mass matrix of the scalar system before diagonalisation, which is proportional to the electroweak scale.

In the limit of large m_ϕ, the Goldstone boson equivalence theorem sets the relations

$$\mathrm{BR}_{\phi\to hh} = \mathrm{BR}_{\phi\to ZZ} = \frac{1}{2}\mathrm{BR}_{\phi\to WW}. \tag{5}$$

The exact formulae for the hhh and ϕhh couplings are reported in reference [1].

2.1 Higgs couplings

The measurement of the Higgs signal strengths provides a constraint on the mixing angle γ through eq. (1). At present, a global fit to 8 TeV LHC data constrain it to be $s_\gamma^2 < 0.23$ at 95% C.L. [2]. Projections for the reach of future hadron and lepton colliders [3] are listed in Table 1.

Large modifications to the triple Higgs coupling can arise in some regions of the parameter space, even if the deviation in the signal strengths is moderate. Future collider experiments, and even the LHC, could in principle be sensitive to these modifications. More details about Higgs couplings can be found in [1].

3 Direct searches

The main decay channels of a heavy singlet are into a pair of W and Z vector bosons, or into a pair of Higgs bosons, if kinematically allowed.

Table 1: *Current and expected precisions on Higgs couplings* [3].

pp	LHC8	LHC14	HL-LHC	HE-LHC	FCC-hh
s_γ^2	0.2	0.08–0.12	0.04–0.08	?	?
$\lvert\Delta g_{hhh}/g_{hhh}^{\mathrm{SM}}\rvert$	–	6	0.5	0.2	0.08
e^+e^-	ILC500	ILC1000	HL-ILC	CLIC	FCC-ee
s_γ^2	0.02	0.02	4×10^{-3}	2–3×10^{-3}	10^{-3}
$\lvert\Delta g_{hhh}/g_{hhh}^{\mathrm{SM}}\rvert$	0.83	0.46	0.1–0.2	0.1–0.2	–

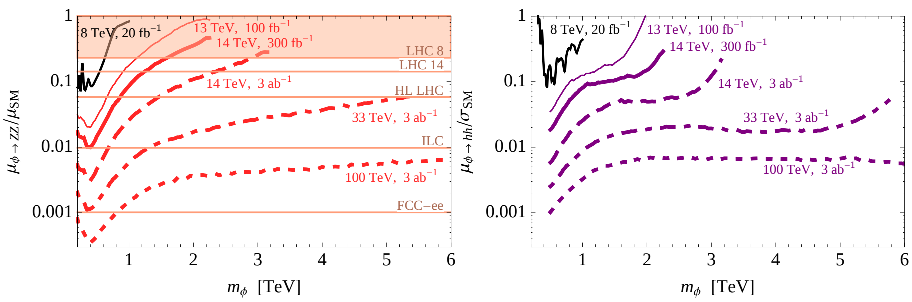

Figure 1: *Excluded values and projected reach for $\mu_{\phi\to ZZ}$ (left) and $\mu_{\phi\to hh}$ (right). In the left panel, the s_γ^2 exclusion from Higgs couplings is also superimposed, assuming a 100% branching ratio into vectors.*

Both the ATLAS and CMS collaborations provide a combined limit from all the WW and ZZ channels, with the strongest bound always coming from searches in the 4ℓ and $2\ell 2\nu$ final states [4)]. In the di-Higgs channel, the main constraint comes from the $4b$ final state [5)]. All these searches are already sensitive to cross-sections smaller than the ones for a SM Higgs at the same mass, and exceed the reach of Higgs coupling measurements for low enough m_ϕ.

Projections for future colliders have been obtained in [1)], rescaling the expected limits from the 8 TeV LHC with the parton luminosities of the backgrounds, following the procedure presented in [6)]. The colliders that have been considered are: the 8 TeV, 13 TeV, and 14 TeV LHC, its high-luminosity upgrade, a possible 33 TeV energy upgrade, and a futuristic 100 TeV FCC-hh.

Figure 1 shows the present and extrapolated limits on the $\mu_{\phi\to VV}$ and $\mu_{\phi\to hh}$ signal strengths, normalised to SM values of the cross-sections. In the left panel the projections for 125 GeV Higgs couplings measurements are also shown, in the limit of small $\mathrm{BR}_{\phi\to hh}$. Figure 2 again shows a comparison between direct and indirect searches, but this time in the m_ϕ–M_{hh} plane, and for $\mathrm{BR}_{\phi\to hh} = 1/4$. The direct exclusion is dominated by $\phi\to VV$.

4 Explicit models

4.1 Supersymmetry

The Higgs sector of the NMSSM [7)] contains the two usual doublets $H_{u,d}$, plus a singlet scalar S, coupled through a Yukawa interaction $\lambda H_u H_d S$ in the

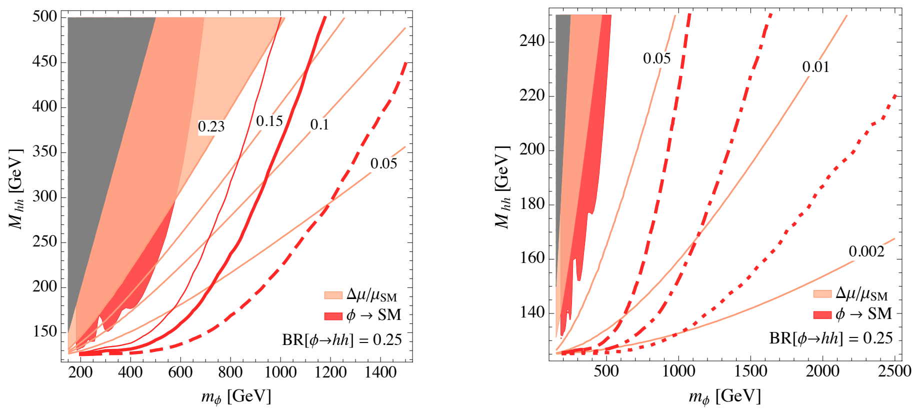

Figure 2: *Comparison between the combined reach of direct searches and Higgs coupling measurements, in the plane m_ϕ–M_{hh}. $\mathrm{BR}_{\phi\to hh}$ has been fixed to 0.25 for simplicity. Left: region relevant for the LHC. Right: projections for future colliders. The notation for the lines is the same as in Figure 1.*

superpotential. An extra contribution to the Higgs mass is generated at tree-level by λ, and reduces the size of the radiative correction needed to obtain 125 GeV. At the same time, the fine-tuning of the electroweak scale v is reduced.

In the decoupling limit for the heavy doublet, the CP-even states are the SM Higgs and the singlet, and can be matched to the previous scenario via [8)]

$$M_{hh}^2 = m_Z^2 c_{2\beta}^2 + v^2\lambda^2 s_{2\beta}^2 + \Delta^2, \tag{6}$$

where Δ is the radiative correction and $\tan\beta = v_u/v_d$. Figure 3 (left) shows the current exclusions and projections from both direct searches and Higgs couplings, in the plane m_ϕ–$\tan\beta$, for fixed values of $\lambda = 1$ and $\Delta = 70$ GeV.

4.2 Twin Higgs

In Twin Higgs models [9)], a naturally light Higgs is obtained without the presence of coloured particles close to the TeV scale. This is achieved introducing a copy of the SM field content and gauge symmetries, $\mathrm{SM_A} \times \mathrm{SM_B}$. The Higgs potential has an approximate global SO(8) symmetry, which is spontaneously broken at a scale f, and the Higgs $h = H_\mathrm{A}\cos\gamma + H_\mathrm{B}\sin\gamma$ is a Goldstone boson of this breaking. Quadratic "divergences" in the Higgs mass cancel between the A and B sectors, while all the new Twin particles are SM singlets.

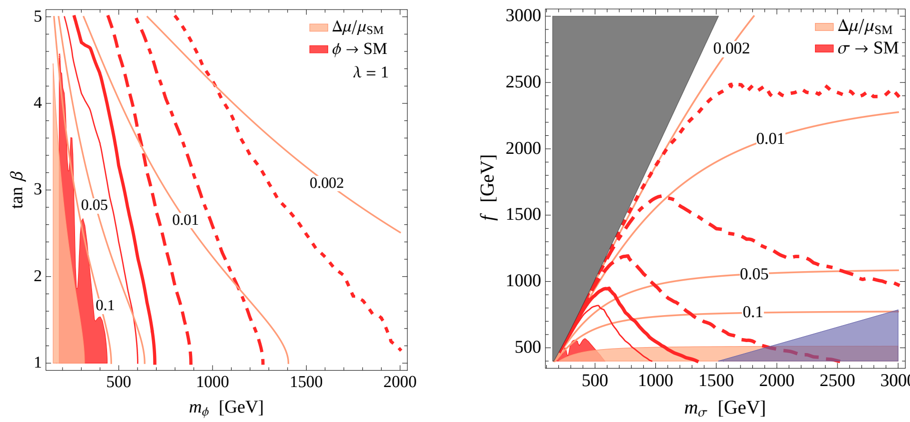

Figure 3: *Current exclusions and projections for the NMSSM singlet with* $\lambda = 1$ *and* $\Delta = 70$ *GeV (left), and the Twin Higgs radial mode (right). The notation is the same as in Figure 1. In the purple region the width* $\Gamma_\phi > m_\phi$*.*

The phenomenology of the "radial mode" $\sigma = H_{\rm B}\cos\gamma - H_{\rm A}\sin\gamma$ is described by eq. (2), (3). The mixing angle is proportional to v/f, and one has

$$M_{hh}^2 = \frac{v^2}{f^2}(m_\sigma^2 + m_h^2). \tag{7}$$

The only difference with respect to the previous cases is the presence of an invisible width into $W_{\rm B}$ and $Z_{\rm B}$ bosons. Figure 3 (right) illustrates the present and future constraints in the plane m_σ–f, which are the only two free parameters of the model. One can see that direct searches for the radial mode are the most powerful probe for a Twin Higgs scenario, at least for not too large values of m_σ and f.

5 Conclusions

Searches for scalar singlets at colliders can be an important probe for the extended Higgs sectors of many physically motivated models, and complementary to the measurement of Higgs couplings. By means of only three parameters that determine the phenomenology in a completely general way, the reach of future colliders in the relevant VV and hh channels has been studied. On the other hand, already the second run of the LHC can efficiently explore this scenario, and will provide valuable information in the near future.

Acknowledgements

I thank Filippo Sala and Andrea Tesi for the stimulating collaboration on which the results presented here are based. This research was supported in part by the Swiss National Science Foundation (SNF) under contract 200021-159720.

References

1. D. Buttazzo, F. Sala, A. Tesi, JHEP **1511**, 033 (2015), [arXiv:1505.05488].

2. P. P. Giardino *et al.*, JHEP **1405**, 046 (2014), [arXiv:1303.3570].

3. S. Dawson *et al.*, Working Group Report: Higgs boson, Community Summer Study 2013: Snowmass on the Mississippi (2013), [arXiv:1310.8361].

4. CMS collaboration, JHEP **1510** 144 (2015), [arXiv: 1504.00936].

5. CMS collaboration, Phys. Lett. B **749**, 560 (2015), [arXiv:1503.04114].

6. A. Thamm, R. Torre, A. Wulzer, JHEP **1507**, 100 (2015), [arXiv:1502.01701].

7. U. Ellwanger, C. Hugonie, A. M. Teixeira, Phys. Rept. **496** 1 (2010), [arXiv:0910.1785].

8. R. Barbieri *et al.*, Phys. Rev. D **87**, 115018 (2013), [arXiv:1304.3670].

9. Z. Chacko, H.-S. Goh, R. Harnik, Phys. Rev. Lett. **96**, 231802 (2006), [hep-ph/0506256].

COSMOLOGICAL HISTORY
OF THE HIGGS VACUUM INSTABILITY

Enrico Morgante
Département de Physique Théorique & Centre for Astroparticle Physics,
Université de Genève
24 quai Ernest-Ansermet, 1211 Genève 4, Switzerland

Abstract

A known property of the Higgs effective potential within the Standard Model is that it develops an instability for very large field values. During inflation, quantum fluctuations can overcome the potential barrier and make the Higgs fall into its true minimum at Planckian scales, forming anti-de Sitter patches that are lethal for the subsequent evolution of our Universe. By analysing the dynamics of the Higgs during and after inflation, we derive a bound on the inflationary Hubble rate that depends on the reheating temperature and on the coupling of the Higgs to the scalar curvature or the inflaton.

1 Introduction

Current measurements of the Higgs boson and top quark masses imply an extremely intriguing result: in the context of the Standard Model with no additional physics, our universe lies at the edge between stability and instability of the Electro-Weak vacuum [1]. Following the SM Renormalization Group equations, the quartic Higgs coupling becomes negative at a scale around $10^{10} \div 10^{11}$ GeV, with a strong dependence on the precise value of m_H and m_t. What is even more puzzling is the fact that, for the present best fit values of m_H and m_t, we live in the peculiar situation in which the EW vacuum is unstable, but the tunnelling probability is so suppressed that its lifetime is larger than the age of the universe. This fact is usually referred to as "metastability".

The issue of vacuum instability becomes of particular interest in the early universe. There are three main effects that can modify the situation, and which can be used, in turn, to put bounds on early-time parameters:

1. During inflation, quantum fluctuations of the Higgs field are governed by the size of the Hubble parameter H. If this is large enough, the Higgs can overcome the potential barrier and fall into its deep minimum with negative energy, leading to the creation of regions of anti-de Sitter space.

2. A non minimal coupling of the Higgs to gravity can generate an effective mass term which stabilises the potential. The same could happen as a consequence of a coupling of the Higgs to the inflaton.

3. Thermal effects during the early phases of radiation dominance are twofold: fluctuations can trigger the "jump" of the barrier, while corrections to the effective potential create an additional effective barrier.

In order to study the evolution of the Higgs field h during the inflatiorary and (pre-)heating phases, one first has to determine under which conditions h can fall into its true minimum, and second determine the evolution of the regions in which this have happened, under the assumption that the large negative potential energy forces the metric to be anti-de Sitter inside the bubble.

The aim of this talk is to summarize the discussion of [2], in which the full process is reconsidered and new conclusion are drawn on the value of the Hubble parameter during inflation and other relevant physical quantities.

2 Higgs fluctuation during inflation

During inflation, quantum fluctuations of long wavelength modes of the Higgs field are governed, in the absence of a large mass term, by a Langevin stochastic equation. Starting from $h = 0$ at $t = 0$ and generating a large set of random evolution of h, the resulting distribution is well approximated by a gaussian distribution

$$P(h,N) = \frac{1}{\sqrt{2\pi\langle h^2\rangle}} \exp\left(-\frac{h^2}{2\langle h^2\rangle}\right) , \qquad \sqrt{\langle h^2\rangle} = \frac{H}{2\pi}\sqrt{N}. \tag{1}$$

The $\sqrt{N}$ behaviour signals the fact that the potential $V(h)$ can be neglected and the evolution is dominated by quantum fluctuations. It's only in the very tail that the distribution becomes non-gaussian: this is due to the fact that the potential term becomes dominant, and the Higgs starts rolling classically down towards its minimum.

2.1 Addition of an effective mass term

Higgs fluctuations during inflation can get damped if the Higgs doublet Φ_H acquires a mass term during inflation. This could happen because of a Higgs-inflaton coupling, because of a non-vanishing temperature generated during inflation by inflaton decays, or thanks to a non minimal coupling of the Higgs to gravity. We will consider here only this last possibility, by adding to the effective lagrangian a term

$$-\xi_H |\Phi_H|^2 R \tag{2}$$

which for constant R produces a large mass $m^2 = \xi_H R = -12\xi_H H^2$. Notice that the presence of this term is unavoidable, since it is generated by RG equations for ξ_H, which have as the only fixed point the conformal value $\xi_H = -1/6$. Assuming $\xi_H < 0$, the potential is stabilized by the effective mass term: if $\xi_H < -3/16$ then fluctuations are exponentially damped, otherwise if $-3/16 < \xi_H < 0$ the distribution at the end of inflation is again quasi gaussian, with

$$\sqrt{\langle h^2\rangle} = \frac{H}{4\pi\sqrt{-2\xi_H}} \, . \tag{3}$$

In this case, the presence of the large mass term invalidates the use of the Langevin equation, and the evolution of the probability must be studied by means of a Fokker-Planck equation, taking $P(h = \pm\infty) = 0$ as boundary conditions. Results are summarized in fig.1. Three regions can be distinguished, depending on the value of h at the end of inflation:

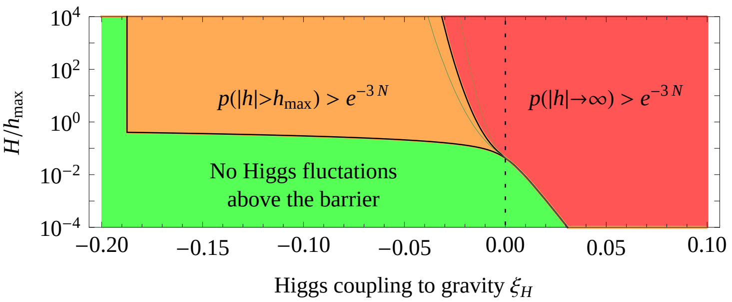

Figure 1: *As a function of* ξ_H *and the Hubble constant in units of the instability scale* $h_{\rm max}$ *(and for* $N = 60$ *e-folds of inflation), we show the three regions where: the probability for the Higgs field to end up in the negative-energy true minimum is larger than* e^{-3N} *(red); the probability for the Higgs field to fluctuate beyond the potential barrier is larger than* e^{-3N} *(orange); the latter probability is smaller than* e^{-3N} *(green). Higgs fluctuations are damped for* $\xi_H < -3/16$. *The uncertainty on the orange/red boundary corresponds to a fudge factor* $1/3 < k < 3$.

1. Regions in which h is smaller than the scale $h_{\rm max} \approx 5 \times 10^{10}$ GeV at which the potential $V(h)$ has its maximum. After inflation ends, h just rolls down its potential, until it reaches the EW vacuum.
2. Regions in which $h > h_{\rm max}$ but quantum fluctuations still dominate over classical rolling, so that at the end of inflation they have not fallen into the true minimun yet.
3. Regions in which h falls into its deep minimum and an AdS bubble forms during inflation.

3 Fate of the AdS bubbles

Understanding the fate of the regions in which the Higgs falls into its true minimum is a very complicated task. An involved GR calculation is presented in [2], under the assumptions of spherical bubbles with a thin wall to separe them from the external background metric. Results can be summarized as follows:

- During inflation (de Sitter background), bubbles can expand or shrink depending on parameters such as the size of the bubble, its internal energy, initial wall velocity and surface tension. Even for expanding bubbles, cosmic expansion is fast enough to hide them behind a de Sitter horizon, so that they don't eat up the whole universe.
- After inflation ends (quasi-Minkowski background), expanding bubbles continue their growth faster than the expansion rate of the universe, and eventually "eat" all space.

As a general conclusion, there is no GR effect that can prevent bubbles from filling the universe. We must then impose that bubbles do not form during inflation: the red region in fig.1 is therefore excluded. As we will discuss in the next section, the orange region can instead be saved by thermal effects during reheating.

4 Thermal effects during radiation dominance

Even if one may naïvely think that the effect of a thermal bath would be that of further destabilize the situation by adding thermal fluctuations, their main consequence is actually the opposite [3]: thermal corrections to the effective potential generate a temperature dependent mass term $m^2 \propto T^2$ which stabilizes the potential. During the reheating phase, temperature (and therefore the thermal mass term) rises up to the value $T_{\rm max}$, then decreases as $a^{-3/8}$ until it reaches $T_{\rm RH}$ at the end of the reheating phase, and finally starts following the a^{-1} behaviour typical of radiation dominance. If $T_{\rm RH}$ is high, the thermal mass is large enough to change the slope of the effective potential $V(h)$ for values $h > h_{\rm max}$ (which correspond to the orange region of fig.1). The Higgs field starts rolling towards zero, and if it crosses the critical value $h_{\rm max}$ before temperature drops then no bubble form. Fig.2 shows the minimal reheating temperature needed in order to avoid bubble formation after inflation, demonstrating that the orange region can be saved by thermal effects.

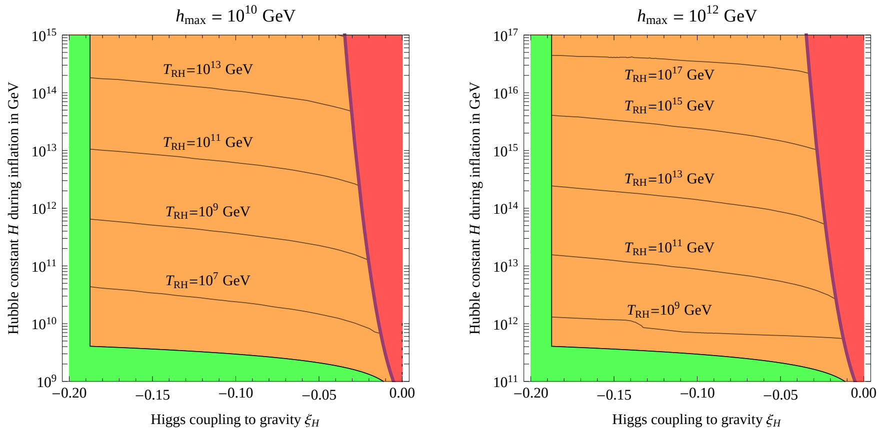

Figure 2: *Minimal reheating temperature* $T_{\rm RH}$ *needed to prevent the fall of the Higgs down into its deep true vacuum, assuming two different values for the instability scale* $h_{\rm max}$ *of the Higgs potential.*

5 Conclusion and possible new directions

We studied the evolution of the Higgs field and its instability, during inflation and during the early phases of radiation dominance. Whenever the Higgs falls in its deep minimum, a bubble of AdS forms, (possibly) expands and eventually eats all the visible universe. Bounds can be put on inflationary parameters by requiring that no bubble forms during inflation. Thermal effects after inflation and induced Higgs mass terms (e.g. non minimal coupling to gravity) play a key role in saving the EW vacuum.

References

1. D. Buttazzo *et al.*, JHEP **1312** 089 (2013), [arXiv:1307.3536 [hep-ph]].
2. J. R. Espinosa *et al.*, JHEP **1509** 174 (2015) [arXiv:1505.04825 [hep-ph]].
3. J. R. Espinosa *et al.*, JCAP **0805** 002 (2008) [arXiv:0710.2484 [hep-ph]].

Recent results from the AMS experiment on the International Space Station after 4 years in Space

Valerio Vagelli, on behalf of the AMS Collaboration.
Istituto Nazionale di Fisica Nucleare – Sezione di Perugia

Abstract

AMS-02 is a cosmic ray detector operating on the International Space Station since May 2011, to conduct a unique mission of fundamental research in space. This contribution reviews the most recent AMS results and the consequent potential advances in the current understanding of cosmic ray origin, acceleration and propagation physics.

1 Introduction

Cosmic rays (CRs) constitute a window to investigate the open problems of fundamental physics in an approach complementary to that of collider physics. The indirect search for Dark Matter (DM) is, indeed, one of the main targets of CR research. With the current detection technology, precision measurements of CR composition, spectra, isotropy and time variability can be finally performed

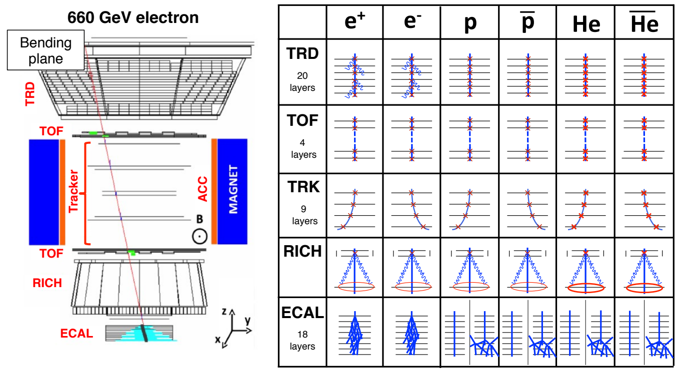

Figure 1: Left – Event display of a 660 GeV e^- detected by AMS-02. Right – Response of the AMS-02 subdetectors for different matter/antimatter CRs.

in space, outside the Earth atmosphere. This contribution reviews the latest results of the space borne experiment AMS.

2 The AMS-02 detector

AMS-02 is a particle physics detector which has been installed on the International Space Station (ISS) in May 2011 to conduct a long-duration (∼20-year) mission of fundamental physics research in space. The main goals of the AMS mission are the detection of primordial antimatter and indirect DM signatures in the fluxes of CRs through the accurate measurement of CR composition and energy spectra up to the TeV scale. The AMS-02 detector is described in details in [1]. It consists of a magnetic spectrometer surrounded by a time of flight system (TOF) for the measurement of the particle rigidity, charge and charge sign. The particle identification capabilities are improved by the measurements of a transition radiation detector (TRD), of a ring imaging Cherenkov detector (RICH) and of an electromagnetic calorimeter (ECAL). Figure 1 shows the AMS-02 detector and the response of its subdetectors for different species of CRs. AMS-02 is continuously operating on the ISS with steady performances, collecting ∼ 1.5 billion CRs each month with no major interruption so far.

3 The hunt for Dark Matter: electrons, positrons and antiprotons

Indirect DM evidence could show up as unexpected features in the spectra of rare components of CRs, like electrons/positrons ($e^{\pm}$) or anti–protons ($\overline{p}$). The DM annihilation – or decay – contribution to the flux of $e^{\pm}$ and $\overline{p}$ could in fact dominate over the purely astrophysical contribution for certain energy ranges.

The independent and complementary measurements of ECAL and TRD allow AMS-02 to separate the tiny $e^{\pm}$ CR component from the overwhelming hadronic CR component, achieving an unprecedented accuracy in the analysis of the $e^{\pm}$ spectral features. The fluxes of e^{+} and e^{-} have been measured by AMS up to, respectively, 500 GeV and 700 GeV [2]. The data show that the $e^{\pm}$ fluxes both harden with increasing energy above 20 GeV, but the e^{-} flux results softer than the e^{+} flux. More sensitive information is provided by the measurement of the positron fraction (PF) $e^{+}/(e^{+}+e^{-})$, for which most of the flux normalization systematic uncertainties cancel to a large extent. The PF has been measured by AMS up to 500 GeV [3]. The PF rises up to $\sim$200 GeV, with its maximum measured to be at 275$\pm$32 GeV. Above this energy, the PF does no longer increase with energy. These observations are not consistent with the expected production of e^{+} from interactions of CRs with the interstellar gas, but they hint to the existence of an additional primary $e^{\pm}$ source, like DM annihilation or production in nearby pulsars, or of unconventional acceleration and propagation mechanisms [4]. Additional distinct information is provided by a dedicated analysis of the total $(e^{+}+e^{-})$ flux, measured disregarding the particle charge sign to achieve an improvement of the systematic uncertainties with respect to the separate $e^{\pm}$ flux measurements. AMS has measured the $(e^{+}+e^{-})$ flux from up to 1 TeV [5]. No features have been observed in the flux, and the $(e^{+}+e^{-})$ spectrum is described by a single power law above 30 GeV.

Figure 2 shows the AMS $e^{\pm}$ measurements. The AMS results are based on 10.6 million $e^{\pm}$ events collected in the first 30 months of operations, and corresponding to $\sim$15% of the expected data sample for the whole AMS mission.

Complementary measurements of different CR channels are essential to identify the dominant source of the $e^{\pm}$ excess observed in the AMS data. The $\overline{p}/p$ ratio is one of the observables which is most sensitive to the DM contribution. AMS-02 has collected 0.29 million $\overline{p}$ CRs during the first 40 months of data taking. These data have been analized to provide a preliminary measurement of the $\overline{p}/p$ ratio up to 450 GV [6]. The AMS result extends the previous $\overline{p}$ measurements towards an energy range never explored so far, and shows that the $\overline{p}/p$ ratio remains almost flat above 50 GV. This behaviour is at the limit of compatibility with the current astrophysical model predictions, for which the $\overline{p}/p$ ratio is expected to decrease for increasing energies [7]. Future data collected by AMS will be critical to lower the uncertainties on the measured

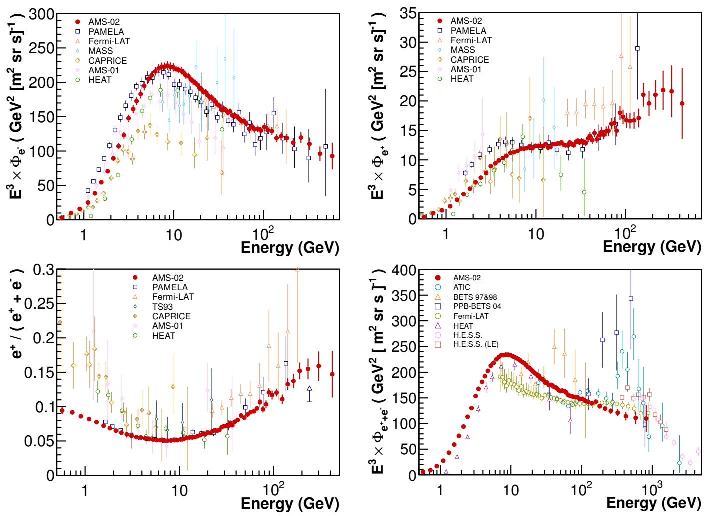

Figure 2: In red, AMS measurements of the e$^-$ flux (top-left), of the e$^+$ flux (top-right), of the positron fraction (bottom-left) and of the (e$^+$ + e$^-$) flux (bottom-right). References in [2, 3, 5].

and on the expected $\overline{\mathrm{p}}$/p ratio and to consequently solve this tension.

4 AMS measurements of light nuclei

Protons (p) and Helium nuclei (He) are the dominant components of CRs. A detailed analysis of their spectral features may provide useful information for the understanding of the origin, acceleration and propagation of CRs. Due to the large statistics of p and He nuclei collected by AMS-02, the accurate measurement of their fluxes requires a detailed understanding of the detector properties and response. All the systematic uncertainties, including among others the rigidity scale, the rigidity resolution and the uncertainty on the nuclear cross sections with the detector materials, have been studied in details with several verifications of the stability of the measurements for different conditions. The p and He fluxes have been measured by AMS with unprecedented accuracy respectively from 1 GV to 1.8 TV and from 2 GV to 3 TV [8].

The resulting spectra are shown in Figure 3. The AMS measurements

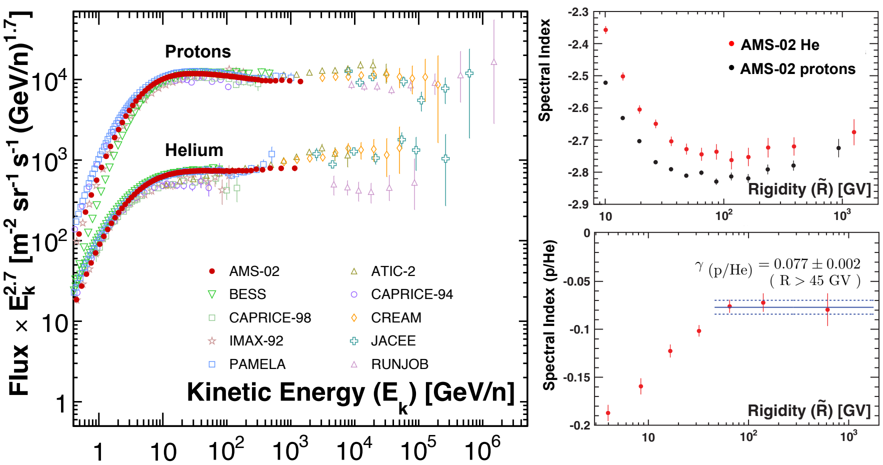

Figure 3: Left – in red, AMS measurements of the p and He fluxes as function of the kinetic energy per nucleon. Right – Spectral index rigidity dependence of the p and He fluxes (top) and of the p/He ratio (bottom). References in [8].

show that both the p and He fluxes deviate from single power laws and that they start to gradually harden above 100 GV. Remarkably, while the p flux differs in magnitude from the He flux, its variation has been observed to be, both in shape and in modulation, analogous to that of the He. A broken power law parametrization applied to the data favors a spectral index break at $\sim 300\,\mathrm{GV}$ for both species. The AMS results are based on the analysis of 300 million p and 50 million He events identified in the data collected in the first 30 months of operations.

AMS-02 has also the capabilities to measure the less abundant heavier nuclei. The measurements of the particle charge at different depths of the detector is crucial to identify the interactions of primary nuclei with the detector materials and to reduce the systematic uncertainties for the measurements of CR nuclei. The AMS data have been analized to provide a preliminary measurement of the Lithium (Li) flux up to 3 TV [9], of the Carbon (C) flux up to 1.8 TV [10] and of the Boron/Carbon (B/C) ratio up to 1.8 TV [11].

The high statistics collected by the AMS-02 detector has allowed to measure the Li flux for the first time with outstanding accuracy. The data favour a break in the Li spectral index in the same rigidity range observed for p and He.

This may hint to an unexpected change of CR origin and propagation regime at these rigidities. The current statistical uncertainties on the C flux prevent to verify if the same break is present also for higher charges.

5 Conclusions

AMS is showing the potential of space borne detectors for precision CR physics. The large data sample collected by AMS-02 and the precise knowledge of the detector performances in space have allowed to measure CR properties at the level of few percents. Further improvements will be reached as the new data will be collected and analized, towards an enriched understanding of the physics of CR origin, acceleration and propagation.

References

1. M. Aguilar *et al*, Phys. Rev. Lett. **110**, 141102 (2013).
2. M. Aguilar *et al*, Phys. Rev. Lett. **113**, 121102 (2014).
3. L. Accardo *et al*, Phys. Rev. Lett. **113**, 121101 (2014).
4. L. Feng *et al*, Phys. Lett. B **728**, 250 (2014); K. Blum *et al*, Phys. Rev. Lett. **111**, 211101 (2013); L. Bergström *et al*, Phys. Rev. Lett. **111**, 171101 (2013); I. Cholis and D. Hooper, Phys. Rev. D **88**, 023013 (2013); T. Linden and S. Profumo, Astrophys. J. **772**, 18 (2013).
5. M. Aguilar *et al*, Phys. Rev. Lett. **113**, 221101 (2014).
6. A. Kounine, in: PoS ICRC **2015**, 300 (2015).
7. G. Giesen *et al*, JCAP **1509**, 023 (2015); C. Evoli *et al*, arXiv:1504.05175 [astro-ph.HE]; R.Kappl *et al*, JCAP **1510**, 034 (2015).
8. M. Aguilar *et al*, Phys. Rev. Lett. **114**, 171103 (2015); M. Aguilar *et al*, Phys. Rev. Lett. **115**, 211101 (2015).
9. L. Derome, in: PoS ICRC **2015**, 303 (2015).
10. M. Heil, in: PoS ICRC **2015**, 289 (2015).
11. A. Oliva, in: PoS ICRC **2015**, 265 (2015).

COSMIC RAY ANTIPROTONS AS A DARK MATTER PROBE

Carmelo Evoli
GSSI and INFN, L'Aquila
Daniele Gaggero
GRAPPA, Amsterdam
Dario Grasso *
INFN, Pisa

Abstract

After PAMELA, the AMS-02 collaboration recently released the preliminary antiproton-to-proton ratio of the cosmic radiation. These experiments also published accurate measurements of several observables relevant for the computation of secondary antiprotons produced by cosmic-ray spallation: in particular, the proton and Helium spectra and the Boron-to-Carbon ratio. These measurements are very important since a discrepancy between the model predictions and experimental data may be interpreted as an evidence of dark matter (DM) annihilation in the Galactic halo. In this contribution we will summarize the basic aspects of the secondary $\bar{p}$ production and discuss the involved astrophysical and nuclear uncertainties. We will then show that, given these uncertainties, no significant evidence of an antiproton excess can be currently claimed on the basis of PAMELA and AMS-02 results, and discuss the corresponding most conservative constraints on the DM annihilation cross section. Interestingly, the parameter space region compatible of the γ-ray GeV excess in the Galactic center region is still allowed by those constraints.

* speaker

1 Introduction

In the latest few years Fermi-LAT, PAMELA and AMS-02 cosmic-ray (CR) observatories led to impressive progresses in particle astrophysics. The study of antiparticle spectra is one of the main goals of these experiments, since these species may show signatures of dark matter (DM) annihilation or decay in the Galactic halo. This search must be complemented by multi-messenger study of many different primary and secondary CR species. This additional study is required: *a)* in order to compute the antiparticles background due to primary CR spallation onto the interstellar medium; *b)* in order to constrain the propagation properties of DM annihilation/decay products.

Those computations require dedicated semi-analytical or numerical tools. Relevant progresses have been performed also on this side, both concerning the computation the spectra of DM annihilation/decay products, by means of codes like `DARKSUSY` [1] or `PPPC4DMID` [2], which now include electroweak corrections [3], and regarding numerical solvers of the CR transport equation like `DRAGON` [4].

In spite of these progresses, large uncertainties are still present in the predictions of both the background and the DM halo function due to the poorly known production cross-sections (CSs) of secondary particles, DM density profiles and CR propagation parameters. In this contribution we will discuss their impact on the sensitivity of current experiments to the main DM properties. We will focus on the antiproton channel since it is one of less affected by astrophysical uncertainties.

2 Secondary antiproton from CR spallation

The differential production rate of secondary antiprotons due to the interaction of CR nuclei with the ISM is given by:

$$Q_{\bar{p}}(E_k) = \sum_{i=\mathrm{H,He}} \sum_{j=\mathrm{H,He}} 4\pi \int_{E_k^{\mathrm{th}}}^{\infty} dE'_k \left(\frac{d\sigma}{dE_k}\right)_{ij} n_i \phi_j(E'_k) \tag{1}$$

where E'_k and E_k are the kinetic energies per nucleon of the incoming nucleus (with threshold energy $E_{\mathrm{th}} = 6m_p$) and the outgoing antiproton, respectively; $d\sigma/dE_k$ is the production differential CS and n_i denotes the interstellar hydrogen density. For the parameterization of the $\bar{p}$ production CSs we use the recent results reported in [5] based on NA49 precision measurements and on a careful treatment of $\bar{p}$ arising from antineutron and hyperon decay.

CR primary nuclei are produced in astrophysical sources and reach the Earth after diffusive propagation in the Galactic magnetic fields. Above 10 GeV/nucleon the spiral arm structure of the Galaxy is irrelevant so that spatial diffusion can be effectively treated as cylindrically symmetric in terms of the Galactocentric radius r and of the distance from the Galactic plane z. While the radial extension of the CR pool does not affect significantly local observables its vertical extension L is more relevant here. In fact, CR are expected to leave the Galaxy mostly along the z axis so that the quantity of matter (*grammage*) encountered by CRs before escaping, and hence the secondary antiproton flux, is determined by the ratio L/D, where D is the diffusion coefficient. L is poorly constrained to be in the range $1 \lesssim L \lesssim 10$ kpc on the basis of the ^{10}Be/^{9}Be radio-clock probe (see however below). The L/D normalization and rigidity dependence can, however, be effectively constrained against secondary/primary CR nuclear ratios - the Boron-to-Carbon (B/C) most importantly. Other propagation parameters as the Alfvèn velocity v_A, which determines the re-acceleration strength, and the advection velocity v_c need also to be constrained on the basis of multi-messenger CR data.

Here we use B/C measurements recently released by the PAMELA collaboration [6] as well as the spectra of protons, Helium (responsible for most $\bar{p}$ production), Carbon (responsible for most Boron production) by the same experiment. Using dataset from the same observatory taken in the same period is important in order to reduce uncertainties related to solar modulation, which are relevant below 10 GeV/nucleon. We scanned 10^4 `DRAGON` models and we computed the secondary $\bar{p}$ spectrum only for those compatible with those data. In the left panel of fig. 1 we compare the envelope of these $\bar{p}$ spectra with PAMELA results [7]. Clearly, no additional antiproton source is required to account for those data. This is also the case for AMS results [8]. Indeed, the $\bar{p}/p$ computed adopting the propagation model giving the B/C best-fit is in excellent agreement with preliminary AMS results [9] (see also [10, 11]). In the right panel of Fig.1 we compare the effect of CS and propagation uncertainties. Upcoming measurements are expected to significantly improve the latter. In that situation, uncertainties on $\bar{p}$ production CSs may become dominant unless a significant experimental efforts will be done to reduce them.

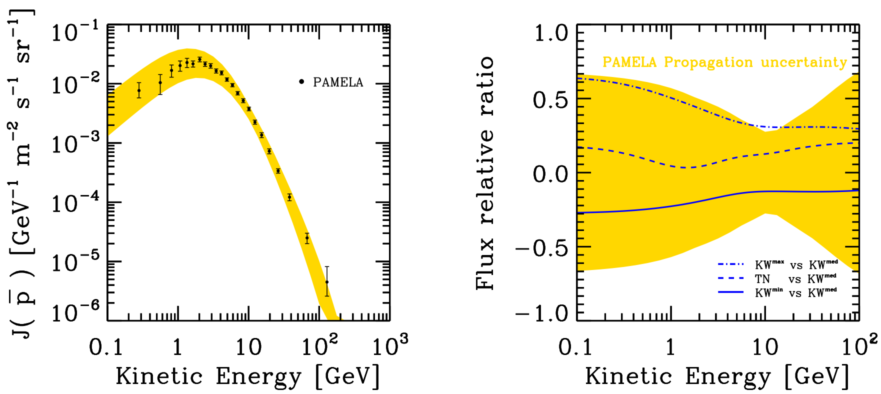

Figure 1: *Left plot: The envelope of the secondary $\bar{p}$ spectra computed with the different propagation models found to reproduce the B/C and primary spectra is compared with PAMELA data. Right plot: Comparison between propagation and nuclear uncertainties. Yellow band: Error on the $\bar{p}$ flux due to the uncertainty in the propagation parameters. Blue lines: The relative difference between the $\bar{p}$ flux computed using the fiducial CS used in this work and its maximal/minimal realization; a comparison is also done with the model conventionally adopted in the related literature (solid line).*

3 Antiprotons from dark matter annihilation

In addition to the spallation of CRs onto the ISM nuclei, antiprotons may be produced in the Galaxy by DM annihilation or decay. Similarly to what done in several previous works, e.g., [12, 13], we compute the DM contribution to the antiproton flux assuming that the source function ($Q_{\rm DM}$) has the general form:

$$Q_{\rm DM}(E_k, r, z) \;=\; \frac{1}{2}\,\frac{\rho^2_{\rm DM}(x)}{m^2_{\rm DM}}\,\langle\sigma v\rangle\,\frac{dN_{\bar{p}}}{dE_k}(E_k) \tag{2}$$

where $\langle\sigma v\rangle$ is the thermally averaged annihilation CS and $\rho_{\rm DM}(x)$ is the DM density profile as function of the galactocentric distance $x = \sqrt{r^2+z^2}$. In our analysis, we adopt two spherically symmetric profiles inferred from N-body simulations: a standard Navarro-Frenk-White (NFW) and a generalized NFW (gNFW) as defined, e.g., in [13]. We consider two benchmark annihilation channels: DM DM $\to b\bar{b}$ and DM DM $\to W^+W^-$, and we take the corresponding $\bar{p}$ yields from the PPPC4DMID. We derive upper limits on the annihilation CSs for those channels requiring that the sum of the background and the DM annihilation products - consistently propagated with DRAGON - does not exceed the PAMELA data with a significance larger than 2σ. More details of our procedure are reported in [9]. We choose $L = 2$ kpc since it is the minimum value compatible with synchrotron diffuse emission observations [14] and it minimizes the $\bar{p}$ flux for a given DM model hence giving the most conservative constraints. Indeed, while the actual value of L is irrelevant for the secondary $\bar{p}$, it is the most important source of uncertainty evaluating DM antiprotons.

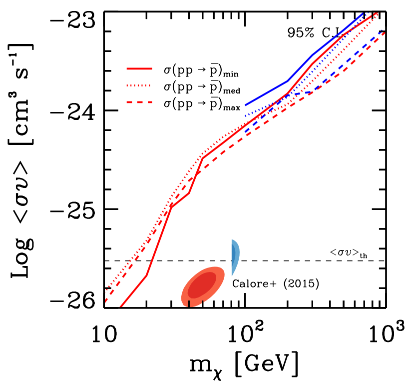

Figure 2: *Antiproton bounds on DM annihilation rate. Red lines: $b\bar{b}$ channel for NFW profile for different assumption for the secondary $\bar{p}$ production. Blue lines: the same for the WW channel. The results obtained with a gNFW profile are indistinguishable from the NFW ones.*

In figure 2 we show our results for the maximum allowed annihilation CS for the $b\bar{b}$ and W^+W^- annihilation channels. They have potential relevance for the DM interpretation of the recently claimed signal in the γ-ray channel located in the inner few degrees around the Galactic center (GC). In [15] the authors show that a DM particle with mass ~ 43 GeV annihilating into $b\bar{b}$ with a CS $\langle\sigma v\rangle \simeq 2.2 \cdot 10^{-26}\,\mathrm{cm}^3\mathrm{s}^{-1}$ and distributed according to a gNFW profile can accomodate the anomalous excess. In figure 2 we compare our findings with the favored regions of annihilation CSs connected to the GC excess as reported in [16].

4 Discussion

The bottom line of this analysis can be summarized as it follows: Although the impressive progresses in the measurements and theoretical modeling of Galactic CRs, a clear signature or a solid exclusion of DM annihilation in the GC region in the $\bar{p}$ channel is still missing. Since the experimental sensitivity to DM in the $\bar{p}$ channel is mostly limited by the large uncertainties on CR propagation parameter - the diffusion halo height most importantly - an effort should be made in order to reduce those uncertainty performing dedicated γ-ray and radio observation campaigns.

References

1. P. Gondolo, *et al.*, JCAP **0407** (2004) 008
2. J. Buch, M. Cirelli, G. Giesen and M. Taoso, JCAP **1509** (2015) 09, 037
3. P. Ciafaloni, *et al.*, JCAP **1103** (2011) 019
4. C. Evoli, D. Gaggero, D. Grasso and L. Maccione, JCAP **0810** (2008) 018
5. R. Kappl and M. W. Winkler, JCAP **1409** (2014) 051
6. O. Adriani *et al.* [PAMELA Coll.], Astrophys. J. **791** (2014) 2, 93
7. O. Adriani *et al.* [PAMELA Coll.], Phys. Rev. Lett. **105** (2010) 121101
8. M. Incagli [AMS Coll.], EPJ Web Conf. **95** (2015) 03017.
9. C. Evoli, D. Gaggero and D. Grasso, arXiv:1504.05175, to appear in JCAP.
10. G. Giesen *et al.*, JCAP **1509** (2015) 09, 023
11. R. Kappl, A. Reinert and M. W. Winkler, JCAP **1510** (2015) 10, 034
12. C. Evoli, *et al.*, Phys. Rev. D **85** (2012) 123511
13. M. Cirelli *et al.*, JCAP **1412** (2014) 12, 045
14. G. Di Bernardo *et al.*, JCAP **1303** (2013) 036
15. T. Daylan, *et al.*, arXiv:1402.6703 [astro-ph.HE].
16. F. Calore, I. Cholis and C. Weniger, JCAP **1503** (2015) 038

ROBUST COLLIDER LIMITS
ON HEAVY-MEDIATOR DARK MATTER

Davide Racco
Département de Physique Théorique, Université de Genève
24 quai Ansermet, CH-1211 Genève 4, Switzerland

Abstract

In these notes we review the proposal of Ref. [2] of a method to derive consistent and reinterpretable bounds from Dark Matter searches at colliders with the use of Effective Field Theories. The results are compared with the reach of Simplified Models, and it is shown that the improved exclusion power of Simplified Models is ultimately due to the resonant production of the mediator. This motivates the interpretation of monojet searches with the Effective Field Theory, to be complemented with dedicated searches of the mediators between Dark Matter and Standard Model.

1 Dark Matter searches at colliders

The search of Dark Matter (DM) is currently one of the main tasks of Particle Physics, and plays an important role in the scientific programme of the LHC.

At colliders, DM shows up as missing energy, and we need the associated production of another object in order to tag the event. This object can be a jet, or a photon, or an electroweak boson or the Higgs boson.
To describe the interaction between DM and the Standard Model we need an appropriate description in terms of a field theory. There is a plethora of microscopic models that include a DM candidate, so it is important to identify an approach that is as model independent as possible in order to interpret the results of these searches. Two possible approaches have been used up to now to interpret the (negative) results of DM searches at colliders.
The first and most obvious one is the use of Effective Field Theories (EFT), in which the Lagrangian is including only the degrees of freedom that are relevant below a given energy threshold, that we denote by $M_{\rm cut}$. The advantages of EFTs are their ample generality, in the sense that they can parametrise potentially *any* model we can think of, and the limited number of parameters they contain, once we state the maximum mass dimension of the operators we want to consider. The downside is that their predictions are reliable only if the energy scale of the event is below the cut-off scale $M_{\rm cut}$. When considering the energy scales involved at the LHC, this condition can be often violated [1].
The second approach that was suggested to partially overcome this problem is the use of Simplified Models, that contain only the essential ingredients for the description of Dark Matter and its interactions: the DM candidate, and its mediator(s) with the Standard Model. Each Simplified Model can still reproduce a class of more complete theories, and has by construction an enlarged regime of validity with respect to EFTs, because we are including in the description another degree of freedom (the mediator). As a consequence, Simplified Models have an higher number of parameters or, generically speaking, of assumptions.

2 Deriving consistent and general bounds using the EFT

The goal of [2] is using the EFT in order to derive, in a consistent way, bounds from DM searches at colliders that can be reinterpreted in any corresponding specific model.
In an EFT there are (at least) three free parameters: the mass $m_{\rm DM}$ of the DM particle, the dimensionful coefficient M_* appearing in the coefficient of the effective operator, and the cut-off scale $M_{\rm cut}$ for the validity of the EFT. It is important to keep in mind that M_* and $M_{\rm cut}$ are two independent parameters.

The meaning of the parameter $M_{\rm cut}$ is illustrated by fig. 1, which sketches the differential cross section, as a function of the centre-of-mass energy $E_{\rm cm}$, for a two-to-two process in two Simplified Models (red and blue lines) and in the corresponding EFT at low energies.

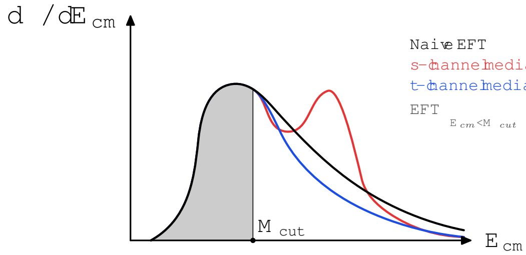

Figure 1: *Schematic representation of the differential cross section for a two-to-two process in two Simplified Models (red and blue lines) and in the corresponding EFT.*

The predictions of the two Simplified Models coincide, by definition, with the prediction of EFT for energies up to $E_{\rm cm} = M_{\rm cut}$. Once we fix a given EFT and we choose a value for the free parameter $M_{\rm cut}$ we do not have *a priori* any guess of the behaviour of the cross-section in the underlying model at energies above $M_{\rm cut}$. Hence, the only robust option, although conservative, to use the cross section predicted by the EFT is to restrict it to the energy range

$$E_{\rm cm} < M_{\rm cut}\,. \tag{1}$$

This corresponds to selecting only the events falling into the grey shaded region in fig. 1. The centre-of-mass energy $E_{\rm cm}$ should be defined, operatively, as the total invariant mass of the hard final states of the process: in the reaction $p\,p \to {\rm DM}_1\,{\rm DM}_2\,j$, where p is a proton and j is a jet, $E_{\rm cm}$ is defined as

$$E_{\rm cm} = \sqrt{\Big(p^\mu({\rm DM}_1) + p^\mu({\rm DM}_2) + p^\mu(j)\Big)^2}\,. \tag{2}$$

The strategy we propose is the following: the simulated signal, which has to be compared with the observed exclusion limit on the cross section, should be restricted to the subset of events that satisfy eq. (1). In this way one systematically underestimates the signal, therefore obtains conservative bounds, but this is the best that can be achieved without making further assumption on

the underlying model.
In [2] we illustrate our procedure with the exclusion limits obtained in the monojet search performed by ATLAS [3] with 10 fb^{-1} at a collision energy $\sqrt{s} = 8$ TeV at the LHC. We choose a model including a Majorana fermion X as DM particle, with an effective interaction with the quarks given by

$$\mathcal{L}_{\mathrm{EFT}} = -\frac{1}{M_*^2}\,\left(\overline{X}\gamma^\mu\gamma^5 X\right)\left(\sum_{\mathrm{flavours}} \overline{q}\gamma_\mu\gamma^5 q\right) . \tag{3}$$

Further details about the experimental search and the analysis we have performed can be found in [3, 2]. For present purposes, it is sufficient to say that the experimental search defines 4 signal regions (SR), each with a different cut on the transverse momentum p_T^{jet} of the leading jet and on the missing transverse energy.
The results of the analysis performed by using the restriction (1) are shown in fig. 2.

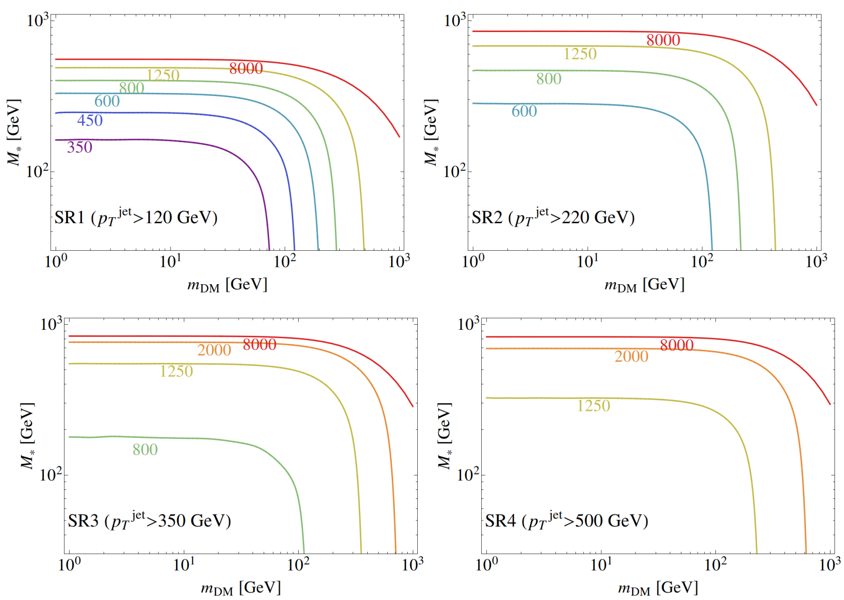

Figure 2: *Lower exclusion bounds on M_* as a function of m_{DM} for different values of M_{cut}, reported in the plots with the same colour of the corresponding lines. The four plots correspond to the four signal regions of* [3].

It is worth noting in fig. 2 that, for values of $M_{\rm cut}$ below ~ 1 TeV, the stronger limit comes from the softer signal region (SR1, at the top left). Indeed, the higher is the cut on $p_T^{\rm jet}$, the higher is the centre-of-mass energy required to produce signal, and the less likely it is for a signal event to pass the requirement (1). This shows that, in order to improve the sensitivity for low values of $M_{\rm cut}$, it is important to improve the sensitivity in the softer signal regions.
By looking at fig. 2, we could ask ourselves what is a plausible value for $M_{\rm cut}$. One can relate two dimensionful parameters of the EFT, M_* and $M_{\rm cut}$, through a relation of proportionality

$$M_{\rm cut} = g_* M_* \,, \tag{4}$$

where g_*, which we call effective coupling strength of the effective theory, must be regarded again as a free parameter. This amounts to trading the free parameter $M_{\rm cut}$ for another free parameter g_*. A possible approach is then deriving the exclusion limits for a fixed value of g_*, rather than for a fixed $M_{\rm cut}$. The corresponding results are shown in fig. 3.

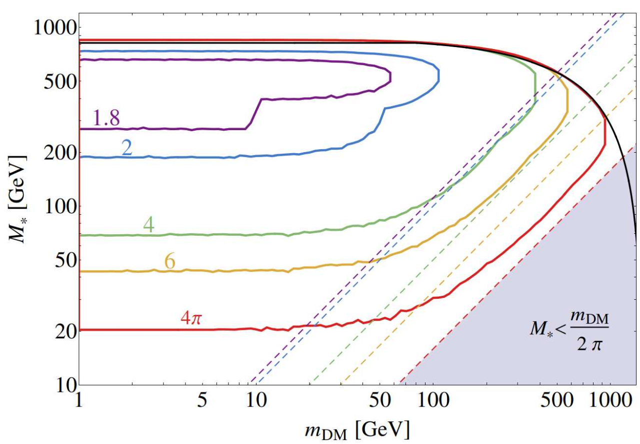

Figure 3: *Combined exclusion limits on M_* as function of $m_{\rm DM}$ for different values of g_*, reported in the plots with the same colour of the corresponding lines. The areas below the dashed lines correspond to the regions where $M_* < 2m_{\rm DM}/g_*$, where the value of g_* is the one corresponding to the colour of the dashed line. Within those regions, the condition (1) for the validity of the EFT is automatically violated.*

The consequence that can be drawn from fig. 3 is that current monojet searches do not set a bound on EFTs with a coupling strength $g_* \lesssim 1$.

3 Comparison with the exclusion reach of Simplified Models

In order to assess the difference between the reach of the exclusion limit obtained within the EFT, restrained as we propose, and within Simplified Models, we identify two Simplified Models leading to the effective operator (3). The first one is a Simplified Model with a Z' vector boson that mediates the process $q\,q \to X\,X$ in the s-channel at tree level, while in the second model (inspired by supersymmetric models) there are coloured scalar mediators exchanged in the t-channel at tree level. For more details about these models, see [2].
The bound obtained in the EFT can be immediately recast once we specify the relation between the expression of the parameters of the EFT in terms of the parameters of the Simplified Model: in the case of model B for example, we identify $M_{\rm cut}$ with the mass $\widetilde{m}$ of the scalar mediators, and M_* turns out to be equal to $2\widetilde{m}/g_{\rm DM}$, where $g_{\rm DM}$ is a coupling parameter. Therefore the exclusion limit shown in fig. 3 can be directly recast as the blue line in fig. 4.
The bound obtained by using the full Simplified Model is shown by the purple lines. It can be seen that they are sensibly different from the bound of the truncated EFT only for mediator massed of the order of 1 TeV. This suggests that the enhanced exclusion power of the Simplified Model is due to the resonant production of the mediator, which enhances the cross section of the signal and thus leads to stronger exclusion bounds. This supposition is confirmed by the red lines, which show the exclusion limit that is obtained by restricting the Simplified Model signal to the events for which the mediator is resonantly produced [1]. As it is evident from fig. 4, the red lines reproduce the bound from the purple ones in the region where they differ from the truncated EFT.
This means that the difference between the bound obtained within the EFT, used in a consistent and robust way with the truncation procedure we propose, and the bound obtained within the Simplified Model approach, is due only to the presence of the mediator in the latter description.

[1] More precisely, this condition is defined as follows: if q^μ is the 4-momentum flowing on the mediator line, we say that the mediator is resonantly produced if $|q^2 - \widetilde{m}^2|$ is smaller than twice the mediator width.

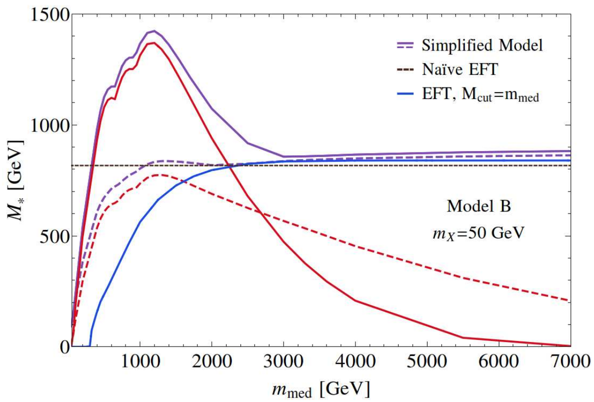

Figure 4: *Exclusion limits on M_* as function of the mediator mass $\widetilde{m}$ for $m_X = 50$ GeV. The blue line shows the recasting, in the Simplified Model, of the limit obtained within the truncated EFT. The purple lines are obtained in the full Simplified Model, while the red ones represent the limit obtained by using the subset of simulated events where the mediator was resonantly produced. Solid and dashed lines correspond to two different values of the mediator width, respectively $\widetilde{m}/(8\pi)$ and $\widetilde{m}/3$.*

4 Conclusions

In ref. [2] we propose a method to derive bounds from the EFT in a consistent and robust way, by reducing the simulated signal to the events for which the centre-of-mass energy $E_{\rm cm}$ is smaller than the cut-off scale $M_{\rm cut}$ of the EFT, which is a free parameter, and using only those events to set a constraint. These bounds, although more conservative than the ones obtainable with the full EFT or with a Simplified Model, can be easily recast in any full theory one can think of.

As a second important point, we show that the enhanced exclusion power of Simplified Models with respect to what achieved with the truncated EFT is due only to the resonant production of the mediator in the Simplified Model. The search of the mediators is clearly better addressed by dedicated searches. Therefore we argue that the most robust and effective way to study exclusion limits on Dark Matter at particle colliders is to interpret mono-particle searches (as monojet ones) with the Effective Field Theory, restricted to its regime of validity, and to complement them with the direct dedicated searches of the mediator(s) between DM and Standard Model, as for example di-jet and multi-jet searches.

References

1. G. Busoni, A. De Simone, E. Morgante and A. Riotto, Phys. Lett. B **728** (2014) 412.

2. D. Racco, A. Wulzer and F. Zwirner, JHEP **1505** (2015) 009.

3. ATLAS Collaboration, ATLAS-CONF-2012-147.

Doubly Charged Leptons at ILC and CLIC

Simone Biondini
Physik-Department, Technische Universität München,
James-Franck-Str. 1, 85748 Garching, Germany
Orlando Panella
Istituto Nazionale di Fisica Nucleare, Sezione di Perugia,
Via A. Pascoli, I-06123 Perugia, Italy

Abstract

We study the production and the corresponding signatures of doubly charged leptons at the forthcoming linear colliders. In the framework of gauge interactions, the interference between the t and u channel is evaluated that has been neglected so far. A pure leptonic final state is considered ($e^- \, e^- \to e^- \, e^- \, \nu_e \, \bar{\nu}_e$) that experimentally translates into a like-sign dilepton and missing transverse energy signature. Including initial state radiation and beamstrahalung, we provide the 3 and 5-sigma statistical significance exclusion curves in the model parameter space. We find that for a doubly charged lepton mass $m^* \approx 2$ TeV the expected lower bound on the compositeness scale at CLIC, $\Lambda > 25$ TeV, is much stronger than the current lower bound from LHC ($\Lambda > 5$ TeV) and remains highly competitive with the expected results at run II of the LHC.

1 Introduction

It is well known that the standard model of particle physics (SM) is performing pretty well. Indeed in terms of few fundamental particles and interactions, we can provide many predictions that have been experimentally confirmed with great accuracy. The SM alone cannot accommodate some observations though, for example, the evidence of neutrino oscillations, the dark matter and the baryon asymmetry in the universe.

The recent discovery of the Higgs boson with a mass $m_h \simeq 125$ GeV offers also a possibility for beyond the SM physics speculations. In particular it is desirable to find an explanation for the Higgs mass to be protected by large quantum corrections. Supersymmetry (SUSY) provides a natural explanation for the cancellation of the large radiative corrections via the existence of superpartners of the SM particles. No evidence of the SUSY particles at the TeV scale provided by its simplest realization has been found yet.

Composite models attempt to explain the Higgs boson as a bound state of some unknown fundamental substructure. The Higgs mass will then arise as a dynamical generation of strongly interacting particles (preons). The compositness models also address the proliferation of the SM fermions in the three generations, though the ordinary matter is made of the the first generation only. One of the main phenomenological consequences of composite models is the possibility to observe excited fermions, that interact with the ordinary ones and may produce interesting signatures at present and future colliders. Many experimental analysis have been carried out in this directions.

Composite models constrained by the weak isospin invariance [1] show the existence of quark and leptons with exotic electromagnetic charges, $Q = 4/3e, 5/3e$ and $Q = 2e$ respectively. For their peculiar electromagnetic charges, such as for the leptons, the corresponding SM background turns out to be lower than the one relevant for the ordinary excited fermion states ($Q = 0, e$). This may provide some signatures to study at the LHC and at future colliders. In [2, 3] the production mechanism for a doubly charged exotic lepton (L^{--}), and the final state originated via its decays has been studied at the LHC. In [4] we show a similar analysis at the forthcoming linear colliders, when the e^-e^- beam option is consider to allow for the single production of the E^{--} (electron flavour).

2 Production cross section

Doubly charged leptons appear in higher isospin multiplets of the compositeness model described in [1]. They read, respectively for the $I_W = 1$ and $I_W = 3/2$

cases:

$$L_1 = \begin{pmatrix} L^0 \\ L^- \\ L^{--} \end{pmatrix}, \qquad L_{3/2} = \begin{pmatrix} L^+ \\ L^0 \\ L^- \\ L^{--} \end{pmatrix},$$

with similar multiplets for the antiparticles. They interact with SM fermions via gauge interactions (GI), the Lagrangian for the different multiplets being

$$\mathcal{L}_{\rm GI}^{(1)} = i\frac{g\,f}{\Lambda}\left(\bar{\psi}_E\,\sigma_{\mu\nu}\,\partial^\nu\,W^\mu\,P_R\,\psi_e\right) + h.c.\,, \tag{1a}$$

$$\mathcal{L}_{\rm GI}^{(3/2)} = i\frac{g\,\tilde{f}}{\Lambda}\left(\bar{\psi}_E\sigma_{\mu\nu}\,\partial^\nu\,W^\mu\,P_L\,\psi_e\right) + h.c. \tag{1b}$$

They also interact via contact interactions (CI). The corresponding Lagrangian is

$$\mathcal{L}_{\rm CI} = \frac{g_*^2}{\Lambda^2}\,\left[\bar{\psi}_\nu(x)\gamma^\mu P_L\psi_e(x)\,\bar{\psi}_E(x)\gamma_\mu P_L\psi_e(x) + h.c.\right]\,. \tag{2}$$

The model parameters are the following: the mass of the excited lepton, m^*, the compositeness scale Λ, the couplings f, $\tilde{f} \sim 1$ and $g_* = \sqrt{4\pi}$. We study in some detail the interference between the t and u channel in the case of GI, that has been neglected so far. The single production of the doubly charged lepton is given by the process (electron flavour) $e^-e^- \to E^{--}\nu_e$ and the results for the corresponding differential cross sections read

$$\begin{aligned}
\left.\frac{d\sigma}{dt}\right|_{I_W=1} &= \frac{1}{4s^2\Lambda^2}\frac{g^4 f^2}{16\pi}\frac{t}{\left(t-M_W^2\right)^2}\,\left[m^{*2}(t-m^{*2}) + 2su + m^{*2}(s-u)\right] \\
&\quad + \frac{1}{4s^2\Lambda^2}\frac{g^4 f^2}{16\pi}\frac{u}{\left(u-M_W^2\right)^2}\,\left[m^{*2}(u-m^{*2}) + 2st + m^{*2}(s-t)\right]\,, \\
\left.\frac{d\sigma}{dt}\right|_{I_W=\frac{3}{2}} &= \frac{1}{4s^2\Lambda^2}\frac{g^4 \tilde{f}^2}{16\pi}\frac{t}{\left(t-M_W^2\right)^2}\,\left[m^{*2}(t-m^{*2}) + 2su - m^{*2}(s-u)\right] \\
&\quad + \frac{1}{4s^2\Lambda^2}\frac{g^4 \tilde{f}^2}{16\pi}\frac{u}{\left(u-M_W^2\right)^2}\,\left[m^{*2}(u-m^{*2}) + 2st - m^{*2}(s-t)\right] \\
&\quad + \frac{1}{8s^2\Lambda^2}\frac{g^4 \tilde{f}^2}{16\pi}\frac{1}{(u-M_W^2)}\frac{1}{(t-M_W^2)}\left(2stu + \frac{3}{4}utm^{*2}\right)\,.
\end{aligned} \tag{3}$$

We summarise the integrated cross sections in fig. 1, where we notice that the cross section is reduced by a factor of almost one third at $\sqrt{s} = 1$ TeV due to the t-u interference. The effect is larger at higher center of mass energies.

Production by CI is more efficient due to the higher value of the coupling that parametrize the effective interaction. For most of the model phase

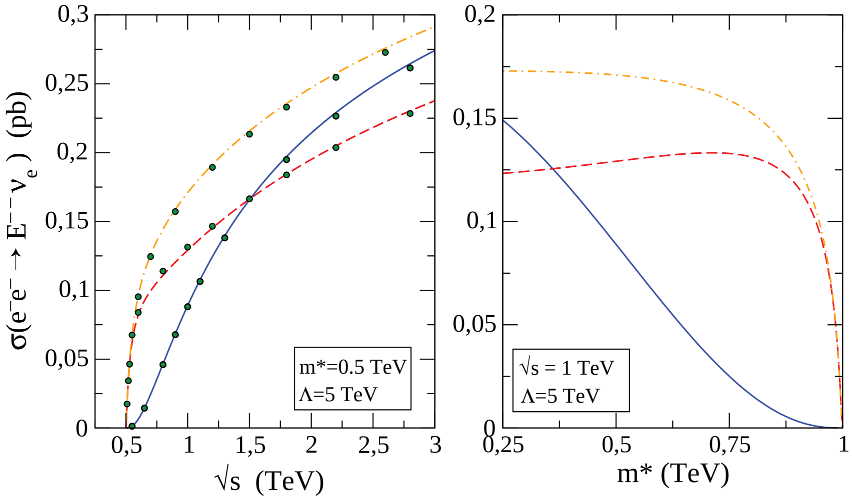

Figure 1: *The total cross sections for the process $e^-e^- \to E^{--}\nu_e$ is shown. In the left panel the total cross section against the center of mass energy is displayed for the different isospin multiplets. The solid blue line stands for $E^{--} \in I_W = 1$, the dashed red (orange dot-dashed) curve for $E^{--} \in I_W = 3/2$ with (without) the interference contribution taken into account. The right panel shows the total cross section against mass. The compositeness parameters are set to ($m^* = 0.5$ TeV, $\Lambda = 5$ TeV). The green dots show the CalcHEP output.*

space, GI are more important for the decay of the E^{--}. We consider all 8 diagrams for the production and decays of the excited lepton (electron flavour) in CalcHEP [5] and we study the final state particle: $e^-e^- \to e^-e^-\nu_e\bar{\nu}_e$, originated from the decay chain $E^{--} \to W^-e^- \to e^-\ell^-\nu_\ell$. This translates into a like-sign dilepton and missing transverse energy experimental signature.

3 SM background and final sate analysis

In order to suggest the detection strategy of such a signal, an estimate of the backgrounds in the e^-e^- beam setting is needed. We start with base kinematic cuts adopted in general purpose detectors for new physics searches. We simulate the SM processes and signal accordingly to the base cuts in table 1. In this work, we consider only the SM induced background by using the CalcHEP [5] and MadGraph [6] generators. We focus on the irreducible backgrounds, since we can estimate the reducible ones to be fairly sub-dominant. The irreducible ones follows in two categories: the SM process $e^-e^- \to e^-e^-\nu_e\bar{\nu}_e$ described

Base Kinematic Cuts		
$p_T^{min}(e^-) > 15$ GeV	$p_T^{max}(e^-) > 50$ GeV	$p_T(\nu) > 15$ GeV
$\lvert\eta(e^-)\rvert < 2.5$	$\Delta R(e^-, e^-) > 0.5$	

Table 1: Kinematic cuts adopted in the first stage of the simulation, based on existing models of general purpose detectors for a linear collider [7, 8].

Improved Kinematic Cuts		
$p_T^{max}(e^-) > 200$ GeV	$-1 < \eta^{max}(e^-) < 2.5$	$\not{E}_T > 100$ GeV

Table 2: The improved kinematic cuts used in addition to the base cuts in the final simulation. Unchanged base cuts from Table 1 are not repeated.

by a total of 28 Feynman diagrams (including those due to the exchange of identical particles) and the SM process $e^-e^- \to e^-e^-\nu_e\nu_e\bar{\nu}_e\bar{\nu}_e$ is described by a total of 301 Feynman diagrams (including those due to the exchange of identical particles).

We study different kinematic distributions of the charged leptons in the final state, together with the missing transverse energy. This procedure leads to a second set of cuts in table 2 that allow to disentangle the signal for the background. To make the phenomenological study more realistic we include the initial state radiation and beamstrahlung effects both for the signal and the SM background. These effect are included in the 3 and 5-sigma statistical significance exclusion curves in the (m^*, Λ) parameter space. Our main result is the comparison between the bounds on the model parameters from the LHC run I and II and the forthcoming linear collider. In figure 2 we show explicitly the result and we notice that CLIC may rather improve the bounds for m^* up to 3 TeV.

4 Conclusions

We discuss the production of heavy exotic doubly charged leptons in the framework of forthcoming linear colliders. Our analysis shows that the bounds on the model parameter space can be rather improved in the case of a 3 TeV energy in the center of mass, as the CLIC facility might offer in the future. In particular, in the region of large excited lepton masses, $m \approx 2$ TeV, the CLIC lower bounds $\Lambda > 22 - 25$ TeV, on the basis of expectations of signatures of the same model at the LHC $\sqrt{s} = 14$ TeV, remains highly competitive with the bound expected for run II of the LHC: $\Lambda > 11.6$ TeV [3].

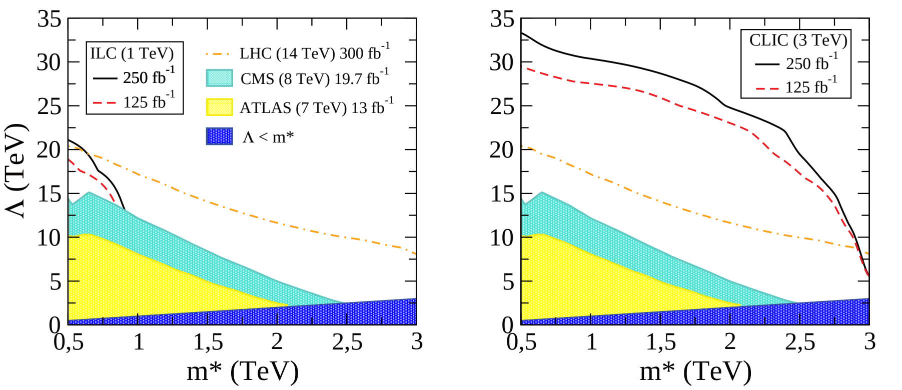

Figure 2: *Comparison of the exclusion curves at 3-sigma level in the parameter space* (Λ, m) *from ILC (left) and CLIC (right), for* $L = 250$ *fb*$^{-1}$ *(solid black) and* $L = 125$ *fb*$^{-1}$ *(solid red), with the bounds from run I at the LHC. Prospects for the same model at the run II is described by the orange dot-dashed line.*

Acknowledgements

The authors would like to thank the organizers of the LC15 workshop held at the ECT*, Villazzano, Trento. The speaker (S. B.) warmly thanks the organizers for the opportunity to give a talk at the workshop.

References

1. G. Pancheri and Y. N. Srivastava, Phys. Lett. B **146** (1984) 87.
2. S. Biondini, O. Panella, G. Pancheri, Y. N. Srivastava and L. Fanò, Phys. Rev. D **85** (2012) 095018
3. R. Leonardi, O. Panella and L. Fanò, Phys. Rev. D **90** (2014) 3, 035001
4. S. Biondini and O. Panella, Phys. Rev. D **92** (2015) 1, 015023
5. A. Pukhov *et al.*, hep-ph/9908288.
6. J. Alwall *et al.*, JHEP **0709** (2007) 028
7. G. Aarons *et al.* [ILC Collaboration], arXiv:0709.1893 [hep-ph].
8. E. Accomando *et al.* [CLIC Physics Working Group Collaboration], hep-ph/0412251.

Flavor mixing effects induced by RGE running in the CMSSM

Mario E. Gómez
Department of Applied Physics, University of Huelva, 21071 Huelva, Spain
Sven Heinemeyer
Instituto de Física de Cantabria (CSIC-UC), 39005 Santander, Spain &
Instituto de Física Teórica, (UAM/CSIC), Cantoblanco, E-28049 Madrid, Spain
Muhammad Rehman
Instituto de Física de Cantabria, 39005 Santander, Spain

Abstract

Even within the Constrained Minimal Supersymmetric Standard Model (CMSSM), it is possible to induce sfermion flavor mixing through the Renormalization Group Equations (RGE) when the full structure of the Yukawa couplings is considered. We analyze the impact of including those effects on the accurate computation of B-physics observables, electroweak precision observables (EWPO) and the Higgs boson mass predictions.

1 Introduction

Supersymmetric (SUSY) extensions of the Standard Model (SM) [1] come with many promises to become the next step in the search for new physics. They offer a solution to the hierarchy problem, a candidate to Dark Matter and many new particles within the LHC energy range. Now, with Run I data of the LHC, we have new bounds for the SUSY observables which constraint the SUSY parameters. We study the impact of these bounds to the SUSY contribution to some of the well measured SM observables. In particular, we include in our analysis flavor violating (FV) contributions arising from the new SUSY particles.

We work in the framework of the Minimal Supersymmetric extension of the SM (MSSM), with the additional assumption that SUSY is broken by universal soft terms at the grand unification scale (GUT). In this framework, called constrained MSSM (CMSSM), FV is present only in the squark sector. This arises due to the presence of the Yukawa couplings in the RGE's, such that the only source of FV is the CKM matrix. Hence, by definition this model fulfills the Minimal Flavor Violation (MFV) hypothesis [2]. However, this model can not explain the experimental evidence for neutrino flavor oscillations. In order to account for those, we must enlarge the CMSSM. This can achieved by augmenting the CMSSM with a type I "see-saw" mechanism. The resulting model, called "CMSSM-seesaw I" predicts also FV in the lepton sector (LFV).

We review in the next sections some results on FV predictions in the CMSSM and their contribution to the evaluation of electroweak precision observables (EWPO), in particular M_W and the effective weak leptonic mixing angle, $\sin^2\theta_{\rm eff}$. The effects on other observables like B physics observables (BPO), in particular BR($B \to X_s\gamma$), BR($B_s \to \mu^+\mu^-$) and ΔM_{B_s}, as well as the masses of the neutral and charged Higgs bosons in the MSSM were found to be small. We refer the reader to refs. [3, 4] for further details of our computation and a complete list of references.

2 Scalar fermion sector with flavor mixing

The MSSM is defined by the superpotential:

$$W_{\rm MSSM} = \epsilon_{\alpha\beta}(Y_e^{ij} H_1^\alpha E_i^c L_j^\beta + Y_d^{ij} H_1^\alpha D_i^c Q_j^\beta + Y_u^{ij} H_2^\alpha U_i^c Q_j^\beta + \mu H_1^\alpha H_2^\beta) \quad (1)$$

where L_i represents the chiral multiplet of a $SU(2)_L$ doublet lepton, E_i^c a $SU(2)_L$ singlet charged lepton, H_1 and H_2 two Higgs doublets with opposite hypercharge. Similarly Q, U and D represent chiral multiplets of quarks of a $SU(2)_L$ doublet and two singlets with different $U(1)_Y$ charges. Three generations of leptons and quarks are assumed and thus the subscripts i and j run over 1 to 3. The symbol $\epsilon_{\alpha\beta}$ is an anti-symmetric tensor with $\epsilon_{12} = 1$. SUSY is

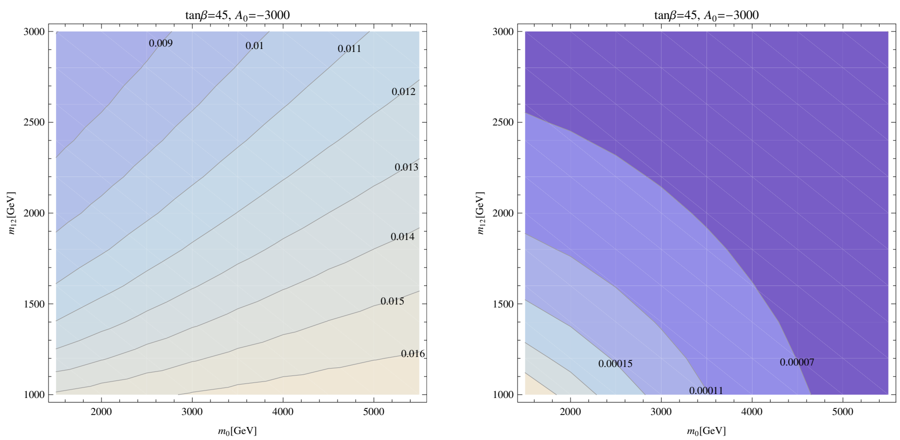

Figure 1: *Contours of* δ_{23}^{QLL} *(left) and* δ_{23}^{ULR} *(right) in the* m_0–$m_{1/2}$ *plane for* $\tan\beta = 45$ *and* $A_0 = -3000$ *GeV in the CMSSM.*

"softly broken" by a scalar potential with bilinear and trilinear combinations of the superpartners. Within the CMSSM the soft SUSY-breaking parameters are assumed to be universal at the Grand Unification scale $M_{\rm GUT} \sim 2 \times 10^{16}$ GeV. All the scalars are assumed to have the same mass, m_0, the trilinear soft terms are proportional to their respective Yukawa couplings and fermionic partners of the gauge bosons have a common mass $m_{1/2}$. Since the soft terms are universal, at the GUT scale, they are invariant under superfield rotations. Hence, it is possible to work in the basis in which the Yukawa couplings are $Y_D = {\rm diag}(y_d, y_s, y_b)$ and $Y_U = V_{\rm CKM}^\dagger {\rm diag}(y_u, y_c, y_t)$ such that FV terms display an explicit dependence on the CKM matrix.

The SUSY spectra have been generated with the code `SPheno 3.2.4` [5]. All the SUSY masses and mixings are then given as a function of m_0, $m_{1/2}$, A_0, and $\tan\beta = v_2/v_1$, the ratio of the two vacuum expectation values (see below). We require radiative symmetry breaking to fix $|\mu|$ and $|B\mu|$ with the tree–level Higgs potential. The non-diagonal entries in this 6×6 general matrix for sfermions can be described in terms of a set of dimensionless parameters δ_{ij}^{FAB} ($F = Q, U, D, L, E$; $A, B = L, R$; $i, j = 1, 2, 3$, $i \neq j$) where F identifies the sfermion type, L, R refer to the "left-" and "right-handed" SUSY partners of the corresponding fermionic degrees of freedom, and i, j indexes run over the three generations. The soft sfermion mass matrices in terms of the δ_{ij}^{FAB} are

$$m^2_{\tilde{U}_L} = \left(\begin{array}{ccc} m^2_{\tilde{Q}_1} & \delta_{12}^{QLL} m_{\tilde{Q}_1} m_{\tilde{Q}_2} & \delta_{13}^{QLL} m_{\tilde{Q}_1} m_{\tilde{Q}_3} \\ \delta_{21}^{QLL} m_{\tilde{Q}_2} m_{\tilde{Q}_1} & m^2_{\tilde{Q}_2} & \delta_{23}^{QLL} m_{\tilde{Q}_2} m_{\tilde{Q}_3} \\ \delta_{31}^{QLL} m_{\tilde{Q}_3} m_{\tilde{Q}_1} & \delta_{32}^{QLL} m_{\tilde{Q}_3} m_{\tilde{Q}_2} & m^2_{\tilde{Q}_3} \end{array} \right) , \qquad (2)$$

$m^2_{\tilde{U}_R}$ and $m^2_{\tilde{D}_R}$ are defined in a similar way, while $m^2_{\tilde{D}_L}$ is given by: $m^2_{\tilde{D}_L} = V^\dagger_{\rm CKM}\, m^2_{\tilde{U}_L}\, V_{\rm CKM}$. The trilinear terms can be written as:

$$v_2 \mathcal{A}^u = \left(\begin{array}{ccc} m_u A_u & \delta_{12}^{ULR} m_{\tilde{Q}_1} m_{\tilde{U}_2} & \delta_{13}^{ULR} m_{\tilde{Q}_1} m_{\tilde{U}_3} \\ \delta_{21}^{ULR} m_{\tilde{Q}_2} m_{\tilde{U}_1} & m_c A_c & \delta_{23}^{ULR} m_{\tilde{Q}_2} m_{\tilde{U}_3} \\ \delta_{31}^{ULR} m_{\tilde{Q}_3} m_{\tilde{U}_1} & \delta_{32}^{ULR} m_{\tilde{Q}_3} m_{\tilde{U}_2} & m_t A_t \end{array} \right) , \qquad (3)$$

the matrix $\mathcal{A}^d$ has a similar form.

We found that the values of the δ_{ij}^{FAB} in the LR or RL part of the mass matrix show a decoupling effect, as it is displayed in Fig. 1 for the case of δ_{23}^{ULR}. However, for LL part of the mass matrix, we found a non-decoupling effect as is shown for the case of δ_{23}^{QLL}. The increase of this term with m_0 produces important contributions to the EWPO as we will see in the next section.

3 Computation of some observables including squark FV.

The flavor violating parameters, generated from the RGE running, enter at one loop in the computation of the physical observables. Numerically, the results have been obtained using the code `FeynHiggs` [6], which contains the complete set of one-loop corrections from (flavor violating) squark and slepton contributions as given in refs. [7, 4].

EWPO, which are known with a great accuracy, have the potential to allow a discrimination between quantum effects of the SM and SUSY models. Examples are the W-boson mass M_W and the Z-boson observables, such as the effective leptonic weak mixing angle $\sin^2\theta_{\rm eff}$, whose present experimental uncertainties are $\delta M_W^{\rm exp,today} \sim 15$ MeV and $\delta \sin^2\theta_{\rm eff}^{\rm exp,today} \sim 15 \times 10^{-5}$. The experimental uncertainty will further be reduced to ~ 4 MeV and $\sim 1.3 \times 10^{-5}$ respectively in future linear colliders.

To show explicitly the contribution of the FV entries to the different observables, we compare the full contribution with the value obtained by setting all $\delta_{ij}^{FAB} = 0$. The results for $\Delta M_W^{\rm MFV} = M_W - M_W^{\rm MSSM}$ and $\Delta \sin^2\theta_{\rm eff}^{\rm MFV} = \sin^2\theta_{\rm eff} - \sin^2\theta_{\rm eff}^{\rm MSSM}$ (where $M_W^{\rm MSSM}$ and $\sin^2\theta_{\rm eff}^{\rm MSSM}$ are the values obtained

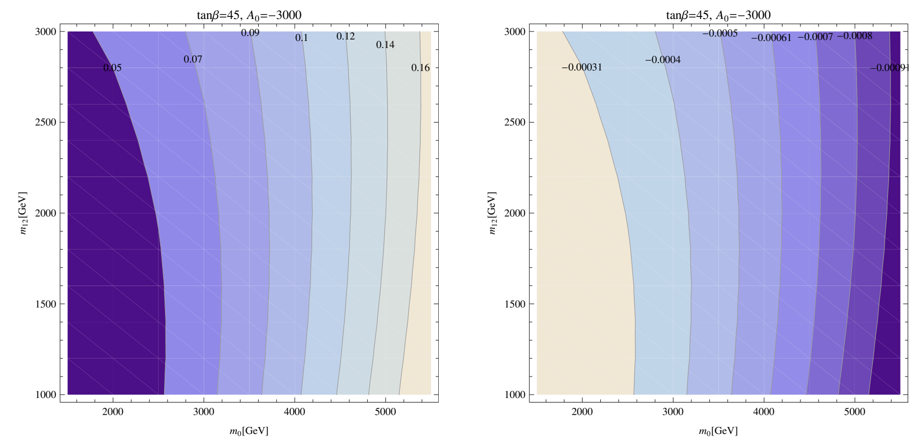

Figure 2: *Contours of* $\Delta M_W^{\mathrm{MFV}}$ *in GeV (left) and* $\sin^2\theta_{\mathrm{eff}}$ *in the* m_0–$m_{1/2}$ *plane for* $\tan\beta = 45$ *and* $A_0 = -3000$ *GeV in the CMSSM.*

with all $\delta_{ij}^{FAB} = 0$) are displayed in Fig. 2. We can observe a non-decoupling behavior for the EWPO, similar to the one observed for δ_{23}^{QLL} as shown in Fig. 1. The FV contributions to M_W and $\sin^2\theta_{\mathrm{eff}}$ can be above the experimental uncertainty for some regions of the parameter space. Therefore, FV contributions should not be neglected in their evaluation. Particularly, in view of a future improved experimental accuracies.

The FV contribution to other observables turn out to be small, the full FV computation does not lead to significant differences with respect to the common approach of setting all the $\delta_{ij}^{FAB} = 0$. In the case of the lightest MSSM Higgs boson, the uncertainties arising from the theoretical computation are larger than the experimental precision of the Higgs mass discovered at the LHC. Even though, we find that the FV effects are below any forseen experimental precision. Similarly, we found that for BPO the approach of taking $\delta_{ij}^{FAB} = 0$ is justified.

4 Conclusion

We studied the impact of including MFV entries in the sfermion mass matrices as they naturally arise in the CMSSM when the CKM matrix is included in the

RGE's. After a careful evaluation of several precision observables, we conclude that the effects are not very significant for BPO and Higgs boson masses. However, EWPO receive contributions that show a non-decoupling behavior as the values of the SUSY spectrum increases. For instance, those effects can be larger than the current experimental accuracy in M_W and $\sin^2\theta_{\rm eff}$. Taking FV effects correctly into account could place new upper bounds on m_0 that are not present in the existing phenomenological analyses. Further applications to FV Higgs decays can be found in ref. [8]. Our conclusions can also apply to popular neutrino motivated extensions of the CMSSM like the CMSSM-seesaw I.

5 Acknowledgements

This work is supported by by the Spanish MICINN's Consolider-Ingenio 2010 Programme under grant MultiDark CSD2009-00064. The authors also acknowledge further support from CICYT (S.H. and M.R. from the grant FPA 2013-40715-P and M.E:G. from FPA2011-23781).

References

1. H. Haber and G. Kane, *Phys. Rept.* **117** (1985) 75;
2. A. Buras et al., *Phys. Lett.* **B 500** (2001) 161.
3. M. E. Gómez, S. Heinemeyer and M. Rehman, Eur. Phys. J. C **75** (2015) 9, 434.
4. M. E. Gómez, T. Hahn, S. Heinemeyer and M. Rehman, Phys. Rev. D **90** (2014) 7, 074016
5. W. Porod, *Comput. Phys. Commun.* **153** (2003) 275 [arXiv:hep-ph/0301101].
6. S. Heinemeyer, W. Hollik and G. Weiglein, *Comput. Phys. Commun.* **124** (2000) 76; T. Hahn, S. Heinemeyer, W. Hollik, H. Rzehak and G. Weiglein, *Comput. Phys. Commun.* **180** (2009) 1426;
7. M. Arana-Catania, S. Heinemeyer, M. J.Herrero and S. Peñaranda, *JHEP* **1205** (2012) 015
8. M. E. Gómez, S. Heinemeyer and M. Rehman, arXiv:1511.04342 [hep-ph].

HUNTING FOR HEAVY COMPOSITE MAJORANA NEUTRINOS AT THE LHC

Roberto Leonardi
INFN Perugia and Università di Perugia, Via A. Pascoli, I-06123, Perugia, Italy
Orlando Panella
INFN Perugia, Via A. Pascoli, I-06123, Perugia, Italy
Luisa Alunni Solestizi
INFN Perugia and Università di Perugia, Via A. Pascoli, I-06123, Perugia, Italy
Livio Fanò
INFN Perugia and Università di Perugia, Via A. Pascoli, I-06123, Perugia, Italy
Francesco Romeo
IHEP, 19B Yuquan Lu, Shijingshan District, Beijing, 100049, China

Abstract

Motivated by the recent observation of an excess in the $eejj$ channel by the CMS collaboration we investigate the search for heavy Majorana neutrinos in the context of the composite model scenario at the LHC RunII at a center of mass energy of 13 TeV. We performed a fast detector simulation based on DELPHES and we computed the exclusion curves finding a great potential of discovery or improving the current bounds on the composite scenario.

1 Introduction

The CMS collaboration has recently reported an excess over the standard model expectation in the $eejj$ final state in two different analysis, one for a search for right-handed gauge boson [1] and one for a search for first generation leptoquarks [2]. Different attempts have been made to explain these excesses in the context of various models, but we want to emphasize that the like-sign di-lepton and di-jet final state is the golden signature to look for heavy Majorana neutrinos [3, 4, 5, 6]. In this work we study the $eejj$ signature in view of a heavy Majorana neutrino arising from the scenario of compositness of quark and leptons, complementing with contact interaction a previous work [3] in which only the gauge interaction was considered.

2 Composite model with gauge and contact interactions

Compositness of fermions can be one possible scenario beyond the standard model. In this approach quarks and leptons are assumed to have an internal structure which should become manifest at some sufficiently high energy scale, the compositness scale Λ. Quite natural, model independent properties of this picture are [7, 8, 9, 10, 11] (i) the existence of excited states of quark and leptons with masses $m^* \leq \Lambda$; (ii) contact interaction that is an effective approach to describe the effects of the unknown internal dynamics. The gauge interaction is described by a magnetic type coupling:

$$\mathcal{L} = \frac{1}{2\Lambda}\,\bar{L}^*_R \sigma^{\mu\nu}\left(gf\frac{\boldsymbol{\tau}}{2}\cdot \boldsymbol{W}_{\mu\nu} + g'f'YB_{\mu\nu}\right)L_L + h.c.\,, \tag{1}$$

The contact interaction is

$$\mathcal{L}_{\rm CI} = \frac{g_*^2}{\Lambda^2}\frac{1}{2}j^\mu j_\mu \tag{2a}$$

$$\begin{aligned} j_\mu = {} & \eta_L \bar{f}_L\gamma_\mu f_L + \eta\prime_L \bar{f}^*_L\gamma_\mu f^*_L + \eta\prime\prime_L \bar{f}^*_L\gamma_\mu f_L + h.c. \\ & + (L \to R) \end{aligned} \tag{2b}$$

3 Cross section and decay width of the composite Majorana neutrino

The heavy Majorana neutrino can be produced in association with a lepton in pp collisions. This process can occur via both gauge and contact interactions. The contact interaction dominates the production of the heavy Majorana neutrino as shown in fig.1a. The heavy Majorana neutrino can decay again through both gauge and contact interactions, the possible decays are

$$N \to \ell q\bar{q}\prime \qquad N \to \ell^+\ell^-\nu(\bar{\nu}) \qquad N \to \nu(\bar{\nu})q\bar{q}\prime.$$

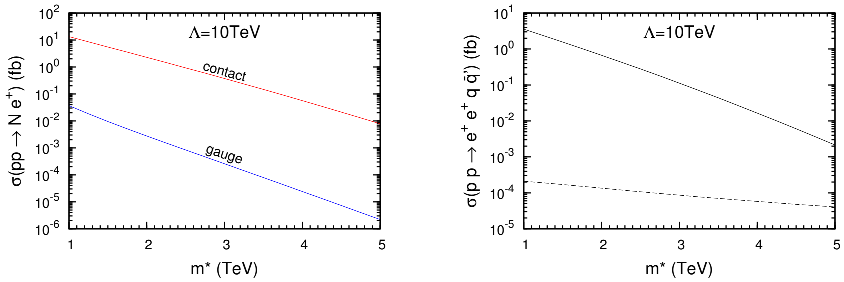

Figure 1: *a)* ^{12}C *Production cross section of* $pp \to Ne^+$ *for gauge and contact interactions at* $\sqrt{s} = 13$ *TeV, with CTEQ6m parton distribution functions and factorization scale* $\hat{Q} = m_N = m^*$ *b) Comparison between the parton-level cross sections of the prosses with resonant production of heavy Majorana neutrino and its subsequent decay (solid line) and that with the exchange of a virtual heavy Majorana neutrino (dashed line).*

We are interestd in the decay $N \to \ell^+ q\bar{q}\prime$, that gives the final signature under examination $\ell^+\ell^+jj$. It is important to remark that this signature can be realized also with a virtual exchange of a heavy Majorana neutrino (see fig.2). However the resonant production rate is dominant relative to the virtual exchange contribution as shown in fig.1b.

4 Signal and background

The main backgrounds for our process are [5]

$$pp \to t\bar{t} \to \ell^+\ell^+\nu\nu jets\,, \tag{3a}$$

$$pp \to W^+W^+W^- \to \ell^+\nu\ell^+\nu jj\,. \tag{3b}$$

From the study of the kinematical distributions of signal and background we found that the background can be drastically reduced applying cuts on the transverse momentum of the leading positron and on that of the second-leading positron:

$$p_T(e^+_{\text{leading}}) \geq 200\,\text{GeV}, \tag{4a}$$

$$p_T(e^+_{\text{second-leading}}) \geq 100\,\text{GeV}. \tag{4b}$$

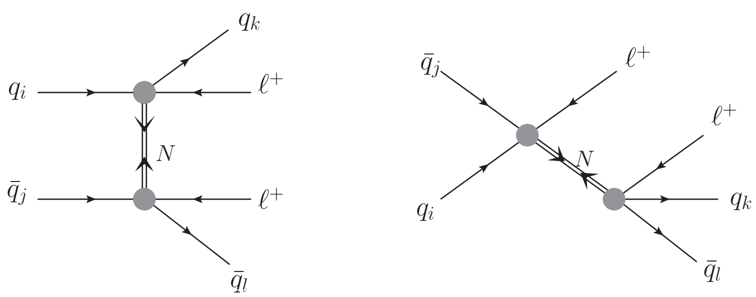

Figure 2: *On the left the process with the exchange of a virtual heavy Majorana neutrino (N), on the right the process with resonant production of N and its subsequent decay.*

5 Fast detector simulation and reconstructed objects

In order to take into account the detector effects, we interfaced the LHE output of CalcHEP with the software DELPHES that simulates the response of a generic detector; we used a CMS-like parametrization. Then we selected the events correctly reconstructed and satisfying the previous cuts, so we can evaluate the reconstruction efficiencies for signal and background (ϵ_s, ϵ_b), then for a given luminosity was possible to estimate the expected number of events for signal (N_s) and background (N_b) and finally the statistical significance (S):

$$N_s = L\sigma_s\epsilon_s \,, \qquad N_b = L\sigma_b\epsilon_b \,, \qquad S = \frac{N_s}{\sqrt{N_b}} \,. \tag{5}$$

In fig.3 we compare our 3-σ contour plot for three different values of integrated luminosity, $L = 30, 300, 3000$ fb^{-1}, with the 95% confidence level exclusion bounds from RunI analyses of ATLAS and CMS.

6 Discussions and conclusions

Our study shows that a full analysis based on this model would have a great potential of discovery or improving the current limits of the $eejj$ signature from a heavy composite Majorana neutrino. Finally we would like to comment about two features of the $eejj$ anomaly. The absence of the excess in the $\mu\mu jj$ channel can be explained by our model assuming that the excited muon state

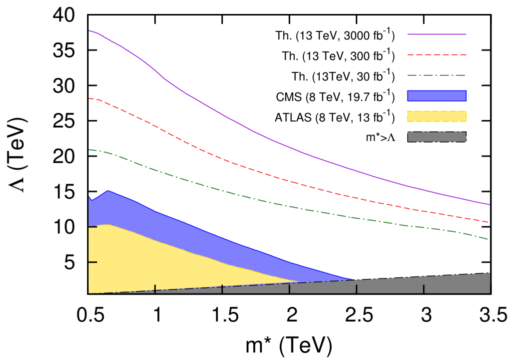

Figure 3: *expected 3-σ contour plots at RunII from heavy composite Majorana neutrino compared to current bounds from CMS and ATLAS searches of excited leptons in RunI.*

is somewhat heavier than the excited electron state and so it would be observabke at higher energies. The predominance of the oppsite-sign events on the same-sign envents in the anomaly observed by CMS can be explained in two ways: (*i*) Assuming the existence of an additional Majorana neutrino with a slightly different mass; it has been shown that the interference between the contributions of the two neutrinos could depress the same-sign yield relative to the opposite-sign [12, 13]. (*ii*) Considering exstended isospin composite models [14] and taking into account the opposite-sign events coming from processes like $pp \to e^+L^{--} \to e^+e^-jj$, $pp \to e^-L^{++} \to e^-e^+jj$.

References

1. V. Khachatryan *et al* (CMS Collaboration), Eur. Phys. J. **C74**, 3149 (2014).
2. S. Chatrchyan *et al* (CMS Collaboration), Phys. Rev. Lett. **109**, 261802 (2012).
3. O. Panella, C. Carimalo and Y.N. Srivastava, Phys. Rev. D **62**, 015013 (2000).

4. O. Panella, M. Cannoni, C. Carimalo and Y. Srivastava, Phys. Rev. D **65**, 035005 (2002).

5. T. Han and B. Zhang, Phys. Rev. Lett. **97**, 171804 (2006).

6. A. Atre, T. Han, S. Pascoli and B. Zhang, Journal of High Energy Physics **2009**, 030 (2009).

7. H. Terazawa, K. Akama and Y. Chikashige, Phys. Rev. D **15**, 480 (1977).

8. H. Terazawa, Phys. Rev. D **22**, 184 (1980).

9. E. Eichten, K.D. Lane and M.E. Peskin, Phys. Rev. Lett. **50**, 811 (1983).

10. N. Cabibbo, L. Maiani and Y. Srivastava, Phys. Lett. B **139**, 459 (1984).

11. U. Baur, M. Spira and P. Zerwas, Phys. Rev. D **42**, 815 (1990).

12. P.S.B. Dev and R.N. Mohapatra, arXive:1508.02277 [hep-ph] (2015).

13. R.L. Awasthi, P.S.B. Dev and M. Mitra, arXive:1509.05387 [hep-ph] (2015).

14. G. Pancheri and Y. Srivastava, Phys. Lett. B **146**, 87 (1984).

THEORY STATUS OF FOUR-FERMION PRODUCTION AT e^-e^+ COLLIDERS

Christian Schwinn*
Institute for Theoretical Particle Physics and Cosmology,
RWTH Aachen University, D-52056 Aachen, Germany
and
Albert-Ludwigs-Universität Freiburg, Physikalisches Institut,
D-79104 Freiburg, Germany

Abstract

The status of predictions for four-fermion production at e^-e^+ colliders is reviewed with an emphasis on the developments after the LEP2 era and an outlook to the challenges posed by the precision program at future colliders.

1 Introduction

After the discovery of a Higgs boson, the search for physics beyond the Standard Model (SM) of particle physics is one of the main objectives of run 2 of the LHC and of future colliders. In case new particles are not directly accessible at these colliders or in non-collider experiments, one can search for indirect evidence for new physics through precise studies of electroweak (EW) or flavour observables,

*Heisenberg Fellow of the German Research Foundation (DFG).

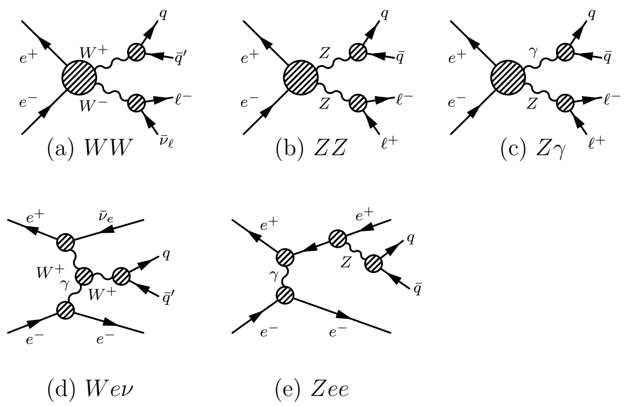

Figure 1: Classification of signatures in four-fermion production.

and the couplings of the gauge bosons and the Higgs boson. Further, accurate measurements of input parameters of the SM such as the masses of the W and Z bosons and the top quark are required for the precision-physics program. Here future e^-e^+ colliders could play a particularly important role by revisiting the LEP precision measurements at higher statistics, and further measuring top-quark and Higgs-boson properties. Currently linear colliders such as ILC and CLIC as well as circular colliders such as FCC-ee or CEPS are investigated. [1)]

An important signature at high-energy e^-e^+ colliders is given by *four-fermion production processes*[1] as shown in Figure 1. They have been explored at LEP2 [2)] for centre-of-mass energies $\sqrt{s} = 161.3$-206.6 GeV, allowing precision tests of the SM through measurements of cross-sections, the mass, width and branching ratios of the W-boson in W-pair production (Fig 1 (a)), and triple-vector boson couplings in W-pair production, $Z\gamma$ and single-W production (Fig 1 (c) and (d), respectively). At future e^-e^+ colliders the precision of these measurements could be increased, for instance by up to two magnitudes for the triple gauge boson couplings. [4)] For M_W, an accuracy of 3–4 MeV is projected for an ILC, while 1 MeV may be possible using a threshold scan of the W-pair production cross section at a future circular e^-e^+ collider. [4)]

[1]Four-fermion final states arising from Higgs-boson production with subsequent decay to b quarks or τ leptons are not considered in this contribution.

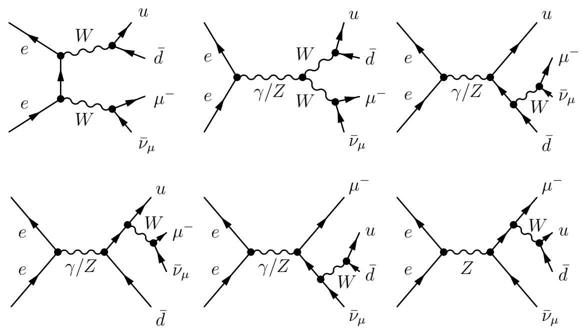

Figure 2: Diagrams contributing at tree-level to the $e^-e^+ \to u\bar{d}\mu^-\bar{\nu}_\mu$ process.

In this contribution, the theoretical challenges and the methods used for four-fermion production are discussed in Section 2. Recent theoretical results are reviewed in Section 3 while an outlook to future developments needed to meet the requirements of planned colliders is given in Section 4.

2 Theoretical challenges and methods

In the theoretical description of four-fermion production, in general all diagrams contributing to a given final state must be taken into account for a consistent, gauge invariant result,[2] resulting in a large number of contributing Feynman diagrams, in particular beyond leading order. These typically include topologies different from the resonant "signal" diagrams of the processes in Figure 1. For instance, as shown in Figure 2, ten tree-diagrams contribute to the final state $u\bar{d}\mu^-\bar{\nu}_\mu$, where only three diagrams include a resonant W-boson pair. Similarly, 20 diagrams contribute to the single-W signature $u\bar{d}e^-\bar{\nu}_e$.

The consistent treatment of the W/Z-boson decay-widths poses a further theoretical challenge. The *Dyson series* allows the resummation of the self-energy Σ_V of the vector boson V to all orders into the denominator of the V-boson propagator, $(p^2 - M_V^2 + \Sigma_V(p^2))$. The complex pole μ_V of the propagator defined by $\mu_V^2 - M_V^2 + \Sigma_V(\mu_V^2) = 0$ provides a gauge invariant definition of the mass M_V and width Γ_V of the vector bosons, $\mu_V^2 \equiv M_V^2 - \mathrm{i}M_V\Gamma_V$.

[2] In some cases, gauge invariant subsets of diagrams can be identified. 3)

The Dyson summation of the self-energy includes only a subset of higher-order diagrams, but neglects other contributions of the same order. A naive application therefore can lead to inconsistencies such as violations of gauge invariance and unitarity, which can can result in dramatically wrong predictions, in particular in the case of single-W production at high energies. [5)]A simple use of a Breit-Wigner propagator with a *fixed width* is sufficient in many leading-order applications, but does not respect electroweak gauge invariance. In the *complex-mass scheme* [6)], the replacement $M_V^2 \to \mu_V^2$ is made in the propagator as well as in the Feynman rules, e.g. in the weak-mixing angle $\cos\theta_w = M_W/M_Z \to \sqrt{\mu_W^2/\mu_Z^2}$. In this way, algebraic identities among vertices and propagators required by gauge invariance are satisfied also for a finite width. The *fermion-loop scheme*, [5)] applied in particular to the single-W process at LEP2, [7)] uses the fact that diagrams with a closed fermion loop form a gauge invariant subset of diagrams. Finally, the *double-pole approximation* (DPA) consistently splits the NLO corrections into factorizable corrections to on-shell vector-boson production and decay, and non-factorizable soft-photon corrections connecting vector-boson production, propagation and decay. The DPA has been applied to W- and Z-boson pair production at LEP2. [8)]

The methods summarized here have been used successfully to describe the LEP2 measurements of four-fermion production with a theoretical accuracy better than 1% for W-pair production and 2–5% for the other processes. [2, 3)]

3 Recent theoretical developments

The high accuracy possible at future e^-e^+ colliders makes it mandatory to improve the theoretical predictions of four-fermion cross sections beyond the level achieved for LEP2. The M_W measurement from a threshold scan requires a calculation of the W-pair production cross section with a precision of a few per-mille in the threshold region $\sqrt{s} \sim 2M_W$, where the accuracy of the DPA degrades. A complete NLO calculation of charged-current 4-fermion production was performed in the complex mass scheme, including loop corrections to singly- and non-resonant diagrams. [6)] The DPA agrees well with the full $e^-e^+ \to 4\mathrm{f}$ calculation for energies $200\,\mathrm{GeV} \lesssim \sqrt{s} \lesssim 500\,\mathrm{GeV}$ while the full calculation is required near threshold $160\,\mathrm{GeV} \lesssim \sqrt{s} \lesssim 170\,\mathrm{GeV}$, and for $\sqrt{s} > 500\,\mathrm{GeV}$, where off-shell effects become important. In a further development, effective-field theory (EFT) methods have been used for a dedicated calculation of four-fermion production near the W-pair production threshold. [9] This method has allowed to isolate and compute the subset of NNLO corrections that is enhanced near threshold due to Coulomb-photon effects. Combining these dominant NNLO corrections, which are of the order of 0.5%, with the full NLO result [6] reduces the theoretical uncertainty of the M_W-measurement from a threshold scan to $\Delta M_W \lesssim 3\,\mathrm{MeV}$, [9] below the ILC precision goal.

At centre-of-mass energies $\sqrt{s} \gtrsim 800$ GeV, which are particularly relevant for measurements of triple gauge couplings, higher-order EW corrections are enhanced by Sudakov logarithms. For W-pair production, NNLO corrections due to NNLL Sudakov logarithms $\alpha^2 \log^m(s/M_W^2)$ with $m = 2, 3, 4$ have been computed [10] and are of the order of 5% (15%) for $\sqrt{s} = 1\,\mathrm{TeV}$ ($3\,\mathrm{TeV}$), so they should be taken into account in the second phase of an ILC or at CLIC.

In addition to these precision calculations, the search for indirect signals of new physics requires a systematic treatment of deviations from the SM in an EFT framework, which has recently been applied to study the sensitivity to anomalous gauge boson couplings in W-pair production. [11]

4 Outlook

Theoretical methods for higher-order calculations have seen remarkable progress after the LEP2 era. The theoretical uncertainty on charged-current four-fermion production has been reduced well below the percent level by a full NLO calculation. [6] The extension of this calculation to the remaining processes of Fig. 1 will be simplified by recent progress on the automation of EW NLO calculations [12] and may provide sufficient precision for future linear e^-e^+ colliders, if supplemented with dominant NNLO effects in special kinematic regions [9, 10] and an improved treatment of initial-state radiation. The precision goals of future circular e^-e^+ colliders may require a full NNLO calculation of EW corrections, where the current state of the art is given by $1 \to 2$ processes. [13] The extension to $2 \to 2$ processes such as on-shell vector-boson pair production is beyond current methods, but may be feasible within several years. This would provide one of the building blocks of the extension of the double-pole approximation [8] or the EFT approach [9] to NNLO, which in addition requires the computation of two-loop soft-photon corrections with finite-width effects. Steps towards a decision on the construction of a future e^-e^+ collider would stimulate theoretical developments to meet these challenges.

References

1. H. Baer *et al.*, arXiv:1306.6352 [hep-ph];
   L. Linssen *et al.*, arXiv:1202.5940 [physics.ins-det];
   M. Bicer *et al.* JHEP **1401**, 164 (2014);
   CEPC project `http://cepc.ihep.ac.cn/`.
2. S. Schael *et al.* Phys. Rept. **532**, 119 (2013).
3. M. W. Grunewald *et al.*, [hep-ph/0005309].
4. M. Baak *et al.*, arXiv:1310.6708 [hep-ph].
5. W. Beenakker *et al.*, Nucl. Phys. B **500**, 255 (1997).
6. A. Denner *et al.*, Phys. Lett. B **612**, 223 (2005) [Erratum-ibid. B **704**, 667 (2011)]. Nucl. Phys. B **724**, 247 (2005) [Erratum-ibid. B **854**, 504 (2012)].
7. E. Accomando *et al.*, Phys. Lett. B **479**, 209 (2000);
   G. Passarino, Nucl. Phys. B **578**, 3 (2000).
8. S. Jadach *et al.*, Phys. Rev. D **56**, 6939 (1997);
   W. Beenakker *et al.*, Nucl. Phys. B **508**, 17 (1997);
   A. Denner *et al.*, Nucl. Phys. B **587**, 67 (2000);
   S. Jadach *et al.*, Phys. Rev. D **65**, 093010 (2002).
9. M. Beneke *et al.*, Nucl. Phys. B **792**, 89 (2008);
   S. Actis *et al.*, Nucl. Phys. B **807**, 1 (2009).
10. J. H. Kühn, F. Metzler and A. A. Penin, Nucl. Phys. B **795**, 277 (2008) [Erratum-ibid. **818**, 135 (2009)].
11. G. Buchalla *et al.*, Eur. Phys. J. C **73** (2013) 10, 2589;
    J. D. Wells and Z. Zhang, arXiv:1507.01594 [hep-ph].
12. S. Kallweit *et al.*, JHEP **1504**, 012 (2015);
    M. Chiesa, N. Greiner and F. Tramontano, arXiv:1507.08579 [hep-ph].
13. S. Actis *et al.*, Nucl. Phys. B **811**, 182 (2009).

MEASURING THE LEADING ORDER HADRONIC CONTRIBUTION TO THE MUON G-2 IN THE SPACE-LIKE REGION

Graziano Venanzoni
Laboratori Nazionali di Frascati dell'INFN, Frascati, Italy

Abstract

After reviewing the traditional way of computing the leading order hadronic correction to the muon $g-2$ through a dispersive approach via time-like data, I will present a novel approach, based on the measurement of the effective electromagnetic coupling in the space-like region extracted from Bhabha scattering data. We argue that this new method may become feasible at flavor factories, resulting in an alternative determination potentially competitive with the accuracy of the present results obtained with the dispersive approach via time-like data.

1 The Muon g-2

The muon anomaly $a_\mu = (g-2)/2$ is a low-energy observable, which can be both measured and computed to high precision [1]. Therefore it provides an important test of the Standard Model (SM) and it is a sensitive search for new physics. Since the first precision measurement of a_μ from the E821 experiment at BNL in 2001 [2], there has been a discrepancy between its experimental value and the SM prediction of $\approx 3\,\sigma$ [1, 3].

Like the effective fine-structure constant at the scale M_z, the SM determination of the anomalous magnetic moment of the muon a_μ is presently limited by the evaluation of the hadronic vacuum polarisation effects, which cannot be computed perturbatively at low energies. However, using analyticity and unitarity, it was shown long ago that this term can be computed from hadronic e^+e^- annihilation data via the dispersive integral [4].

Two recent compilations of e^+e^- data give [5, 6]:

$$a_\mu^{\mathrm{had;LO}} = (6\ 923 \pm 42) \times 10^{-11}\,, \quad (1)$$

$$a_\mu^{\mathrm{had;LO}} = (6\ 949 \pm 43) \times 10^{-11}\,, \quad (2)$$

respectively.

Important earlier global analyses include those of Hagiwara et al. [7], Davier, et al., [8], Jegerlehner and Nyffler [9].

Therefore the leading-order hadronic vacuum polarization contribution, a_μ^{HLO} is known with a fractional accuracy of 0.7%, i.e. to about 0.4 ppm. The $\mathrm{O}(\alpha^3)$ hadronic light-by-light contribution, a_μ^{HLbL}, is the second dominant error in the theoretical evaluation. It cannot at present be determined from data, and relies on using specific models. Although its value is almost two orders of magnitude smaller than a_μ^{HLO}, it is much worse known (with a fractional error of the order of 30%) and therefore it still give a significant contribution to $\delta a_\mu^{\mathrm{TH}}$ (between 2.5 and 4 $\times 10^{-10}$).

From the experimental side, the error achieved by the BNL E821 experiment is $\delta a_\mu^{\mathrm{EXP}} = 6.3 \times 10^{-10}$ (0.54 ppm) [10]. This impressive result is still limited by the statistical errors, and a new experiment, E989 [11], to measure the muon anomaly to a precision of 1.6×10^{-10} (0.14 ppm) is under construction at Fermilab.

2 Measuring a_μ^{HLO} with space-like data

The leading-order hadronic contribution to the muon $g-2$ can be expressed in the form [12]

$$a_\mu^{\rm HLO} = \frac{\alpha}{\pi}\int_0^1 dx\,(1-x)\,\Delta\alpha_{\rm had}[t(x)]\,. \tag{3}$$

where

$$t(x) = \frac{x^2 m^2}{x-1} < 0 \tag{4}$$

is a space-like squared four-momentum.

Equation (3), involving the hadronic contribution to the running of the effective fine-structure constant at space-like momenta, can be computed by measurements of the effective electromagnetic coupling in the space-like region.

3 $\Delta\alpha_{\rm had}(t)$ from Bhabha scattering data

The hadronic contribution to the running of α in the space-like region, $\Delta\alpha_{\rm had}(t)$, can be extracted comparing Bhabha scattering data to Monte Carlo (MC) predictions.

Before entering the details of the extraction of $\Delta\alpha_{\rm had}(t)$ from Bhabha scattering data, let us consider a few simple points. In fig. 1 (left) we plot the integrand $(1-x)\Delta\alpha_{\rm had}[t(x)]$ of Eq. (3) using the output of the routine `hadr5n12` [13] (which uses time-like hadroproduction data and perturbative QCD). The range $x \in (0,1)$ corresponds to $t \in (-\infty, 0)$, with $x=0$ for $t=0$. The peak of the integrand occurs at $x_{\rm peak} \simeq 0.914$ where $t_{\rm peak} \simeq -0.108$ GeV^2 and $\Delta\alpha_{\rm had}(t_{\rm peak}) \simeq 7.86 \times 10^{-4}$ (see fig. 1 (right)). Such relatively low t values can be explored at e^+e^- colliders with center-of-mass energy $\sqrt{s}$ around or below 10 GeV (the so called "flavor factories") where

$$t = -\frac{s}{2}\,(1-cos\theta)\left(1-\frac{4m_e^2}{s}\right), \tag{5}$$

θ is the electron scattering angle and m_e is the electron mass. Depending on s and θ, the integrand of Eq. (3) can be measured in the range $x \in [x_{\rm min}, x_{\rm max}]$, as shown in fig. 2 (left). Note that to span low x intervals, larger θ ranges are needed as the collider energy decreases. In this respect, $\sqrt{s} \sim 3$ GeV appears to be very convenient, as an x interval $[0.30, 0.98]$ can be measured varying θ between $\sim 2°$ and $28°$. Furthermore, given the smoothness of the integrand, values outside the measured x interval may be interpolated with some theoretical input. In particular, the region below $x_{\rm min}$ will provide a relatively small contribution to $a_\mu^{\rm HLO}$, while the region above $x_{\rm max}$ may be

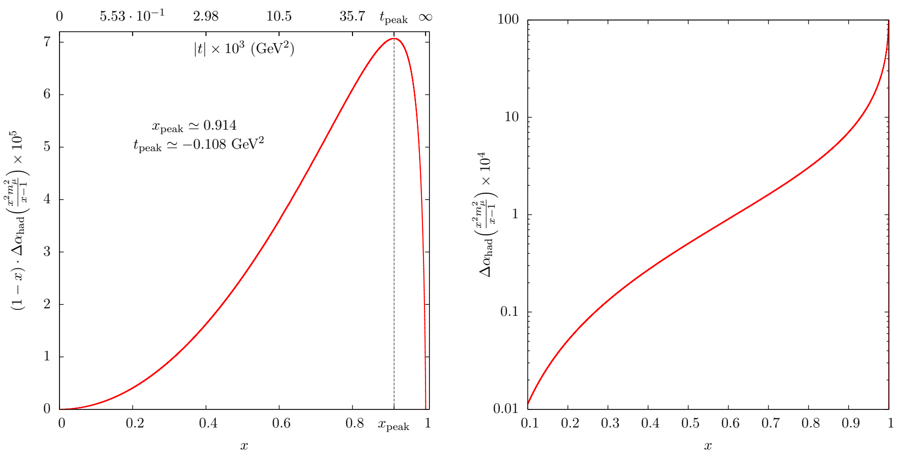

Figure 1: Left: The integrand $(1-x)\Delta\alpha_{\rm had}[t(x)] \times 10^5$ as a function of x and t. Right: $\Delta\alpha_{\rm had}[t(x)] \times 10^4$.

obtained by extrapolating the curve from $x_{\rm max}$ to $x = 1$, where the integrand is null, or using perturbative QCD.

The analytic dependence of the MC Bhabha predictions on $\alpha(t)$ (and, in turn, on $\Delta\alpha_{\rm had}(t)$) is not trivial, and a numerical procedure has to be devised to extract it from the data [14].

In order to assess the achievable accuracy on $\Delta\alpha_{\rm had}(t)$ with the proposed method, we remark that the LO contribution to the cross section is quadratic in $\alpha(t)$, thus we have:

$$\frac{1}{2}\frac{\delta\sigma}{\sigma} \simeq \frac{\delta\alpha}{\alpha} \simeq \delta\Delta\alpha_{\rm had} \tag{6}$$

Equation (6) relates the *absolute* error on $\Delta\alpha_{\rm had}$ with the *relative* error on the Bhabha cross section. From the theoretical point of view, the present accuracy of the MC predictions [15] is at the level of about 0.5 per-mil, which implies that the precision that our method can, at best, set on $\Delta\alpha_{\rm had}(t)$ is $\delta\Delta\alpha_{\rm had}(t) \simeq 2 \cdot 10^{-4}$. Any further improvement requires the inclusion of the NNLO QED corrections into the MC codes, which are at present not available (although not out of reach).

From the experimental point of view, we remark that a measurement of $a_\mu^{\rm HLO}$ from space-like data competitive with the current time-like evaluations would require an $\mathcal{O}(1\%)$ accuracy. Statistical considerations show that such a

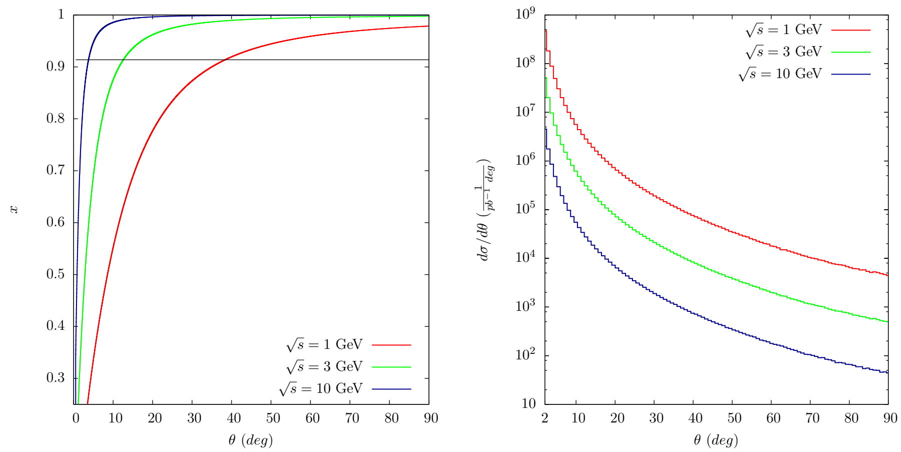

Figure 2: Left: Ranges of x values as a function of the electron scattering angle θ for three different center-of-mass energies. The horizontal line corresponds to $x = x_{\rm peak} \simeq 0.914$. Right: Bhabha differential cross section obtained with `BabaYaga` [16] as a function of θ for the same three values of $\sqrt{s}$ in the angular range $2^\circ < \theta < 90^\circ$.

statistics could be obtained at current flavor factories [14]. The experimental systematic error must match the same level of accuracy.

4 Acknowledgements

It's a pleasure to thank the LCF15 local organizing committee, for running a smooth and productive meeting in a very friendly atmosphere, and ECT* for the financial support. I thank C. Calame, M. Passera, and L. Trentadue for the common work which led to the proposal discussed in the text. This talk is dedicated to the memory of my friend and colleague Eduard A. Kuraev.

5 References

References

1. F. Jegerlehner, "The anomalous magnetic moment of the muon," Springer Tracts Mod. Phys. **226** (2008) 1.

2. H. N. Brown *et al.* [Muon g-2 Collaboration], Phys. Rev. Lett. **86** (2001) 2227.

3. T. Blum, A. Denig, I. Logashenko, E. de Rafael, B. Lee Roberts, T. Teubner and G. Venanzoni, arXiv:1311.2198 [hep-ph].

4. M. Gourdin and E. De Rafael, Nucl. Phys. B **10** (1969) 667.

5. M. Davier, A. Hoecker, B. Malaescu and Z. Zhang, Eur. Phys. J. **C71** (2011) 1515, Erratum-ibid. **C72** (2012) 1874.

6. K. Hagiwara, R. Liao, A. D. Martin, D. Nomura and T. Teubner, J. Phys. **G38** (2011) 085003.

7. K. Hagiwara, A. D. Martin, D. Nomura and T. Teubner, Phys. Lett. **B649** (2007) 173.

8. M. Davier,Nucl. Phys. Proc. Suppl. **169** (2007) 288.

9. F. Jegerlehner and A. Nyffeler, Phys.Rept. **477** (2009) 1.

10. G. W. Bennett *et al.* [Muon G-2 Collaboration], Phys. Rev. D **73** (2006) 072003.

11. J. Grange *et al.* [Muon g-2 Collaboration], arXiv:1501.06858 [physics.ins-det]; R.M. Carey *et. al.* [New Muon (g-2) Collaboration], see http://lss.fnal.gov/archive/testproposal/0000/fermilab-proposal-0989.shtml.

12. F. Jegerlehner, J. Phys. G **29** (2003) 101.

13. S. Eidelman, F. Jegerlehner, Z. Phys. C **67** (1995) 585; F. Jegerlehner, Nucl. Phys. Proc. Suppl. **181-182** (2008) 135.

14. C. M. Carloni Calame, M. Passera, L. Trentadue and G. Venanzoni, Phys. Lett. B **746** (2015) 325 doi:10.1016/j.physletb.2015.05.020.

15. S. Actis *et al.* [Working Group on Radiative Corrections and Monte Carlo Generators for Low Energies Collaboration], Eur. Phys. J. C **66** (2010) 585.

16. G. Balossini, C.M. Carloni Calame, G. Montagna, O. Nicrosini, F. Piccinini, Nucl. Phys. B **758** (2006) 227.

TOTAL CROSS-SECTIONS AT LHC AND COSMIC RAY ENERGIES

Giulia Pancheri
INFN Frascati National Laboratories, Via E. Fermi 40, I00044 Frascati
Daniel Fagundes
Universidade Federal de Santa Catarina, 89065-300 Blumenau, SC, Brazil
A. Grau
Departamento de Fisica Teorica y del Cosmos, Universidad de Granada, Spain.
O. Shekhovtsova
NSC KIPT, Kharkov, Ukraine, and INP of PAS Cracow, Poland
Y. N. Srivastava
Department of Physics & Geology, University of Perugia, Perugia, Italy

Abstract

An overview of the present status of measurements and modeling of the total *pp* cross-section is presented. Open problems and some proposed solutions are discussed.

1 Introduction

Early observation of high energy particle scattering were made through cosmic ray showers. They were followed by measurements with particle beam accelerators beginning in the mid 1950's. Since then, the energy behavior of the total hadronic cross-section, be it with proton, photon, pion or kaon beams, is still of fundamental interest to a vast community of physicists. In this brief note, we shall discuss questions posed by the present data and some proposed solutions.

Presently, measurements range in energy from a few GeV (in the center of mass frame) to almost 100 TeV, the latter obtained through cosmic ray experiments. In Fig.(1), we show a compilation of data from measurements which probe at least the 100 GeV c.m. region, where all data clearly exhibit the common feature of a rise in the total cross-section with energy. This excludes πp and Kp, whose measurements are still limited in the energy reach by having been done at fixed target accelerators, and hence are not included in the figure.

The common features exhibited by these different processes can be seen by normalizing them around the observed minimum. As indicated in the figure, this can be done with a factor proportional to α_{QED} for γp and the same factor, but squared, for $\gamma\gamma$.

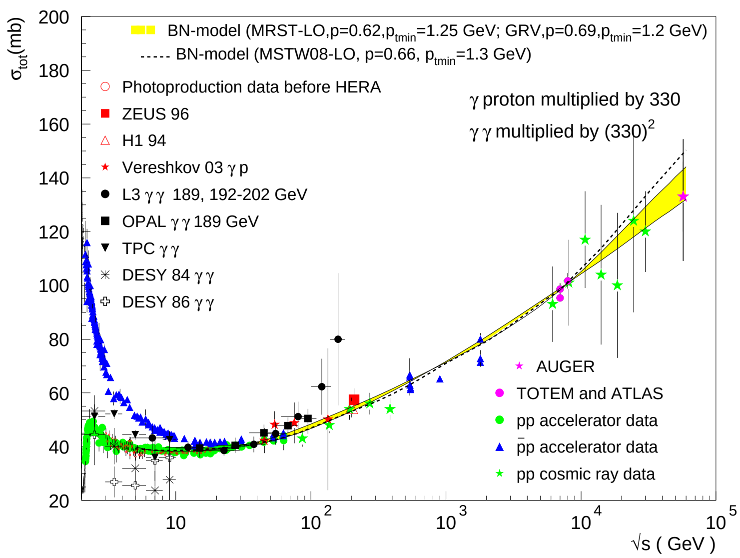

Figure 1: pp, $p\bar{p}$, γp and $\gamma\gamma$ total cross-sections, normalized to the same scale. The figure is from [1].

Two properties come to immediate attention: In $p\bar{p}$, the data show an apparent minimum around $\sqrt{s} \simeq 20\ GeV$, with a sharp rise and a continuous increase past $\sqrt{s} \simeq 200\ GeV$, but with a softer slope, i.e. one notices a softening of the rise. The minimum is less pronounced in the pp case, but the increase is the same. In $\gamma\gamma$ and γp the lack of really high energy data does not allow to establish beyond doubt that the increase has the same slope as in purely hadronic processes. As the energy increased and new measurements were made, models adapted their parameters to accommodate the new features. Thus one may ask what does one learn from present models when compared to the data since most models accommodate new data just by changing the parameters? Another question is related to the fact that there are large uncertainties concerning the very high energy *pp* data, which are extracted from cosmic rays: which machines and which type of experiments can give new information to move ahead with models and get understanding of the underlying dynamics?

2 A brief history

A first realistic model was provided by Heisenberg in 1952, who studied the dynamics of production of the pion cloud emitted in a high energy collision [2], and predicted that it should possible to describe the energy behavior according to two extreme models: either $\sigma_{tot} \sim constant$ or $\sigma_{tot} \sim [\ln s]^2$.

A most successful model for the total and the elastic cross-section is based on the Gribov-Regge theory, where the elastic amplitude is given as

$$\mathcal{A}(s,t) \propto i \sum s^{\alpha_i(t)-1} \tag{1}$$

with $\alpha_i(t)$ the Regge trajectories exchanged in the t-channel. Using the optical theorem, Donnachie and Landshoff in 1992 proposed the simple and universal expression [3]

$$\sigma_{tot}(s) = X s^{-\eta} + Y s^{+\epsilon} \tag{2}$$

with $\eta, \epsilon \geq 0$. The above expression contradicts the Froissart-Martin bound which requires all total cross-sections to increase asymptotically not more than $[\ln s]^2$. This behaviour is requested by the existence of a cut-off in the range of the interaction or, equivalently, the existence of a finite mass, such as the pion mass. Thus, the dilemma is shown in Fig. (2): what is the dynamical mechanism which makes the cross-section rise and which mechanism limits the rise to be "tamed" into a logarithmic behavior? To comply with unitarity, the Gribov-Regge theory was extended to an eikonal approach, which includes Pomeron exchanges and a multichannel formalism, as for instance in [4, 5].

An answer to the above questions has been proposed [6] in the context of QCD mini-jet models, in which the rise with energy is driven by the increasing number of low-x partons participating to the scattering. At the same time,

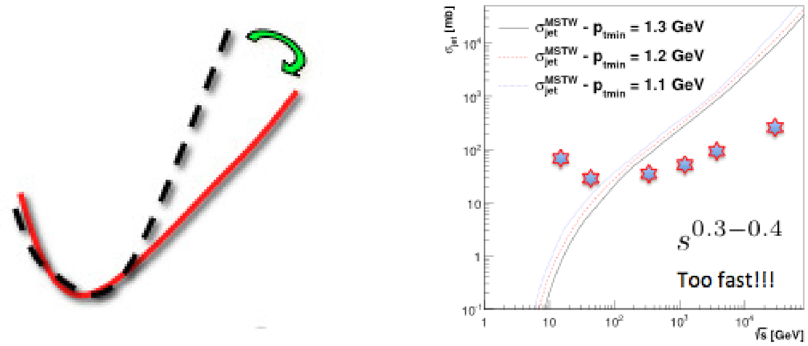

Figure 2: At left a cartoon describing the transformation of the initial fast rise of the cross-section, compatible with a power-law, into a smooth asymptotic behavior, compatible with a logarithmic behavior. At right the energy behavior of a QCD cross-section compared with a typical hadronic cross-section (stars).

while more and more low-x gluons produce QCD mini-jets, softer and softer gluons accompanying the scattering increase the a-collinearity of the colliding particles and *de facto* decrease the cross-section. These two mechanisms act together to produce the observed logarithmic increase of the cross-section. We show a calculation of a QCD mini-jet cross-section in the right hand panel of Fig. (2), where the curve is from [7)] and the stars describe qualitatively a typical hadronic total cross-section. Related to this is the transition between the region where the cross-section is decreasing and the one where it rises. As clearly seen in Fig. (1) such a transition seem to occur around 20 GeV in the pp c.m. system. This behavior reflects the transition from non-perturbative to perturbative QCD (pQCD) dynamics. The argument runs as follows [7)]: the regime of applicability of pQCD requires parton transverse momenta to be $p_t >> \Lambda_{QCD} \simeq 0.2 \div 0.4\ GeV$ so as to allow the perturbation expansion in the asymptotic freedom expression for the coupling constant $\alpha_s(p_t)$. One can then calculate the contribution of parton-parton scattering to the proton-proton cross-section, so-called *mini-jet cross-section*.

Call p_{tmin} the minimum transverse moment for pQCD applicability, and let us take $p_{tmin} \geq 1\ GeV$. Partons with such transverse momentum carry a fraction of the proton momentum $x \gtrsim 2p_{tmin}/\sqrt{s}$ and are characterized by a 1/x spectrum. As the energy increases, their contribution to the proton-proton cross-section becomes more important, and increasing: typically one needs $x \leq (0.1-0.2)$-values, namely $\sqrt{s} \geq 2p_{tmin}/0.1 \geq 20\ GeV$, precisely the energy where the change in curvature of the total cross-section appears. Observation of an *edge* in the impact parameter space by Block and collaborators around the same energy values is indicative of the occurrence of a transition to a different regime [8].

3 The single-channel eikonal mini-jet model with infrared soft gluon resummation

In this section, we describe the results of a single channel mini-jet model for the total pp [6] and $p-air$ [9] cross-section, based on the expressions:

$$\sigma_{total}^{pp} = 2\int d^2\mathbf{b}[1-e^{-\chi_{pp}(b,s)}],\ 2\chi_{pp}(b,s) = n_{pp}^{soft} + A(b,s)\sigma^{QCD}(p_{tmin},s) \quad (3)$$

$$\sigma_{inel}^{pp} = \int d^2\mathbf{b}[1-e^{-2\chi_{pp}(b,s)}] \quad (4)$$

$$\sigma_{prod}^{p-air} = \int d^2\mathbf{b}[1-e^{-2\chi_{p-air}(b,s)}],\ 2\chi_{p-air}(b,s) = n_{p-air}^{soft} + T_{air}(b)\sigma_{inel}^{pp} \quad (5)$$

where the impact space distributions $A(b,s)$ and $T_{air}(b)$ are obtained from a soft gluon resummation model and a gaussian-like nuclear distribution function respectively. The mini jet cross-sections $\sigma^{QCD}(p_{tmin},s)$ are obtained from standard parton-parton cross-sections folded with parton densities (PDFs). The curves of Fig. (1) were obtained from Eq. (3) using GRV and MSTW2008 PDFs [7]. As for the $p-air$ cross-sections, details of the model (and references) can be found in [9] and we show in Fig. (3) the results of the single-channel eikonal mini-jet model of Eq. (5) compared with cosmic ray data, up to the latest Auger and Telescope Array data.

4 Conclusions

Presently, some of the questions posed by total hadronic cross-section measurements are still unanswered, in particular the one related to whether the limit of the Froissart bound has been reached. It appears that for quite some time the answer can only come from cosmic ray experiments, which are still however affected by large errors, both statistical and systematic. In this note we have presented a proposal to extract the information from mini-jet models and soft gluon resummation, which reproduces both pp and $p-air$ available data, with errors due to present uncertainty in the parton densities at very low-x values.

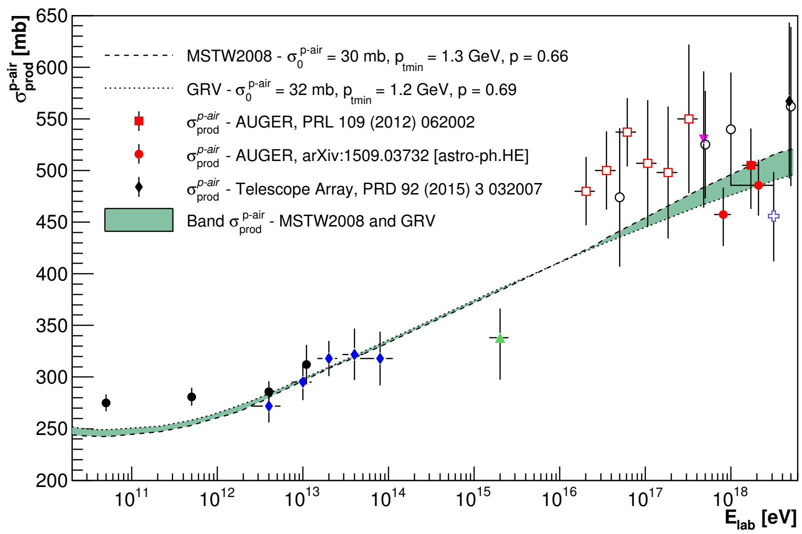

Figure 3: $p - air$ production cross-section as deduced from the mini-jet model of [6] and [9], and its comparison with cosmic ray data. The band indicates uncertainties due to low-x behavior of the PDFs.

References

1. F. Cornet *et al.*, Phys. Rev. **D13**, 138, (2015).
2. W. Heisenberg, Z. Phys. **133**, 65, (1952).
3. A. Donnachie and P.V. Landshoff, Phys. Lett. **B296**, 227, (1992).
4. M.G. Ryskin *et al.*, Eur.Phys.J. **C54**, 199, (2008).
5. E. Gotsman *et al.*, Eur.Phys.J. **C57**, 689, (2008).
6. A. Grau *et al.*, Phys. Rev.**D60**, 114020, (1999); R.M. Godbole *et al.*, Phys. Rev. **D72**, 076001, (2005).
7. D. Fagundes *et al.* Phys. Rev. **D91**, 11, 114011(2015).
8. M.M. Block *et al.*, Phys.Rev. **D92**, 1, 014030 (2015).
9. D. Fagundes *et al.*, EPJ Web Conf. **90**, 03002, (2015), arXiv:1408.2921.

QCD AT THE LHC: STATUS AND PROSPECTS

Ruggero Turra
Università degli Studi di Milano & INFN

Abstract

This article summarizes most of the QCD-related analyses made by the ATLAS and CMS experiments at the LHC with the first proton-proton collisions collected in 2015 at $\sqrt{s} = 13\,\mathrm{TeV}$ (integrated luminosity in the range $170\,\mathrm{\mu b^{-1}T} - 85\,\mathrm{pb^{-1}}$, according to the analysis under discussion) and a selected review of the most important results of Run1 at $\sqrt{s} = 7\,\mathrm{TeV}$, $8\,\mathrm{TeV}$ and $2.76\,\mathrm{TeV}$. QCD processes play an important role at LHC: first, many QCD predictions can be tested and precision measurements can be done; second, QCD processes represent the vast majority of background for many searches of New Physics (NP). Both soft and hard QCD results are presented, including the measurement of α_s. Data show a good agreement with the QCD theoretical predictions.

1 Introduction

In QCD phenomenology, thanks to factorization, the production cross section of the hard process can be factorized as the parton-parton cross section times the parton distribution function (pdf). The first term can be computed with perturbative QCD (pQCD), while the second term must be measured combining different experiments. To obtain the final and physically interesting observables, non-perturbative effects must be accounted for. They include hadronization and underlying event (UE) and are simulated via Monte Carlo generators, which are tuned using data.

QCD production is the most common process at LHC due to the hadronic nature of the proton-proton collisions. Many pQCD predictions can be tested at the LHC, in a new phase space region where some measurements become sensitive to NLO QCD. In addition, QCD processes are a source of uncertainty for many other important processes since they constitute a common background, for example for the Higgs boson studies or BSM searches. QCD processes can be used to determine non-perturbative quantites like PDFs, which are a large source of uncertainty for different processes ($gg \to H$, $t\bar{t}$ production, …) or UE deternination.

The results presented in this review are from proton-proton collisions at the LHC by ATLAS and CMS, from Run1 and the first months of data taking of Run2. Run1 includes $\simeq 5\,\mathrm{fb}^{-1}$ of data collected at $\sqrt{s} = 7\,\mathrm{TeV}$ and $\simeq 20\,\mathrm{fb}^{-1}$ collected at $\sqrt{s} = 8\,\mathrm{TeV}$. Run2 data used in the presented analyses are from 50 ns collisions and an integrated luminosity in the range $170\,\mu\mathrm{b}^{-1}$-$85\,\mathrm{pb}^{-1}$.

Section 2 shows results of non-perturbative QCD, including minimum bias and underlying event in Run2. The following sections are organized with respect to the probe used to study QCD: jets in section 3, including cross section measurements (inclusive, dijet, multijet) and the measurement of α_s, photons in section 4 and vector bosons in section 5.

2 Non-perturbative QCD

Both ATLAS and CMS measured the distribution of charged particles at $\sqrt{s} = 13\,\mathrm{TeV}$ [1] [2]. This provides insight into the strong interaction in the low energy, non-perturbative QCD region, which is described by QCD-inspired models, implemented in MC event generators with free parameters that can be constrained by measurements. The ATLAS distributions of the pseudorapidity η, transverse momentum p_T and charge multiplicity highlight clear differences with respect to MC models. Among the models considered, EPOS provides the best data description, PYTHIA 8 A2 and MONASH give reasonable data descriptions and HERWIG++ and QGSJET-II provide the worst descriptions of the data. CMS presented only η distributions: in the central region, the measurement is consistent with predictions of the PYTHIA 8 and EPOS event generators, while those in a wider η range are better described by the latter.

The underlying event refers to the aspects of a given collision event not identified with the hard process, and its description in MC generators must be tuned to data. This is done studying the track multiplicity density and E_T flow in the transverse region ($60° < |\Delta\phi| < 120°$, where $\Delta\phi$ is the azimuthal angle with respect to the leading jet). ATLAS showed first results at 13 TeV [3], at detector level: the underlying event increased by 20% with respect to $\sqrt{s} = 7$ TeV, and data agree with all tested models. CMS complements the underlying event measurement using data at $\sqrt{s} = 2.76$ TeV [4], showing a good agreement with PYTHIA6, PYTHIA8, and HERWIG++ within 5% to 10%.

3 QCD with jet

Jet production at high-p_T at LHC allows the validation of pQCD predictions at the TeV scale. It is sensitive to soft QCD, comparing different jet clustering and it is sensitive to the gluon-PDF at high-x. ATLAS analyzed the first data with 78 pb^{-1} at 13 TeV. Figure 1a shows the measured p_T differential cross section, in the kinematic region $346 \leq p_T \leq 838$ GeV and jet rapidity $|y| < 0.5$, consistent with NLO calculations. This analysis complements previous analyses at 8 TeV [21] [22] , 7 TeV [26] [24] and 2.76 TeV [23] [25], which span a wide range of p_T from few dozens of GeV to few TeV: as an example, figure 1b shows the jet cross section at 8 TeV measured by CMS. Similarly, dijet cross sections [27] [28] show a good agreement with NLO predictions, are able to discriminate PDF sets and can constrain gluon-PDFs at high-x.

3.1 α_s measurement

The α_s constant is the only free parameter of the massless QCD theory. At LHC $\alpha_s(Q)$ can be measured at high-Q, where it can become sensitive to NP

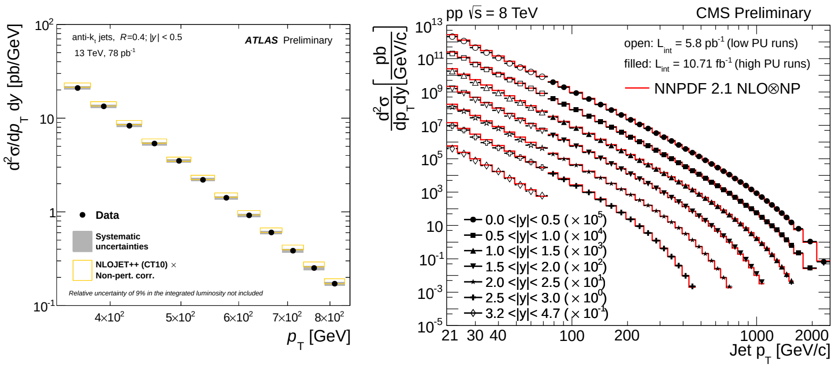

(a) (b)

Figure 1: (a) jet cross section in $|y| < 0.5$ at $\sqrt{s} = 13\,\mathrm{TeV}$ by ATLAS. (b) jet cross section in several $|y|$ regions at $8\,\mathrm{TeV}$ by CMS.

contributions. Many measurements are sensitive to its value: inclusive jet cross section [6], 3-jet mass [7], R_{32} [8] (3-jet / 2-jet cross section ratio), transverse energy-energy correlation (TEEC) [5] and $t\bar{t}$ cross section [9]. Measurements show a very good agreement of the α_s running with the prediction, up to the TeV scale, including results from CMS. The most precise value of $\alpha_S(m_Z)$ comes from $t\bar{t}$ cross section by CMS $\alpha_s(m_Z) = 0.1151^{+0.0028}_{-0.0027}$. The most precise value from ATLAS comes from the TEEC in dijet events $\alpha_S(m_Z) = 0.1173 \pm 0.0010(\mathrm{exp})^{+0.0065}_{-0.0026}(\mathrm{theo})$ [5].

4 QCD with photons

Compared to jets, the cross section of isolated photons, produced in QCD processes, provides a test of pQCD in a cleaner environment, without the hadronization complications. As shown in [10] these measurements can be used to constrain the gluon-PDF. ATLAS showed the first study on inclusive photons at 13 TeV [13]; the good agreement between the detector level measurement using $6.4\,\mathrm{pb}^{-1}$ with Sherpa is shown in figure 2a. This new analysis complements previous measurements of the inclusive cross section [11] [12], photon-jet cross section [14] [15] and diphoton cross section [16] [17]. Figure 2b shows the major discrepancy, observed in the low azimuthal angle between two photons because initial-state soft gluon radiation is divergent at NLO, without soft gluon resummation.

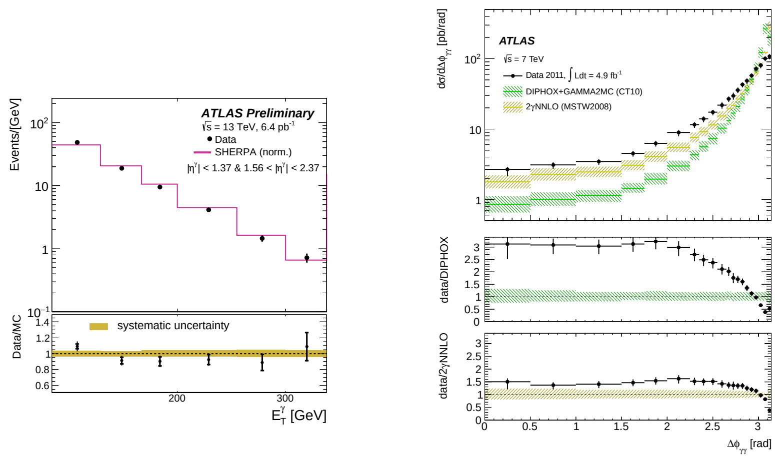

(a) (b)

Figure 2: (a) E_T^{γ} distribution from inclusive photon at 13 TeV by ATLAS and (b) $\Delta\phi_{\gamma\gamma}$ distribution from diphoton at 7 TeV by ATLAS.

5 QCD with $W^{\pm}$ and Z boson

Vector boson production at 13 TeV is enhanced by a factor 2 with respect to 7 TeV. First results from ATLAS in the leptonic channels show agreement of the inclusive cross section with NNLO predictions [19]. Ratios of cross sections W^+/W^- (R_{W^+/W^-}) or $W^{\pm}/Z$ ($R_{W/Z}$) cancel out several experimental systematics, in particular those related to the luminosity (9%). The uncertainty on these ratios are 2.5% and 3.2% respectively. In particular R_{W^+/W^-} (figure 3a) is starting to be sensitive to different sets of PDFs. Figure 3b shows the Z differential production cross section as a function of the number of jets in $Z+$jets, compared with predictions with matrix elements calculated for up to two partons at NLO, and up to four additional partons at LO.

A new analysis from CMS at 8 TeV studied the exclusive $Z+\geq 1b$ and

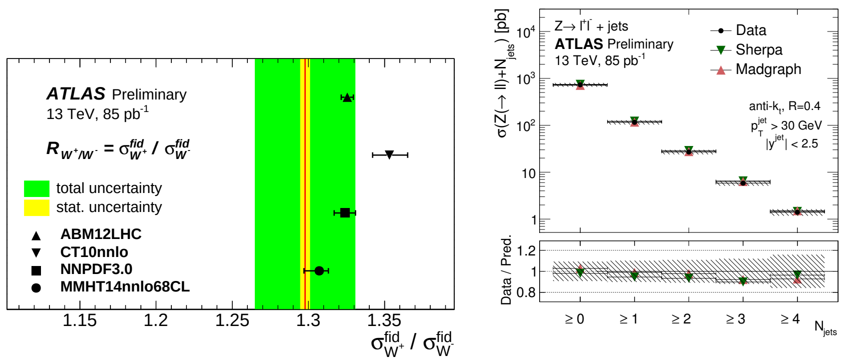

(a) (b)

Figure 3: (a) ratio of W^+ and W^- cross section and (b) jet multiplicity in Z+jet by ATLAS at 13 TeV.

$Z+ \geq 2b$ cross sections and the ratio with the $Z + j$ as a function of several variables that can be sensitive to b-PDF, gluon splitting, gluon radiation in the final state and NP [20]. Good agreement is observed, except for a discrepancy of about 20% in the overall normalization for the 4FS-based prediction of $Z+ \geq 1b$, of the same order of magnitude of its estimated theoretical uncertainty.

In summary, ATLAS and CMS produced a large amount of results on QCD in a new phase space region, some of them sensitive to NLO effects. Both collaborations showed first results at $\sqrt{s} = 13$ TeV: results from soft-QCD are used to tune non-perturbative components of MC simulations, while others are already used to test pQCD. The compatibility between theoretical predictions and data shows that QCD gives an accurate description of the measured observables.

References

1. ATLAS collaboration, ATLAS-CONF-2015-028.
2. CMS Collaboration, Phys. Lett. B **751** (2015) 143
3. ATLAS Collaboration, ATL-PHYS-PUB-2015-019

4. CMS Collaboration, JHEP **1509** (2015) 137
5. ATLAS Collaboration, Phys. Lett. B **750** (2015) 427
6. CMS Collaboration, Eur. Phys. J. C **75** (2015) 6, 288
7. CMS Collaboration, Eur. Phys. J. C **75** (2015) 5, 186
8. CMS Collaboration, Eur. Phys. J. C **73** (2013) 10, 2604
9. CMS Collaboration, Phys. Lett. B **728** (2014) 496
10. ATLAS Collaboration, ATL-PHYS-PUB-2013-018
11. ATLAS Collaboration, Phys. Rev. D **89** (2014) 5, 052004
12. CMS Collaboration, Phys. Rev. D **84** (2011) 052011
13. ATLAS Collaboration, ATL-PHYS-PUB-2015-016
14. ATLAS Collaboration, Nucl. Phys. B **875** (2013) 483
15. CMS Collaboration, JHEP **1406** (2014) 009
16. ATLAS Collaboration, JHEP **1301** (2013) 086
17. CMS Collaboration, Eur. Phys. J. C **74** (2014) 11, 3129
18. CMS Collaboration, JHEP **1510** (2015) 128
19. The ATLAS collaboration, ATLAS-CONF-2015-039.
20. CMS Collaboration, CMS-PAS-SMP-14-010.
21. CMS Collaboration, CMS-PAS-SMP-12-012.
22. CMS Collaboration, CMS-PAS-FSQ-12-031.
23. CMS Collaboration, CMS-PAS-SMP-14-017.
24. ATLAS Collaboration, JHEP **1502** (2015) 153
25. ATLAS Collaboration, Eur. Phys. J. C **73** (2013) 8, 2509
26. CMS Collaboration, Phys. Rev. D **87** (2013) 11, 112002
27. ATLAS Collaboration, JHEP **1405** (2014) 059
28. CMS Collaboration, CMS-PAS-SMP-14-002

THE GROWING TOOLBOX OF PERTURBATIVE QCD

Lorenzo Magnea
Dipartimento di Fisica, Università di Torino, and INFN, Sezione di Torino

Abstract

Advances in perturbative QCD techniques have been crucial for the successful interpretation of the data collected in Run I of LHC, and for the discovery of the Higgs boson. I will very briefly highlight some recent additions to the QCD toolbox, and note how these new tools are likely to be essential for future precision physics, both in Run II at the LHC, and in view of future hadron and lepton colliders.

1 Introduction

The first run of the LHC was a resounding success, culminating in the Nobel-prize-winning discovery of the Higgs boson: a great achievement, although the discovery was to a large extent expected. Strikingly, on the other hand, the Standard Model of particle physics held up, and it is now tested and verified to an unexpected, even amazing degree of accuracy all the way up to the TeV energy scale: no new physics turned up in Run I. This seems to have heightened the expectations for Run II: indeed, the recent announcement by CMS and ATLAS of a small excess of events in the di-photon channel triggered the publication, in less than one week, of more than one hundred papers with tentative theoretical interpretations, with the first papers appearing within minutes of the announcement. In a few months we will know if this outburst of speculative activity will be justified by further data. The task of this Workshop, however, is to look further ahead, to the next generation of machines which are currently being discussed and planned, and which will succeed or complement the LHC at the high-energy frontier.

The lesson that I would like to draw from the experience of the past years, leading up to the LHC operation and the data analyses of Run I, is that the role of precision Standard Model phenomenology has been crucial to develop a sufficient understanding of the immensely complex processes underlying LHC collisions, and will remain crucial for our ability to adequately exploit any future high-energy collider [1)].

The past ten to fifteen years have seen remarkable progress in our quantitative control of the three stages of hadron collisions. The parametrisation of initial states by means of parton distributions (PDFs) has undergone a radical overhaul, and we now have several independent and reliable sets of PDF's, with credible determinations of their uncertainties [2)]; our understanding of the hadron jets that characterise most final states has similarly evolved from qualitative to precisely quantitative, with the development of fast infrared-safe jet algorithms allowing for precise predictions for complex final states, including studies of the internal structure of the jets themselves [3)]. Finally, our capabilities to compute the hard-scattering partonic cross sections at the heart of LHC collisions has progressed much beyond what might have been expected: NLO calculations of multi-particle final states matched to parton showers are now the standard, and the extension of these techniques to NNLO and beyond is well under way [4)].

It is easy to argue that the splendid results of LHC Run I would not have been possible without this vast body of work, stemming from many collaborations involving hundreds of phenomenologists. Similarly, exploiting future colliders, which will operate at even higher energies, and likely require even higher precisions, will not be possible without a continued effort to refine our understanding of Standard Model processes.

In the limited space of this contribution, I will begin by emphasising the non-trivial role played by QCD predictions even at future lepton colliders; I will continue by giving some examples of the QCD tools developed in the past few years to handle high-order perturbative calculations, and I will conclude by briefly summarising some recent progress in the field of soft-gluon resummation, which may soon shed light on a new class of all-order contributions to interesting hadronic cross sections.

2 QCD at future (lepton) colliders

There is clearly no need to make the case for the importance of perturbative QCD studies at future hadron colliders, such as foreseen upgrades of the LHC, or the prospected 100 TeV collider [5]. On the other hand, preliminary physics assessment of proposed lepton colliders, such as TESLA, ILC or CLIC, have often focused (quite understandably) on their new physics potential, leaving the Standard Model on the sidelines. On occasions, this emphasis can be misleading, and further analysis shows that a detailed high-precision Standard Model analysis is necessary in order to exploit the full potential of the machine. Here are a few examples, focusing on QCD studies.

2.1 Hadronic jets

Lepton colliders are designed as precision machines, but, at high energies, many important final states will be characterised by a very high jet multiplicity. Such states are not easy to characterise accurately. As an example, consider $t\bar{t}H$ production, with all particles decaying hadronically: this leads to an eight-jet final state, with at least four b-quark jets. If colored supersymmetric particles were to be discovered, they would easily lead to even more complex final states. At a hadron collider, one might sidestep the problem by focusing on (semi) leptonic final states, but given the lower number of events to be expected for example at ILC, exploiting fully hadronic final states may prove necessary. Such high-multiplicity final states are likely to require the most advanced available QCD techniques for jet identification, tagging and mass reconstruction. One may also note that some of these techniques will need to be retuned (see for example [6]): boost invariance of the jet-finding algorithm will be less relevant, and jet-substructure studies will have a more limited impact since heavy states are unlikely to be heavily boosted.

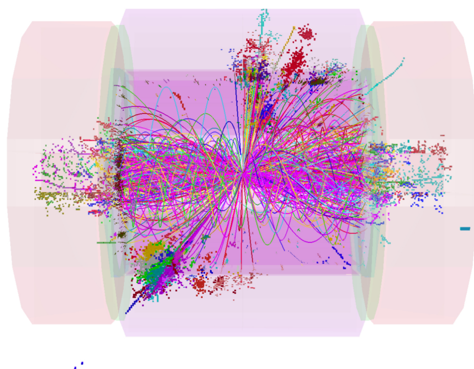

Figure 1: *A simulated event including the production of a $t\bar{t}$ pair at CLIC, with $\sqrt{s} = 3$ TeV, and overlaid background from $\gamma\gamma \to$ hadrons, from* [7].

2.2 Underlying event

One of the reasons why lepton colliders are (correctly) touted as 'clean' precision machines is the absence of the 'underlying event', the complex low p_T scattering of hadron remainders that surrounds the hard scattering at hadron colliders. It is however well understood by now that at sufficiently high energy a very significant 'underlying event' develops at lepton colliders as well. Just as protons at high energy can be seen as made mostly of gluons, leptons acquire an increasingly dominant photon component, which materialises as an underlying event through photon scattering, via $\gamma\gamma \to$ hadrons. Fig. 1, taken from the CLIC Conceptual Design Report [7] shows the simulation of a hard scattering event including the production of a $t\bar{t}$ pair, at $\sqrt{s} = 3$ TeV, with the hadron background generated by photon collisions. At this CM energy, the background deposits 1.2 TeVs of energy per event in the detector, which will have to be subtracted using refinements of recently developed tools such as jet areas [8].

2.3 Standard Model parameters

Lepton colliders hold the promise to give the most precise determinations of key Standard Model parameters, for example m_{top} and α_s. This was discussed elsewhere in this Workshop, it has recently been reviewed in detail in [9, 10], and certainly cannot be discussed in this very limited space. Once again, however, it is worth emphasizing that these determinations must rely upon state-of-the-art, high-order, precision QCD calculations. A case in point is the recently computed three-loop correction to the near-threshold production of $t\bar{t}$ pairs [11], which will play a key role in the determination of m_{top} with better than permil precision through a threshold scan: only at this level, reached through a combination of effective field theory techniques with high-level tools for loop calculations, one observes that the theoretical uncertainty comes under full control.

3 Selected examples of new tools

Recent years have seen a remarkable degree of progress in our ability to compute gauge theory amplitudes and cross sections to very high perturbative orders. To some extent, this was certainly triggered by the needs of LHC, but it is interesting to note that several of the new techniques that have been deployed are connected to purely theoretical developments originating from studies of $N = 4$ Super-Yang-Mills (SYM) theory and thus ultimately related to string theory. Altogether, the new developments are feeding a 'NNLO revolution' which has already yielded a number of phenomenologically relevant results for $2 \to 2$ LHC processes. Some aspects of these recent developments are briefly touched upon below.

3.1 High-order amplitudes and iterated integrals

The development of unitarity-based methods to compute scattering amplitudes, together with several pioneering high-order calculations in $N = 4$ SYM, brought the focus on the concept of 'transcendental weight' of the functions arising in Feynman diagram calculations. We now know that a vast class of gauge-theory scattering amplitudes can be expressed in terms generalized polylogarithms that can be generated by means of iterated integrals, which in turn encode in a simple way the singularity structure of the amplitude as a function of the

Mandelstam invariants. Understanding the class of functions that make up the result for a scattering amplitude can often turn an extremely difficult analytic problem into a relatively simple algebraic one, so these new mathematical tools (recently reviewed in [12]) have quickly found application in a number of phenomenological calculations. While the tools turn out to be especially powerful for a conformal theory like $N = 4$ SYM, it has become clear that they have direct applications also to QCD and electroweak amplitudes and cross sections. The breakthrough [13] was the realization that well-known method of differential equations for the computation of Feynman amplitudes could be optimized to a truly remarkable degree by choosing (when possible) a basis of master integrals belonging to the class of iterated integrals mentioned above. The method, reviewed in [14], is proving very powerful, and the list of NNLO calculations that have become available in its wake is already much too long to be referenced here. More generally, it is remarkable that, after many decades of intensive studies, perturbative quantum field theory can still surprise us, with the discovery of new and beautiful mathematical structures and entirely novel viewpoints.

3.2 NNLO subtraction

The calculation of loop-level partonic cross section requires the cancellation of infrared and collinear divergences which appear separately in virtual corrections and when real emission corrections are integrated over the phase space of undetected partons. The problem has been well understood in principle for decades, but the construction of a sufficiently general and efficient algorithm to perform the cancellation at NNLO has proved much harder than expected. Crucially for phenomenological applications, several practical solutions to this problem have now been proposed and are in different stages of being applied or tested [15, 16, 17, 18, 19]. As a matter of principle, the optimal 'subtraction algorithm' should have several attributes: complete generality across all IR-safe observables with arbitrary numbers of final state partons, exact locality of the IR and collinear counterterms, which should be computed analytically to optimize speed and theoretical understanding, exact independence on external parameters introduced to 'slice' away the singular regions of phase space, and overall computational efficiency. In this sense, none of the existing methods qualifies as a 'silver bullet' enjoying all these properties. The methods however have proven sufficiently powerful to perform pioneering and highly non-trivial NNLO calculations, such as the $t\bar{t}$ production cross section [20] and the Higgs-plus-jet cross section [19]. Rapid further developments towards the automatisation of NNLO calculations, similarly to what has been done at NLO in recent years, are under way.

3.3 Threshold resummation beyond leading power

To conclude this bird's eye overview with a theme where I have made a direct contribution, I will now briefly discuss the all-order summation of soft and collinear gluon effects, which is often necessary to extend the applicability of perturbative calculations to regions of phase space where large logarithms of ratios of mass scales appear order by order in the coupling. Specifically, I consider the common situation in which a partonic cross section has a threshold for the production of some heavy state, for example a vector boson, a Higgs boson, or a heavy coloured final state such as a $t\bar{t}$ pair. In these circumstances, the cross section $\sigma(\xi)$ depends logarithmically on the distance from threshold ξ, according to

$$\frac{d\sigma}{d\xi} = \sum_{n=0}^{\infty} \left(\frac{\alpha_s}{\pi}\right)^n \sum_{m=0}^{2n-1} \left[c_{nm}^{(-1)} \left(\frac{\log^m \xi}{\xi}\right)_+ + c_n^{(\delta)}\, \delta(\xi) + c_{nm}^{(0)} \, \log^m \xi \, + \, \ldots \right] . \tag{1}$$

The leading-power logarithms determined by the coefficients $c_{nm}^{(-1)}$ are directly related to the infrared and collinear divergences of the amplitudes, and, as a consequence, they can be resummed to all-orders in perturbation theory, using a technology which has been well understood for decades and is now routinely applied to increasing logarithmic accuracy. For massless gauge-theory scattering amplitudes, soft and collinear effects factorise [21], according to

$$\mathcal{A}_n(p_i) \, = \, \prod_{i=1}^{n} \left[\frac{J_i(p_i)}{\mathcal{J}_i(\beta_i)} \right] \cdot \mathcal{S}_n(\beta_i) \cdot \mathcal{H}_n(p_i) \, , \tag{2}$$

where I wrote the particle momenta as $p_i = Q\beta_i$, with Q a hard scale, the soft function $\mathcal{S}_n(\beta_i)$ parametrises soft-gluon effects, and the jet functions J and $\mathcal{J}$ contain collinear dynamics. Each function has a gauge invariant operator definition, for example for a quark

$$J(p,n)\, u(p) \, = \, \langle 0 \, | \Phi_n(\infty, 0) \psi(0) | \, p \rangle \ , \tag{3}$$

where Φ_n is a Wilson line factor and n is an auxiliary 'factorization vector'. For well-behaved IR-safe observables, the factorization in Eq. (2) leads to resummation of leading-power threshold logarithms. At next-to-leading power (NLP), an increasing body of evidence has been suggesting that a similar organization of the logarithms determined by the coefficients $c_{nm}^{(0)}$ should be possible [22]. In the soft sector, it is indeed possible to extend the soft exponentiation theorem beyond leading power [23, 24], but this proves insufficient to generate all NLP logarithms starting at two loops. The reason is the interference of collinear singularities with (next-to-) soft emissions, which prevents their complete factorization. This obstacle was first overcome by Del Duca [25], and recently revisited and applied to electroweak annihilation cross sections in [26, 27]. The result is a generalisation of the leading-power factorization in Eq. (2), which, in its simplest form, reads

$$\mathcal{A}^\mu(p_j, k) \, = \, \sum_{i=1}^{2} \left(q_i \, \frac{(2p_i - k)^\mu}{2p_i \cdot k - k^2} + q_i \, G_i^{\nu\mu} \, \frac{\partial}{\partial p_i^\nu} + G_i^{\nu\mu} \, J_\nu(p_i, k) \right) \mathcal{A}(p_i; p_j) \, , \quad (4)$$

where $\mathcal{A}^\mu$ is an amplitude including the radiation of an extra soft gluon, $G_{\mu\nu}$ is a kinematic projection, and J_μ is a 'radiative jet' function defined by

$$J_\mu \left(p, n, k \right) u(p) \, = \, \int d^d y \; \mathrm{e}^{-\mathrm{i}(p-k)\cdot y} \; \langle 0 \mid \, \Phi_n(y, \infty) \, \psi(y) \, j_\mu(0) \, | \, p \rangle \; , \qquad (5)$$

where j_μ is the current for the production of the extra soft gluon. Using Eq. (4), it is possible to exactly reproduce all NLP logarithms at two loops for vector boson production cross sections, in terms of universal soft and collinear factors. This strongly suggests that a complete resummation formalism for NLP logarithms is at hand, which would then lead to a number of phenomenological applications to precision calculations of QCD cross sections of relevance for LHC and future colliders. Work is in progress to proceed in this direction.

4 Acknowledgements

Work supported by the Research Executive Agency (REA) of the European Union under the Grant Agreement PITN-GA-2012-316704 (HIGGSTOOLS); by MIUR (Italy), under contract 2010YJ2NYW_006, and by the University of Torino and the Compagnia di San Paolo under contract ORTO11TPXK.

References

1. For a more detailed discussion see: S. Forte *et al.*, Eur. Phys. J. C **75** (2015) 11, 554, `arXiv:1505.01279 [hep-ph]`.
2. See, for example: J. Butterworth *et al.*, `arXiv:1510.03865 [hep-ph]`.
3. See, for example: D. Adams *et al.*, Eur. Phys. J. C **75** (2015) 9, 409, `arXiv:1504.00679 [hep-ph]`.
4. See, for example: J. R. Andersen *et al.*, `arXiv:1405.1067 [hep-ph]`.
5. N. Arkani-Hamed, T. Han, M. Mangano and L. T. Wang, `arXiv:1511.06495 [hep-ph]`.
6. M. Boronat, J. Fuster, I. Garcia, E. Ros and M. Vos, Phys. Lett. B **750** (2015) 95, `arXiv:1404.4294 [hep-ex]`.
7. L. Linssen, A. Miyamoto, M. Stanitzki and H. Weerts, `arXiv:1202.5940 [physics.ins-det]`.
8. M. Cacciari, Int. J. Mod. Phys. A **30** (2015) 31, 1546001, `arXiv:1509.02272 [hep-ph]`.
9. S. Moch *et al.*, `arXiv:1405.4781 [hep-ph]`.
10. D. d'Enterria *et al.*, `arXiv:1512.05194 [hep-ph]`.
11. M. Beneke, Y. Kiyo, P. Marquard, A. Penin, J. Piclum and M. Steinhauser, Phys. Rev. Lett. **115** (2015) 19, 192001, `arXiv:1506.06864 [hep-ph]`.
12. C. Duhr, `arXiv:1411.7538 [hep-ph]`.
13. J. M. Henn, Phys. Rev. Lett. **110** (2013) 251601, `arXiv:1304.1806 [hep-th]`.
14. J. M. Henn, J. Phys. A **48** (2015) 153001, `arXiv:1412.2296 [hep-ph]`.
15. J. Currie, `http://inspirehep.net/record/1323546/files/thesis.pdf`.
16. M. Czakon and D. Heymes, Nucl. Phys. B **890** (2014) 152, `arXiv:1408.2500 [hep-ph]`.

17. R. Bonciani, S. Catani, M. Grazzini, H. Sargsyan and A. Torre, Eur. Phys. J. C **75** (2015) 12, 581, `arXiv:1508.03585 [hep-ph]`.

18. V. Del Duca, C. Duhr, G. Somogyi, F. Tramontano and Z. Trocsanyi, JHEP **1504** (2015) 036, `arXiv:1501.07226 [hep-ph]`.

19. R. Boughezal, F. Caola, K. Melnikov, F. Petriello and M. Schulze, Phys. Rev. Lett. **115** (2015) 8, 082003, `arXiv:1504.07922 [hep-ph]`.

20. M. Czakon, P. Fiedler and A. Mitov, Phys. Rev. Lett. **110** (2013) 252004, `arXiv:1303.6254 [hep-ph]`.

21. L. J. Dixon, L. Magnea and G. F. Sterman, JHEP **0808** (2008) 022, `arXiv:0805.3515 [hep-ph]`.

22. E. Laenen, L. Magnea and G. Stavenga, Phys. Lett. B **669** (2008) 173, `arXiv:0807.4412 [hep-ph]`.

23. E. Laenen, G. Stavenga and C. D. White, JHEP **0903** (2009) 054, `arXiv:0811.2067 [hep-ph]`.

24. E. Laenen, L. Magnea, G. Stavenga and C. D. White, JHEP **1101** (2011) 141, `arXiv:1010.1860 [hep-ph]`.

25. V. Del Duca, Nucl. Phys. B **345** (1990) 369.

26. D. Bonocore, E. Laenen, L. Magnea, L. Vernazza and C. D. White, Phys. Lett. B **742** (2015) 375, `arXiv:1410.6406 [hep-ph]`.

27. D. Bonocore, E. Laenen, L. Magnea, S. Melville, L. Vernazza and C. D. White, JHEP **1506** (2015) 008, `arXiv:1503.05156 [hep-ph]`.

Parton Distribution Functions at present and future colliders

Alberto Guffanti
Università degli Studi di Torino & INFN Torino

Abstract

In this contribution we give a brief overview of the status of Parton Distribution Function (PDF) determinations as of September 2015, with particular emphasis on the impact of Run I LHC data already included in the fits. We then move to discuss which measurements could be performed during the LHC Run II and at future colliders that could provide relevant constraints for PDF determinations.

1 Introduction

Parton Distribution Functions (PDFs) encode the information on the longitudinal momentum carried by quarks and gluons inside a hadron when it undergoes an high energy collision. In this respect, they are one of the fundamental building blocks of theoretical predictions for observables at experiments carried out at hadron colliders.

In perturbative QCD the cross-section for inclusive production of a massive final state (X) in an hadron-hadron collision can be written, according to the Factorization Theorem [1], in a convolution form as

$$\sigma_X = \sum_{a,b} \int_0^1 dx_1 dx_2 f_a(x_1, \mu_F) f_b(x_2, \mu_F) \hat{\sigma}_{ab\to X} \left(x_1, x_2, \alpha_s(\mu_R), \frac{Q^2}{\mu_R}, \frac{Q^2}{\mu_F} \right) , \tag{1}$$

where the sum runs over the partonic content (quarks, antiquarks and gluon) of the hadrons, f_a and f_b are the Parton Distribution Functions of the incoming hadrons, $\hat{\sigma}$ denotes the partonic cross-section, μ_F and μ_R are the factorisation and renormalisation scales and Q is the typical hard scale of the process.

Parton densities are non-perturbative quantities, which cannot be determined from first principle computations in perturbative QCD. They are extracted from global fits to a wide variety of data from Deep Inelastic Scattering (ep) and hadron collider (pp) experiments.

2 Overview of Parton Distribution Function determinations

Different groups regularly produce PDF fits and recently released updated versions of their sets [2, 3, 4, 5, 6]. The most recent PDF determinations differ primarily because of the data sets on which they are based. On the one side there are the global fits (CT [3], MMHT [5] and NNPDF [6]), which aim to include a large number of different processes and observables in order to constrain most combinations of parton densities. On the other side there are those PDF determinations, like ABM [2] and especially HERAPDF [4], which are based on restricted, but more homogeneous data sets for which theoretical predictions are available at the highest perturbative order (NNLO). Aside from the data set, PDF determinations difffer in many aspects of the fits. For example the way heavy flavour mass effects are taken into account, the number of PDF combinations parametrized at the initial scale and the form of parametrisation (either fixed functional forms or neural networks). In Table 1 we collect relevant information about the ingredients entering the most recent updates of the mentioned PDF determinations.

Due to the assumptions made by the various groups the parton densities and their uncertainties determined by different collaborations show differences both in central values and uncertainties size which are suggestive of the fact

Table 1: *Parton Distribution Function fits routinely used in the experimental analyses at the LHC experiments and their characterisitics: the perturbative QCD order, the scheme in which the heavy flavour contibutions are treated (Fixed Flavour Number Scheme or General Mass Variable Flavour Number Scheme), whether the strong coupling constant is fitted along with the PDF parameters, how many independent PDF combinations are parametrised at the initial scale and whether polynominal functional forms or Neural Networks are used and the form of PDF uncertainties are represented, whether Hessian (with or without tolerance) or Monte Carlo.*

PDF set	**PT Order**	**HQ Treat.**	α_s	**Param.**	**Uncert.**
ABM12 [2]	NLO NNLO	FFN	Fit	6 indep. PDF Polynom.	Hessian
CT14 [3]	LO NLO NNLO	GM-VFNS	Input	6 indep. PDF Polynom.	Hessian Tolerance
HERAPDF2.0 [4]	NLO NNLO	GM-VFNS	Input	5 indep. PDF Polynom.	Hessian
MMHT14 [5]	LO NLO NNLO	GM-VFNS	Fit	7 indep. PDF Polynom.	Hessian Tolerance
NNPDF3.0 [6]	LO NLO NNLO	GM-VFNS	Input	7 indep. PDF Polynom.	Monte Carlo

that a single group might underestimate the uncertainties and a combination of individual PDF sets is required for a reliable estimation of uncertainties on LHC cross-sections. Such a combination has recently been performed in the context of the PDF4LHC working group [7] and PDFs made available through the LHAPDF interface [8].

3 Impact of LHC Run I data on PDF fits

The three global fits (CT, MMHT and NNPDF) already include in their fits a substantial number of data sets from the LHC experiments (ATLAS, CMS and LHCb). In particular, the NNPDF3.0 data set includes ATLAS and CMS inclusive jet data and top pair production total cross-section, W and Z rapitidy distributions from ATLAS and LHCb. W asymmetry and double differential Drell-Yan data from CMS and associated production of W boson with a charm quark.

These data provide moderate, but already noticeable, constrains on different PDF distributions. In Fig. 1 we illustrate the impact of LHC Run I data by comparing the outcome of two fits from the NNPDF3.0 series [6], one with and one without LHC data. It is clear how different data sets do provide constraints on different PDF combinations. In particular, the impact of inclusive jet data is seen in the reduction of the uncertainties on the gluon distribution and medium-/large-x, the light quark flavours are affected by the inclusion in the fit of the CMS W boson asymmetry and double-differential Drell-Yan data and, finally, the CMS associated production of a W boson with a charm quark data provide the best constraint on the strange quark distribution.

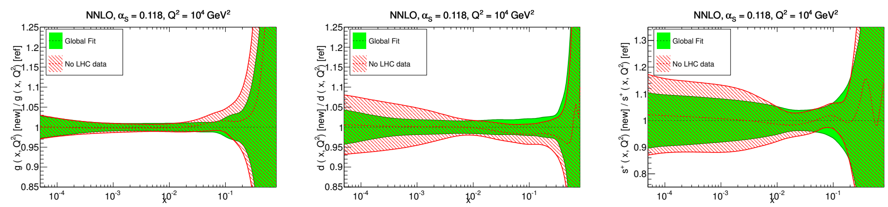

Figure 1: *Impact of the LHC data included in the NNPDF3.0 analysis on different PDF combinations: the gluon parton distribution (left), the d quark distribution (center) and the* $(s + \overline{s})$ *distribution (right).*

4 More constraints to come from LHC Run I and Run II data

A detailed study of PDF related issues at the LHC experiments has recently been completed [9]. This includes a thorough assessment of the impact of LHC Run I data on PDF fits and the identification of a number of measurements, both with Run I and Run II data, which could provide important constraints when included in PDF determinations.

Among the measurements performed by ATLAS, CMS and LHCb at the LHC Run I, which have the potential to substantilly constrain PDFs and have not yet been included in PDF fits we find the associated production of vector bosons (W, Z) with heavy quarks (c, b) which provide independent constraints on the charm and bottom distributions, allowing us to measure eventual intrinsic heavy quark components. The Z transverse momentum distribution measurements, either in the inclusive or the $Z + jet$ channel, give an independent constrain to the gluon distribution in the x range relevant for Higgs production in gluon-gluon fusion. Multi-jet (dijet and three-jets) distributions, when cross-correlations with inclusive jet production are properly accounted, strenghten the constraints on the gluon distribution at large x. Other measurments that have the potential to constrain the gluon distribution in the medium-/large-x region are direct photon production and top quark pair differential distributions. Finally, it is important to keep in mind that the LHCb experiment, with its unique coverage of the forward kinematic region, allows us to explore the small-x region [10]. In particular, the LHCb measurements of low-mass Drell-Yan are sensitive to quark distributions at x values as low as $8 \cdot 10^{-6}$ for $Q^2 = 25$ GeV^2 and the measurements of J/Ψ and Υ photo-production can put strong constraints on the low-x gluon.

During the Run II period the LHC will collide protons at 13 TeV center-of-mass energy, with an expected integrated luminosity up to 300 fb^1. The higher center-of-mass energy compared to Run I implies larger cross sections and extended kinematic reach for many processes which are of interest in PDF fits. The expected increase in the inclusive cross-section is by a factor of 2 for W and Z production an a factor of 4 for top pair production. At the same time the kinematic coverage for processes like inclusive jets and prompt photons will be substantially extended. This means that Run II data will not only strenghten the constraints from LHC data already included in PDF fits but will provide constraints in regions not probed by present data.

Finally, the possibility of using ratios of measurements at different center-of-mass energy, taking into account the full information on systematic cross-correlations, will prove to be a crucial tool to fully exploit the physics potential of the LHC data for constraining PDFs and, at the same time, looking for new physics. A study of the potential impact of LHC Run II data in PDF fits, based on a profiling analysis performed using the HERAFitter code [11], has been presented in the PDF4LHC report [9]. In Fig.2 we show as an example the expected impact on the up and down valence distributions of adding Run II W asymmetry pseudodata to each of the three global fits (CT10, MMHT14 and NNPDF3.0).

5 Outlook to future (possible) colliders

Looking down the road to possible future colliders it is clear that Parton Distribution Functions and their uncertainties will remain one of the fundamental

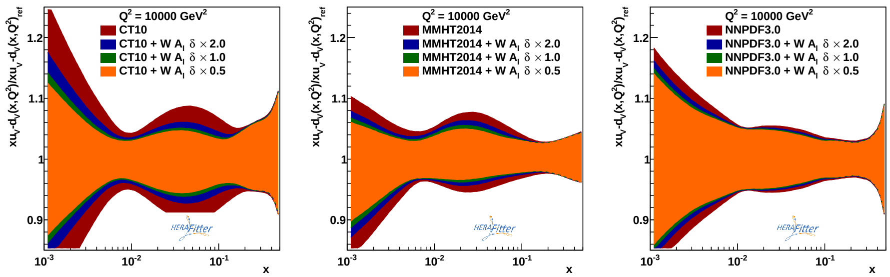

Figure 2: *Relative uncertainty of the $u_V - d_V$ distribution as a function of x for $Q^2 = 10^4$ GeV^2 estimated based on CT10nnlo (left), MMHT14 (middle) and NNPDF3.0 (right) PDF sets, respectively. The outer uncertainty band corresponds to the original PDF uncertainty. The embedded bands represent results of the PDF profiling using the W asymmetry measurements pseudo-data at 13 TeV corresponding to (from outermost to innermost band) a conservative, a baseline and an aggressive model of the data uncertainties. (Figure taken from the PDF4LHC report [9]).*

ingredients of our theoretical predictions based on perturbative QCD, often being one of the limiting factors to fully exploit their potential for discovery of new physics. Conversly, a large number of measurements could be performed that would help us to better determine PDFs.

Primary examples are acurate measurements of high-mass tails of distributions, forseen in the preliminary studies for the High-Luminosity phase of the LHC (HL-LHC). These measurements, the precision of which is limited by statistics at the LHC Run I and II, will allow us to probe and constrain PDFs in the large-x region.

Further down the road, the LHeC machine [12], a Large Hadron Electron Collider at CERN, could offer unique possibilities to reach the ultimate precision in PDF determinations by probing kinematic regions which are far from the reach of current experiments. For example, exploring in detail the small-x region ($x \sim 10^{-6}$) to look for evidence of deviations from DGLAP evolution due to BFKL resummation or saturation effects.

References

1. J. C. Collins, D. E. Soper and G. F. Sterman, Adv. Ser. Direct. High Energy Phys. **5** (1989) 1 [hep-ph/0409313].

2. S. Alekhin, J. Blumlein and S. Moch, Phys. Rev. D **89** (2014) 5, 054028 [arXiv:1310.3059 [hep-ph]].

3. S. Dulat *et al.*, arXiv:1506.07443 [hep-ph].

4. H. Abramowicz *et al.* [H1 and ZEUS Collaborations], Eur. Phys. J. C **75** (2015) 12, 580 [arXiv:1506.06042 [hep-ex]].

5. L. A. Harland-Lang, A. D. Martin, P. Motylinski and R. S. Thorne, Eur. Phys. J. C **75** (2015) 5, 204 [arXiv:1412.3989 [hep-ph]].

6. R. D. Ball *et al.* [NNPDF Collaboration], JHEP **1504** (2015) 040 [arXiv:1410.8849 [hep-ph]].

7. J. Butterworth *et al.*, J. Phys. G **43** (2016) 023001 [arXiv:1510.03865 [hep-ph]].

8. A. Buckley, J. Ferrando, S. Lloyd, K. Nordstrm, B. Page, M. Rfenacht, M. Schnherr and G. Watt, Eur. Phys. J. C **75** (2015) 132 [arXiv:1412.7420 [hep-ph]].

9. J. Rojo *et al.*, J. Phys. G **42** (2015) 103103 doi:10.1088/0954-3899/42/10/103103 [arXiv:1507.00556 [hep-ph]].

10. R. S. Thorne, A. D. Martin, W. J. Stirling and G. Watt, doi:10.3360/dis.2008.30 arXiv:0808.1847 [hep-ph].

11. S. Alekhin *et al.*, Eur. Phys. J. C **75** (2015) 7, 304 doi:10.1140/epjc/s10052-015-3480-z [arXiv:1410.4412 [hep-ph]].

12. J. L. Abelleira Fernandez *et al.* [LHeC Study Group Collaboration], J. Phys. G **39** (2012) 075001 doi:10.1088/0954-3899/39/7/075001 [arXiv:1206.2913 [physics.acc-ph]].

A DATA-DRIVEN APPROACH TO PILE-UP AT HIGH LUMINOSITY

F Hautmann
RAL, University of Oxford and University of Southampton

Abstract

We discuss recent results on pile-up based on a data-driven jet-mixing method. We illustrate prospects for experimental searches and precision studies in high pile-up regimes at high-luminosity hadron colliders, showing how the jet mixing approach can be used, also outside tracker acceptances, to treat correlation observables and effects of hard jets from pile-up.

Experiments at high-luminosity hadron colliders face the challenges of very large pile-up, namely, a very large number of overlaid hadron-hadron collisions per bunch crossing. At the Large Hadron Collider (LHC), for instance, in data taken at Run I the pile-up is about 20 *pp* collisions on average, while it reaches the level of over 50 at Run II, and increases for higher-luminosity runs [1, 2, 3, 4, 5, 6, 7, 8, 9, 10, 11].

Current methods to deal with pile-up at the LHC employ precise vertex and track reconstruction, in regions covered by tracking detectors. More generally, they rely on Monte Carlo simulations to model pile-up for data comparisons. This however brings in a model dependence which is particularly significant in regions where no detailed and precise measurements are available to constrain Monte Carlo generators.

Ref. [12] proposes a complementary approach to pile-up treatment, using data-driven methods rather than Monte Carlo modeling. The main purpose of this approach is to deal with potentially large contributions from jets with high transverse momenta, produced from pile-up events independent of the primary interaction vertex, in a region where tracking devices are not available to identify pile-up jets. The goal is to treat not only inclusive observables but also correlations, and to rely on data recorded in high pile-up runs, rather than requiring dedicated runs at low pile-up.

The basic idea of Ref. [12] can be illustrated using Drell-Yan lepton pair production associated with jets. This can straightforwardly be extended to a large variety of processes affected by pile-up. Fig. 1 shows a cartoon picture of different effects due to pile-up in Z-boson + jets production. One effect, denoted as jet pedestal, consists of additional pile-up particles in the jet cone, leading to a bias in the jet transverse momentum. Another is the overlapping of soft particles from pile-up, which are clustered into jets. A further effect is the misidentification of high transverse momentum jets produced from independent pile-up events.

Several methods exist to take the first two effects into account and correct for them. These include techniques based on the jet vertex fraction [3] and charged hadron subtraction [5, 13], the Puppi method [14], the SoftKiller method [15], the jet cleansing method [16]. These methods correct for transverse momenta of individual particles, but not for any misidentification. The objective of the approach [12] is to analyze and treat the third effect, due to the mistagging of high transverse momentum pile-up jets.

Fig. 2 illustrates the overall contributions of pile-up to Z-boson + jet correlation variables. In the top plot is the leading jet p_T spectrum, while in the bottom plot is the Z-boson p_T spectrum. Event samples for Z-boson + jet production, with boson rapidity and invariant mass $|\eta^{(\text{boson})}| < 2$, 60 GeV $< m^{(\text{boson})} < 120$ GeV, and jet transverse momentum and rapidity $p_T^{(\text{jet})} > 30$ GeV, $|\eta^{(\text{jet})}| < 4.5$, are generated, using the anti-k_T jet algorithm [17] with distance parameter $R = 0.5$, by Pythia 8 [18] with the 4C tune [19] for the

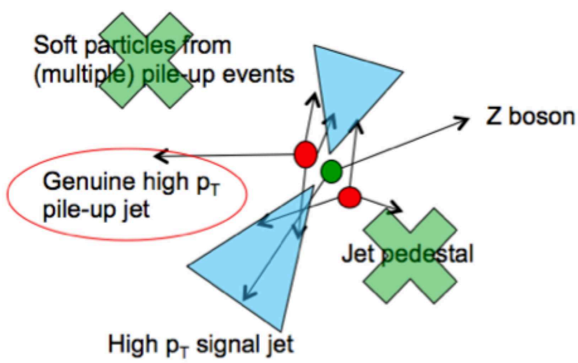

Figure 1: *Pile-up contributions to the reconstruction of jets in Z-boson + jet production.*

different scenarios of zero pile-up and N_{PU} additional pp collisions at $\sqrt{s} = 13$ TeV. The solid black curve is the signal, represented by the result in absence of any pile-up collision. The dot-dashed black curve is the result for $N_{\mathrm{PU}} = 50$ pile-up collisions. The dashed blue curve is the result of applying the method SoftKiller [15)] to remove contributions of soft pile-up particles in the event. We see from Fig. 2 that the effects of pile-up on Z-boson + jet spectra are large. Further we see that, while the leading jet p_T spectrum can be corrected well by the pile-up removal method SoftKiller, the Z-boson p_T spectrum is still affected by significant deviations from the signal even after applying SoftKiller. Ref. [12)] interprets this as an effect of mistagged pile-up jets, and devises an approach based on jet mixing to treat it.

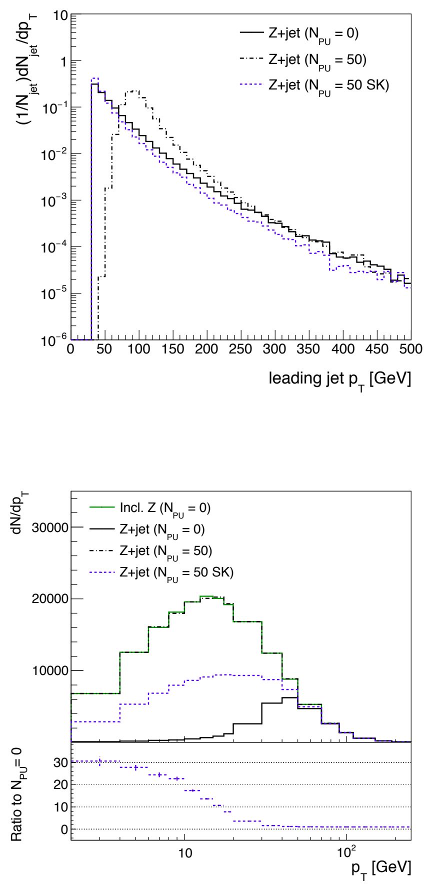

Figure 2: *Effects of pile-up in Z-boson + jet production at the LHC: (top) the leading jet p_T spectrum; (bottom) the Z-boson p_T spectrum* [12].

The jet mixing method [12] uses uncorrelated event samples to express the signal in the pile-up scenario in terms of the signal without pile-up and a minimum bias sample of data at high pile-up. The results of this approach are shown in Fig. 3, where samples containing N_{PU} minimum bias events are used for the mixing, in the cases $N_{\mathrm{PU}} = 50$ (top plot) and $N_{\mathrm{PU}} = 100$ (bottom plot). The solid black curve is the "true" Z-boson plus jet signal. The dashed blue curve is the high pile-up, SoftKiller-corrected result ($N_{\mathrm{PU}} = 50$ SK and $N_{\mathrm{PU}} = 100$ SK), representing the pseudodata in high pile-up. The long-dashed red curve is the jet-mixed curve obtained from mixing the signal with the minimum bias sample. The solid red curve is the final result, obtained by a simple "unfolding", defined by multiplying the signal by the ratio of the pile-up (dashed blue) curve to the jet-mixed (long-dashed red) curve.

We see from Fig. 3 that without the need to use Monte Carlo events to simulate pile-up the true signal is extracted nearly perfectly from the mixed sample.[1] This conclusion can be strengthened by checking [12] that if the mixing is applied to a different starting distribution the unfolding still returns the true signal. Also, control checks on the jet resolution are carried out in Ref. [12], verifying that features of the "true" signal in the parton-jet p_T correlation and ΔR distribution are well reproduced by the jet mixing. As Fig. 3 indicates, the performance of the mixing technique, unlike the SoftKiller pile-up removal method, improves with increasing N_{PU}.

In summary, the approach described in this article, while not addressing the question of a full detector simulation including pile-up, focuses on how to extract physics signals with the least dependence on pile-up simulation, and how to use real data, rather than Monte Carlo events, at physics object level. It can be applied to the high pile-up regime relevant for the LHC and for future high-luminosity colliders, and does not require data-taking in special runs at low pile-up, so that there is no loss in luminosity. It implies good prospects both for precision Standard Model studies at moderate scales affected by pile-up, e.g. in Drell-Yan [20, 21] and Higgs production [22, 23], and for searches for rare processes beyond Standard Model in high pile-up regimes.

[1]Here we use a Monte Carlo to generate minimum bias events but under real running conditions this sample should be taken from real events recorded at high pile-up.

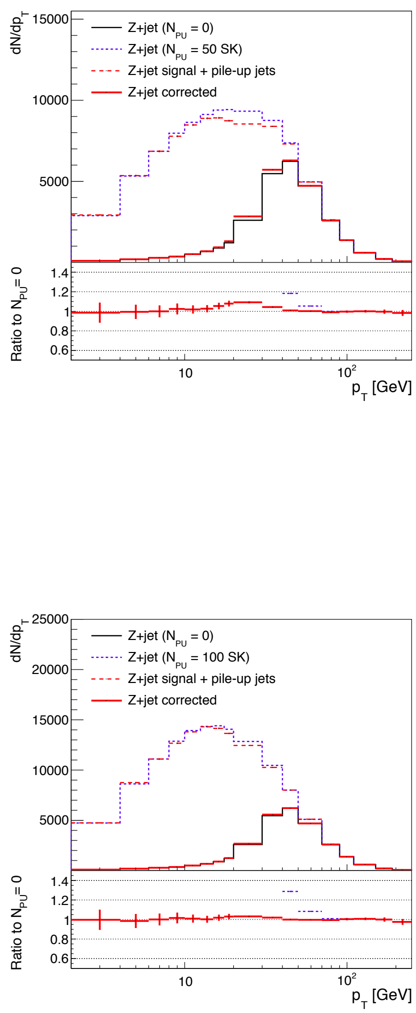

Figure 3: *The Z-boson p_T spectrum in Z + jet production from the jet mixing method* [12]*: (top)* $N_{\mathrm{PU}} = 50$*; (bottom)* $N_{\mathrm{PU}} = 100$.

Acknowledgments. Many thanks to the organizers of the Workshop *LFC15* for the invitation to a very interesting meeting. The results presented in this article have been obtained in collaboration with H. Jung and H. Van Haevermaet. Useful comments from M. Dittmar, E. Gallo, B. Murray, P. Van Mechelen and M. Wielers are gratefully acknowledged. This work is supported in part by the DFG SFB 676 programme "Particles, String and the Early Universe" at the University of Hamburg and DESY.

References

1. ATLAS Collaboration, ATLAS-CONF-2014-018.
2. ATLAS Collaboration, ATLAS-CONF-2014-019.
3. ATLAS Collaboration, ATLAS-CONF-2013-083.
4. Z. Marshall [ATLAS Collaboration], J. Phys. Conf. Ser. **513** (2014) 022024.
5. CMS Collaboration, CMS-PAS-JME-14-001.
6. CMS Collaboration, CMS-PAS-JME-13-005.
7. S. S. Ghosh [CMS Collaboration], arXiv:1502.05207 [hep-ex].
8. J. Anderson *et al.*, Snowmass Energy Frontier Simulations White Paper (2013).
9. A. Haas [ATLAS Coll.], talk at LHC Detector Simulations Workshop, CERN, March 2014.
10. M. Hildreth [CMS Coll.], talk at LHC Detector Simulations Workshop, CERN, March 2014.
11. S. Fartoukh, Phys. Rev. ST Accel. Beams **17** (2014) 111001.
12. F. Hautmann, H. Jung and H. Van Haevermaet, arXiv:1508.07811 [hep-ph].
13. H. Kirschenmann [CMS Collaboration], PoS EPS-HEP2013 (2013) 433.
14. D. Bertolini, P. Harris, M. Low and N. Tran, JHEP **1410** (2014) 59.
15. M. Cacciari, G. P. Salam and G. Soyez, Eur. Phys. J. C **75** (2015) 59.

16. D. Krohn, M. D. Schwartz, M. Low and L. T. Wang, Phys. Rev. D **90** (2014) 065020.

17. M. Cacciari, G. P. Salam and G. Soyez, JHEP **0804** (2008) 063.

18. T. Sjöstrand, S. Mrenna and P. Z. Skands, Comput. Phys. Commun. **178** (2008) 852.

19. R. Corke and T. Sjöstrand, JHEP **1103** (2011) 032.

20. S. Dooling *et al.*, Phys. Lett. B **736** (2014) 293; F. Hautmann and H. Jung, Nucl. Phys. B **883** (2014) 1.

21. R. Angeles-Martinez *et al.*, Acta Phys. Polon. B **46** (2015) 2501.

22. P. Cipriano *et al.*, Phys. Rev. D **88** (2013) 097501.

23. H. Van Haevermaet *et al.*, PoS DIS **2014** (2014) 163.

Possible discrepancies between theory and data at high energy colliders

Leandro Cieri
Physik-Institut, Universität Zürich, CH-8057 Zürich, Switzerland

Abstract

We are interested in final states containing at least one photon. We enumerate possible sources of discrepancies that could appear between the data and the theory, for those final states, taking into account measurements from the Tevatron and the Run I of the LHC. We investigate the origin of each discrepancy and the way in which we can solve it. We use this study as a way to understand the possible issues that could appear at future high energy colliders but also at the Run II of the LHC.

1 Introduction

We are interested in $pp(\bar{p})$ collisions, in particular in final states F containing at least one photon and their comparison with fixed order theoretical tools [1]

[1]This contribution doesn't treat the comparison of the data with Monte Carlo generators (parton–shower Monte Carlo).

(with or without considering in addition transverse momentum resummation).

These processes are very important in order to check the validity of perturbative Quantum-Chromodynamics (QCD) [1], to test soft gluon resummation techniques, and to extract information about the parton distribution functions [2] (PDF) of the proton. Some of them also constitute irreducible backgrounds for Higgs boson searches and studies [3, 4], and also backgrounds for Beyond the Standard Model (BSM) searches [5]. The determination of the Higgs boson couplings [6] and of self couplings of the electro-weak gauge bosons [7] or the search of the anomalous triple gauge boson couplings [8] are also another motivations to study those final states. In order to extract precise information from comparisons between the data and theory, and for all the precedent enumerated tasks, we need the best theoretical calculations to not introduce large uncertainties from the theory side.

The common feature of all the processes that we are considering here, is the presence of at least one photon in the final state. Therefore all these measurements and all the calculations used to describe them are sensible to the issues related to the photon isolation. Photons can be produced through to two possible mechanisms. Photons produced *directly* from the hard part of the interaction are called *direct* photons. A photon can be obtained also from the fragmentation of a parton. This is a non-perturbative phenomenon which requires the photon fragmentation function to describe it.

Experimentally photons must be isolated to reduce the large reducible background, in which photons are faked by jets, mainly pions decaying in photons. The isolation that is applied to suppress the reducible background affects the signal itself, reducing the size of the fragmentation component.

This contribution is organized as follows. In Section 2 we comment about three subject areas, which could represent the origin of possible discrepancies between the data and theory. We specify the distinct types of discrepancies belonging to each case and how to reduce them. In Section 3 we summarize our results.

2 Possible discrepancies between theory and data

We are interested in the QCD corrections for processes initiated by hadron-hadron collisions with final states composed by at least one photon. For almost all the phenomenological relevant processes containing at least one photon in the final state, the next-to-leading-order (NLO) or next-to-next-to-leading-order (NNLO) perturbative corrections with respect to the QCD coupling α_S are available. The NLO calculations can also include fragmentation at leading-order (LO) or NLO. The numerical codes belonging to the `PHOX` family [9, 10] have NLO fragmentantation.

2.1 Isolation

In this section we briefly present the standard and "smooth" cone isolation criteria, and their advantages and difficulties concerning theoretical and experimental implementations. We also comment on possible issues that could appear by increasing the energy of the accelerator; and discrepancies that could appear comparing cross-sections obtained with different isolation prescriptions.

2.1.1 The "smooth" and the standard cone isolation criteria

The smooth cone isolation prescription is the criterion proposed by Frixione [11] (see also Ref. [12]). A photon is said to be isolated if, inside any cone of radius r (with $r < R$) in rapidity and azimuthal angle around the photon direction, the amount of deposited hadronic transverse energy E_T^{had} is smaller than some value $E_{T\,max}\ \chi(r)$:

$$\sum E_T^{had} \leq E_{T\,max}\ \chi(r)\ ,$$
$$\text{inside any}\ \ r^2 = (y - y_\gamma)^2 + (\phi - \phi_\gamma)^2 \leq R^2\ , \tag{1}$$

with fixed values of $E_{T\,max}$ and R and with a suitable choice for the function $\chi(r)$. The constant value $E_{T\,max}$ can be replaced with a fraction of the transverse momentum of the photon ($p_T^\gamma \epsilon$, where typically $0 < \epsilon \leq 1$). The $\chi(r)$ function has to vanish smoothly when its argument goes to zero ($\chi(r) \to 0$, if $r \to 0$), and it has to verify $0 < \chi(r) < 1$, if $0 < r < R$. One possible choice is

$$\chi(r) = \left(\frac{1 - \cos(r)}{1 - \cos R}\right)^n\ , \tag{2}$$

where n is typically chosen to be $n = 1$. This condition implies that, closer to the photon, less hadronic activity is allowed inside the cone. The cancellation of soft gluon divergences takes place as in ordinary infrared-safe cross-sections, since no region of the phase space is forbidden. That is the main advantage of this criterion: it entirely eliminates the fragmentation component in an infrared-safe way. By contrast, it can't be implemented within the usual experimental conditions.

The standard way of implementing isolation in experiments is to use the prescription of Eq. 1 with a constant $\chi(r) = 1$. If we consider this isolation criterion, or any other than the smooth one, we have to consider the fragmentantation contribution and the direct component (in our theoretical tools) in order to obtain infrared-safe cross-sections.

Comparing the two isolation criteria it is easy to observe that both of them coincide at the outer cone ($r = R$, $\chi(R) = 1$), and due to the presence of the $\chi(r)$ function, which verifies $0 \leq \chi(r) \leq 1$, the smooth cone isolation criterion is always more restrictive than the standard one. This directly implies that we expect smaller cross-sections when we use the Frixione criterion than when we implement the standard one, if the same parameters $(E_{T\,max}, R)$ or (ϵ, R) are used in both criteria:

$$\sigma_{Frix}\{R, E_{T\ max}\} \leq \sigma_{Stand}\{R, E_{T\ max}\}\ . \tag{3}$$

The constraint in Eq. 3 is certainly fullfilled experimentally and it should also be fullfilled by any reliable theoretical prediction.

As shown in Ref. [13], for various kinematical configurations there are values of isolation parameters for which the standard and smooth cone isolation criteria produce very similar quantitative results in theoretical calculations. For example, from a purely pragmatic point of view, it was shown [13] that if the isolation parameters are tight enough (e.g., $E_{T\ max} < 6$ GeV, $R = 0.4$), the standard and the smooth cone isolation prescription coincide at the 1% level at NLO, which is well within the theoretical uncertainty of the NLO results.

Matching experimental conditions to theoretical calculations always implies a certain degree of approximation. Considering the large QCD corrections to processes involving photons (e.g the size of the NNLO correction is essential to match diphoton data [14]) and the agreement (tipically at the % level for the diphoton case studied in [13]) between the standard and smooth cone theoretical calculations, the use of the latter for theoretical purposes is well justified.

The *Les Houches 2013* or "pragmatic" accord proposed in Ref. [13] is as follows: the experiment can proceed to the analysis of the data with the usual standard isolation with cuts tight enough if the interesting observable needs to be an isolated cross-section or distribution. While the theoretical calculation can apply the smooth cone isolation prescription with the same isolation parameters used by the experiment $(E_{T\,max}, R)$ or (ϵ, R). While the definition of "tight enough" might slightly depends on the particular observable (this can always be checked performing a lowest order calculation). The analysis of Ref. [13] shows that the LHC isolation parameters $E_T^{max} \leq 5$ GeV (or $\epsilon < 0.1$), $R \sim 0.4$ and $R_{\gamma\gamma} \sim 0.4$ are safe enough to proceeed.

This procedure would allow to extend available NLO calculations to one order higher (NNLO) for a number of observables [14, 15, 16], since the direct component is always much simpler to be evaluated than the fragmentation part, which identically vanishes by using the smooth cone isolation.

2.1.2 *Possible issues*

If we consider a very narrow isolation cone in the standard cone criterion, the NLO theoretical predictions (as well as calculations at subsequent fixed orders) are unstable [10]. In the limit $R \ll 1$ (practically if $R \lesssim 0.1$), the available phase-space for parton emission inside the isolation cone is strongly restricted and this leads to a collinear sensitivity in the form of a fairly large dependence on $\ln(1/R)$, which could make the theoretical prediction unreliable[2] unless these logarithms are resummed to all perturbative orders as in Ref. [17], restoring the reliability of the calculation.

Since the effects of pile-up are sensible to the area of the isolation cone (*i.e* R^2), one could decrease the typical size of the radius $R \simeq 0.4$ (used at the Tevatron and at the Run I of the LHC) to values closer to $R \simeq 0.2$ (or even smaller) in order to avoid large contamination from pile-up effects. This can leads to theoretical issues, not only for future high energy colliders but also for the Run II of the LHC. If we use the standard cone isolation criterion in our theoretical tools we have to be aware of the results of Ref. [17]. If we use the smooth cone isolation, which is less sensitive to $\ln(1/R)$, we also have to check always to which extent the result doesn't violate unitarity [3]. In the diphoton case, using the acceptance criteria used by the CMS collaboration in recent Higgs boson searches and studies at $\sqrt{s} = 7$ TeV [3], we have checked

[2]This could even lead to an unphysical result such as an isolated cross-section is larger than the inclusive one [10], thereby violating unitarity.

[3]The isolated result has to be smaller than the inclusive cross-section.

that using the smooth cone prescription with values of $R \simeq 0.1$ the NLO result remains smaller than the inclusive value obtained with `DIPHOX`.

It is clear that if we relax the set of isolation parameters proposed by the Les Houches accord we can see the effects of fragmentation. Then if the experiment use very loose isolation parameters and if we compare the measurement with theoretical tools using the smooth cone isolation criterion, discrepancies could appear due to this feature.

The measurement performed by the ATLAS collaboration on $V\gamma$ (V being Z or W) production [18] use a very large $\epsilon = 0.5$ parameter. We learnt from the diphoton case that the theoretical cross-section obtained using the smooth isolation can be at least a 10% smaller than the result with fragmentation at NLO using $\epsilon = 0.5$ [13]. Can we extend these considerations to the $V\gamma$ case? Can this large $\epsilon = 0.5$ parameter explain the discrepancies that we have respect to the NNLO result using smooth isolation? Or are these discrepancies due to missing higher order QCD correction terms? The latter question is the subject of the next section.

2.2 Missing higher order QCD correction terms

In 2011 the CDF collaboration presented a measurement [19] of the diphoton cross-section by separately considering two phase space regions: i) the region in which the transverse momentum of the diphoton pair is larger than its invariant mass ($p_T^{\gamma\gamma} > M_{\gamma\gamma}$); ii) the region in which $p_T^{\gamma\gamma} < M_{\gamma\gamma}$. In the region i) we reduce the effects of the Born-like contributions which have $p_T^{\gamma\gamma} = 0$. And in the region ii) we reduce the effects of the real radiation which have $p_T^{\gamma\gamma} > 0$. If the discrepancies that we found in the general case (the case without extra cut) are incremented in the case i) and reduced to a level in which we have a good agreement in the case ii) we can understand that the next subsequent order QCD corrections are necessary to describe the phenomenology of the data. The same cuts could be replaced by any other set of cuts that allows to separate the kinematic regions in which the real radiation is stronger than the Born-like contributions and *viceversa*. For example we can consider the regions $\Delta\phi_{\gamma\gamma} \gtrless \pi/2$, where $\Delta\phi_{\gamma\gamma}$ is the azimuthal separation between the two photons. Similarly the measurements can be performed in $V\gamma$ production by considering the exclusive (0 jet) and the inclusive case (N jets). In Ref. [16], it was shown that the NNLO results can reduce the discrepancies between the

NLO result and the data from 2σ to 1σ in the inclusive case and from 1.6σ to 1.2σ in the exclusive case. Which is the origin of the remaining discrepancies? Missing N^3LO QCD correction terms? Missing electro–weak corrections? As we wrote in Section 2.1 it would be nice to have under control the issue with the large $\epsilon = 0.5$ used by the ATLAS collaboration. If a study similar to that of Ref. [13], should show that at NLO the effects of fragmentantation can't be neglected with $\epsilon = 0.5$, the use of the smooth cone isolation would represent a large source of uncertanty.

2.3 Transverse momentum q_T resummation

The aim of the transverse momentum resummation program is resum all the large logarithmic terms of the type $\ln(q_T^2/M^2)$ that appear in theoretical fixed order calculations, in the small transverse momentum limit $q_T \ll M$ (with M the invariant mass of the final state F). It is not only important for the q_T distribution of the final state F. Also other observables which are related to the kinematic region $q_T \simeq 0$ are affected (with subleading logarithmic terms) by transverse momentum resummation. Transverse momentum resummation recovers the reliability of the fixed order tools in those kinematic regions, reducing also the discrepancies between the data and the theory. Other specific discrepancies that could apperar are related to the position of the peak in the transverse momentum distribution (which also depends on non-perturbative effects) and the height of the peak (which is related to the finite part of the virtual corrections of the parent Born-level process). Transverse momentum resummation at the next-to-next-to-leading logarithmic accuracy (NNLL) combined with the complete NNLO calculation of diphoton production [15] recover the reliability of the calculation in the low q_T region of the transverse momentum distribution and it leads to the right description of the phenomenology of the data in kinematical regions directly related to the limit $q_T \to 0$. The $\Delta\phi_{\gamma\gamma}$ distribution in the region $\Delta\phi_{\gamma\gamma} \simeq \pi$ constitutes an example of this subleading effects [15].

3 Conclusions

We have enumerated three sources of discrepancies that could appear in the comparison of theoretical calculations with the data. We also briefly specified the origin of these discrepancies and how to reduce them. Taking into account measurements of the Tevatron and the LHC it was possible understand how these discrepancies depend on the energy of the collider. And, in this way, it is possible to address the potential discrepancies that could appear between theoretical calculations and data obtained in the Run II of the LHC and future high energy colliders.

4 Acknowledgements

We are very grateful to Stefano Catani for valuable comments on the manuscript.

References

1. S. Chatrchyan *et al.* [CMS Collaboration], JHEP **1201** (2012) 133 ;T. Aaltonen *et al.* [CDF Collaboration], Phys. Rev. D **84** (2011) 052006 ;S. Chatrchyan *et al.* [CMS Collaboration], Eur. Phys. J. C **74** (2014) 11, 3129 ;V. M. Abazov *et al.* [D0 Collaboration], Phys. Lett. B **725** (2013) 6 ;G. Aad *et al.* [ATLAS Collaboration], Phys. Rev. D **85** (2012) 012003. ;G. Aad *et al.* [ATLAS Collaboration], JHEP **1301** (2013) 086 ; S. Chatrchyan *et al.* [CMS Collaboration], Phys. Rev. D **89** (2014) 9, 092005 ; CMS Collaboration [CMS Collaboration], CMS-PAS-SMP-14-021. ; G. Aad *et al.* [ATLAS Collaboration], Phys. Rev. D **87** (2013) 11, 112003 [Phys. Rev. D **91** (2015) 11, 119901] ;G. Aad *et al.* [ATLAS Collaboration], Phys. Rev. Lett. **115** (2015) 3, 031802 ;S. Chatrchyan *et al.* [CMS Collaboration], Phys. Rev. D **84** (2011) 052011 ; G. Aad *et al.* [ATLAS Collaboration], Phys. Lett. B **706** (2013) 150

2. J. Cantero [ATLAS Collaboration], PoS DIS **2014** (2014) 160.

3. S. Chatrchyan *et al.* [CMS Collaboration], Phys. Lett. B **716** (2013) 30

4. G. Aad *et al.* [ATLAS Collaboration], Phys. Lett. B **716** (2013) 1

5. **ATLAS** Collaboration, G. Aad et al., , *Phys.Lett.* **B718** (2012) 411–430, ; S. Chatrchyan *et al.* [CMS Collaboration], JHEP **1303** (2013) 111 ;G. Aad *et al.* [ATLAS Collaboration], New J. Phys. **15** (2013) 043007 ;**CMS** Collaboration, S. Chatrchyan et al., , *Phys. Lett. B.* (2012) ;G. Aad *et al.* [ATLAS Collaboration], Phys. Rev. D **92** (2015) 3, 032004 ; G. Aad *et*

al. [ATLAS Collaboration], Phys. Lett. B **738** (2014) 428 ; G. Aad *et al.* [ATLAS Collaboration], Phys. Lett. B **728** (2014) 562

6. CMS Collaboration [CMS Collaboration], CMS-PAS-HIG-15-002.
7. G. Aad *et al.* [ATLAS Collaboration], Phys. Rev. Lett. **115** (2015) 3, 031802
8. V. Khachatryan *et al.* [CMS Collaboration], JHEP **1504** (2015) 164
9. T. Binoth, J. P. Guillet, E. Pilon and M. Werlen, Eur. Phys. J. C **16** (2000) 311
10. S. Catani, M. Fontannaz, J. P. Guillet and E. Pilon, JHEP **0205** (2002) 028
11. S. Frixione, Phys. Lett. B **429** (1998) 369
12. S. Frixione and W. Vogelsang, Nucl. Phys. B **568** (2000) 60 ;S. Catani, M. Dittmar, D. E. Soper, W. J. Stirling, S. Tapprogge, S. Alekhin, P. Aurenche and C. Balazs *et al.*, In *Geneva 1999, Standard model physics (and more) at the LHC* 1-115 [hep-ph/0005025].
13. J. Butterworth, G. Dissertori, S. Dittmaier, D. de Florian, N. Glover, K. Hamilton, J. Huston and M. Kado *et al.*,
14. S. Catani, L. Cieri, D. de Florian, G. Ferrera and M. Grazzini, Phys. Rev. Lett. **108** (2012) 072001
15. L. Cieri, F. Coradeschi and D. de Florian, JHEP **1506** (2015) 185
16. M. Grazzini, S. Kallweit and D. Rathlev, JHEP **1507** (2015) 085 ; M. Grazzini, S. Kallweit, D. Rathlev and A. Torre, Phys. Lett. B **731** (2014) 204
17. S. Catani, M. Fontannaz, J. P. Guillet and E. Pilon, JHEP **1309** (2013) 007
18. G. Aad *et al.* [ATLAS Collaboration], Phys. Rev. D **87** (2013) 11, 112003 [Phys. Rev. D **91** (2015) 11, 119901]
19. T. Aaltonen *et al.* [CDF Collaboration], Phys. Rev. D **84** (2011) 052006

An alternative subtraction scheme for NLO QCD calculations

Tania Robens
IKTP, TU Dresden, Zellescher Weg 16, 01069 Dresden, Germany

Abstract

We discuss an alternative subtraction scheme for NLO QCD calculations, which is based on the splitting kernels of an improved parton shower. As an example, we show results for the C parameter of the process $e^+ e^- \rightarrow 3$ jets at NLO used for the verification of this scheme.

1 Introduction

It is indisputable that higher order corrections are needed to correctly predict fully differential distributions for scattering processes at high precision. However, the implementation of NLO calculations into numerical tools exhibits a caveat stemming from the infrared divergence of real and virtual NLO contributions, which originate from different phase spaces: although in the sum of all contributions, the infinite parts exactly cancel, the behaviour of the divergence needs to be parametrized, e.g. by infinitesimal regulators. In practise, this can result in large unphysical numerical uncertainties. A way to circumvent this problem is the introduction of subtraction schemes. We here discuss a specific scheme and its properties [1], using splitting kernels as well as mapping prescriptions which were already suggested in the framework of an improved parton shower [2, 3, 4, 5]. It was further developed for processes with an arbitrary number of final states in [6], with a review in [7]. Furthermore, the scheme has been implemented within the HelacNLO framework [8].

2 Subtraction Schemes

Higher order subtraction schemes make use of factorization of the real-emission matrix element in the soft or collinear limits, leading to the decomposition $|\mathcal{M}_{m+1}(\hat{p})|^2 \longrightarrow \mathcal{D}_\ell \otimes |\mathcal{M}_m(p)|^2$ [9, 10, 11]. Here and in the following, we follow the notation presented in [1, 6, 7]. The subtracted contributions are then given by

$$\sigma^{\text{NLO}} = \underbrace{\int_{m+1} \left[d\sigma^R - d\sigma^A\right]}_{\text{finite}} + \underbrace{\int_{m+1} d\sigma^A + \int_m d\sigma^V}_{\text{finite}} \tag{1}$$

where

$$\begin{aligned} \int_m \left[d\sigma^B + d\sigma^V + \int_1 d\sigma^A\right] &= \int dPS_m \left[|\mathcal{M}_m|^2 + |\mathcal{M}_m|^2_{\text{1-loop}} + \sum_\ell \mathcal{V}_\ell \otimes |\mathcal{M}_m|^2\right], \\ \int_{m+1} \left[d\sigma^R - d\sigma^A\right] &= \int dPS_{m+1} \left[|\mathcal{M}_{m+1}|^2 - \sum_\ell D_\ell \otimes |\mathcal{M}_m|^2\right], \end{aligned} \tag{2}$$

and where $\int dPS$ denotes the integration over the respective phase space, including all symmetry and flux factors. The symbols $d\sigma^B$, $d\sigma^V$, $d\sigma^R$ stand for the Born, virtual and real-emission contributions of the calculation, while real-emission subtraction terms are summarized as $d\sigma^A$. Since $|\mathcal{M}_{m+1}|^2$ and $|\mathcal{M}_m|^2$ live in different phase spaces, their momenta need to be mapped via a mapping function. Furthermore, the subtraction term $\mathcal{D}_\ell$ and its one-parton integrated counterpart $\mathcal{V}_\ell$ are related by $\mathcal{V}_\ell = \int d\xi_p \, \mathcal{D}_\ell$, where $d\xi_p$ is an unresolved one-parton integration measure. In the scheme discussed here, we apply a momentum mapping which leads to an overall scaling behaviour $\sim N^2$ for a process with N partons in the final state.

3 Scheme setup

We denote four-momenta in the Born-type kinematics by unhatted quantities p_i, while the real emission phase space momenta are denoted by hatted quantities $\hat{p}_i$; initial state momenta are labelled p_a and p_b, where $Q = p_a + p_b$ and with Q^2 being the squared centre-of-mass energy, with equivalent relations in the real emission phase space; generally, $\hat{p}_\ell$ labels the emitter, $\hat{p}_j$ the emitted parton and $\hat{p}_k$ the spectator.

The real emission matrix element $\mid \mathcal{M}_\ell(\{\hat{p}, \hat{f}\}_{m+1})\rangle$ is related to the Born one $\mid \mathcal{M}(\{p, f\}_m)\rangle$ via [2]

$$\mid \mathcal{M}_\ell(\{\hat{p}, \hat{f}\}_{m+1})\rangle = t_\ell^\dagger(f_\ell \to \hat{f}_\ell + \hat{f}_j) \, V_\ell^\dagger(\{\hat{p}, \hat{f}\}_{m+1}) \mid \mathcal{M}(\{p, f\}_m)\rangle, \tag{3}$$

In our scheme, soft/ collinear divergences from interference terms are treated using dipole partitioning functions $A_{\ell k}$ [4], which have been explicitely discussed in [1, 6, 7]. All (integrated) subtraction terms are specified in the same reference.

The improved scaling behaviour of our scheme mainly results from the specific mapping between the real emission and Born-type kinematic phase spaces for final state emitters. For final state mappings, we use the whole remainder of the event as a spectator in terms of momentum redistributions:

$$p_\ell = \frac{1}{\lambda_\ell}(\hat{p}_\ell + \hat{p}_j) - \frac{1 - \lambda_\ell + y_\ell}{2\lambda_\ell \, a_\ell} Q, \; p_n^\mu = \Lambda(K, \hat{K})^\mu{}_\nu \, \hat{p}_n^\nu, \; n \notin \{\ell, j = m+1\}, \tag{4}$$

with $\Lambda(K, \hat{K})^\mu{}_\nu = g^\mu{}_\nu - \frac{2\,(K+\hat{K})^\mu \,(K+\hat{K})_\nu}{(K+\hat{K})^2} + \frac{2\,K^\mu \,\hat{K}_\nu}{\hat{K}^2}$, where $y_\ell = \frac{P_\ell^2}{2\,P_\ell \cdot Q - P_\ell^2}$ and we introduced $\lambda_\ell\,(y_\ell, a_\ell) = \sqrt{(1+y_\ell)^2 - 4\,a_\ell\,y_\ell}$, $K = Q - p_\ell$, $\hat{K} = Q - P_\ell$, $a_\ell\,(P_\ell, Q) = \frac{Q^2}{2\,P_\ell \cdot Q - P_\ell^2}$, with $P_\ell = \hat{p}_\ell + \hat{p}_j$. It is the *global* mapping for all remaining particles in Eqn. (4) that is responsible for the reduced number of Born-type matrix reevaluations. For the real emission subtraction terms, we then obtain the total contribution

$$d\sigma^{A}_{ab}(\hat{p}_a,\hat{p}_b) \;=\; d\sigma^{A,a}_{ab}(\hat{p}_a,\hat{p}_b) + d\sigma^{A,b}_{ab}(\hat{p}_a,\hat{p}_b) + \sum_{\ell \neq a,\, b} d\sigma^{A,\ell}_{ab}(\hat{p}_a,\hat{p}_b), \qquad (5)$$

with the sum over all possible final state emitters.

In the setup of the scheme, the finite remainders of some subtraction terms are currently evaluated numerically. This poses no impediment for the implementation of our scheme. We have approximated all remainders for numerical integrals by approximation functions, cf. [12] for a first preliminary discussion.

4 Results

We here show the results for the C parameter in the process $e^+ e^- \to 3$ jets [6]. For this, the real emission processes are given by

$$e^+ e^- \;\to\; q\,\bar{q}\,q\,\bar{q},\; e^+ e^- \;\to\; q\,\bar{q}\,g\,g. \qquad (6)$$

These contributions call for $(8 + 10)$ matrix element reevaluations per phase space point in the Catani-Seymour [13] and $(4{+}5)$ reevaluations in our scheme, respectively. We display our results in terms of the C distribution [14]

$$C^{(n)} \;=\; 3\left\{1 - \sum_{i,j\,=\,1,\, i<j}^{n} \frac{s_{ij}^2}{(2\,p_i\cdot Q)\,(2\,p_j\cdot Q)}\right\},\; (s_{ij} \;=\; 2\,p_i\cdot p_j). \qquad (7)$$

Figure 1 shows that we reproduce the literature result [15], as well as agreement between implementations of both schemes. We want to point out that this is indeed a non-trivial statement, as the *differences* between the two schemes for both subtracted real emission as well as virtual contributions are sizeable.

5 Summary

We here reported on an alternative NLO subtraction scheme for QCD calculations, which uses the splitting functions of an improved parton shower as subtraction kernels. We have briefly discussed the setup, and especially the

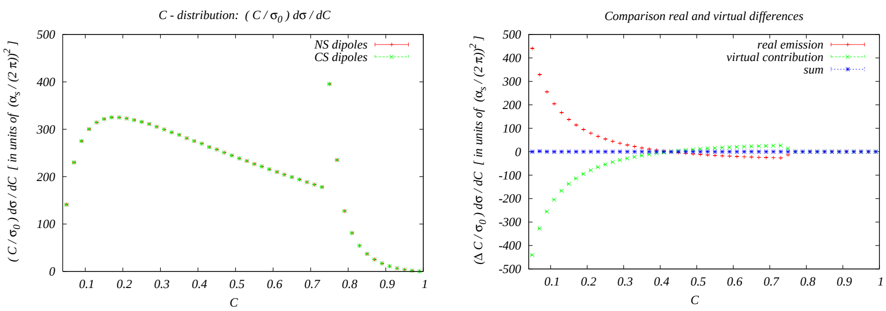

Figure 1: *Left:* Total result for differential distribution $\frac{C}{\sigma_0}\,\frac{d\sigma^{\mathrm{NLO}}}{dC}$ using both our dipoles (red, "NS") and Catani-Seymour dipoles (green, "CS"). The standard literature result obtained using the CS scheme is completely reproduced with the NS dipoles. *Right: Differences* $\Delta_{\text{CS-NS}}$ for real emission (red, upper) and virtual (green, lower) contributions, showing that especially for low C values the contributions in the two schemes significantly differ. Adding up $\Delta^{\mathrm{real}}+\Delta^{\mathrm{virt}}$ renders 0 as expected.

features leading to an improved scaling behaviour of our scheme. Results for the process $e^+e^- \to 3$ jets have been presented. Summarizing, we regard the scheme discussed here as a viable alternative to standard schemes.

6 Acknowledgements

TR wants to thank the organizers for an excellent workshop at ECT*.

References

1. C.H. Chung, M. Kramer, and T. Robens. An alternative subtraction scheme for next-to-leading order QCD calculations. *JHEP*, 1106:144, 2011.

2. Zoltan Nagy and Davison E. Soper. Parton showers with quantum interference. *JHEP*, 09:114, 2007.

3. Zoltan Nagy and Davison E. Soper. Parton showers with quantum interference: leading color, spin averaged. *JHEP*, 03:030, 2008.

4. Zoltan Nagy and Davison E. Soper. Parton showers with quantum interference: leading color, with spin. *JHEP*, 07:025, 2008.

5. Zoltan Nagy and Davison E. Soper. A parton shower based on factorization of the quantum density matrix. *JHEP*, 06:097, 2014.

6. Cheng-Han Chung and Tania Robens. Nagy-Soper subtraction scheme for multiparton final states. *Phys.Rev.*, D87:074032, 2013.

7. Tania Robens. Nagy-Soper Subtraction: A Review. *Mod.Phys.Lett.*, A28:1330020, 2013.

8. G. Bevilacqua, M. Czakon, M. Kubocz, and M. Worek. Complete Nagy-Soper subtraction for next-to-leading order calculations in QCD. *JHEP*, 1310:204, 2013.

9. Guido Altarelli and G. Parisi. Asymptotic Freedom in Parton Language. *Nucl. Phys.*, B126:298, 1977.

10. A. Bassetto, M. Ciafaloni, and G. Marchesini. Jet Structure and Infrared Sensitive Quantities in Perturbative QCD. *Phys. Rept.*, 100:201–272, 1983.

11. Yuri L. Dokshitzer, Valery A. Khoze, Alfred H. Mueller, and S. I. Troian. Basics of perturbative QCD. Gif-sur-Yvette, France: Ed. Frontieres (1991) 274 p. (Basics of).

12. Markus Bach, Cheng Han Chung, and Tania Robens. An alternative subtraction scheme for NLO QCD calculations using Nagy-Soper dipoles. *PoS*, RADCOR2013:014, 2013.

13. S. Catani and M. H. Seymour. A general algorithm for calculating jet cross sections in nlo qcd. *Nucl. Phys.*, B485:291–419, 1997.

14. R. Keith Ellis, D. A. Ross, and A. E. Terrano. The Perturbative Calculation of Jet Structure in e+ e- Annihilation. *Nucl. Phys.*, B178:421, 1981.

15. http://hepwww.rl.ac.uk/theory/seymour/nlo/event2_02.f.